

---

**Core Loss During a Severe Accident (COLOSS Project)**

**Contract FIKS-CT-1999-00002  
(Cost-shared action)**

**IRSN/DPAM/Dir/2004-0279, SAM-COLOSS-P079**

**COLOSS Final Extended Report**

**Part 1**

**Experimental and analytical activities**

**Main outcomes from the project**

B. Adroguer, F. Bertrand, P. Chatelard, J.P. Van Dorsselaere,  
N. Cocuaud, C. Duriez, (IRSN-DPAM), L. Bellenfant (IRSN-DSR),  
A. Miassoedov, M. Steinbrück, J. Stuckert, G. Schanz, W. Krauss, W. Hering, C. Homann (FZK),  
D. Bottomley, D. Knoche (JRC/ITU),  
V. Vrtilkova (ÚJP-PRAHA),  
L. Belovsky (ALIAS CZ),  
K. Müller (JRC/IE),  
Z. Hózer, L. Matus, I. Nagy, Gy. Gyenes, A. Pintér, P. Windberg (AEKI),  
G. Bandini, S. Ederli, (ENEA),  
J. Birchley (PSI),  
T. v. Berlepsch, I. Kleinhietpass (RUB),  
M. Buck (IKE),  
J. A. Fernandez Benitez, F. Martin-Fuertes (UPM),  
E. Virtanen (LTKK),  
S. Marguet (EDF),  
G. Azarian, A. Caillaux (Framatome ANP SAS), H. Plank (Framatome ANP GmbH),  
M. Veshchunov, A. Berdyshev, A. Boldyrev (IBRAE),  
V. Kobzar, A. Volchek, Y. Zvonarev, (NSI/RRC-KI),  
A. Goryachev, V. Smirnov (RIAR)

Dissemination level: RE (Distribution of this document is restricted to the partners of the project and to co-ordinators of some EC projects)

## COLOSS distribution list

B. Adroguer	IRSN/DPAM/Dir/Cadarache	(5ex)
J.P. Van Dorsselaere	IRSN/DPAM/Dir/Cadarache	
C. Duriez	IRSN/DPAM/SEREA/Cadarache	
N. Cocuau	IRSN/DPAM/SEREA/Cadarache	
P. Chatelard	IRSN/DPAM/SEMCA/Cadarache	
F. Bertrand	IRSN/DPAM/SEMCA/Cadarache	
B. Chaumont	IRSN/DSR/SAGR/Far	
L. Bellenfant	IRSN/DSR/SAGR/Far	
H. Plitz	FZK/Karlsruhe	
G. Schanz	FZK/Karlsruhe	
W. Krauss	FZK/Karlsruhe	
A. Miassoedov	FZK/Karlsruhe	
M. Steinbrück	FZK/Karlsruhe	
J. Stuckert	FZK/Karlsruhe	
W. Hering	FZK/Karlsruhe	
C. Homann	FZK/Karlsruhe	
D. Knoche	JRC/Karlsruhe	
D. Bottomley	JRC/Karlsruhe	
J. P. Glatz	JRC/Karlsruhe	
J. Kubant	ÚJP-PRAHA, Prague	
V. Vrtilkova	ÚJP-PRAHA, Prague	
L. Belovsky	ALIAS CZ, ÚJP consultant/Prague	
K. Müller	JRC/Petten	
Z. Hózer	AEKI/Budapest	
I. Nagy	AEKI/Budapest	
Gy. Gyenes	AEKI/Budapest	
P. Winberg	AEKI/Budapest	
A. Pinter	AEKI/Budapest	
M. Pezzilli	ENEA/Roma	
G. Bandini	ENEA/Bologna	
S. Ederli	ENEA/Roma	
S. Guentay	PSI/Villigen	
J. Birchley	PSI/Villigen	
M. K. Koch	RUB/Bochum	
I. Kleinhietspass	RUB/Bochum	
M. Buck	IKE/Stuttgart	
S.A. Alonso	UPM/Madrid	
E. Gallego	UPM/Madrid	
F. Martin-Fuertes	UPM/Madrid	
J. Fernandez Benitez	UPM/Madrid	
E. Virtanen	LTKK/Lappeenranta	
S. Marguet	EDF/Clamart	
Y. Dutheillet	EDF/Clamart	
G. Azarian	Framatome ANP/Paris	
A. Caillaux	Framatome ANP/Paris	
H. Plank	Framatome ANP/Erlangen	
M. Veshchunov	IBRAE/Moscow	
A. Berdyshev	IBRAE/Moscow	
A. Boldyrev	IBRAE/Moscow	
Y. Zvonarev	KI/Moscow	
V. Kobzar	KI/Moscow	
V. Smirnov	RIAR/Dimitrovgrad	
A. Goryachev	RIAR/Dimitrovgrad	

**ENTHALPY and EVITA projects**

A. De Bremaecker	IRSN/PDAM/SEMIC/Cadarache
H.J. Allelein	GRS/Cologne
K. Traumbauer	GRS/Munich

**THENPHEBISP project**

B. Clément	IRSN/DPAM/SEMIC/ Cadarache
T. Haste	PSI/Villigen

**EC distribution**

A. Zurita	DG Research J.4 /Bruxelles
-----------	----------------------------

**IRSN distribution list**

De Franco	IRSN/Pg/Clamart
J. Bardelay	IRSN/Pg/Clamart
R. Dallendre	IRSN/RI/Clamart
M. Durin	IRSN/DSR/Clamart
S. Roche	IRSN/DSR/Clamart
J. Lewi	IRSN/DESTQ/Clamart
M. Schwarz	IRSN/DPAM/Dir/Cad
G. Hache	IRSN/DPAM/Dir/Cad
J.C. Micaelli	IRSN/DPAM/Dir/Cad
M. Faury	IRSN/DPAM/SEREA/Cad
R. Gonzalez	IRSN/DPAM/SEMIC/Cad
P. Giordano	IRSN/DPAM/SEMIC/Cad
N. Alpy	IRSN/DPAM/SEMIC/Cad
M. Barrachin	IRSN/DPAM/SEMIC/Cad
F. Barré	IRSN/DPAM/SEMCA/Cad
F. Camous	IRSN/DPAM/SEMCA /Cad
S. Pignet	IRSN/DPAM/SEMCA/Cad
G. Repetto	IRSN/DPAM/SEMCA/Cad
S. Bourdon	IRSN/DPAM/SEMCA/Cad

Blank page

**Institut de Radioprotection et de Sûreté Nucléaire  
Direction de Prévention des Accidents Majeurs**

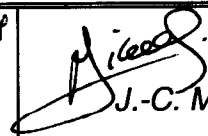
Nat. Document	Rapport Technique DPAM/Dir 2004-0279 SAM-COLOSS-P079	
<b>TITRE</b>	<b>COLOSS Final Extended Report : Part 1</b> Experimental and analytical tasks. Main outcomes from the project	
Auteur(s)	<i>B. Adroguer et al.,</i>	
Type de Diffusion :	"Mots clés" : COLOSS project, Severe Accidents, core degradation, plant calculations	Nbre de pages : 229 Nbre annexes: 1

Résumé :

Ce rapport final COLOSS résume les activités du projet relatives aux activités expérimentales et de modélisation (WP1 à WP7). Les principaux résultats des calculs réacteurs (WP8) détaillés dans la Partie 2 du rapport y sont également rappelés et pris en compte dans les conclusions et recommandations finales du projet

Abstract :

This report gives a summary of the experimental and modelling work-packages (WP1 to WP7). Main outcomes from plant calculations (WP8) detailed in the Part 2 of the report are also summarised. Finally main conclusions from the project are drawn along with recommendations for further activities.

 <b>B. ADROGUER</b> 21/06/04	 22/06/04 <b>B. CLEMENT</b>	 24.6.4 <b>J.-C. MICAELLI</b>
Rédaction : Nom/Visa/Date	Vérification : Nom/Visa/Date	Approbation DPAM : Nom/Visa/Date

## Content

Executive Summary .....	10
<b>1 Introduction .....</b>	<b>15</b>
<b>2 Objectives and description of the project .....</b>	<b>16</b>
2.1 Objectives .....	16
2.2 Work programme .....	17
2.3 Modification of the work programme.....	18
<b>3 Experimental tasks (WP1 to WP6).....</b>	<b>20</b>
3.1 WP1.1: SETs on dissolution of fresh and high burn-up UO <sub>2</sub> and MOX (JRC/ITU) ...	20
3.2 WP1.1: SETs on melting point of U-O-Zr mixtures .....	26
3.3 WP1.2: Analytical support to tests on dissolution of irradiated fuel (IRSN).....	27
3.4 WP2.1: SETs on simultaneous dissolution of UO <sub>2</sub> and ZrO <sub>2</sub> by molten Zr (JRC/IE and RIAR).....	27
3.5 WP2.2: PWR and VVER single rod degradation tests (AEKI/KFKI) .....	31
3.6 WP2.3: Analytical support to PWR and VVER degradation tests .....	39
3.6.1 SVECHA/QUENCH calculations (IBRAE) .....	40
3.6.2 ICARE/CATHARE and SCDAP/RELAP5 calculations (ENEA) .....	41
3.6.3 ICARE/CATHARE calculations (KI).....	46
3.7 WP3.1: Experiments on dissolution of ZrO <sub>2</sub> and on oxidation of U-Zr-O mixtures....	50
3.7.1 Experiments on oxidation of solid U-Zr-O mixtures (ÚJP-PRAHA).....	50
3.7.2 ZrO <sub>2</sub> dissolution tests and oxidation of molten Zr-O mixtures (FZK) .....	60
3.8 WP3.2: Analytical support to tests on the oxidation of U-Zr-O mixtures.....	65
3.8.1 Interpretation of the results with ICARE2 (IRSN - ALIAS CZ) .....	65
3.8.2 Interpretation of the UJP-PHAHA results (RUB).....	68
3.9 WP4: SETs on B <sub>4</sub> C and related analysis tasks (IRSN, FZK) .....	69
3.9.1 SETs with VERDI on oxidation of B <sub>4</sub> C (IRSN).....	70
3.9.2 SETs with BOX on oxidation of B <sub>4</sub> C (FZK) .....	74
3.9.3 SETs on degradation of B <sub>4</sub> C control rod segments and oxidation of B <sub>4</sub> C-rich mixtures (FZK).....	80
3.9.4 Thermogravimetric SETs on B <sub>4</sub> C oxidation and analytical evaluation (FZK).....	83
3.10 WP5.1: VVER bundle test with a central B <sub>4</sub> C control rod (AEKI).....	89
3.11 WP5.2: Analytical support to the VVER-B <sub>4</sub> C control rod (KI, AEKI).....	98
3.11.1 Calculations with ICARE/CATHARE (KI).....	98
3.11.2 Calculations with ICARE/CATHARE (AEKI) .....	102
3.12 WP6.1: PWR bundle tests with a central B <sub>4</sub> C control rod (FZK) .....	106
3.12.1 Quench facility .....	106
3.12.2 Main Results of QUENCH-07 Test .....	108
3.12.3 Main Results of QUENCH-09 Test .....	112
3.12.4 Main outcomes from QUENCH-07 and QUENCH-09 tests .....	117

<b>3.13 WP6.2: Analytical support for QUENCH-07 and -09 tests (FZK, EDF, PSI, IKE, UPM, ENEA and IRSN)</b> .....	<b>117</b>
3.13.1 Analytical support for QUENCH-07 (FZK) .....	117
3.13.2 Post-test calculations of QUENCH-07 (EDF) .....	129
3.13.3 Analytical support for QUENCH-09 test (FZK).....	131
3.13.4 Analytical support for QUENCH-07 and QUENCH-09 (PSI) .....	142
3.13.5 Analytical support for QUENCH-07 and QUENCH-09 (IKE) .....	149
3.13.6 Analytical support for QUENCH-07 and QUENCH-09 (UPM) .....	150
3.13.7 Analytical support for QUENCH-09 (ENEA) .....	157
3.13.8 Post-test calculations of QUENCH-09 (IRSN).....	164
<b>4 Modelling tasks (WP7).....</b>	<b>176</b>
<b>4.1 B<sub>4</sub>C-CR degradation and oxidation models (IRSN, EDF, FZK).....</b>	<b>176</b>
4.1.1 B <sub>4</sub> C oxidation model from IRSN .....	176
4.1.2 B <sub>4</sub> C-CR degradation and oxidation models from EDF.....	183
4.1.3 B <sub>4</sub> C oxidation model from FZK.....	184
<b>4.2 Oxidation of U-O-Zr mixtures (IRSN, ALIAS CZ, JRC, IBRAE, RUB).....</b>	<b>185</b>
4.2.1 Modeling task on oxidation of solid U-Zr-O mixtures (ALIAS CZ).....	185
4.2.2 Modeling task on oxidation of liquid Zr-O and U-Zr-O mixtures (JRC, IBRAE) .....	187
4.2.3 Modeling on oxidation of liquid U-Zr-O mixtures (IRSN) .....	190
4.2.4 Investigation on the melt oxidation above the liquidus temperature (RUB) .....	190
<b>4.3 Dissolution of fuel (IRSN, ALIAS CZ, IBRAE).....</b>	<b>192</b>
4.3.1 Dissolution of irradiated fuel (UO <sub>2</sub> & MOX) by molten Zr (IRSN, ALIAS CZ).....	193
4.3.2 Simultaneous dissolution of UO <sub>2</sub> and ZrO <sub>2</sub> by molten Zr (IBRAE).....	197
<b>4.4 Main improvements of SA codes in the project.....</b>	<b>200</b>
<b>5 Summary of the WP8 devoted to plant calculations of SA sequences .....</b>	<b>202</b>
<b>5.1 Assessment of SA codes on H<sub>2</sub> production, B<sub>4</sub>C effects and corium formation.....</b>	<b>203</b>
<b>5.2 Needs for short-term code improvements .....</b>	<b>204</b>
<b>5.3 Safety implications of results .....</b>	<b>205</b>
<b>6 European added value and dissemination of the results .....</b>	<b>205</b>
<b>7 Main achievements.....</b>	<b>206</b>
<b>7.1 Fulfilling the terms of the contract.....</b>	<b>206</b>
<b>7.2 Main achievements and perspectives .....</b>	<b>207</b>
<b>Acknowledgements .....</b>	<b>211</b>
<b>Appendix 1: COLOSS reports .....</b>	<b>212</b>

## LIST OF ABBREVIATIONS AND SYMBOLS

AECL	Atomic Energy of Canada Limited
AEKI	Atomic Energy Research Institute from the Hungarian Academy of Sciences
ANL	Argonne National Laboratory, US
ASTEC	Accident Source Term Evaluation Code
B <sub>4</sub> C-CR	B <sub>4</sub> C Control Rod
BWR	Boiling Water Reactor
CEA	Commissariat à l'Energie Atomique
CEC	Commission of the European Communities
CIT	Corium Interactions and Thermochemistry project (4 <sup>th</sup> FP)
COBE	Core Behaviour project (4 <sup>th</sup> FP)
COLOSS	Core Loss project (5 <sup>th</sup> FP)
ECCS	Emergency Core Coolant System
EC	European Commission
EDF	Electricité de France
EDX	Energy Dispersive Micro-Analysis
ENEA	Ente per le Nuovo Tecnologie, l'Energia e l'Ambiente
EU	European Union
EPMA	Electron Probe Micro-Analysis
EPR	European Pressurized Reactor
EVITA	European Validation of the Integral Code <u>A</u> STEC (5 <sup>th</sup> FP)
Ex-V.	Ex-Vessel
FLHT	Full Length High Temperature
FP	Fission Product
5 <sup>th</sup> FP	5 <sup>th</sup> Framework Programme of the EC
FZK	Forschungszentrum Karlsruhe (formerly Kernforschungszentrum Karlsruhe (KfK))
GRS	Gesellschaft für Anlagen und Reaktorsicherheit, Germany
HFI	High Frequency Induction
IBRAE	Nuclear Safety Institute of Russian Academy of Sciences
IKE	Institut für Kernenergetik und Energiesysteme, Universität Stuttgart, Germany
In-V.	In-Vessel
IRSN	Institut de Radioprotection et de Sureté Nucléaire (formerly IPSN)
ISTC	International Science and Technology Center (Moscow)
ITU	Institut des Trans-Uraniens
JRC	Joint Research Centre
KfK	see FZK
KI	Russian Research Centre “ Kurchatov Institute “
LOCA	Loss of Coolant Accident
LTKK	Lappeenranta University of Technology, Finland
LSK	Saint Petersburg Electrotechnical University, Russia
LWR	Light Water Reactor
MP	Melting Point
MOX	Mixte Oxides
NAS	New Associated States

NPP	Nuclear Power Plant
NoE	Network of Excellence
NSI	Nuclear Safety Institute (IBRAE) from the Russia Academy of Sciences
OPSA	Oxidation Phenomena in Severe Accidents project (4 <sup>th</sup> FP)
OECD	Organisation for Economic Cooperation and Development
PAG	Plant Analysis Group in COLOSS
PBF	Power Burst Facility, United States
PIRT	Parameter Identification and Ranking Table
PNL	Pacific Nord-Est Laboratory
PORV	Power Operated Relief Valve
PSI	Paul Scherrer Institute, Swiss
PWR	Pressurised Water Reactor
RCS	Reactor Coolant System
RIAR	Institute for engineering and scientific research for Nuclear Power Plants Dimitrovgrad (Russia)
RUB	Ruhr Universität Bochum, Germany
SARNET	Severe Accident Research Network (6th FP)
SBO	Station Blackout sequence
SCDAP/R5	SCDAP/RELAP5 code (S/R5)
SET	Separate Effects Tests
RPV	Reactor Pressure Vessel
SA	Severe Accident
SAM	Severe Accident Management
SEM/EDX	Scanning Electron Microscopy/Energy-Dispersive X-ray analysis
SNL	Sandia National Laboratory, US
SOAR	State of the Art Report
TMI-2	Three Mile Island Unit 2
UJP-Praha	formerly SKODA-UJP, Zbraslav, Czech Republic
UPM	Universidad Politecnica De Madrid
U-Zr-O	Mixtures involving core materials resulting from the liquefaction of fuel rods (UO <sub>2</sub> , Zr, ZrO <sub>2</sub> )
VVER	Pressurized Water Reactor of Russian type

# Executive Summary

## Description and objectives of the project

The COLOSS project was a 3-year shared-cost action which started in February 2000. The objective was concerned with the consequences that core degradation, occurring under Severe Accident (SA) conditions, may have on H<sub>2</sub> production, melt generation and the source term. Unresolved in-vessel risk-relevant issues were studied, in particular:

- dissolution of fresh and high burn-up UO<sub>2</sub> and MOX by molten Zircaloy,
- simultaneous dissolution of UO<sub>2</sub> and ZrO<sub>2</sub> by molten Zircaloy in rod geometry,
- oxidation of U-O-Zr mixtures,
- oxidation of pure B<sub>4</sub>C material and
- degradation-oxidation of prototypic B<sub>4</sub>C control rods.

The main challenge addressed was the in-depth analysis of experimental results produced and the development of models for SA codes. The priority was put on the application of results in SA codes and on the implications of results on the safety viewpoint. Efforts were focussed on the following risk-relevant aspects:

- Fuel dissolution responsible for liquefaction of the fuel ~1000 K below the UO<sub>2</sub> melting point (~3100 K), was characterized by large uncertainties on the effect of burn-up and no data were available on MOX dissolution. Effects of burn-up on the corium formation and early fuel rod liquefaction and collapse were not correctly understood in spite of significant effects on FP release and corium behavior (amount and timing of molten mixture formation and composition).
- Metal-rich U-O-Zr mixtures oxidise in steam during relocation and once frozen at lower core zones. This is a key source of H<sub>2</sub> during core degradation and particularly during reflooding. The corresponding modelling is either missing or inadequate in SA codes. The main concern was the high H<sub>2</sub> production rates which can reduce the efficiency of H<sub>2</sub> mitigation measures in the containment or even create a H<sub>2</sub> explosion risk.
- Effects of B<sub>4</sub>C, a neutron-absorbing material used in high power nuclear plants, were poorly understood, and models in SA codes were either missing or inadequate. The main concern was to identify the gas production (H<sub>2</sub>, CO, CO<sub>2</sub>, CH<sub>4</sub>, B-compounds) from B<sub>4</sub>C oxidation suspected to affect the chemistry and transport of volatile fission products out of the core, in particular that of iodine which represents the main radiological risk in the short-term of SA's.

## Partnership

Eighteen partners from 13 countries of the EU, 2 NAS and 3 Russian laboratories having an excellent expertise on core degradation under SA conditions were involved in the project, including plant designers, R&D organisations working on nuclear safety, the French Utility and four Universities. Significant progress on knowledge as well as on SA codes was made possible thanks to a close cooperation inside the project between experimentalists and analysts and outside with the EVITA and ENTHALPY 5<sup>th</sup> FP projects and also with the PHEBUS FP and QUENCH programmes.

## Main achievements

*Sophisticated experimental tasks were carried out with success. Some with existing facilities and five with small-scale rigs constructed at the beginning of the project.*

Several experimental programmes to study the effects of B<sub>4</sub>C on core degradation and gas production were carried out using test rigs at different scales for B<sub>4</sub>C material, from B<sub>4</sub>C fragments to B<sub>4</sub>C Control Rods (B<sub>4</sub>C-CR) in rod bundles. A large experimental database was produced covering a wide scope of conditions and phenomena.

- Separate Effects Tests (SET) enabled the measurements of B<sub>4</sub>C oxidation kinetics and the related formation of gases and B-compounds. Different conditions and various B<sub>4</sub>C materials representative of different plant designs were studied. Production of gases such as H<sub>2</sub>, CO, CO<sub>2</sub>, very low CH<sub>4</sub> and very large amounts of aerosol were measured.

- Small scale B<sub>4</sub>C control rod tests enabled the identification of main degradation processes such as B<sub>4</sub>C/steel and Zr/steel eutectic interactions, crucible effect of the external ZrO<sub>2</sub> layer of the guide tube, failure conditions and final oxidation of the remaining B<sub>4</sub>C fragments (undissolved part of the B<sub>4</sub>C pellets) and metallic B<sub>4</sub>C-rich mixtures.

- Preliminary data on the oxidation of B<sub>4</sub>C-rich metallic mixtures showed much more rapid kinetics than the oxidation of solid materials. This could enhance the H<sub>2</sub> peak production generated during the quenching of degraded cores due to oxidation of relocated B<sub>4</sub>C-rich mixtures.

- Three key large-scale fuel rod bundle experiments characterized by a central B<sub>4</sub>C control rod have been carried out in the QUENCH and CODEX facilities with bundles representative of PWR (2 tests) and VVER designs respectively. The B<sub>4</sub>C was found to be a contributor to the core degradation nevertheless its specific contribution could not be quantified. No significant differences could be observed between PWR and VVER designs. For the first time, the gas production from B<sub>4</sub>C oxidation was measured during the core degradation. Significant quantities of CO, CO<sub>2</sub> and B-compounds (as large aerosol source) were produced during the degradation of the bundles while CH<sub>4</sub> release was very low. The gas production resulting from the B<sub>4</sub>C control rod degradation and oxidation was found to be closely dependent on the oxidizing thermal-hydraulic conditions in the bundle. These results are of particular interest for the preparation of the future PHEBUS FPT3 test planned also with a central B<sub>4</sub>C control rod.

- The knowledge acquired from the large B<sub>4</sub>C experimental database produced enabled significant progress regarding modeling and validations studies.

Experimental data on the oxidation of U-O-Zr solid and molten mixtures were obtained from two experimental programmes.

- In both cases, faster kinetics than for pure Zr were found. These data confirm that Zr-rich metallic mixtures can be a significant source of rapid H<sub>2</sub> production during core degradation and, mainly, during core reflooding. This is a key insight for modelling the oxidation of mixtures, this phenomenon being, in general, absent or inadequately considered in SA codes. These code

deficiencies could explain why the H<sub>2</sub>-peak production observed during core reflooding is usually significantly underestimated by SA codes. This knowledge was taken into account in the related modeling task.

Experimental data on fuel dissolution by molten Zr were obtained from three experimental programmes involving fresh fuel and irradiated fuel.

- New results were produced on simultaneous dissolution of fresh UO<sub>2</sub> and ZrO<sub>2</sub> by molten Zr. This interaction was investigated in a crucible geometry and in the fuel rod configuration. These data enabled progress in the understanding of the mechanisms driving this double interaction and responsible of the early fuel liquefaction and failure of the external ZrO<sub>2</sub> layer of the cladding. The related modeling was upgraded.

- Unique data could be obtained on dissolution of high burn-up UO<sub>2</sub> (65 and 90 GWd/tU) and MOX fuel (~45 GWd/tU) by molten Zr. Compared with fresh fuel, enhanced kinetics and greater apparent dissolution and fuel decohesion were observed in both cases due to fuel cracking and gaseous fission product (FP) release and bubbling. Whether UO<sub>2</sub> or MOX fuel of similar burn-up dissolves faster cannot be concluded from these experiments, since the burn-ups of the two fuels were too different. These preliminary results require confirmation with additional experiments covering a wider range of experimental conditions, in particular medium burn-up UO<sub>2</sub> fuel, and carried out with improved post-test examinations.

### ***Modelling and transfer of knowledge in SA codes:***

Each experimental task was accompanied by a significant analytical activity enabling the production of models on B<sub>4</sub>C oxidation, fuel dissolution and oxidation of solid and molten mixtures.

- Models produced were implemented in SA codes ASTEC, ATHLET-CD, ICARE/CATHARE and SVECHA. This activity ensured the transfer of knowledge from experimental programmes to SA codes used for safety studies.

- Models developed on B<sub>4</sub>C, fuel dissolution and oxidation of mixtures were applied in the calculation of the bundle tests QUENCH-07, QUENCH-09 and CODEX-B<sub>4</sub>C for validation purposes. Modelling improvements and related validation was planned to continue after the project to take full account of experimental results produced near the end of the project.

- Preliminary versions of SA codes developed during the project need to be consolidated and validated with complementary experimental results on B<sub>4</sub>C, fuel dissolution and oxidation of mixtures expected from ongoing PHEBUS FP, QUENCH and ISTC projects funded by the EC on core degradation and corium behaviour.

- Large user-effects were found in various calculations regarding the choice of oxidation kinetics law and that of fuel rod degradation criteria (ZrO<sub>2</sub> clad failure and fuel rod collapse). Based on an in-depth analysis of existing data, recommendations were given by FZK for the oxidation laws and by IRSN for the degradation criteria on the choice of these user-specified models in SA codes. The latter were based on PHEBUS PF results. For the Zr oxidation, the use of Leistikow (or Cathcart) correlation at low temperature (T <1800K) and Prater-Courtright

correlation at high temperature ( $T > 1900\text{K}$ ) were recommended in the calculations of the project. More investigations are needed to conclude on the best Zr oxidation correlations, in particular there is a need at high temperature of modeling improvements regarding the steam supply limitation before recommending Zr oxidation correlations for plant calculations.

### ***Application of results to plant calculations of selected SA sequences:***

Two large series of eleven severe accident sequences involving different plant designs such as PWR-900, PWR-1300, EPR, BWR and VVER and the TMI-2 accident were calculated using three integral codes ASTEC, MELCOR and MAAP4 and two mechanistic codes ICARE/CATHARE and SCDAP/RELAP5. The final calculations were run with improved codes and taking into account the knowledge acquired during the project.

- Each series of plant calculations was enriched by sensitivity studies on key parameters of the core degradation and by code-to-code benchmark exercises. This effort enabled a) the assessment of codes to calculate core degradation with the identification of main uncertainties and needs for short-term improvements and b) the identification of safety implications of new results.

- Three “Risk Relevant Parameters and Ranking Tables” have been deduced from plant calculations to identify relevant parameters affecting the modelling of  $\text{H}_2$  production,  $\text{B}_4\text{C}$  effects and corium behaviour. These tables include a ranking of each parameter for the related safety risks:  $\text{H}_2$  explosion in the containment, impact of  $\text{B}_4\text{C}$  on the source term and in-vessel corium retention. These tables provide also valuable indications for future R&D efforts.

- The project organized a large code-to-code comparison exercise involving plant calculations carried out in the project. Valuable results on respective code capabilities and uncertainties were obtained. Code-to-code benchmarks were recognized as useful exercises for code assessment. Recommendations to optimise future benchmarks could be given regarding the harmonization of input decks, the choice of SA scenario and the need to limit user-effects.

- Key points arriving from plant calculations were:

*H<sub>2</sub> production:* Sensitivity studies on early degradation models showed more significant effects on *H<sub>2</sub> rate* during early core heat-up or during quenching than on *total H<sub>2</sub> production*. The scattering of code predictions on the total  $\text{H}_2$  release was found to be in the range of 20-35%.

*ZrO<sub>2</sub> clad failure:* The assessment of codes on the  $\text{ZrO}_2$  clad failure criteria evidenced large uncertainties, the effect being dependent on core conditions and also dependent on code modelling. The uncertainties would affect significantly the hydrogen release rate during core heat-up as well as the corium formation via the fuel dissolution by Zircaloy and its composition.

*Fuel rod collapse:* The fuel rod collapse criteria are clearly characterised by large uncertainties. Significant effects were found in plant applications on the mass of corium that is formed. It was recommended that sensitivity studies have to be performed on these criteria for plant applications.

*Oxidation of mixtures:* In general, this phenomenon is a key weakness of SA codes, related models being either missing or inadequate. Consequently, the  $\text{H}_2$  production rate during melt relocation or during quenching is certainly underestimated due to the poor melt oxidation models (or even to the lack of models). The proposed models, which enabled larger  $\text{H}_2$  production during core degradation, need to be consolidated and validated with complementary data.

*B<sub>4</sub>C oxidation:* Effects on core degradation were calculated as limited although experimental observations suggest more important effects. H<sub>2</sub> from B<sub>4</sub>C was often found to be less than 10% of the total H<sub>2</sub> production. Very little CH<sub>4</sub> was directly produced. It was found that CO and CO<sub>2</sub> can be converted into CH<sub>4</sub> in the cooler zones of the primary circuit during H<sub>2</sub>-rich phases. Then, non-negligible quantities of volatile CH<sub>3</sub>I, a key factor of radiological risk, could be formed. Large effects of B-compounds were also found on Cs chemistry.

*UO<sub>2</sub> dissolution:* Substantial uncertainties were evidenced by large differences between models and results on UO<sub>2</sub> liquefaction. The *burn-up effect* known to enhance significantly UO<sub>2</sub> liquefaction and suspected to favour early rod collapse and FP release has to be modelled in SA codes. Again the provisional models need to be consolidated using complementary data.

*Corium behaviour:* Large discrepancies were found between comparable calculations in the amount and timing of corium formation, in its composition and in the distribution between core, core by-pass and lower head. MAAP4, SCDAP/RELAP5 and ICARE/CATHARE were found to largely underestimate the mass of corium that was formed in TMI-2. Corium behaviour was found to be more dependent on the late melt progression modelling than on that of the early degradation. One exception is the *fuel rod collapse criterion*, which causes an early and large corium formation and significantly affects late corium behaviour.

#### ***Perspectives:***

Remaining uncertainties and SA code weaknesses in safety-relevant phenomena of core degradation have been transmitted to the PIRT review on SA carried out in the EURSAFE thematic network (5<sup>th</sup> FP) to be addressed in the SARNET network of excellence (6<sup>th</sup> FP). In particular results on dissolution of irradiated fuel and oxidation of metal-rich mixtures during core degradation and reflooding should be consolidated. The follow-up of the COLOSS activity on plant calculations with sensitivity studies and benchmarking exercises has also been recommended, the priority being put in SARNET on the European ASTEC code

# 1 Introduction

From the beginning of nuclear power plant developments, it has been realized that a severe accident in which the core cooling is lost could lead to fuel elements melting and FP release beyond the plant limits. Nuclear power plants are designed with engineering systems and associated operational procedures which provide a defense-in-depth against such accidents. Even if the probability to have a Severe Accident is very low, in view of the potential large radiological consequences of such severe accidents, it is now a common practice to assess the risks associated with SA conditions using computer codes to model the accident progression, and potential source term to the environment. The reliability of the assessment strongly depends on the predictive capability of the computer codes. Ensuring such a capability requires to collect the scientific information needed to better understand and describe the physical phenomena playing a role during the progression of the accident. This approach is usually done by the means of experimental programmes and modelling activities.

A severe accident (SA), which can arise in a nuclear reactor in case of safety systems failure, could develop via core heat-up in steam, interaction phenomena between core components, loss of core integrity, melt relocation and corium melt pool formation if other counteracting measures are not successful. Core degradation and liquefaction are the source of risk from gas and fission products (FP) releases and corium formation and progression. This, in turn, raises the problem of corium retention in the reactor vessel. Consequently, the mechanisms of core degradation and the related core material interactions require detailed analysis and quantification. Powerful computer codes are used for safety studies to evaluate these effects and improve the accident management and hence reduce the overall risk of radioactive contamination.

The aim of the COLOSS project (COre LOSS during a Severe Accident) was to improve the knowledge on key core degradation phenomena affecting the corium formation, and thus the related gas and FP release.

Three kinds of activities were performed: experiments at different scales including global tests with fuel rod bundles, modelling for SA codes and plant calculations of significant severe accident sequences occurring on various plant designs: PWR, BWR, VVER-1000, EPR and the TMI-2 accident.

This report is the Part 1 of the final extended COLOSS report which is divided as follows:

## **Part 1 is devoted to experimental, analytical and modeling work-packages.**

It involves:

- Small-scale experiments and related analysis tasks in work-packages WP1 to WP4.
- Large-scale experiments and related analysis tasks in WP5 and WP6
- Modelling and validation tasks in WP7

In order to have a report involving all aspects of the project, Part 1 also includes a summary of the WP8 on plant calculations. The last section give the main achievements and relates to all WPs of the project.

## **Part 2 is only devoted to plant calculations:**

Part 2 gives a synthesis of the activity of the project's Plant Analysis Group composed of the eleven partners of the project involved in plant calculations (WP8) (Ref.[1]).

A large series of plant calculations was done, including the final runs with codes improved by the project. Sensitivity studies and code-benchmarks enabled code uncertainties on core degradation to be evaluated. The implications of results produced for safety were identified as well as strengths and weaknesses of SA codes to predict core degradation. Recommendations for SA code users and for future plant calculations were also given.

## 2 Objectives and description of the project

### 2.1 Objectives

In spite of significant progress in the last 20 years on the understanding of the core degradation, remaining areas have not advanced enough to resolve the following key issues:

- a) What is the impact of  $\text{UO}_2$  and  $\text{ZrO}_2$  dissolution on the loss of core geometry and how can the burn-up effect affect the dissolution of  $\text{UO}_2$  and MOX?
- b) How does the oxidation of U-O-Zr mixtures contribute to the  $\text{H}_2$  peak production during the reflood of degraded cores?
- c) What is the  $\text{B}_4\text{C}$  effect (from the absorber elements) on core degradation and melt progression?
- d) Can the oxidation of  $\text{B}_4\text{C}$  material affect the chemistry of volatile FPs, in particular the production of volatile organic iodine?

These issues were addressed by the COLOSS project, which involved 18 partners including experimentalists, analysts, code developers and code users. The main objective was to improve the knowledge on key core degradation phenomena affecting the corium formation, and thus the gas and FP release. Unresolved risk-relevant issues regarding  $\text{H}_2$  production, melt generation and  $\text{B}_4\text{C}$  control rod degradation and oxidation were studied, through a large number of experiments. In parallel, corresponding models were developed for SA computer codes. These codes were also used to apply experimental results in plant calculations and evaluate their consequences on key SA sequences in different plants involving  $\text{B}_4\text{C}$  and in the TMI-2 accident.

Issues of fuel dissolution and quench effects relevant to questions a) and b) were previously addressed in the CIT ([2], Ref.[8]) and COBE (Ref.[3]) projects of the previous EC Nuclear Fission Safety Programme which respectively dealt with core material interactions and quench effects during core degradation. At that time, experimental results on fuel dissolution and on quenching indicated strong effects on early core liquefaction and  $\text{H}_2$  peak production but the database was not sufficient for understanding and modelling in SA codes. At the beginning of the project, the status of codes on fuel dissolution and quench effects was as follows:

- Existing fuel dissolution models in SA codes did not take into account the following aspects: a) the simultaneous dissolution of the external  $\text{ZrO}_2$  layer of the cladding (Ref.[9]) which occurs, in the fuel rod geometry, during the  $\text{UO}_2$  dissolution by molten Zr, b) the burn-up effect and c) the dissolution of MOX. The first two effects were suspected of being driving factors in fuel liquefaction, the clad failure, the loss of rod geometry and the kinetics of FP release.
- Models for the oxidation of Zr-rich compounds in degraded cores could not predict on a physical basis the risk-relevant  $\text{H}_2$  peak during quench conditions. This was illustrated several years ago in the International Standard Problem ISP-31 on the CORA-13 test (Ref.[4]) and very recently in the ISP-45 on the QUENCH-06 test (Ref.[5]). The proposal of the project was to study the oxidation of Zr-rich mixtures suspected to be a key source of  $\text{H}_2$  during quench.

- The project was also focused on B<sub>4</sub>C oxidation and B<sub>4</sub>C control rod degradation in order to answer questions c) and d). These topics were poorly understood and models in SA codes were either unsuitable or missing. The main concern here was to identify the impact of B<sub>4</sub>C on core liquefaction, on H<sub>2</sub> production and on the formation of boron and carbon gaseous species (CO, CO<sub>2</sub>, CH<sub>4</sub>, B<sub>2</sub>O<sub>3</sub> and boric acids), which could modify the chemistry and the transport of certain volatile FPs, in particular iodine (gaseous forms) and caesium. This is of prime importance for the evaluation of the source term from the containment.

In order to reduce uncertainties on the effects of fuel dissolution, B<sub>4</sub>C oxidation and quench conditions, well-targeted experimental programmes were performed involving tests at different scales. The objective was to provide a sufficient database to enable modelling improvements and validation activities as well as applications to the main SA codes used in the EU. This experimental and analytical effort was tightly linked to plant calculations of key SA sequences for different European LWRs, in particular those with B<sub>4</sub>C-CR such as PWR-1300, VVER-1000, EPR and BWR. Results produced by the project were used in plant calculations (Ref.[1]).

## 2.2 Work programme

The COLOSS project, which was a 3-year shared-cost action, started in February 2000. The work-programme performed by 18 partners was shaped around complementary experimental and analytical activities aimed at improving severe accident (SA) codes.

**Table 1: COLOSS Work-Packages and Partners**

Work-Packages	Description of the tasks and partners involved
<b>WP1 : SET on dissolution of irradiated fuel</b>	WP1.1 Irradiated UO <sub>2</sub> and MOX dissolution tests (JRC/ITU) WP1.2 Analysis of tests (IRSN)
<b>WP2: SET on simultaneous UO<sub>2</sub> and ZrO<sub>2</sub> dissolution</b>	WP2.1 Simultaneous UO <sub>2</sub> and ZrO <sub>2</sub> dissolution tests (RIAR, JRC/IE) WP2.2 PWR and VVER single rod degradation tests (AEKI) WP2.3 Analysis of WP2 tests (IRSN, KI, IBRAE, JRC/IE, ENEA)
<b>WP3: SET on U-O-Zr oxidation</b>	WP3.1 U-O-Zr oxidation tests (ÚJP) WP3.2 Analysis of U-O-Zr oxidation tests (IBRAE, JRC/IE, RUB, IRSN)
<b>WP4: SET on B<sub>4</sub>C oxidation &amp; control rod degradation</b>	WP4.1 B <sub>4</sub> C oxidation tests (FZK, IRSN) WP4.2 B <sub>4</sub> C control rod degradation tests (FZK) WP4.3 Analysis of B <sub>4</sub> C oxidation/degradation tests (IRSN, ENEA, EDF)
<b>WP5: VVER bundle test</b>	WP5.1 VVER bundle test with a central B <sub>4</sub> C control rod (AEKI) WP5.2 Analysis of the VVER bundle test (AEKI, KI, ENEA, IKE, LTKK)
<b>WP6: PWR bundle tests</b>	WP6.1 PWR/BWR bundle tests with a central B <sub>4</sub> C control rod (FZK) WP6.2 Analysis of the bundle tests (FZK, PSI, IKE, UPM, IRSN, EDF)
<b>WP7: Modelling</b>	WP7.1 B <sub>4</sub> C oxidation/degradation (IRSN, ENEA, EDF, IKE) WP7.2 U-O-Zr oxidation (IBRAE, JRC/IE, RUB, IRSN) WP7.3 Simultaneous UO <sub>2</sub> and ZrO <sub>2</sub> dissolution by Zr (IBRAE, JRC/IE, IRSN)
<b>WP8: Plant calculations of SA sequences</b>	WP8.1 PWR-1300, VVER-1000, BWR, EPR: Impact of new B <sub>4</sub> C models (IRSN, FZK, PSI, KI, LTKK, EDF, Framatome-ANP/Fr & Ge) WP8.2 TMI-2: Impact of new fuel models (ENEA, IRSN, EDF) WP8.3 Synthesis / Feedback on SA codes and safety (All WP8 partners)

The work plan involved 8 Work-Packages (WP) (Table 1):

a) Experiments on different scales were carried out for the investigation of the following phenomena:

- The dissolution of fresh and high burn-up UO<sub>2</sub> and MOX by molten Zircaloy (Zry),

- The simultaneous dissolution of  $\text{UO}_2$  and  $\text{ZrO}_2$  by molten  $\text{Zr}$  (for PWR and VVER rods),
- The oxidation of U-O-Zr and O-Zr mixtures and the related  $\text{H}_2$  production,
- The oxidation of pure  $\text{B}_4\text{C}$  material from different plant designs,
- The degradation-oxidation of single PWR and VVER  $\text{B}_4\text{C}$  control rods (CR).

WP1 to WP4 include Separate-Effects Tests (SET) and WP5 and WP6 were characterised by three large-scale experiments with VVER and PWR representative bundles with central  $\text{B}_4\text{C}$  control rod in each case. Each experimental task was supported by pre- and post-test calculations in order to analyse the results and contribute to the validation of SA codes used in the project.

b) Model development and coupling in SA computer codes used by Utilities, Industry and Safety Authorities such as the detailed ICARE/CATHARE, ATHLET-CD and SVECHA codes, and the integral ASTEC and MAAP4 codes. This activity was performed in WP7.

c) Plant calculations to assess the consequences of new experimental data and models on key SA sequences for different plant designs such as PWR-1300, PWR-900, VVER-1000, BWR, EPR and also for the TMI-2 reference accident. The large WP8 involved 11 partners using several SA codes such as ASTEC, MAAP4, MELCOR, ICARE/CATHARE, ATHLET-CD and SCDAP/RELAP5. Calculations of key SA sequences were mainly focussed on core degradation. Benchmarks and sensitivity studies were planned to identify code weaknesses and give recommendations for SA code users and for future code developments.

## **2.3 Modification of the work programme**

### **Experimental tasks**

In the initial project two experimental programmes were proposed by IPSN (renamed IRSN since 28 February 2002) in the WP2.2 and WP4.2 aimed at studying respectively the degradation of single "long  $\text{UO}_2$  rods" and "long  $\text{B}_4\text{C}$  control rods". These experiments were planned for the MADRAGUE facility under construction at the beginning of the project. The construction of this new furnace was faced with unexpected difficulties to design a new "long furnace" able to sustain temperatures up to  $2400^\circ\text{C}$  in oxidizing conditions. Finally these tests could not be kept within the timescale of the project due to delays and partners agreed at the Mid-Term Assessment meeting (Ref.[6]) to carry out new experimental activities to replace the withdrawn MADRAGUE tests.

The following alternative tests proposed by AEKI and FZK were accepted by all partners at the Mid-Term Assessment meeting.

- **WP2.2:** Additional tests with short  $\text{UO}_2$  rods by AEKI (extension of the existing WP on short fuel rod dissolution initially named WP2.3)
- **WP6.1:** A second test in the QUENCH facility using a bundle characterised by a central  $\text{B}_4\text{C}$  control rod (extension of the existing WP 6.1).

### **Analytical tasks**

The resulting changes of the experimental programmes of IRSN, AEKI and FZK induce changes of the accompanying analytical tasks (Table 2).

### **Plant calculation tasks**

- During the PAG meetings, the following changes have been proposed and agreed regarding the plant calculations:
  - EDF proposed to participate on a free basis in the TMI-2 calculation using the MAAP4 code,
  - PSI proposed to calculate a BWR SA sequenced using MELCOR instead of SCDAP/R5 in order to take advantage of the assistance of the MELCOR modelling team (NRC/Sandia), in particular regarding the B<sub>4</sub>C models. This activity was planned within the framework of a PSI-NRC agreement to carry out pre- and (later) post-test analysis of PHEBUS FPT3. In addition, PSI proposed a 2<sup>nd</sup> calculation of a BWR SA sequence (large break LOCA) not planned at the beginning of the contract.

**Table 2:** Impact of alternative tests on analytical tasks (WP2.3 and WP6.2).  
 (\*) I/C: ICARE/CATHARE code

Partners initially involved in analysis of MADRAGUE tests	Revised analytical efforts for the AEKI alternative tests	Revised analytical efforts proposed for the FZK alternative test
<b>WP2.4 partners (fuel rod tests)</b>  IRSN (I/C*support) IBRAE (Svetcha validation) ENEA (Pre-, Post-test with I/C)  UPM (Pre and Post-test with I/C)	<b>Previous WP2.4 became WP2.3 with the following revised contributions</b>  IRSN (I/C support) KI (enlarged to new tests) JRC/IE and IBRAE (SVECHA validation) ENEA (Pre- and post-test calculations with I/C & S/R5) UPM effort transferred to FZK test	
<b>WP4.3 partners (B<sub>4</sub>C-CR tests)</b>  IRSN (I/C support & analysis) ENEA (Pre, Post-test with I/C) UPM (Pre and Post-test with I/C) EDF (Post-test with MAAP4)		<b>Revised WP6.2</b> FZK (new test) PSI and IKE (enlarged to new tests) IRSN (I/C support & analysis) ENEA (Post-test with I/C) UPM ( <i>Mainly</i> Pre-test with I/C) EDF (Post-test with MAAP4)

- A partial reorientation of the strategy of plant calculations was decided before the 2<sup>nd</sup> set of calculations during the progress meeting held in Madrid mid-2002 (Ref.[7]). It was decided to focus on sensitivity studies related to modeling uncertainties suspected to be the cause of large differences observed between first calculations. The following studies were recommended:
  - check the choice of the Zr oxidation kinetics at high temperature proposed by FZK,
  - check the choice of clad failure and the fuel rod collapse criteria derived by IRSN from the analysis of PHEBUS tests.
  - check parameters of the new B<sub>4</sub>C models and melt relocation-oxidation models available in the new versions of SA codes.
- Benchmarks between plant calculations have been proposed and agreed mid-2002 (Ref.[7]). These comparisons have been reported in Part 2 of the final report. Other benchmarks

between calculations carried out in COLOSS and EVITA projects were organized also outside the framework of the two projects.

### 3 Experimental tasks (WP1 to WP6)

In spite of unexpected difficulties in some experimental programmes leading to delays or even redefinition of some tasks, significant experimental results have been produced enabling progress in related modelling tasks.

#### 3.1 WP1.1: SETs on dissolution of fresh and high burn-up UO<sub>2</sub> and MOX (JRC/ITU)

In the previous CIT project the accelerating effect of irradiation on fuel dissolution behaviour was demonstrated to be considerable, and it was evident that the effect of burn-up needed to be further investigated. Thus the COLOSS project WP1.1 objectives were the examination of a) high burn-up fuel, and b) to investigate the behaviour of MOX fuel during Zircaloy dissolution. The chosen UO<sub>2</sub> fuel had a burn-up higher than 80 GWd/tU (few tests were performed with a burn-up of 65 GWd/tU), while the MOX fuel had a burn-up of about 46 GWD/tU. Samples were slices of clad fuel rods, approximately 4mm thick.

A new furnace (Fig. 1) was constructed to investigate the burn-up effect on UO<sub>2</sub> and MOX dissolution. The construction of this furnace was faced with difficulties which caused delays.



Fig. 1: Oven freshly installed in caisson 106

#### **Oven commissioning in hot cell**

The oven was tested thoroughly in the workshop during March and April 2002. Different tests carried out with Y<sub>2</sub>O<sub>3</sub> crucibles confirmed that these crucibles are suitable for use. Thereafter the oven was put in the hot cell using a fork-lift truck (Fig 1) and various electric and thermalhydraulic connections were carried out with electric supplies and water-cooling systems in the basement.

#### **Initial natural UO<sub>2</sub> testing**

The first inactive tests of the furnace at 2000°C for 100s in a mixture of (He +2%H<sub>2</sub>) using a natural UO<sub>2</sub> clad slice were successfully performed mid 2002. The natural UO<sub>2</sub> samples were embedded and polished, and under the microscope revealed a clear Zircaloy/UO<sub>2</sub> interaction with both ceramic phase and metallic phase zones.

### **1<sup>st</sup> series of tests on dissolution of irradiated MOX in (He + 2% H<sub>2</sub>) and in pure He**

Initial testing was done at 2000°C for 100 sec and 5 min in *He - 2% H<sub>2</sub> gas mixture* with UO<sub>2</sub>, irradiated UO<sub>2</sub> (65 GWd/tU), and MOX (~45 GWd/tU).

The irradiated material tests resulted in the complete break up of the sample especially the cladding and failure of the crucible. The fuel and crucible broke into pieces while the cladding was in a powder form. By contrast, the natural UO<sub>2</sub> material showed the expected reaction with cladding melting and uniform attack of the fuel.

The fact that the intact fuel segment caused the crucible to rupture is probably due to stresses caused by the cladding swelling with H<sub>2</sub> uptake. It is believed that the fuel prevented any inward swelling so that the crucible ruptured.

Two following tests were carried out with irradiated MOX at 2000°C for 5 mins in *pure He* (without H<sub>2</sub>) ramping to temperature with the following two rates:

- 10 min from 1700 to 2000°C and,
- ramping at 1 min from 1700 to 2000°C.

Both tests showed considerable attack from the central underside (where melt had collected) to dissolve upward into the cracking and disintegrating fuel (Fig. 2). The degradation of MOX was heterogeneous (Figure 2). The faster ramp rate appeared to have the greater attack and had practically fluxed the whole central zone. It is thought that faster ramps means the Zircaloy melts before it can dissolve the oxide layer and therefore melts at a lower temperature ( $Zr_{mp} = 1760^{\circ}C$ , but  $\alpha-Zr(O)_{mp}$  can rise to nearly 2000°C) so that there is more time for liquefied Zr attack at faster ramp rates.

A 3<sup>rd</sup> comparative experiment in the conditions of the second test with irradiated MOX fuel, i.e. with a rapid heating, was performed using three Y<sub>2</sub>O<sub>3</sub> crucibles with natural urania and two irradiated MOX fuel. It has been observed a more “regular” degradation of the natural fuel.

Long-term testing for 60mins at 2000°C in He atmosphere show that there is complete dissolution of the fuel by the cladding in a standard fuel rod geometry and a Zr/MOX weight ratio of 0.25. Although there was complete dissolution of the fuel the melt was quite viscous (phase composition shows however a homogeneous pattern). By contrast, the addition of a second ring of Zry cladding to a clad fuel segment to raise the Zr/MOX weight ratio to 0.50 results in a very fluid melt which will probably also have completed the fuel dissolution within a shorter time. This could easily occur in a degrading core as the molten Zry candles down the rod and accumulates at certain points.

These initial results on irradiated MOX indicate that the U/(U+Zr) percentage in the melt would rise already after 10 mins. at 2000°C to over 60%, and was beyond the maximum values measured in the previous CIT project (4<sup>th</sup> FP) by Hayward of AECL from natural UO<sub>2</sub> at 2100°C & 2200°C after longer term exposures. This large value of the fuel dissolution shows that the 1<sup>st</sup> saturation stage of the melt has been reached and that the 2<sup>nd</sup> precipitation stage has developed.

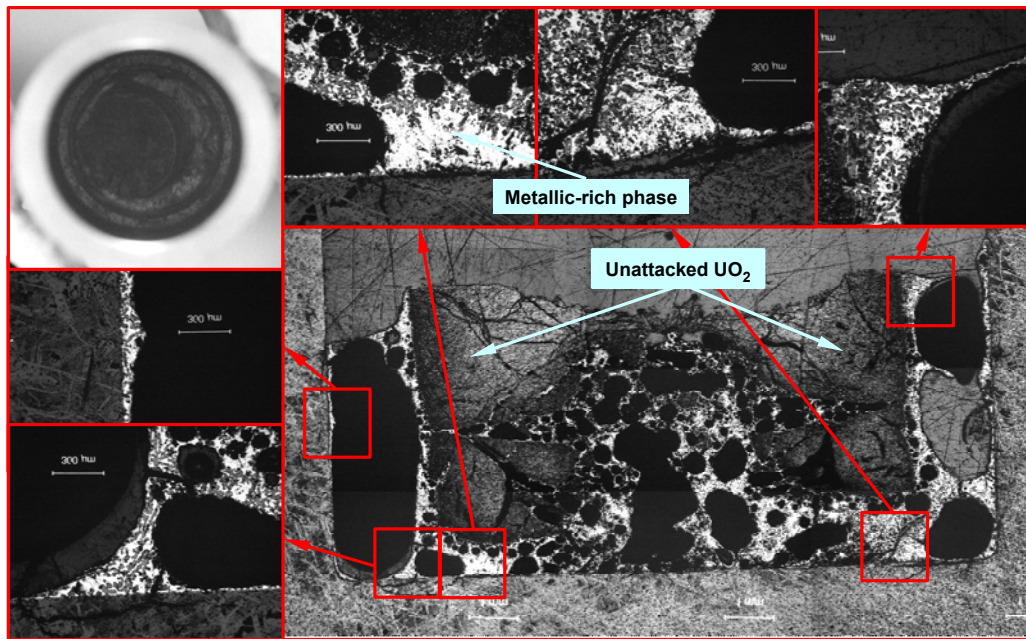


**Figure 2:** Dissolution of irradiated MOX at 2000°C.

## 2<sup>nd</sup> series of tests on dissolution of irradiated MOX and UO<sub>2</sub> in pure He

A new series of fuel dissolution tests at high temperature was successfully carried out in 2003. The test matrix used irradiated and un-irradiated MOX and UO<sub>2</sub> fuel segments that were heated up to temperatures of 2000°C for times varying from 0 to 600 seconds with one test for MOX being carried out at 2200°C.

The samples were - as in the 1<sup>st</sup> test series - heated to 1700°C at 1K.s<sup>-1</sup> and then at 5K.s<sup>-1</sup> from 1700°C to 2000°C to minimise the effect of interactions between the liquefied Zircaloy (alloy melting point ~1760°C) and the fuel before the sample had reached the operating temperature. One irradiated fuel segment (3-5mm thick) in an inert yttria crucible was placed directly on top of a corresponding non-irradiated fuel segment (also 3-5mm high and placed in an yttria crucible) with both crucibles being located inside an external tungsten crucible. The two samples were then heated up together in the furnace installation: thus both samples underwent the same temperature history. After testing, the segments were removed from the furnace and photographed using the periscope from above in their crucibles. After photography the fuel samples were embedded in raisin and cut vertically.

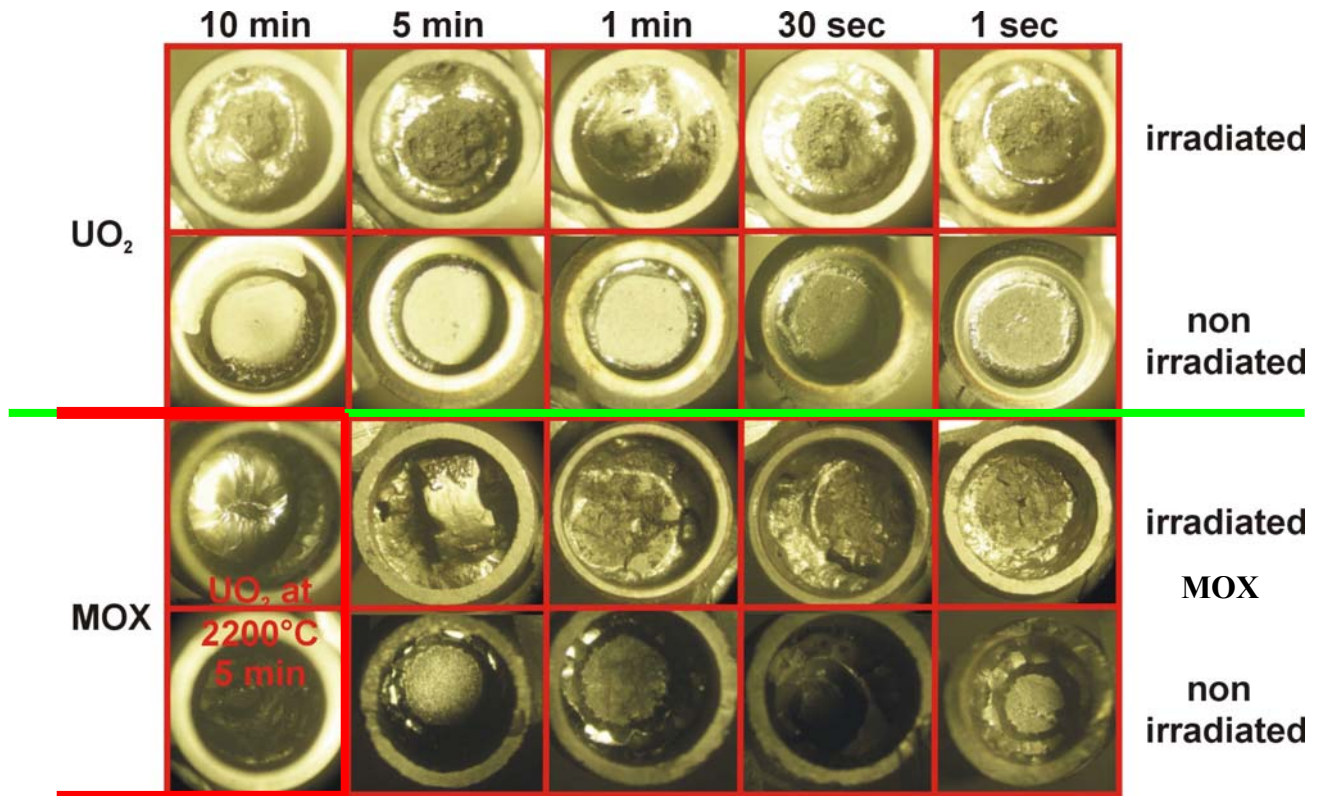


**Figure 3:** Matrix of results of the 3<sup>rd</sup> test series using irradiated and non-irradiated UO<sub>2</sub> and MOX fuel heated to 2000°C for various times and to 2200°C for two MOX tests at 5min. Upper views of the crucibles.

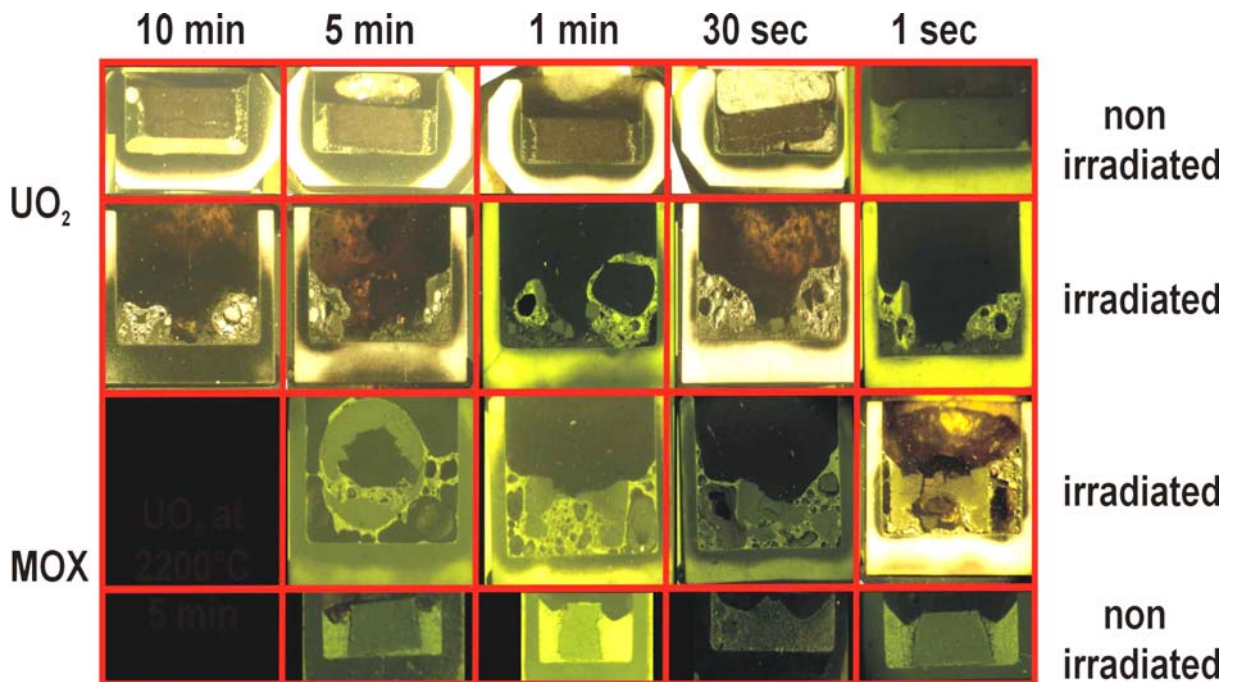


**Figure 4:** Matrix of results of the 3<sup>rd</sup> test series using irradiated and non-irradiated UO<sub>2</sub> heated to 2000°C for various times. Axial views of the crucibles.

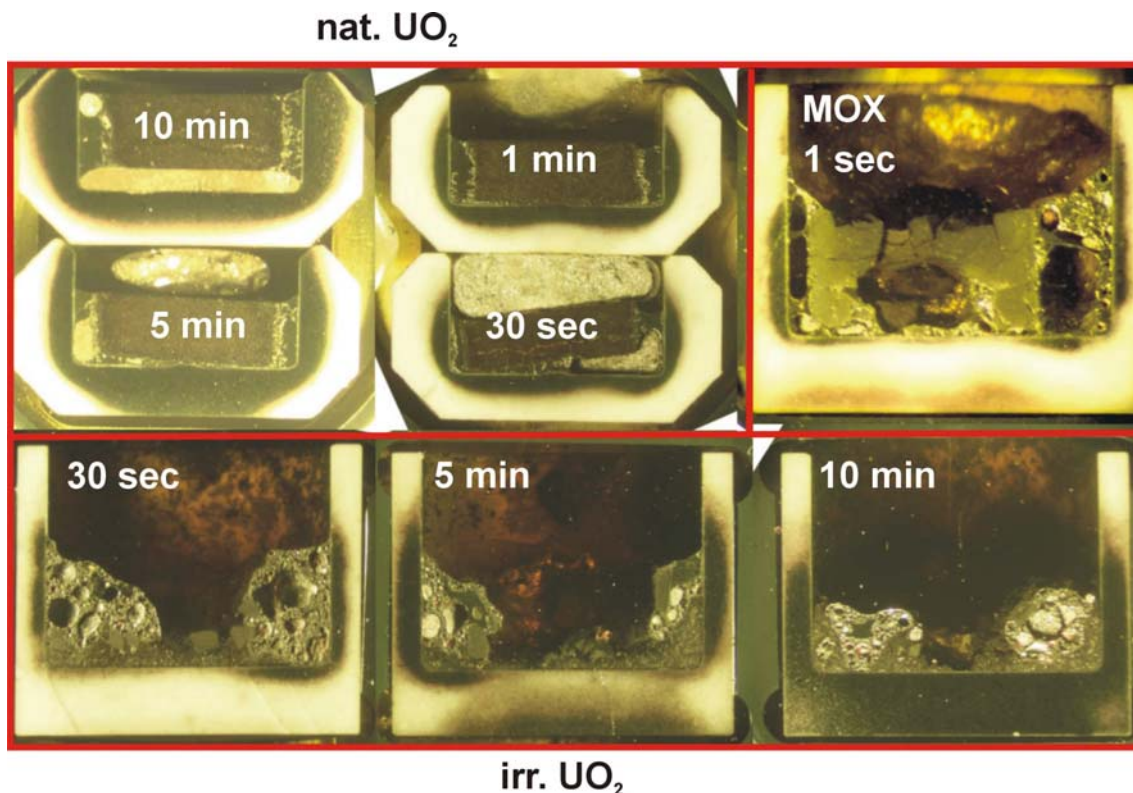


**Figure 5:** Cross-sectional macrographs of the natural and irradiated UO<sub>2</sub> samples at 2000°C for various times showing the uniform progression of the natural UO<sub>2</sub> dissolution and the rapid attack of the irradiated UO<sub>2</sub> fuel. The attack of the irradiated MOX shown in the upper right corner shows less dissolution than for irradiated UO<sub>2</sub> fuel at 30s.

#### **Post-test analysis:**

The post-test analysis method was developed to quantify the fuel dissolution. This required the samples to be sectioned in half vertically and then embedded and polished metallographically. Optical micrographs were taken of the sections and then the photos built up into a composite of the whole cross-section. This was then converted into a colour figure for the zones of porosity, the melt, the fuel, and the embedding resin.

These cross-sections for the various zones could then be measured using a phase analysis device, so that the relative as well as the absolute change in cross-section could be estimated. From these results and knowing the initial dimensions of the fuel samples the extent of the fuel dissolution as a percentage of the consumption of the fuel pellets could be established. This data could then be used in the work package WP7 for the modelling of the irradiated fuel dissolution.

#### **Periscope Photos**

The test matrix is shown in Figure 3 along with these top views.

The un-irradiated UO<sub>2</sub> and MOX dissolution show a slow uniform progression. Comparison between the irradiated UO<sub>2</sub> and MOX samples does not show any substantial differences between them. (The irradiated MOX sample exposed for 5 mins. has turned on its side during the experiment.)

The un-irradiated reference UO<sub>2</sub> sample of the 10min test had a smaller diameter since it came from a different batch of UO<sub>2</sub> pellets, unfortunately there was no time to have a special smaller yttria (Y<sub>2</sub>O<sub>3</sub>) crucible made. Consequently the molten Zircaloy flowed into the free space

and did not attack the natural  $\text{UO}_2$  as uniformly as in the other natural  $\text{UO}_2$  tests, since the attacked surface was smaller and the dissolution of the fuel less.

The melted Zircaloy cladding around the fuel has a smooth reflective surface under the periscope light and appears to have expanded during the test above the fuel segment.

Already from the top view of the un-irradiated reference samples a smooth, unattacked surface is shown whereas the irradiated  $\text{UO}_2$  and MOX fuel segments- show a very irregular surface in which break-up and/or attack of the surface is visible.

### **Vertical cross-sectional examination (Fig. 4 and 5)**

The uniform nature of the attack for the non-irradiated MOX and  $\text{UO}_2$  fuel is also confirmed by the first examination of the vertical cuts. However for the irradiated  $\text{UO}_2$  fuel the process seems both faster and more erratic. For example in Figure 4 (top view), the cross-section shows that for irradiated fuel the dissolution process is already almost completed after 1min - where only a few small fuel fragments can be recognised - and very well advanced after 10 mins., by contrast the dissolution of fresh fuel is considerably less advanced after 5 and 10 min.

The molten cladding material appears to be mainly metallic in nature at the sides of the crucible, whereas it is mainly a darker material at the bottom of the crucible sometimes surrounding the vestiges of the original fuel. This darker material may possibly be the ceramic-rich phase of the molten material, compared to the metallic -rich phases at the crucible sides. The fact that metallic-rich phase of the melt is still concentrated at the location of the cladding ring also shows how viscous this cladding becomes as it takes up oxygen from the fuel. The melt viscosity is a further important factor determining the dissolution behaviour and rates. This was shown in one of the first series of tests, and is a factor that should be investigated further.

The high burn-up  $\text{UO}_2$  fuel segments seems to be almost completely dissolved, so that it is very difficult to infer the mechanism by which it has broken up. At even longer times only tiny fuel particles were found. It may be in some cases that the rapid fission gas release is capable of causing a complete fragmentation and can cause fuel dissolution since at this high burn-up thermal stresses and gas release can be considerable. The individual result maybe considerably more variable since it was seen that after 1min dissolution is practically complete.

**Irradiated  $\text{UO}_2$ :** Given the results from earlier  $\text{UO}_2$  tests of this series and results from the CIT project (Ref.[8]) where the interaction was not so advanced, it is still supposed that the fissures present in the irradiated  $\text{UO}_2$  play an important role in the segment's fragmentation. The release of fission gas is also very important, but the volume of fission gas from all the irradiated  $\text{UO}_2$  samples of this series would be of the same order of magnitude, i.e. the whole inventory is released from the fuel. Release rates would also be similar since the samples all underwent the same temperature ramp.

**Irradiated MOX:** MOX fuel also dissolves rapidly but with slower kinetics than the irradiated  $\text{UO}_2$  fuel. The vertical cut (Fig. 4) displays the more uniform progression of the attack with penetration of the liquefied cladding along the pre-existing cracking in the fuel and even at after 5 min considerable amounts of fuel are still intact. The fission gas released from the MOX fuel during the experiments also was of the same order of magnitude for all MOX samples including the longer duration tests: it can be assumed that large majority of the inventory is released. Nevertheless the releases would be smaller than that of the  $\text{UO}_2$  fuel samples since the MOX had a lower burn-up.

### **Concluding remarks**

All the available results show that the burn-up is an important parameter in the process of fuel dissolution during a severe accident.

Irradiated fuel (both MOX and  $\text{UO}_2$ ) dissolves much faster than fresh fuel for two reasons: (i) the thermal cracking in the irradiated fuel assists the fuel break-up, as well as allowing the melt to penetrate into the fuel; (ii) the fission gas release causes bubbling of the melt and generally improves the melt-fuel contact.

The high burn-up  $\text{UO}_2$  fuel ( $\sim 90$  GWd/tU) from these tests appears to dissolve faster than the medium burn-up MOX fuel ( $\sim 45$  GWd/tU). Whether  $\text{UO}_2$  or MOX fuel of similar burn-up dissolves faster could not be concluded from these experiments, since the burn-ups of the two fuels are too different.

Final tests with irradiated MOX (44 GWd/tU) and  $\text{UO}_2$  (90 GWd/tU) showed a wide scattering of results. Additional data are needed for quantification of the kinetics.

### **3.2 WP1.1: SETs on melting point of U-O-Zr mixtures**

ITU was also involved in tests to measure the melting point (MP) of some U-O-Zr mixtures using the laser flash method. ITU has been asked by IRSN to fabricate some sub-stoichiometric U-Zr-O pellets and perform melting point measurements on these samples to examine the metal-rich part of the U-Zr-O phase diagram in an area useful for the modelling of the Urania fuel solubility in molten Zircaloy. This experimental programme was also of interest to investigate more precisely the miscibility gap of the U-O-Zr phase diagram through the measurement of the liquidus temperatures of sub-stoichiometric samples. Two TMI-2 samples coming from the homogeneous central core molten pool were also included in the test matrix.

#### ***Preliminary results***

Five batches of mixtures were prepared, at  $1700^\circ\text{C}$ , by sintering Urania, Zirconium and Zirconia together. The compositions of the batches correspond to zirconium-rich mixtures. The first of the sub-stoichiometric U-Zr-O samples have been tested. The metallography showed that batch No 1 (50at.%  $\text{UO}_2$  - 50at.% Zr) was composed of metallic precipitates in a ceramic matrix, while the opposite batch, No 5 (13 %  $\text{UO}_2$  25 %  $\text{ZrO}_2$  and 57 % Zr) was effectively ceramic precipitates in a metallic matrix (strong heterogeneities).

Preliminary MP tests were performed in mid-2002. The procedure of the transition temperature determination was the following: the sample was heated by laser heating above its presumed liquidus temperature; the laser was then switched off and the liquidus temperature determination was based on the detection of the thermal arrests on the cooling curve. The temperature was measured by a pyrometer.

One composition has been investigated twice and the results showed a large dispersion of 275 K on the liquidus temperature.

The first tests showed variable phase transition temperatures. It was thought that the metallic phase with its higher conductivity and lower emissivity / higher reflectivity could be melting preferentially, dissolving the ceramic phase in a second stage. EDX analysis of the melt spot showed layers of Zr-rich and  $\text{UO}_2$ -rich phases in the spot, so that it was suspected that the homogeneous melt separated out into separate phases even on rapid cooling. Such a difference was never observed in previous MP tests.

#### ***Improvement of the test rig***

Additional investigations showed the need to improve the experimental device, in particular the power of the laser flash. The occasion was taken to design and improve the device with a more powerful laser with combined beams and a better pyrometer as well as a new method for the identification of liquidus temperature by measuring surface reflectivity. Measurements will be restarted after the project on the U-Zr-O system using newly-prepared samples of the UO<sub>2</sub>-Zr system (20-80%, 40-60%, 60-40%, and 80-20 wt. %). It is thought that using a simplified system will enable a more precise MP determination than with the old technique, yielding data both during heating and cooling of the temperature transient.

These experiments on the liquidus temperature of existing U-O-Zr and TMI-2 could not be carried out within COLOSS. These tests are postponed in the SARNET NoE (6<sup>th</sup> FP) in which additional fuel dissolution tests will be done.

(1) Complementary irradiated UO<sub>2</sub> dissolution tests with a medium burn-up (around 50-60Mwd/tU) are planned in order to compare the burn-up effect between MOX and UO<sub>2</sub> dissolution kinetics more clearly,

(2) The melting point determinations of the existing UO<sub>2</sub>-Zry mixtures and TMI-2 samples are also expected in SARNET using the improved MP test rig.

### **3.3 WP1.2: Analytical support to tests on dissolution of irradiated fuel (IRSN)**

This activity was tightly linked with the modelling of the burn-up effect. The ICARE/CATHARE code was used for pre-test and post-test calculations, sensitivity studies. This activity is described in §4 devoted to modelling.

### **3.4 WP2.1: SETs on simultaneous dissolution of UO<sub>2</sub> and ZrO<sub>2</sub> by molten Zr (JRC/IE and RIAR)**

These tests were carried out by RIAR-Dimitrovgrad acting as a subcontractor of JRC-Ispra. This experimental task has been proposed in continuation to the exploratory tests carried out in the previous CIT project of the 4<sup>th</sup> FP wherein unexpected results were produced (Ref.[9]). Some of the previous partners of this topic in the CIT project were still involved in this activity:

- IBRAE for analytical and modelling efforts using the SVECHA code (WP2.3 and WP7.3),
- FZK for the delivery of the ZrO<sub>2</sub> rods, Zry and Y<sub>2</sub>O<sub>3</sub> materials

The same UO<sub>2</sub>-Zr-ZrO<sub>2</sub> configuration was used as in the CIT project. A ZrO<sub>2</sub> rod was located at the centre of the UO<sub>2</sub> crucible with a Y<sub>2</sub>O<sub>3</sub> disc at the bottom of the crucible to prevent the interaction between molten Zircaloy and the crucible bottom. The RIAR has manufactured the UO<sub>2</sub> crucibles.

Tests were performed in an electric resistance furnace filled with argon at atmospheric pressure (Fig. 6). The test matrix (Table 3) involved two test series at 2100 and 2200°C with different time period from 100 to 600s. The sample temperature was determined by a two-beam pyrometer focused on the Zry charge and two thermocouples installed into the recesses at the crucible sidewall. Calibrating tests have been carried out to check the uniformity of the heating and calibrate readings of the thermocouple and pyrometer measurements.

The test procedure consisted in fast heating of the sample to a specified temperature, holding the sample at this temperature and final cooling. During the tests there was a simultaneous dissolution of the crucible wall and central ZrO<sub>2</sub> rod by the Zircaloy-rich melt (Figures 8 and 9).

**Table 3:** RIAR test matrix.

Melt Temperature [°C]	2100					
Time period of constant temperature [s]	100	200	300	400	500	600
Melt Temperature [°C]	2200					
Time period of constant temperature [s]	100	200	300	400	500	600

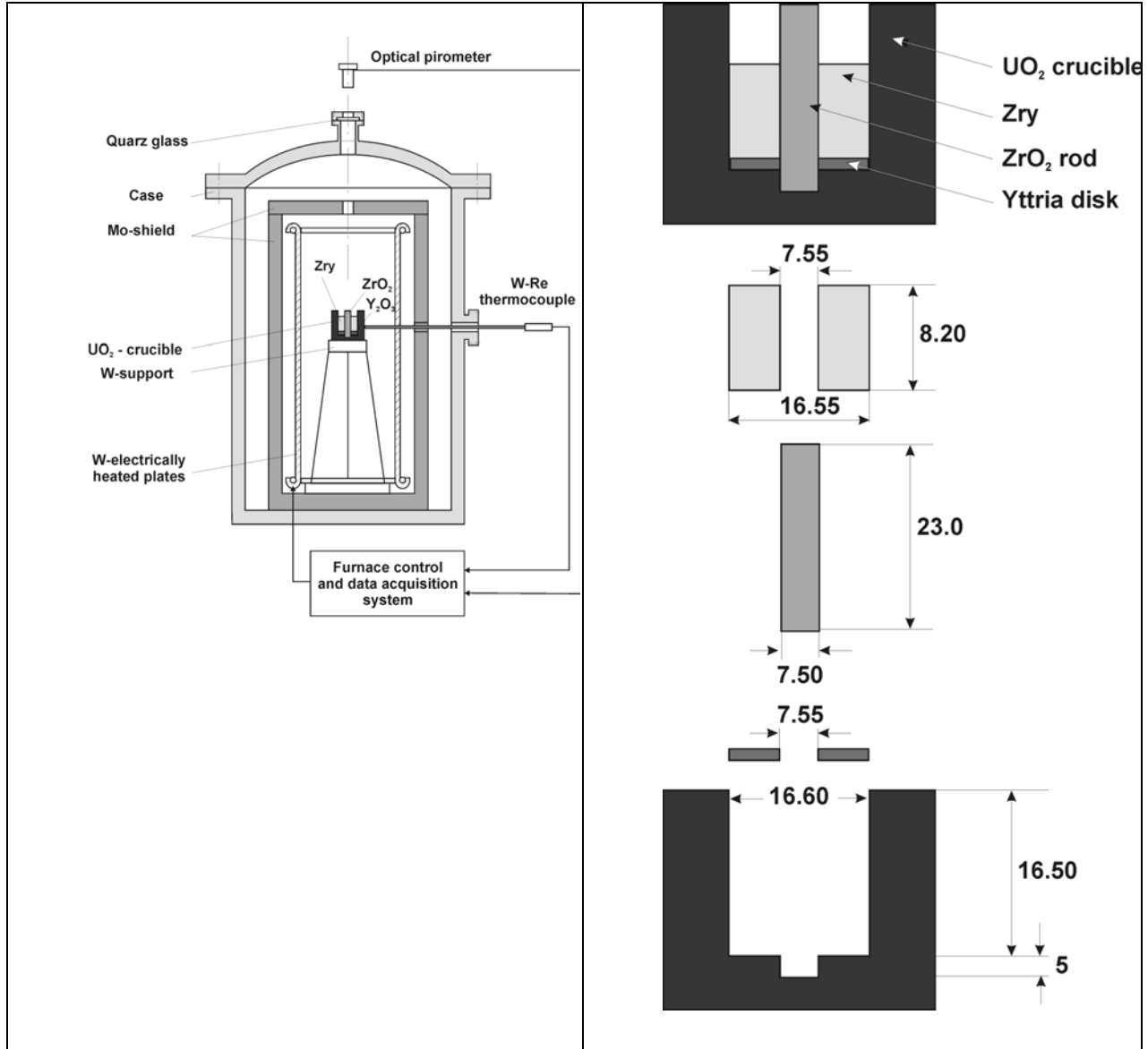


**Fig. 6:** Schemes of the RIAR facility and samples used in the UO<sub>2</sub> and ZrO<sub>2</sub> dissolution tests.

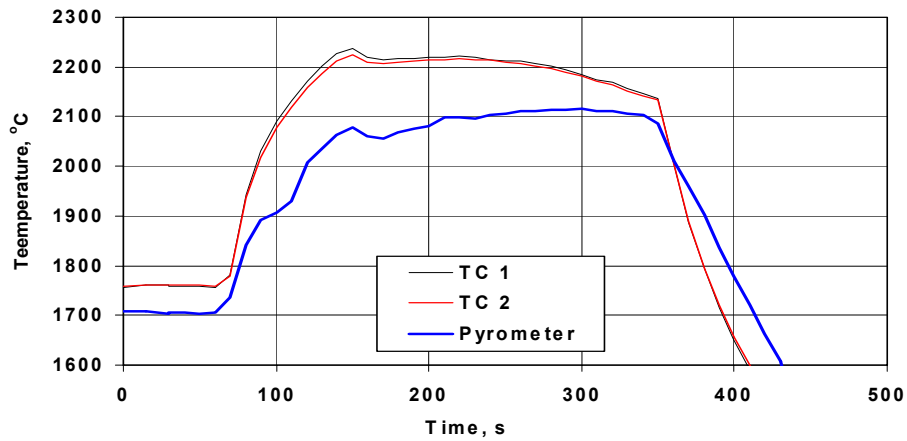


**Fig. 7:** Temperature versus time in the RIAR Test 2 (2100°C, 200s).

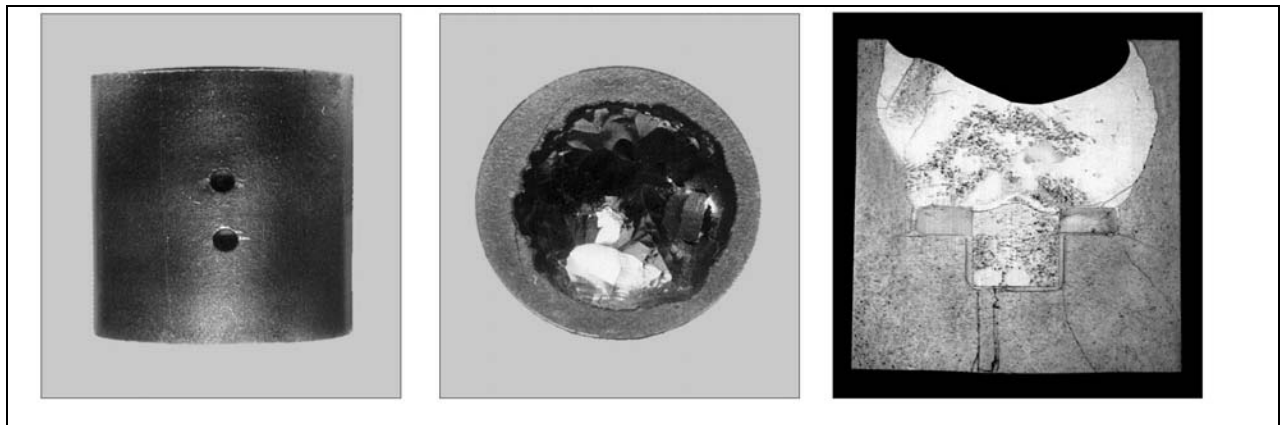


**Fig. 8:** Test (2100°C, 200s) of the 1<sup>st</sup> series on simultaneous dissolution of UO<sub>2</sub> and ZrO<sub>2</sub>. (The revised temperature is indicated, the initial temperature was 2200°C)

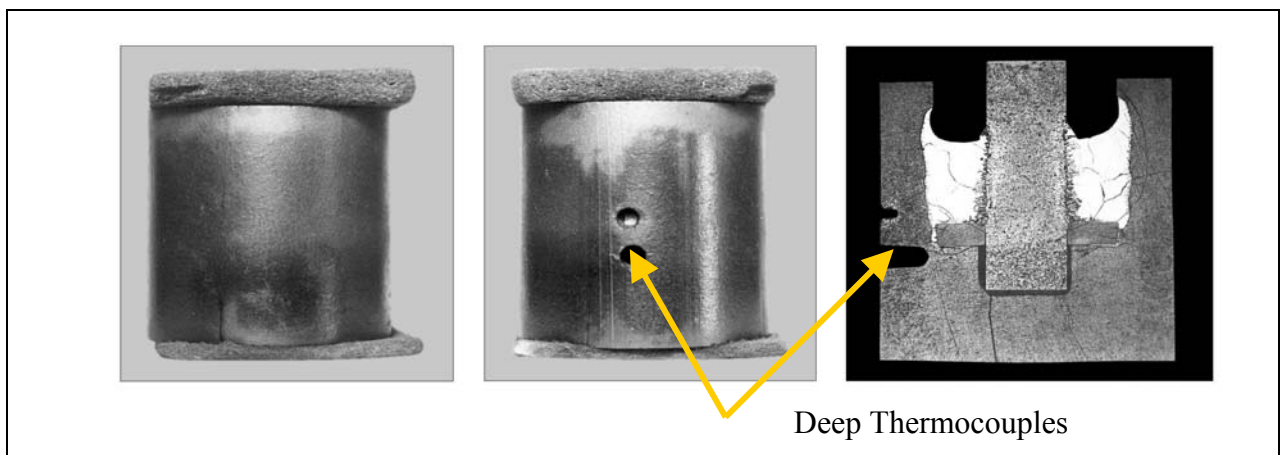


**Fig. 9:** Test (2100°C, 400s) of the 2<sup>nd</sup> series on simultaneous dissolution of UO<sub>2</sub> and ZrO<sub>2</sub>.

Figure 7 illustrates the temperature recording in tests of the 1<sup>st</sup> series. Two thermocouples TC1 and TC2 measured the external crucible sidewall temperature at different axial locations and

gave the reference temperature. The pyrometer measuring the temperature at the upper part of the crucible was considered during the tests of the 1<sup>st</sup> series to give the reference temperature of the melt.

Results obtained at 2100 and 2000°C showed a significant dissolution of the UO<sub>2</sub> and ZrO<sub>2</sub> material (Figures 8 and 9). In the test series at 2200°C, the crucible failed at 260s due to dissolution of the UO<sub>2</sub> wall. A complete dissolution of the central ZrO<sub>2</sub> rod was observed for tests carried out at ~ 2100° (revised temperature) during 200, 300 and 400s (Fig. 9).

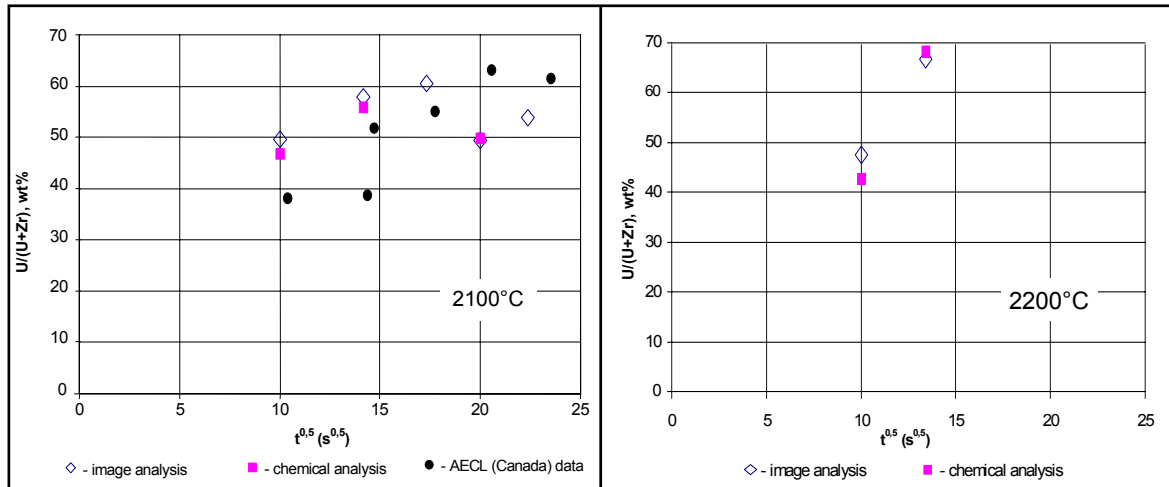


**Fig. 10:** U/(U+Zr) ratio in the melt, results of chemical and image analysis

The analysis of the first tests showed that the temperature difference between the melt and the crucible could have been a driving parameter of the dissolution. For the 2<sup>nd</sup> series of tests, an upper insulating layer was added to reduce axial heat losses and crucible wall temperature gradients (Fig. 9). The location of the two TC was changed (the internal TC was implemented in a hole near the bottom of the crucible and near the inner crucible wall surface) in order to have a better control of temperature differences. Finally the last set of five tests showed that the temperature gradient through the crucible wall was in fact lower than initially expected when taking into account the pyrometer reading as the reference temperature. Finally TC readings were confirmed as the right temperature reference showing that experiments were carried out between 2100 and 2300°C. The temperature difference in the crucible wall was finally found to be negligible.

The post-test examinations included the determination of the ratio of the dissolved uranium mass to the mass of the created melt. The determination of the dissolved uranium amount was carried out by two methods:

- the quantitative image analysis using photos of longitudinal sections of the tested samples,
- the chemical analysis of the melt.

The melt was characterized by an homogeneous distribution of two main phases: (U,Zr)O<sub>2-x</sub> and U-Zr metallic phase. The two methods showed similar results and indicated results consistent with previous AECL results of the CIT project (Fig. 10).

This experimental database was used for dissolution modelling and validation of the SVECHA code.

### 3.5 WP2.2: PWR and VVER single rod degradation tests (AEKI/KFKI)

The high temperature interaction of reactor core materials during a severe accident leads to the oxidation and melting of metal components. The interactions of molten Zr cladding with  $\text{UO}_2$  and  $\text{ZrO}_2$  are important factors in the determination of cladding failure conditions and play a role in the loss of fuel rod like geometry and in the formation of debris bed and molten pool in the core.

At the beginning of the project, the existing database on fuel dissolution involved various experiment including dissolution of  $\text{UO}_2$ , dissolution of  $\text{ZrO}_2$  and simultaneous dissolution of  $\text{UO}_2$  and  $\text{ZrO}_2$  by molten Zr. All these past experiments were carried out using crucibles with different sizes, different  $\text{UO}_2/\text{Zr}$  mass and melt surface to volume ratios. These factors are known to affect the dissolution process and differences between various experiments were responsible of difficulties regarding the interpretation of results and the modeling of fuel dissolution in prototypic fuel rod conditions. In particular, the comparison of simultaneous dissolution tests of  $\text{UO}_2/\text{ZrO}_2$  and separate  $\text{UO}_2$  and  $\text{ZrO}_2$  showed faster dissolution and larger extent of dissolution in the case of simultaneous tests which was difficult to explain.

These observations emphasized the importance of prototypic conditions to study the dissolution processes in order to facilitate the fuel dissolution modeling (simultaneous dissolution of inner  $\text{UO}_2$  pellets and outer  $\text{ZrO}_2$  scale of the cladding). For these reasons experiments with short fuel rod segments were carried out by AEKI in the framework of the COLOSS project. The analytical support regarding pre and post-test calculations was provided by some COLOSS partners.

The complementary experimental programme initially planned by IRSN in the MADRAGUE facility with long prototypic fuel rod tests could not be carried out due to unexpected difficulties and delays in the construction of a new furnace. It was replaced by ten additional tests in the AEKI programme involving more tests with PWR and VVER fuel rods (Ref.[6]). The final test matrix is given in Table 4.

The main objectives of the short fuel rod dissolution tests with PWR and VVER type fuels were the followings:

- Quantification of the simultaneous dissolution of  $\text{UO}_2$  (pellets) and  $\text{ZrO}_2$  (external oxide layer on the clad) by molten Zr using prototypic rods,
- Measurement of clad failure conditions (in inert atmosphere for modeling purposes),
- Production of rod degradation data suitable for code validation,
- Comparison of PWR and VVER fuel rod behaviour under similar severe accident conditions.

#### **Experimental facility and test procedure**

A high temperature experimental facility with an inductive furnace was improved to carry out tests with fuel rod segments (Fig. 11). The rod specimen was placed into a crucible, which had connections for steam and argon supply. The furnace configuration was changed to overcome technical difficulties found during the first test series. In particular the inductive direct heating mode on the inner non-oxidized layer of the cladding induced a system effect after melting of Zr. Liquid Zr moved down and impacted the power and temperature distribution. Several improvements have been implemented to the experimental set up. The use of metallic crucibles (Mo or W) enabled indirect heating of the fuel rod and improved thermal behaviour of the sample. In order to reduce axial the temperature profile, final tests were carried out using shorter rods with two pellets instead of four.

Temperature measurements were taken from a thermocouple, which was located in the centre of the fuel rod. In two tests additional pyrometers were applied as well.

The test procedure was based on a first oxidation phase at temperature followed, without intermediate cooling down, by a dissolution stage at a higher temperature in the range 1930-2230°C.

Stage 1: isothermal oxidation in steam (~1100 °C) for the formation of an external ZrO<sub>2</sub> oxide layer.

Stage 2: isothermal dissolution in inert gas atmosphere (~2000 °C) for the interaction between molten Zr and UO<sub>2</sub> and ZrO<sub>2</sub>.

**Table 4 :** Thermal characteristics of short fuel rod dissolution tests

Sample No.	Type	Oxidation temperature [°C]	Oxidation time [s]	Maximum dissolution temperature [°C]	Dissolution temperature <sup>1</sup> above 1850 °C [°C]	Dissolution time [s]
D1	VVER	1150	10600	1950	1943	205
D2	PWR	1150	10600	2050	2027	398
D4	VVER	1050	10800	2074	2035	357
D6	PWR	1150	12000	1797/1737	1738/1710	25/20
D7	PWR	1050	10800	1998/1776	1918/1750	63/132
D8	VVER	1050	10800	1923	1898	56
D9	VVER	1050	5700	2032	1916	104
D10	PWR	1050	10700	2176	2124	358
D16	VVER	1050	10800	1900	1878	79
D17	VVER	1050	5400	2056	1980	287
D18	VVER	1050	5400	1764	1732	96
D19	PWR	1050	7200	2027	1947	228
D20	PWR	1050	10800	2160	1908	47
D21	PWR	1150	10800	2147	2073	530
D22	VVER	1210	3600	1892	2015	49
D23	VVER	1050	3600	1892	1863	70
D26	PWR	1150	5360	1882/2057	1859/1913	195/212
D27	PWR	1150	4000	2066/1897	1925/1879	166/111
D28	PWR	1050	2550	2084	2000	180
D29	PWR	1050	1650	2212	2022	195

<sup>1</sup>Average dissolution temperature above 1850 °C during the dissolution stage: indication of two numbers means two temperature levels. Value below 1850 means low temperature and an average value calculated above 1700 °C.

After revision of the test protocol, the steam flow-rate was stopped immediately after the oxidation phase, and so the intermediate heat-up between oxidation and dissolution took place in pure Ar. The typical flow-rates were the followings:

Argon flow: 2-5 liter/minute (atmospheric pressure, room temperature)

Steam flow: ~0.1 g/s.

Short VVER type (Zr1%Nb cladding) and PWR type (Zircaloy-4 cladding) fuel rods of ~5 cm length, with prototypic UO<sub>2</sub> pellets were used in the tests.

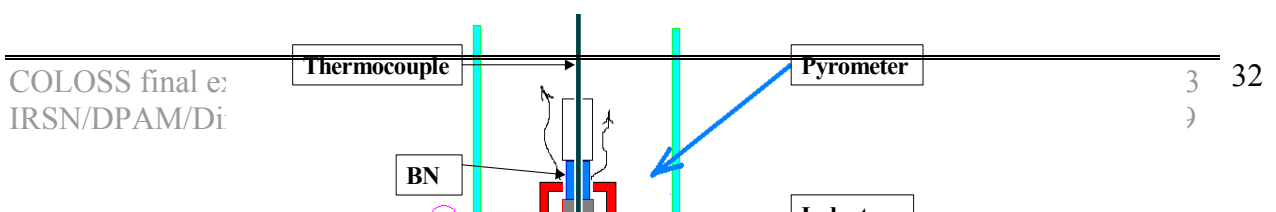


**Fig. 11:** Improved AEKI facility for fuel rod dissolution tests

### **Test matrix and experimental conditions**

The original test matrix included 20 tests with different oxidation and dissolution conditions and with two types of fuel rods; 9 VVER and 11 PWR with four or two fresh  $\text{UO}_2$  pellets (Table 4). The conditions were selected to make possible the following comparisons:

- PWR and VVER fuel under the same oxidation and dissolution conditions,
- fuels rods with the same oxidation but different dissolution conditions,
- fuel rods with the same dissolution but different oxidation conditions.

After the first tests it turned out that the originally planned test conditions could not be kept, especially in the dissolution phase. In fact, the isothermal dissolution plateau was not stabilised in most of the cases due to the relocation of molten material. On-line measurements and post-test examinations showed large uncertainty in the temperature distribution.

The main thermal characteristics of the tests are given in Table 4. The average dissolution temperature was calculated from the part of the temperature history curve above 1850 °C and the related period is given as dissolution time. A typical temperature history is given in Fig. 12. In addition to the short fuel rod dissolution tests, 12 separate oxidation tests were performed with Zr1%Nb and Zircaloy-4 cladding in order to provide data on the initial oxide scale before dissolution phase. The tests were carried out similarly to the oxidation phase in the dissolution tests: the temperatures were 1050 and 1150 °C and the oxidation time between 1800-10800s.

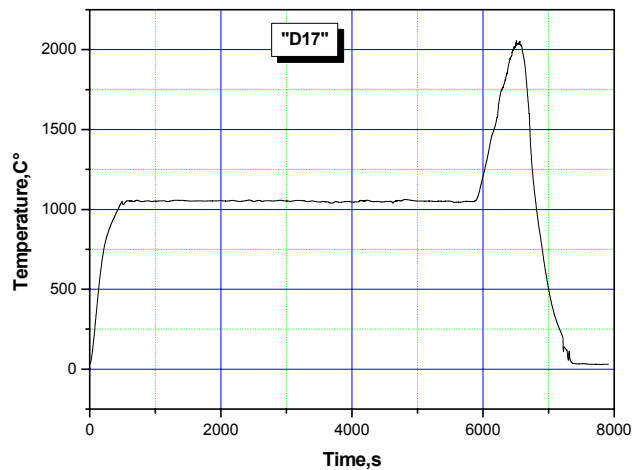


**Fig. 12:** Temperature history of test short fuel rod dissolution test D17

### Post-test examinations

The aim of the post-test examination was to get information on the degree of dissolution of  $\text{UO}_2$  and  $\text{ZrO}_2$  in the molten Zr alloys. The original samples were filled up with epoxy and horizontal and longitudinal cross sections were cut, polished and ground. Horizontal cross sections were prepared mainly from the central part of the rods, close to the position of thermocouple. Typical cross sections are shown in Figures 13, 14 and 15.

All samples were studied by optical microscopy in order to identify the structural changes in the fuel. Scanning electron microscopy (SEM) and energy dispersive microanalysis (EDX) were applied to investigate the microstructure and the elemental composition of some cross sectional samples selected for these investigations.

The main sizes including oxide layer thickness were measured by optical microscopy. No measurements were taken for samples without noticeable oxide layer and for fully oxidized samples. Knowing the estimation for the initial  $\text{ZrO}_2$  scale and the measured data of its final thickness, the dissolution of  $\text{ZrO}_2$  layer of the cladding could be calculated (Table 5) showing  $\text{ZrO}_2$  dissolution up to 100% during the second dissolution stage in steam-starved conditions. In the tests D7, D8 and D16, the final oxide layer was thicker than the estimated initial thickness. In those test probably thicker initial oxide scale was created in the oxidation phase, or some impurities of the inlet gas made possible further oxidation in the dissolution phase as well. The fuel rod failure was indicated on the basis of cladding state in the examined cross sections. Most of the claddings failed in the test series, only 4 of the 20 samples could keep intact cladding. Those samples had thick oxide layer after the tests. Complex clad failure mechanisms were also observed but no differences were observed between VVER and PWR rods.

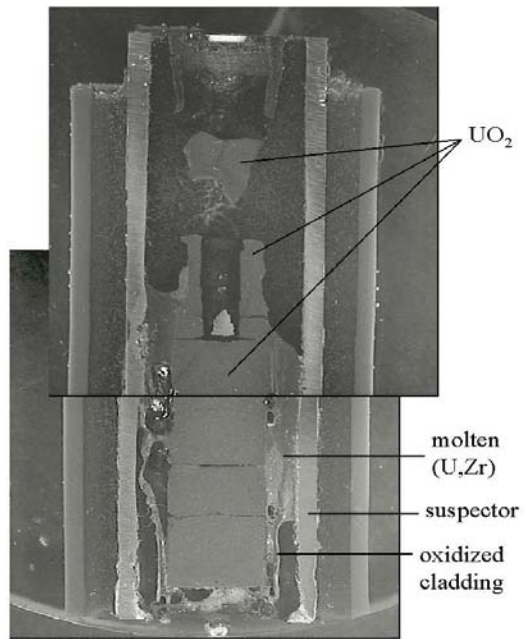


**Fig. 13:** Longitudinal cross section of sample D23

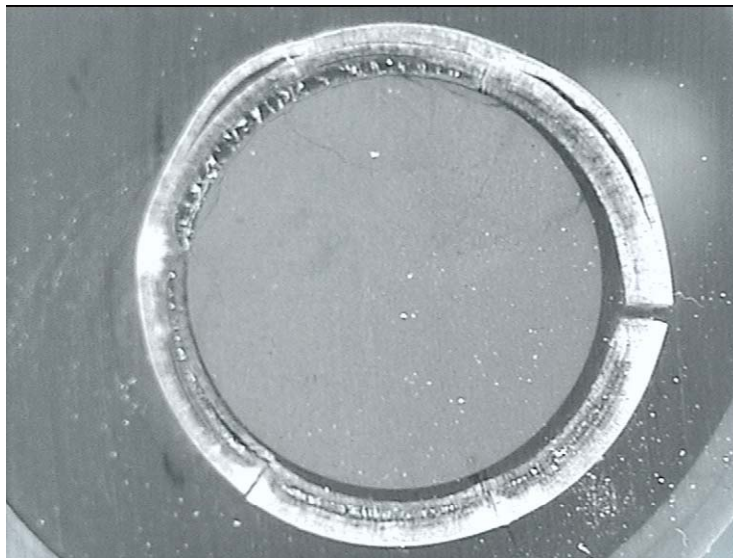


**Fig. 14:** Cross section of D6 sample with fully oxidized cladding, showing no interaction between pellet and cladding

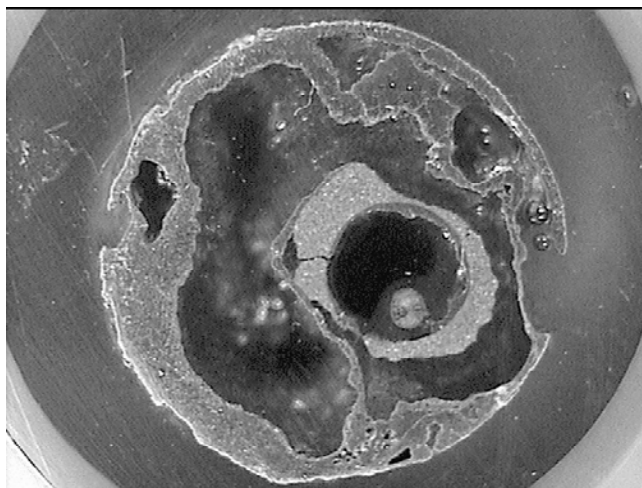


**Fig. 15:** Cross section of D20 sample showing large part of pellet dissolved

**Table 5:** Summary of ZrO<sub>2</sub> dissolution data

Sample No.	Type	Estimated ZrO <sub>2</sub> scale before dissolution [μm]	Measured ZrO <sub>2</sub> scale after dissolution <sup>1</sup> [μm]	Fraction of dissolved ZrO <sub>2</sub> [%]	Clad failure yes/no
D1	VVER	326	317	2,7	no
D2	PWR	625	338	46	no
D4	VVER	129	73	43	yes
D6	PWR	707	full	0	yes
D7	PWR	114	200	~0	yes
D8	VVER	129	160	~0	yes
D9	VVER	65	50	23	no
D10	PWR	113	100	12	yes
D16	VVER	129	317	~0	no
D17	VVER	61	50	18	yes
D18	VVER	61	0	100	yes
D19	PWR	97	19	80	yes
D20	PWR	114	0	100	yes
D21	PWR	637	0	100	yes
D22	VVER	155	0	100	yes
D23	VVER	38	0	100	yes
D26	PWR	123	0	100	yes
D27	PWR	127	0	100	yes
D28	PWR	60	0	100	yes
D29	PWR	48	0	100	yes

<sup>1</sup>Oxide scale thickness: "full" means no metallic Zr, only ZrO<sub>2</sub>,  
0 value means no clear oxide scale (complete dissolution of ZrO<sub>2</sub>)

Two types of measuring methods were used: EDX analysis and image analysis to establish the amount of the uranium dissolved by molten Zr. These measurements were performed on images (areas) with relatively small magnification, i.e. at relatively large areas to have average elemental composition and relatively large surface areas of the sample. In Table 6 the results for the average U content gained by the two methods are summarized.

**Table 6:** Average U content of various mixtures measured by EDX and image analysis

Sample	2/1K	2/2K	D7	D8	10K	D19	D20A	D21
U content by EDX (mass%)	5.6	15.9	10	2.5	25.1	28	58.7	69.1
Area % of the U-rich features	-	20.6	-	-	21.6	22.5	73.2	-
Melt location	center	center	center	center	center	center	bottom	center

**Table 7:** Summary of UO<sub>2</sub> dissolution data

Sample No.	Type	Dissolved volume of UO <sub>2</sub> pellet <sup>1</sup> [%]	U content in the melt <sup>2</sup> [mass %]
D1	VVER	0	
D2	PWR	8	10
D4	VVER	0	
D6	PWR	0	
D7	PWR	3	10
D8	VVER	2	2.5
D9	VVER	4	
D10	PWR	10	25.1
D16	VVER	0	
D17	VVER	0	
D18	VVER	0	
D19	PWR	10	28
D20	PWR	50	58.7
D21	PWR	60	69.1
D22	VVER	20	
D23	VVER	30	
D26	PWR	35	
D27	PWR	60	
D28	PWR	70	
D29	PWR	60	

<sup>1</sup>Dissolved UO<sub>2</sub> volume estimated on the basis of metallographic examinations

<sup>2</sup>U content based on EDX studies

Table 7 summarizes the data on UO<sub>2</sub> dissolution. The dissolved volume of UO<sub>2</sub> was estimated on the basis of metallographic examinations. U content in the melt was determined by EDX as average of the studied samples and series for the given tests. The maximum U content in the studied claddings was found to be 69 mass %. This value was measured on sample 21, which reached a high degree of degradation. UO<sub>2</sub> dissolution was observed by optical microscopy (Fig. 16) and the elemental composition of the resulting melt was analyzed by EDX method across the pellet cladding interface (Fig. 17).

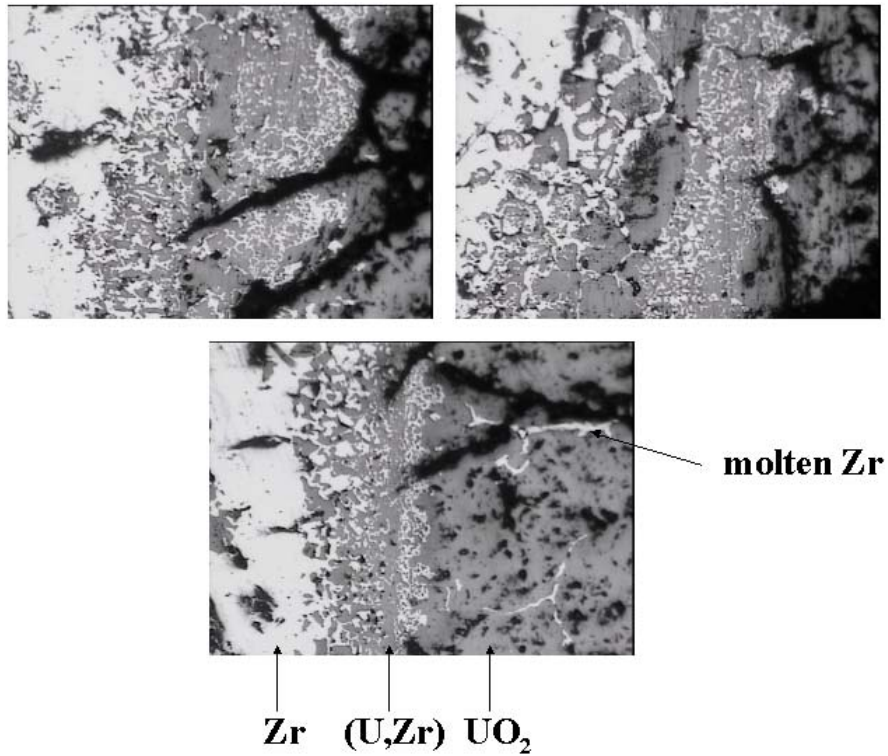


**Fig. 16:** Series of optical micrographs from sample D2 showing the interaction zone between  $UO_2$  pellet and the cladding and the penetration of molten Zr into the cracks of the pellet

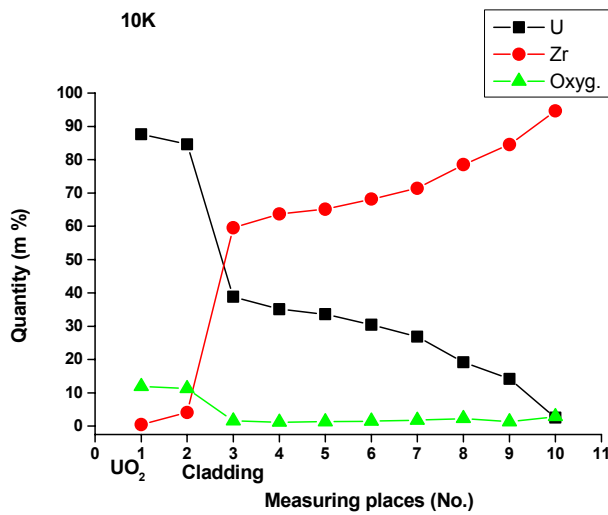


**Fig. 17:** EDX results for D10. Zone 1-2 is in  $UO_2$ , Zone 3-10 is in the cladding

## Main results

- The short fuel rod dissolution tests indicated large differences and **additional** phenomena compared to crucible tests. The internal relocation of the melt to lower positions and its accumulation in the bottom part, the penetration of molten material into the space between pellets complicates the picture of dissolution process.
- Dissolution of both  $\text{UO}_2$  and  $\text{ZrO}_2$  in the molten Zr was evidenced. High dissolution of  $\text{UO}_2$  by molten Zr was observed for higher temperature tests with partial oxidation of the cladding. The extent of dissolution and fuel rod degradation increased at higher temperatures.
- The dissolution interactions were non-uniform in axial and radial directions. Small cracks and local effects were able to accelerate the local dissolution and the movement of molten materials. The dissolution of  $\text{UO}_2$  was larger when the cladding was closed or got into touch with the  $\text{UO}_2$  pellet.
- As expected, no dissolution was seen in case of completely oxidized cladding.
- Steel impurity accelerated local dissolution in one case.
- The clad failure behavior showed no significant difference between PWR and VVER rods. Complex clad failure mechanisms were observed. The expected failure mechanism - local dissolution of oxide layer and flowing out of molten Zr - was not seen in none of the tests. However most of the samples failed. The most typical way of loss of fuel integrity was the radial cracking of cladding and the complete dissolution of external oxide layer. Fragmentation of samples was observed in many cases. It could happen not only during the experiments, but after the tests, during handling as well.
- Higher  $\text{UO}_2$  dissolution was observed in the PWR tests, however the dissolution temperatures were generally higher than in case of VVER tests and whether  $\text{UO}_2$ -PWR or  $\text{UO}_2$ -VVER dissolves faster could not be concluded from these tests.

Experimental data were provided for model development and validation purposes. The electronic database includes temperature histories and a complete set of optical micrographs.

The experimental conditions were not prototypical and were selected in order to provide data on the main aspects of specific phenomena for modeling purpose. Inert atmosphere was used during the dissolution phase to avoid the additional effect of Zr oxidation. In power plant conditions, steam atmosphere is also expected during the fuel dissolution at least during the early stage of the interaction. In these conditions cladding oxidation and fuel dissolution occur simultaneously. For this reason the experimental results (e.g. failure conditions) can not be applied directly for severe accident analysis, but are intended to be used first of all for model development.

According to the results obtained, local contact between  $\text{UO}_2$  pellet and Zr cladding plays an important role in the dissolution process. For this reason, in case of high burnup fuel with closed gap, more intense interaction can be expected than with fresh fuel.

### **3.6 WP2.3: Analytical support to PWR and VVER degradation tests**

Calculations were provided to assist in the preparation of the tests and in the analysis of results. The final objective was modelling improvement on early fuel liquefaction and cladding failure. Three codes were involved in this task: SVECHA/QUENCH, ICARE/C. and S/R5.

### 3.6.1 SVECHA/QUENCH calculations (IBRAE)

The upgraded model for simultaneous dissolution of  $\text{UO}_2$  and  $\text{ZrO}_2$  by molten Zr, which was developed by IBRAE (see WP7, § 4.3) and implemented in the SVECHA/QUENCH (S/V) code, was validated against AEKI data on fuel rod dissolution.

At first, pre-test calculations of AEKI tests were performed with the S/Q code, Figs. 18 and 19. Calculation results show that the oxide scale (formed in the pre-oxidation stage) and uranium pellets are attacked by molten Zircaloy during annealing stage. Before metal Zircaloy melting the oxide thickness was found to decrease (during heat-up stage) owing to “chemical thinning” under steam starved conditions (re-dissolution of  $\text{ZrO}_2$  in the underlying metallic Zr).

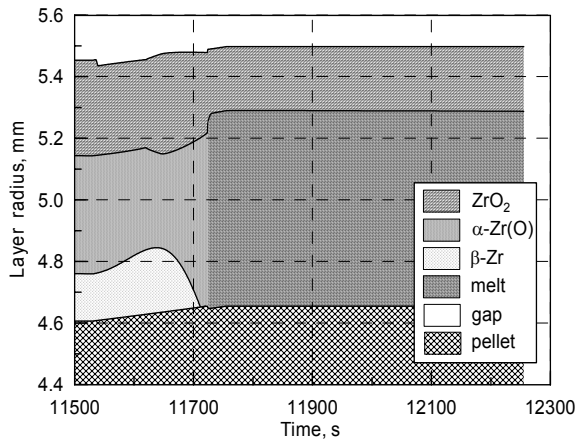


**Fig. 18:** Pre-test calculation of the fuel rod layers evolution in test D7.

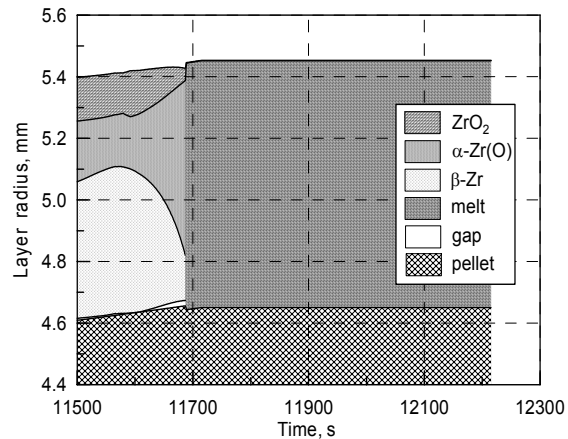


**Fig. 19:** Pre-test calculation of the fuel rod layers evolution in test D10.

Analysis of experimental data shows that observed oxide scale thickness is much thicker than predicted one (D10 test: 100  $\mu\text{m}$  in the test). In order to explain this disagreement, it was assumed that steam starved conditions were not completely realised in the tests and that significant amount of oxygen was accessible also in the final high temperature stage of the tests.

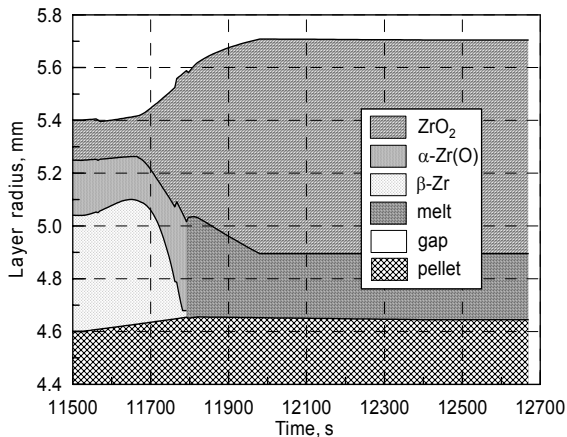


**Fig. 20:** Post-test calculation of the fuel rod layers evolution in test D7. Oxygen flow is 0,1 g/s during the test.

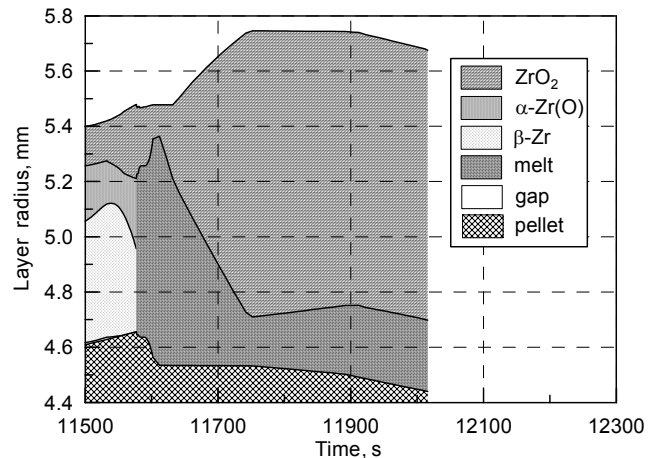


**Fig. 21:** Post-test calculation of the fuel rod layers evolution in test D10. Oxygen flow is 0,1 g/s during the test.

Post-test calculations under assumption of steam supply in the final stage of the tests give a qualitative agreement with experimental data, i.e. thick oxide scale and noticeable uranium pellets dissolution in test D10, Fig. 21. The demonstrative calculations of tests D7 and D10 confirms the possible oxygen access to the system as was later recognized by AEKI experimentalists (final data report). Nevertheless these calculations indicate an overestimation of the  $ZrO_2$  thickness ( $\sim 1000 \mu m$  calculated instead of  $\sim 100 \mu m$  in the D10 test).

### 3.6.2 ICARE/CATHARE and SCDAP/RELAP5 calculations (ENEA)

Pre-test analysis of AEKI tests has been performed by ENEA using ICARE/CATHARE and SCDAP/RELAP5 codes in order to support the test conduct and better define the test matrix. Code to code result comparison using different default oxidation and dissolution models in the two codes has put in evidence that code result differences depend mainly on different default modelling for the degradation phenomena. Post-test analysis has been performed by ENEA using the same codes to verify the ability of these codes to model fuel rod dissolution and try to identify the best code modelling.

#### Pre-Test Analysis

Short PWR fuel rod samples of 5 cm length have been used in a high temperature experimental facility with and inductive furnace to carry out the tests.

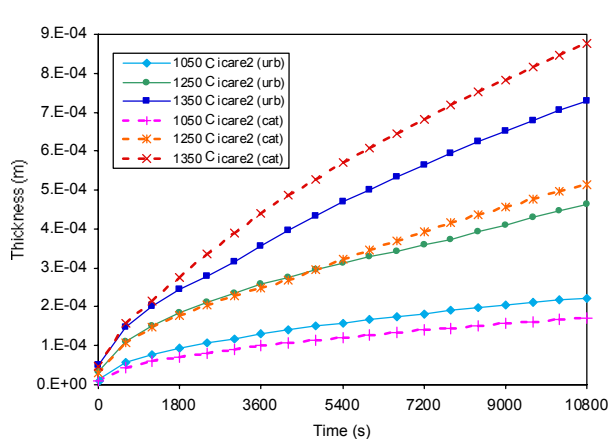


**Fig. 22:** Oxide layer by ICARE/CATHARE code using Urbanic and Cathcart correlations

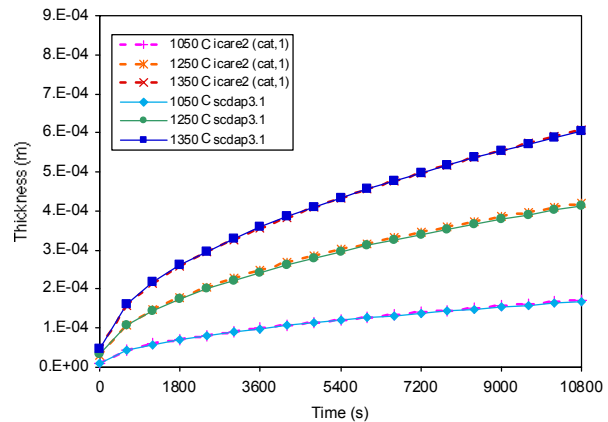


**Fig. 23:** Oxide layer by I/C and S/R5 codes using Cathcart correlation

A parametric analysis with both codes has been performed to investigate:

- the oxide scale growth under isothermal conditions in steam at different temperatures and using different oxidation kinetics correlations;
- the  $UO_2$  and  $ZrO_2$  dissolution by molten zircaloy under isothermal conditions in argon at different temperatures, for different oxide scale thicknesses, and using different dissolution kinetics correlations and solubility limits;

with the aim to assess the influence on the results of different codes and kinetics models used.

One of the major outcomes from this analysis was that code result differences do not depend on the code itself but on the different models used to compute oxidation and dissolution phenomena.

Figure 22 shows the oxide layer growth calculated by ICARE/CATHARE at different temperatures and using different kinetics correlations. The Urbanic-Heidrick correlation gives, at low temperature, faster oxidation than the Cathcart-Pawel one. When the same correlation (Cathcart-Pawel) is used by the two codes, they give identical results (Fig. 23).

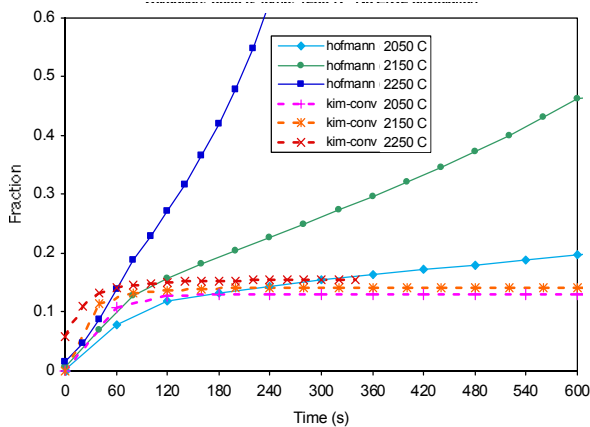


**Fig. 24:** UO<sub>2</sub> dissolution by ICARE/CATHARE code using Kim-convective and Hofmann-diffusive models

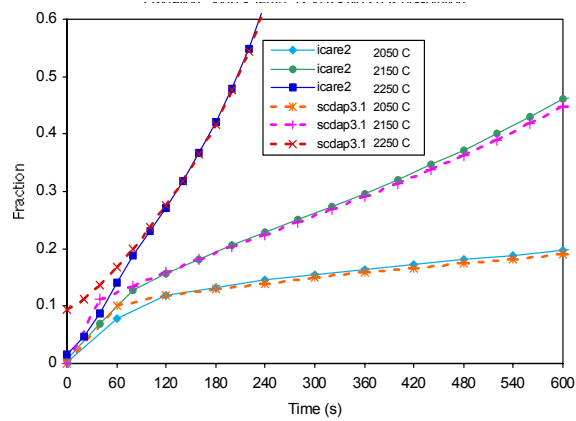


**Fig. 25:** UO<sub>2</sub> dissolution by I/C and S/R5 codes using the Hofmann-diffusive model

Fig. 24 shows the UO<sub>2</sub> dissolution calculated by ICARE/CATHARE code using two different dissolution models and solubility limits (dissolution of oxide scale was not taken into account). The Hofmann diffusive model (solidus line of U-Zr-O phase diagram as solubility limit) gives, in general, much more dissolution than the Kim-Olander convective model (liquidus line as solubility limit). UO<sub>2</sub> dissolution calculated by the two codes using the Hofmann model is compared in Fig. 25. Except for the initial transient, the codes give very similar results.

### Pre-test analysis of the extended part of the test matrix (PWR fuel rod tests)

**Table 8:** Fuel rod oxidation and dissolution modelling

PHENOMENA	CODE MODEL	
	ICARE/CATHARE	SCDAP/RELAP5
Zircaloy oxidation	Urbanic correlation	Cathcart correlation
Oxide scale dissolution by molten zircaloy	Hofmann model	No model
Clad failure and material mixture relocation	Chemical dissolution of oxide scale	No criteria applied
UO <sub>2</sub> dissolution by molten zircaloy	Kim-convective model Solubility limit: liquidus line of ternary phase U-Zr-O diagram	Hofmann diffusive model Solubility limit: solidus line of ternary phase U-Zr-O diagram

The five new PWR fuel rod tests have been analysed with both ICARE/CATHARE and SCDAP/RELAP5 codes, using default code models for material oxidation and dissolution (Table. 8).

The tests consisted of two phases: first an isothermal oxidation phase in steam at 1523 K followed by an isothermal dissolution phase in argon. The parameters to be varied in the different tests were the oxidation time, the dissolution time and the dissolution temperature. Figs. 26 and 27 show code results for the test n. 20 regarding fuel rod thickness evolution.

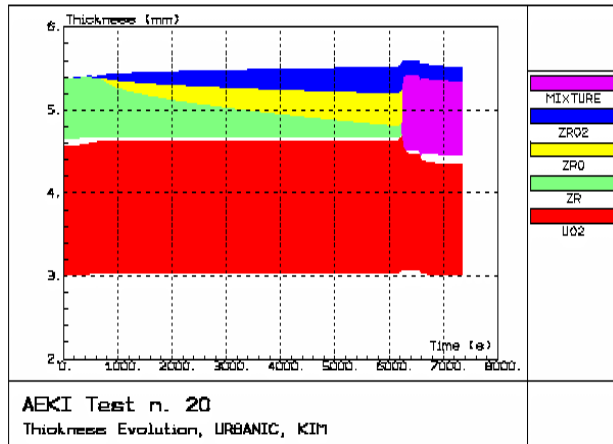


**Fig. 26:** Fuel rod thickness evolution by I/C code

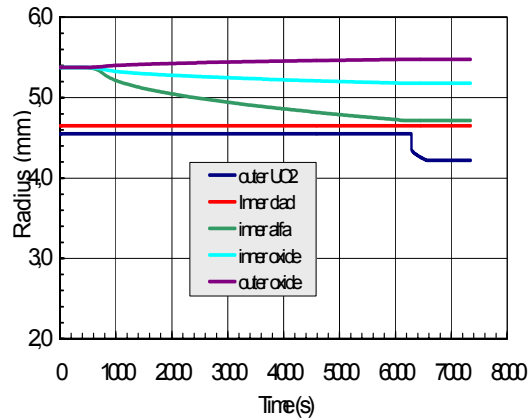


**Fig. 27:** Fuel rod thickness evolution by S/R5 code

Table 9 summarizes the results of pre-test analysis. In general the analysis of the tests have shown sufficient agreement in the prediction of the oxide scale thickness at the end of oxidation phase; while large discrepancies have been found in the amount of  $UO_2$  dissolution calculated by the two codes. These discrepancies have been mainly attributed to different solubility limits of dissolution model used, and the lack of an oxide scale dissolution model in SCDAP/RELAP5.

**Table 9:** Summary of results of pre-test analysis

AEKI TEST	Test Conditions		RESULTS				
	Tox (°C) tox (s)	Tdis (°C) tdis (s)	CODE	ZrO2 layer thickness (µm)	ZrO2 dissolution (%)	Clad failure	UO2 dissolution (%)
n. 16	1250	2250	ICARE	257	100	yes	19
	3600	120	SCDAP	243	-	no	51.6
n. 17	1250	2250	ICARE	257	100	yes	19
	3600	180	SCDAP	243	-	no	77.6
n. 18	1250	2250	ICARE	257	100	yes	19
	3600	300	SCDAP	243	-	no	100
n. 19	1250	2050	ICARE	257	69.3	no	18.8
	3600	180	SCDAP	243	-	no	23.1
n. 20	1250	2050	ICARE	312	48.4	no	16.7
	5400	300	SCDAP	296	-	no	24.8

On the basis of the analysis performed, a revised test matrix has been proposed. The importance of test conducted at high dissolution temperature was recognized due to the lack of

data. One more test at high temperature was suggested replacing the test n. 20. One test with a longer oxidation phase was suggested to avoid complete chemical dissolution of oxide scale at high temperature, as computed by ICARE/CATHARE at 2250 °C.

### Post-Test Analysis

Due to difficulties in performing the tests, the originally planned test conditions could not be kept, especially in the dissolution phase. The isothermal dissolution plateau was not constant in most of the cases due to relocation of molten material. Therefore, the test matrix was different from that it was considered in the pre-test analysis.

Twelve PWR fuel rod tests have been analysed with both ICARE/CATHARE and SCDAP/RELAP5 codes. Comparison of code results with experimental data was difficult due to large uncertainties in the interpretation of data.

Main characteristics of analysed PWR fuel rod tests and code results are summarized in Table 10 below.

**Table 10:** Summary of results of post-test analysis

AEKI TEST	Test Conditions		RESULTS					
	Tox (°C) tox (s)	Tdis (°C) tdis (s)	CODE	ZrO2 layer thic. (µm)	Clad failure	ZrO2 layer dissol. (%)	UO2 dissol. (%)	% of UO2 in the mixture
D2	1150	2050	ICARE	317	no	55.2	17.4	32.6
	10600	272	SCDAP	270	no	0	26	51
D7	1050	2000	ICARE	223	no	38.1	6.4	15.6
	10800	--	SCDAP	168	no	0	0	0
D10	1050	2150	ICARE	222	yes / no	100 / 0	16.1 / 31.8	-- / 50.9
	10700	225	SCDAP	167	no	0	51.3	62
D16	1050	1900	ICARE	248	no	1.6	0.6	2.8
	13400	--	SCDAP	187	no	0	0	0
D17	1050	2050	ICARE	158	yes / no	100 / 0	11.4 / 31.8	-- / 49.2
	5400	--	SCDAP	119	no	0	26.5	44
D18	1050	1760	ICARE	159	no	1.9	0	0
	5400	--	SCDAP	120	no	0	0	0
D19	1050	2026	ICARE	186	no	19.9	0.4	1.3
	7200	--	SCDAP	140	no	0	22.3	41
D20	1050	1900	ICARE	223	no	8.1	1.2	4.1
	10800	50	SCDAP	168	no	0	18.3	39
D23	1050	1900	ICARE	130	no	1.5	0.8	3.2
	3600	129	SCDAP	98	no	0	0	0
D27	1150	2061	ICARE	199	yes / no	100 / 0	15.5 / 22.9	-- / 42.1
	4000	--	SCDAP	169	no	0	23.2	43
D28	1050	2084	ICARE	110	yes / no	100 / 0	7.9 / 32.9	-- / 48.7
	2550	58	SCDAP	83	no	0	25.4	42
D29	1050	2160	ICARE	89	yes / no	100 / 0	6.2 / 35.1	-- / 49.8
	1650	78	SCDAP	67	no	0	27.9	44

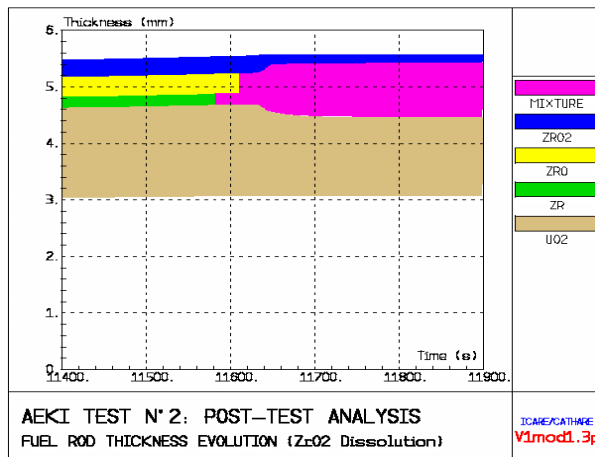


**Fig. 28:** Fuel rod thickness for D2 test by I/C code

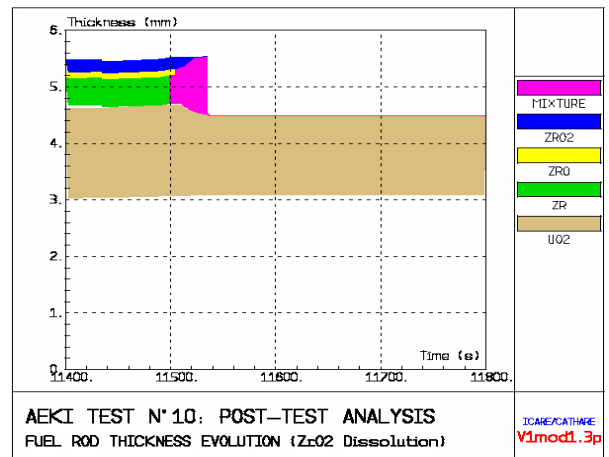


**Fig. 29:** Fuel rod thickness for D10 test by I/C code

Discrepancies in the code results depend mainly on different code models as verified in the pre-test analysis. In general SCDAP/RELAP5 overpredicts UO<sub>2</sub> dissolution with respect to ICARE/CATHARE. No ZrO<sub>2</sub> dissolution is modelled by SCDAP/RELAP5. The fuel dissolution calculated by ICARE/CATHARE can be significantly limited by oxide scale chemical dissolution and molten mixture relocation, as observed in the analysis of test D10 (Fig. 29).

### ***Comparison with Experimental Data***

In many tests, the relocation of the melt to lower positions and the penetration of molten material into the space between pellets complicates the pictures of dissolution process. Furthermore, the interactions were non-uniform in axial and radial directions. Small cracks and local effects were able to accelerate the local dissolution and the movement of molten materials. Because of that, the comparison of code results with experimental data is somewhat difficult.

High dissolution of UO<sub>2</sub> by molten Zircaloy was observed in the tests, when the temperature of the cladding was high enough to promote the interaction between the UO<sub>2</sub> and the cladding. High UO<sub>2</sub> dissolution is calculated by the codes, for tests at higher temperature (over 2000 °C), in reasonable agreement with experimental data. In general, SCDAP/RELAP5 code seems to overpredict fuel dissolution, while ICARE/CATHARE underpredicts it, owing to different dissolution limit. In general, both codes tend to underpredict fuel dissolution for tests conducted at temperature below 2000 °C.

Complete dissolution of external oxide scale took place in some tests with thin initial oxide layer. This behaviour is quite well captured by ICARE/CATHARE which models chemical dissolution of ZrO<sub>2</sub>.

### **Conclusions**

Pre-test analysis of AEKI tests with different codes has provided valuable data for test conduct and the definition of the test matrix. The parametric analysis performed using different oxidation and dissolution models has demonstrated that code result differences depend, quite exclusively, on different default models used by the codes.

In spite of the difficulties in performing the tests and interpretation of data, the fuel rod tests have provided very valuable information on fuel rod dissolution for code model

development and validation. Comparison of code results with experimental data has shown the ability of codes to model fuel dissolution in the higher temperature range. The use of the Kim-Olander convective model for fuel dissolution with a solubility limit between the liquidus and solidus lines of U-Zr-O phase diagram (Extra option in ICARE/CATHARE as solubility limit dissolution model) can be recommended to better reproduce experimental data. The evaluation of fuel dissolution in the lower temperature range is much more uncertain. The need to model oxide scale dissolution, as in ICARE/CATHARE, has been confirmed while this effect seems overestimated in the current model.

### 3.6.3 ICARE/CATHARE calculations (KI)

Pre-test calculations of AEKI single rod tests were done with the ICARE/CATHARE V1 code in order to help the experimental team in the preparation of the tests.

Key results were obtained in variant calculations, which included 240 ICARE2 runs for 20 tests with PWR and VVER short fuel rods of 5 cm long. The particular attention was given to the analysis of extent of cladding oxidation and UO<sub>2</sub> dissolution. Calculations were carried out using the following ICARE2 modules:

- Zr oxidation module (ZROX);
- UO<sub>2</sub> and ZrO<sub>2</sub> dissolution module (UZRL);
- Ternary phase diagram module (PHADI).

The output responses included ZrO<sub>2</sub> thickness after oxidation, final ZrO<sub>2</sub> thickness after dissolution and amount of UO<sub>2</sub> dissolved. The latter value is the most sensitive to deviation of modelling parameters and for the same test its variation can be very significant. Simulations confirm that such large uncertainties can be the result of not only weak knowledge UO<sub>2</sub> dissolution process in fuel rods, but also on the uncertainty (20-30%) on the cladding oxidation state before the dissolution stage.

For low temperature tests, main findings are the following:

- Amount of UO<sub>2</sub> dissolved is very small. The uncertainty in simulations depends on  $\alpha$ -Zr(O) melting point. The simulations with PHADI module gave higher melting temperatures Zr(O) than simulations based on simple approach.
- Dissolution stage of the transients exceeds the characteristic time needed for saturation of U-Zr-O melt.
- The main uncertainty for the process of UO<sub>2</sub> dissolution concerned the saturation limit of U concentration in U-Zr-O melts. Two possibilities exist: the process is stopped reaching the liquidus line of ternary phase diagram or continues up to some limit (KIM option in ICARE2 input deck).

For high temperature tests, main findings are the following:

- Poor knowledge of ternary U-Zr-O line exists. As a result, the amount of UO<sub>2</sub> dissolved is up to two times greater for calculations with PHADI module than without it.
- Account of ZrO<sub>2</sub> dissolution option in the ICARE2 input deck led to decrease both the final oxide scale and the UO<sub>2</sub> dissolved. The latter effect appeared with additional oxygen in the melt and is a consequence of the dependence of UO<sub>2</sub> solubility on oxygen content.

It is suspected that the current ICARE2 dissolution modelling over-predicts the dissolution of  $ZrO_2$ .

- The extent of  $UO_2$  dissolution is greatly influenced by uncertainties in Zr oxidation (initial thickness of  $\alpha$ -Zr(O) and  $ZrO_2$ ). Actually, the uncertainties in oxidation kinetics are found to strongly affect the  $UO_2$  dissolution.

The discrepancy in simulations was foreseen to be partially resolved on the basis of the post-test metallographical examination, thus leading to diminishing of uncertainty gap in this field. For situation with several quite different physical phenomena (Zr oxidation,  $UO_2$  and  $ZrO_2$  dissolution) it was proposed to experimental team to perform a number of additional single rods tests, focusing more on the characterization of the Zr oxidation in order to improve the analysis of the fuel dissolution.

Post-test calculations were carried out. with an improved version of the ICARE/CATHARE V1 code, which includes the upgraded ICARE2 V3 Mod1.2 code. For that purpose available test transients were examined, taking into account the results of post-test metallographical measurements.

Preliminary examination of experiments from AEKI series of single rod tests revealed complex geometry of the melts, which appeared in cladding metallic parts and expanded in the course of  $UO_2$  dissolution. Melt spreading inside pellet holes and over upper pellet surface was observed experimentally, potentially leading to higher melt heterogeneity than is was supposed in pre-test ICARE2 simulations. Some part of the melt penetrated even in small gap between pellets.

Therefore a correspondence between measured and calculated values had to be re-characterized in order to facilitate the code-to-data comparison. The problem was discussed with AEKI specialists and it was considered reasonable to provide the experimental results as solubility of uranium in the melt on oxygen free basis, i.e. the  $U/(U+Zr)$  wt% ratio in specific parts of the sample. The latter values can be easily compared with the simulated amount of  $UO_2$  dissolved and with the results of other experimental groups. It should be mentioned that the same approach was used in previous experiments of Hayward and George (Ref.[10]) AECL, Canada, 1994] and both test data can be easily compared.

The conduct of the test led to have, before the dissolution stage, a cladding mainly composed of oxygen rich  $\alpha$ -Zr(O) phase underlying the external  $ZrO_2$  scale. This condition was confirmed by the D21 test simulations, where  $\alpha$ -Zr(O) and  $ZrO_2$  layers were found to represent 95% of the cladding after the oxidation stage (base case simulation). In such situation the results can be compared with the ones obtained previously by another experimentalists from AECL, who examined the  $UO_2$  dissolution reaction in crucibles with  $\alpha$ -Zr(O) charge. Figure 30 presents the comparison between present AEKI and AECL results on solubility limit, defined as  $U/(U+Zr)$  mass ratio, i.e. on oxygen free basis.

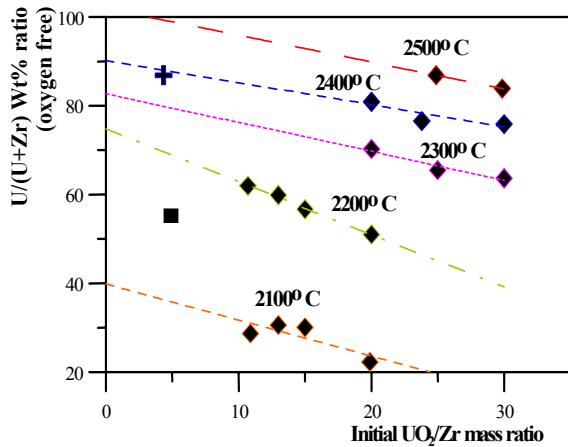


**Figure 30:** Comparison of AEKI and AECL results on solubility limit. ■ D21 experiment, ◆ - Hayward-George data.

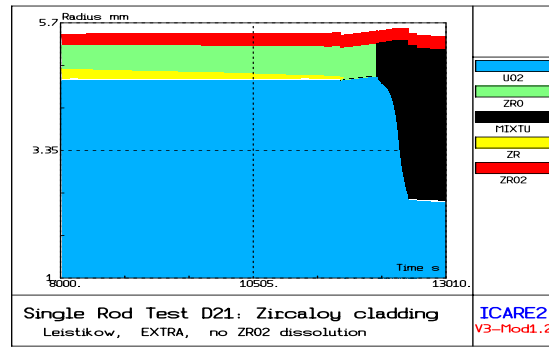


**Figure 31:** Evolution of cladding layers during simulated D21 transient.

As it was established by Hayward-George, who examined the crucibles of different sizes, the U solubility limit depends smoothly on initial  $\text{UO}_2/\text{Zr}$  mass ratio. Physically this phenomenon was explained using arguments based on the effects of O diffusion on stoichiometry of the dissolved fuel. Hayward-George examined a number of crucible in the range 10 to 30 of  $\text{UO}_2/\text{Zr}$  mass ratio, while AEKI results are characterized by ratios of 4.2 and 4.8 for VVER and PWR fuel rods. One can see that extrapolation of previous Hayward-George crucible results at examined dissolution temperature  $\sim 2150^\circ\text{C}$  is consistent with currently obtained data. Here near 60 wt% of  $\text{U}/(\text{U}+\text{Zr})$  mass ratio on oxygen free basis while it was  $\sim 69$  mass % of total sample mass in the test.

Post-test calculations were carried out with the following modules of ICARE2 V3 Mod1.2:

- Zr oxidation module (ZROX) (allows possible  $\text{ZrO}_2$  thinning in conditions of steam starvation after oxidation phase);
- Simultaneous  $\text{UO}_2$  and  $\text{ZrO}_2$  dissolution module (UZRL);
- Ternary phase diagram module (PHADI).

Table 11 displays the modelling parameters, which were chosen in current studies for the examination of the simulated uncertainty range. Some of options are given by general name and short description of each option is presented below.

Sensitivity calculations on Zr oxidation model were carried out in pre-test calculations. The additional Zr and O resulting from the dissolution of the external  $\text{ZrO}_2$  shell can penetrate into the melt and influence of the rate and solubility limit of the  $\text{UO}_2$  dissolution. Impact of  $\text{ZrO}_2$  dissolution in current ICARE2 code version was examine by simple switch on or off the option in UZRL module driving the  $\text{ZrO}_2$  dissolution. Additionally sensitivity was carried out on the option EXTRA. It accounted  $\text{UO}_2/\text{Zr}$  mass ratio and extrapolated results of crucible solubility measurements to fuel rod dimensions. This option was developed by KI and implemented in official ICARE V3 Mod1 code version just after the beginning of the COLOSS project.

Main analytical efforts were based on results for D21 sample because the full set of the experimental data on temperature history and metallography was not available during a large part of the project. The output of 15 ICARE2 runs was chosen for comparison with different

modelling options. It was obtained that outputs for U/(U+Zr) mass ratio appeared to be as higher than experimentally reported. The best fit in the modelling equals to 80.2 wt% and corresponds to following modelling options:

- Oxidation: Leistikow-Schantz correlations at low temperatures;
- UO<sub>2</sub> dissolution: option EXTRA;
- ZrO<sub>2</sub> dissolution: neglected.

**Table 11:** Varied parameters and options used in the ICARE2 calculations

Physical phenomena	General name		ICARE2 options	Objective
Zr Cladding Oxidation (ZROX)	VVER	Sokolov	User defined	Analyses of initial conditions before UO <sub>2</sub> dissolution
		URBANIC	URBANIC	
	PWR	Leistikov, Prater + Courtright	User defined	
		URBANIC	URBANIC	
UO <sub>2</sub> dissolution (UZRL)	KIM		SOLU = KIM	Analyses of UO <sub>2</sub> solubility limit
	LIQUIDUS		SOLU = LIQUIDUS	
	PHADI		SOLU = LIQUIDUS, PHADI = YES (OPTI)	
	EXTRA		SOLU=EXTRA	
ZrO <sub>2</sub> dissolution (UZRL)	YES		ZRO2 = YES	Analyses of ZrO <sub>2</sub> dissolution impact on UO <sub>2</sub> dissolution
	NO		ZRO <sub>2</sub> = NO	

As mentioned in the modelling description, the option EXTRA was implemented into ICARE2 code to provide extrapolation of UO<sub>2</sub> dissolution results from crucibles to fuel rod geometries. Therefore the agreement of the option with current measurements for fuel rods seems natural. An evolution of cladding layers during oxidation phase, heat-up to high temperature and dissolution stage is given in Figure 31. The  $\alpha$ -Zr(O) phase occupied almost all the metallic part of the cladding. This oxygen rich phase appeared as a result of oxidation and certain solid-solid fuel-cladding interaction during heat-up phase. Very low UO<sub>2</sub>/Zr liquefaction was predicted in solid state after closing of cladding-fuel gap.

When considered, the influence of the ZrO<sub>2</sub> dissolution on AEKI was predicted negligible. In the conditions of the tests, it is suspected that the rate of ZrO<sub>2</sub> dissolution derived from crucible tests with pure Zr should be updated for  $\alpha$ -Zr(O) melts representative of moderate and heavy cladding oxidation.

Main findings are the following:

- ICARE2 V3 Mod1.2 code version predicts the results of the single rod tests in agreement with experimental observations;
- Closest agreement was found with the following code options (for D-21 test): Oxidation with Leistikow-Schantz correlations, UO<sub>2</sub> dissolution with option EXTRA, switch-off the ZrO<sub>2</sub> dissolution option.
- AEKI measurements of UO<sub>2</sub> solubility in D-21 test are compatible with the extrapolated Hayward ones for UO<sub>2</sub>/Zr mass ratio representative of fuel rods

### **3.7 WP3.1: Experiments on dissolution of ZrO<sub>2</sub> and on oxidation of U-Zr-O mixtures**

The key objective of these experiments was the development of models that can simulate the oxidation of U-Zr-O and Zr-O mixtures suspected to be the main cause of temperature escalation and large H<sub>2</sub> release during the quenching of degraded cores. The experimental effort involved two areas of investigation: 1) ÚJP-PRAHA tests on U-O-Zr oxidation of solid mixtures (T<1400°C) and 2) FZK melt oxidation tests (T>2100°C) based on small scale ZrO<sub>2</sub> dissolution by molten Zr. The latter tests, not included in the initial project, were proposed by FZK to facilitate and validate the modeling work of IBRAE (see § 4.2) on oxidation of molten Zr-O mixtures.

#### **3.7.1 Experiments on oxidation of solid U-Zr-O mixtures (ÚJP-PRAHA)**

ÚJP-PRAHA (SKODA-ÚJP) at the beginning of the project) did experiments on the oxidation behaviour of selected solid U-Zr-O alloys between ~400-1400 °C in 0.1 MPa Ar/steam mixture. The objective of the experiments was to map the oxidation behaviour of the U-Zr-O alloys, to quantify the role of U and O for the oxidation kinetics and to provide data for severe accident (SA) codes (Ref.[11]). Former unpublished data of ŠKODA-ÚJP indicated that the presence of U and O in the alloys enhances the oxidation kinetics. It is to note that most of the SA codes were still based on the modelling of the U-Zr-O oxidation using the oxidation kinetics for pure Zircaloy.

##### **Outline of the programme**

The first year of the project (2000) was devoted to construction of a new LABIO Test Facility with continuous H<sub>2</sub> measurement (Fig. 32), to fabrication of 16 U-Zr-O alloys & cylindrical specimens and to ignition tests aimed at studying the pyrophoric behaviour of the tested alloys. As the LABIO Test Facility was available only at the beginning of the second year and the fabrication of cylindrical specimens was delayed due to difficult machining of the brittle alloys, the ignition tests were performed with provisional irregular specimens (Table 12).

The second year (2001) was devoted to first isothermal oxidation tests with 12 U-Zr-O alloys between 700-1200 °C using one exposure time of 10 minutes in the LABIO Test Facility. There was a limited number of specimens, ~20 per alloy. Based on the results of these tests two alloys E2\* (5U-90Zr-5O in wt%) and C2\* (30U-65Zr-5O in wt%) were selected for subsequent measurements of their oxidation kinetics during the third year.

The third year (2002) was devoted to fabrication of a sufficient quantity of the E2\* and C2\* alloys, to fabrication of specimens and to measurements of the oxidation kinetics for E2\* and C2\*. The isothermal tests were performed in the LABIO Test Facility between 650-1400 °C and in a resistance furnace CLASIC with a stainless steel reaction tube for tests between 400-600 °C.

Measured and evaluated parameters are given below:

- specimen weight gain,
- continuous measurement of the released H<sub>2</sub>,
- specimen state after exposition,

- optical metallography of sectioned specimens,
- oxide thickness (where possible),
- determination of the H<sub>2</sub> content in the exposed specimens.

**Table 12 : Summary of the tests with the U-Zr-O alloys (RF: resistance furnace).**

Furnace	Type of test	Number of alloys	Sample geometry	Test objectives
RF CLASIC	Exploratory ignition tests (transient)	2	irregular	To demonstrate that U-Zr-O alloys can ignite already <1000 °C.
	Ignition tests (transient)	14	irregular	To determine the approximate ignition temperature in steam and air.
RF LABIO & RF CLASIC with SS tube	Preliminary oxidation tests (isothermal) 700 - 1200 °C	12	cylindrical	To assess the reproducibility of the tests and the influence of U & O on the oxidation of the tested alloys (compared against Zr1Nb alloy).
	Oxidation tests (isothermal) 400 - 600 °C	2	cylindrical	To quantify the oxidation kinetics of selected alloys.

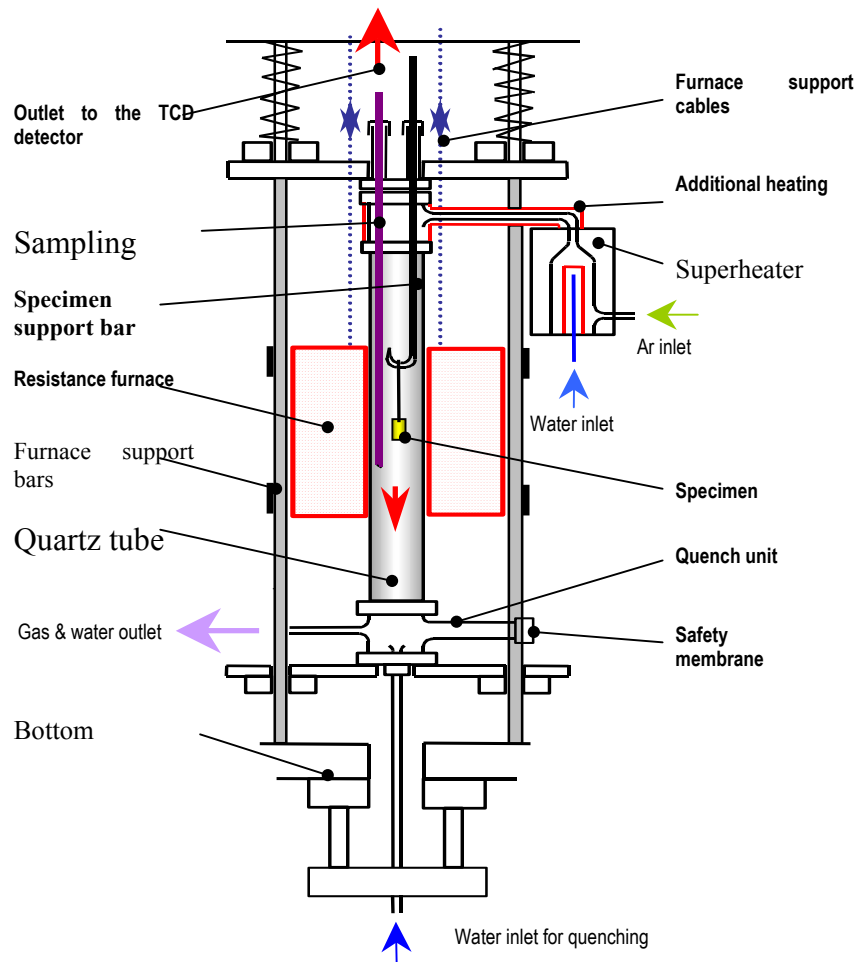


**Fig. 32: Scheme of the LABIO furnace**

**Table 13:** Nominal composition [wt%] of the studied U-Zr-O alloys.

Alloy	U	Zr	O	Exploratory ignition tests	Ignition tests	Preliminary oxidation tests	Detailed oxidation kinetics
Specimens				few	~50	~100	~250
<b>A</b>	50	50	0	x			
<b>B</b>	30	60	10	x			
<b>C</b>	33	66	0		x	x	
<b>C1</b>	30	66	2		x	x	
<b>C2</b>	25	67	5		x	x	
<b>C3</b>	26	62	8		x		
<b>D</b>	66	33	0		x	x	
<b>D1</b>	63	33	2		x	x	
<b>D2</b>	52	41	5		x	x	
<b>D3</b>	52	37	8		x		
<b>E</b>	5	95	0		x	x	
<b>E1</b>	5	93	2		x	x	
<b>E2</b>	5	90	5		x	x	
<b>F</b>	15	85	0		x	x	
<b>F1</b>	15	83	2		x	x	
<b>F2</b>	15	80	5		x	x	
<b>E2* a-e</b>	5	90	5				x
<b>C2* a-e</b>	30	65	5				x

#### Fabrication of U-Zr-O alloys and specimens

The tested U-Zr-O alloys shown in **Table 13** were prepared at ÚJP-PRAHA from depleted U, iodide Zr and ZrO<sub>2</sub> in an arc-melting furnace under He atmosphere (ingots ~10 x 5 x 1 cm). The oxygen-containing alloys were very brittle, badly machinable and pyrophoric. There was usually one ingot produced per alloy C to F2 and five ingots (a to e) per alloy E2\* and C2\*.

The specimens for the ignition tests (alloys **A** to **F2**) were irregular pieces (~1 g). The specimens for oxidation tests (alloys **C** to **F2**, **E2\*** and **C2\***) were solid cylinders  $\phi 7 - 10$  mm fabricated from ingots using electro-spark method (max. ~20-30 specimens per ingot).

#### Experimental facilities and test method

The qualitative ignition tests with the alloys were performed in a high-temperature resistance furnace CLASIC. The specimen temperature was measured with a two-colour pyrometer. The specimen was heated in flowing Ar/steam mixture from ~300 °C at ~20 °C/min up the ignition temperature. The temperature at which uncontrolled temperature escalation started

was measured. The Ar/steam mass flow rates were not measured but were high enough to prevent steam starvation.

The oxidation experiments between 650-1400 °C were performed in the LABIO Test Facility build within COLOSS equipped with a resistance furnace and with a continuous measurement of the hydrogen generated during oxidation (Fig. 32). The temperature of the heated zone of the furnace was measured with a thermocouple. The direct temperature of the specimen could not be measured (oxide spalling or specimen disintegration). The specimen was inserted into the heated zone at test temperature under flowing Ar and then oxidised in Ar/steam mixture.

The oxidation tests between 400-600 °C were performed in a resistance furnace CLASIC with a stainless steel reaction tube. The temperature was measured with thermocouples located close to the specimen placed into quartz ampoules with holes at periphery. The specimens were inserted into the furnace under flowing Ar and then oxidised in Ar/steam mixture.

## Results

### Ignition tests

The ignition tests in steam showed that the U-Zr-O alloys start to rapidly oxidise at temperatures ~380-500 °C, accompanied with uncontrolled temperature escalation up to ~1100 °C. The higher was the U and O content in the alloy the higher was the peak temperature during escalation and the lower was the temperature from which the escalation started.

### Preliminary oxidation tests with 12 U-Zr-O alloys between 700-1200 °C

The tests with alloys C to F2 were aimed at selection of alloys suitable for detailed study of the oxidation kinetics. The results are shown in Figure 33, where the weight gain after 10 min exposure time is plotted against reciprocal temperature and compared with the data for Zr1Nb and for the 66U-30Zr-4O alloy studied by Prater-Courtright (Ref.[15]). All the U-Zr-O alloys exhibit higher weight gain than Zr1Nb. High weight gains were measured in the temperature range 700-1000 °C for alloys with high U and O contents for which important temperature escalations were also observed. Based on these results two alloys were selected for detailed study of the oxidation kinetics: C2\*: 30U-65Zr-5O wt% and E2\*: 5U-90Zr-5O wt%. The 5 wt% O represents the highest oxygen content for which the specimen treatment is technologically feasible.

### Oxidation tests with the 30U-65Zr-5O (C2\*) and 5U-90Zr-5O (E2\*) alloys (400-1400 °C)

Oxidation kinetics are given on Figure 34. Main points are:

- The oxidation of alloy E2\* is approximately parabolic above 1100°C and the oxide remains adherent up to high temperatures, where slight crumbling was observed. The highest experimental scatter was observed at 600 °C. The weight gains for 600 and 700 °C were almost identical. Under 600°C, the oxidation kinetics is quite linear.
- The oxidation of alloy C2\* is approximately parabolic at 400 °C and at temperatures  $\geq 1000$  °C. It is quit linear under 600°C (with an exception at 400°C). The slope of the oxidation curves progressively increases at temperatures between 450-900 °C. When the weight gain reaches the values measured for tests at 1000 °C, the oxidation kinetics decreases and further follows the parabolic law Figure 35. The largest temperature scatter was observed at temperatures 450 and 1100 °C. The isothermal curves for temperatures 1000 to 1300 °C are very similar.

The oxidation rate versus reciprocal temperature is shown in Figures 37 A, B. One can see that the oxidation kinetics of E2\* can be described by a Arrhenius-type correlation. The transition below 700 °C is probably due to temperature escalation due to pyrophoric behaviour. The oxidation are not isothermal at these temperatures. Similarly, for the alloy C2\* the oxidation tests were not isothermal at test temperatures between 450-1000 °C.

In these temperature-escalation zones, the temperature behaviour was characterized by instabilities that can be explained by the cracking and spalling of the protective ZrO<sub>2</sub> layer. After spalling, the temperature escalation occurs. It is followed by a decrease of the oxidation rate due to the formation of a new protective oxide layer and finally the temperature of the specimen decreases to the test temperature. Afterward, the oxide layer separates again from the underlying metal and the oxidation of the fresh surface starts again causing a new temperature escalation. The sequence of “temperature escalation-oxide formation- decrease of the oxidation rate and temperature decrease to the test temperature” continued in a cyclic way. The evidence for this behaviour was seen on the H<sub>2</sub> generation record during oxidation, (Figure 36). On-line visual observation of the specimens at temperature shows changes in specimen brightness and on the oxide morphology (oxide composed of several sub-layers). This non-parabolic behaviour was found for O-rich alloys such as E2 and C2.

#### Amount of absorbed hydrogen in the oxidised alloy.

The maximum measured H<sub>2</sub> content for alloy E2\* was ~800 ppm (cracked specimen). In most cases the H<sub>2</sub> content was max. 400 ppm and for temperatures above 1000 °C max. it was 200 ppm only. The maximum measured H<sub>2</sub> content for alloy C2\* was ~1300 ppm (cracked specimen). The maximum usual H<sub>2</sub> content of ~800 ppm was observed at 900 °C. The H<sub>2</sub> content decreased with increasing temperature (>1000 °C) up to ~300 ppm at 1300 °C.

#### Visual evaluation of the exposed specimens (Figure 38 and 39).

- On alloy E2\* an adherent oxide formed that slightly crumbled at high temperatures only.
- For alloy C2\* oxide crumbling was visible already at 450 °C, but significant oxide spalling was observed in the temperature range 600-800 °C. Relatively adherent oxide formed at temperatures above 900 °C that cracked and spalled on cooling outside the furnace. At temperatures above 1200 °C and short reaction times an oxide formed that spalled on cooling together with a part of the metallic  $\alpha$ -Zr(O). An adherent oxide was formed after long exposure times. This oxide was dark in contrast to that formed on E2\*.

#### Oxide morphology and thickness (including the oxide/metal interface) (Figures 49 and 41).

On specimens of alloy E2\* a not uniform porous oxide with preferential oxidation of grain boundaries and fine cracks formed at low temperatures. Oxide sub-layers parallel to the oxide/metal interface formed after long exposures. Oxide layers similar to the oxides grown on Zr-alloys but with cracks perpendicular to the oxide/metal interface formed at temperatures >1000 °C. The metal layer close to oxide was often cracked. A thin (U, Zr)O<sub>x</sub> layer formed near the oxide/metal interface at temperatures above 1200 °C.

On specimens of alloy C2\* a non-uniform oxide as well formed at low temperatures. As in the case of E2\*, it was possible to observe the preferential oxidation of both the grain boundaries and the cracks within metal. The oxide was composed of sub-layers and was porous on specimens with long exposure times. The oxide porosity was visibly smaller on specimens exposed at 900 °C with long exposure times. An oxide with columnar grains similar to that

observed on Zr-alloys formed at temperatures  $\geq 1000$  °C. This oxide had cracks perpendicular to the oxide/metal interface. At temperatures  $\geq 1100$  °C it was possible to observe a cracked  $\alpha$ -Zr(O) layer free of (U, Zr)O<sub>x</sub> strings.

The (U, Zr)O<sub>x</sub> phase formed just close to the  $\alpha$ -Zr(O) layer and it is evident that this phase was liquid, Figure 39.

The relation between oxide thickness and weight gain can be expressed by a linear relationship for both alloys,

$$\tau_{\text{ox}} = K(\text{alloy}) \cdot \Delta G,$$

$$K(\text{E2}^*) = 0.0634 \mu\text{m}/(\text{mg}/\text{dm}^2) \text{ and } K(\text{C2}^*) = 0.0743 \mu\text{m}/(\text{mg}/\text{dm}^2).$$

$\Delta G$ : Weight gain

## Conclusions

- All U-Zr-O alloys oxidised faster than pure Zr-based cladding materials in the temperatures range 400-1400 °C. This fact should be considered in the severe accident codes, where it is usually assumed that the oxidation of the cladding material is the fastest. This behaviour will generate more hydrogen than assumed up to now.
- Alloys with higher U content show oxide spalling and cracking already at the test temperature and also during cooling. These effects were responsible for the non-parabolic behaviour of the oxidation resulting in enhanced H<sub>2</sub> release. The enhanced oxidation was observed when uranium and oxygen were simultaneously present in the alloy. Similar oxidation was found for oxygen contents  $\geq 2$  wt%, whereas the oxidation increases with the uranium content, especially above 15 wt% U.
- Alloys with 30 wt% U and  $\geq 2$  wt% O oxidised between 450-1000 °C much faster than ZrNb ( $\gg 10$  times). This fact is probably associated with the ability of the alloys to ignite at temperatures 380-800 °C (fast oxidation & temperature escalation).
- The existing Prater reaction kinetics for a ~60 wt% U alloy underestimate significantly oxidation of studied mixtures when extrapolated to temperatures below 1400 °C. Nevertheless this law is in agreement at 1400 °C with the reaction rate measured for the U-rich alloys studied.

These results support the hypothesis that the unexplained enhanced H<sub>2</sub> production during the reflood of degraded fuel could be caused partly by oxidation of relocated U-Zr-O alloys. This key oxidation process is not considered presently in SA codes which cannot predict on any physical basis the H<sub>2</sub> peak observed during reflood.

Oxidation of U-Zr-O alloys during “temperature transient conditions” (either heating or cooling) were not studied in this programme and should be investigated in the future. In these conditions, temperature variations could induce additional ZrO<sub>2</sub> layer cracking and spalling able to reinforce the oxidation kinetics increase observed under isothermal conditions.

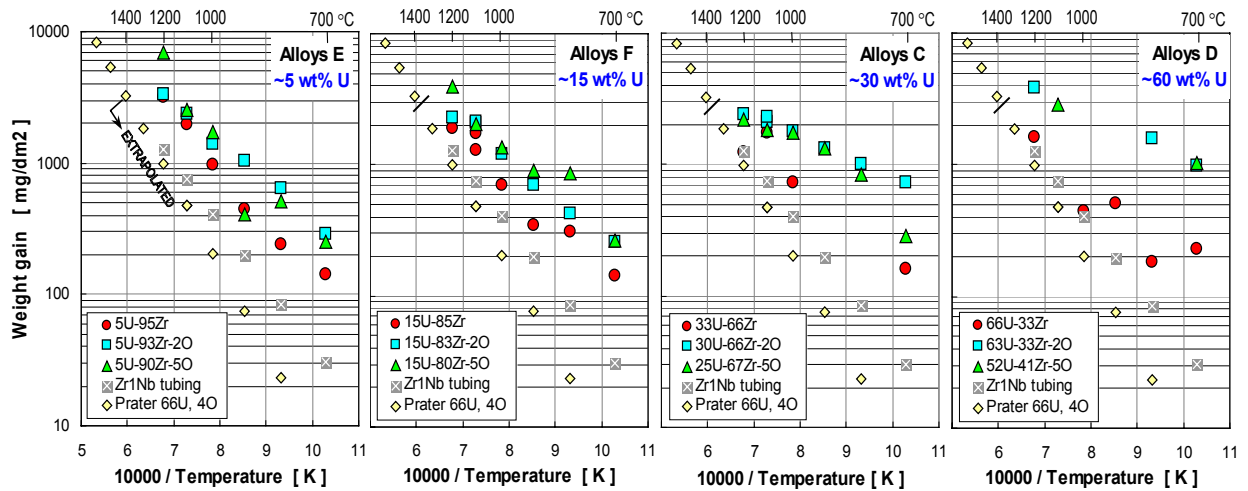


**Fig. 33:** Preliminary oxidation tests with 12 U-Zr-O alloys. The weight gain after 10 min. exposure time is plotted against reciprocal temperature and compared with the data for Zr1Nb and the 66U-30Zr-4O alloy of Prater-Courtright.

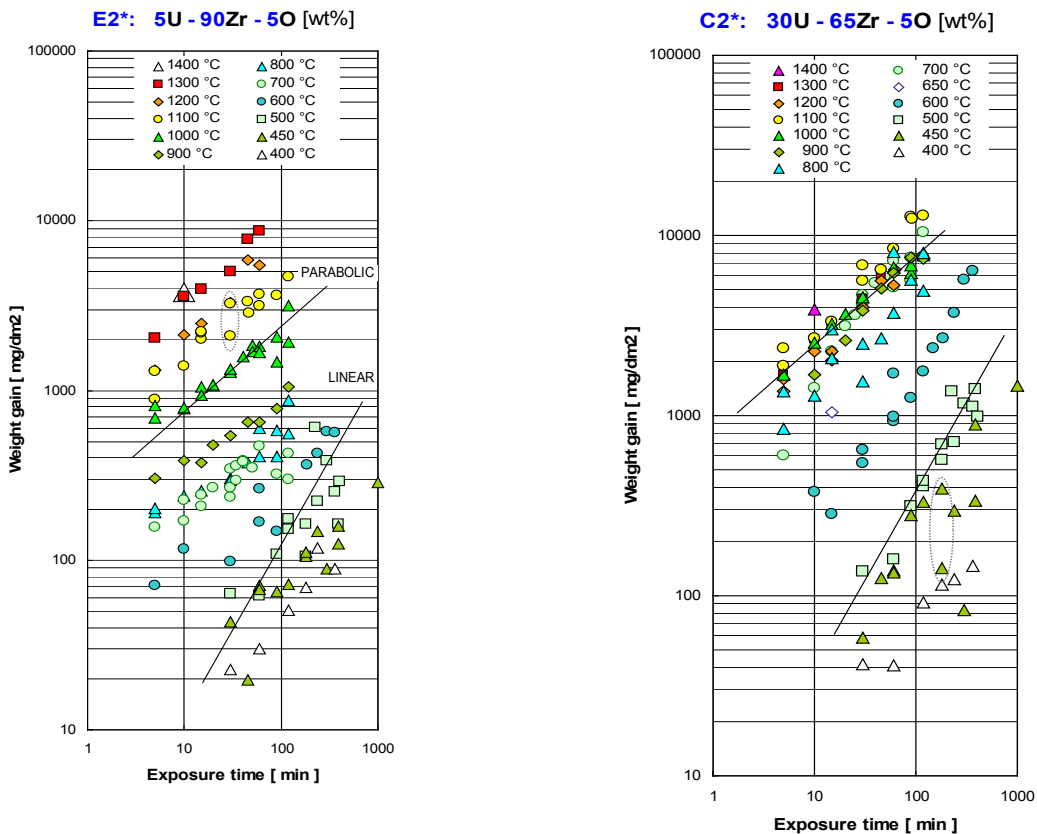


**Fig. 34:** Oxidation kinetics for E2\* and C2\* alloys in Ar/steam mixture.

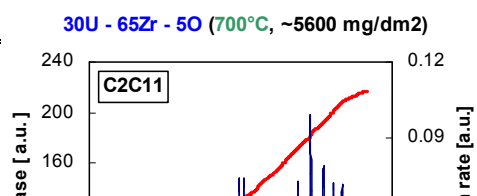
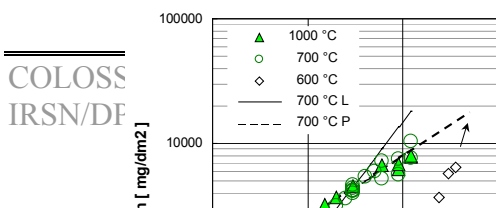


**Fig. 35:** Oxidation of alloy C2\* at 700 °C: for  $T > 1000^\circ\text{C}$ , oxidation kinetics follows that at  $1000^\circ\text{C}$  follows this curve.

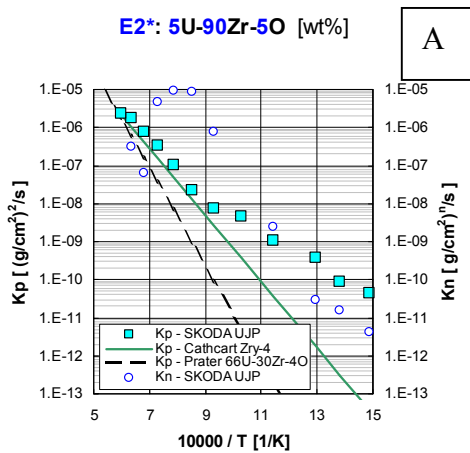


**Fig. 36:** Oxidation of alloy C2\* at 700 °C: Example of continuous H<sub>2</sub> record showing instabilities during oxidation.

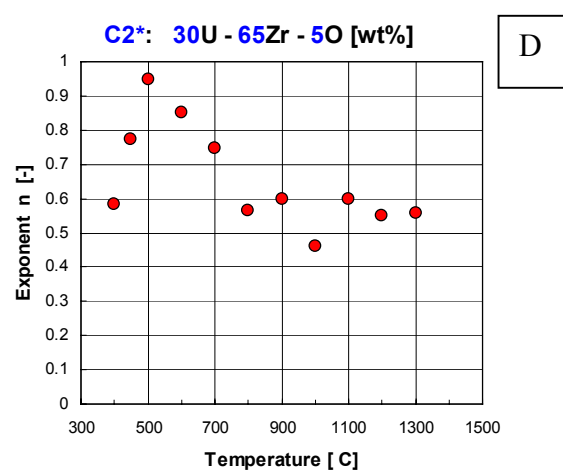
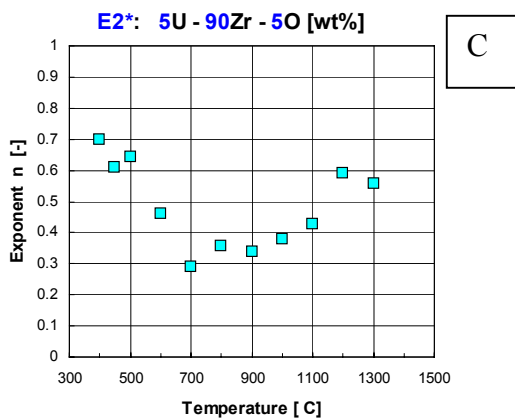
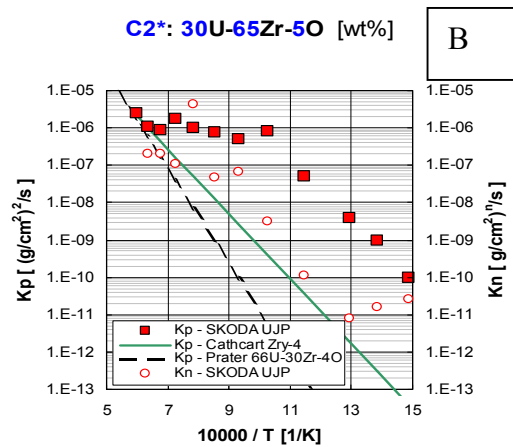


**Fig. 37:** Alloys E2\* and C2\*: Reaction rate constants (A, B) compared to Cathcart (Zry-4) and Prater (66U-30Zr-4O). The rate constant  $K_p$  corresponds to a parabolic law ( $n = 2$ ). The rate constant  $K_n$  ( $\Delta G^n = K_n \cdot t$ , where  $\Delta G$  = weight gain,  $K_n$  = rate constant) is approximated for each individual temperature that fits best the measured data ( $n$  values given in Fig. C, D).

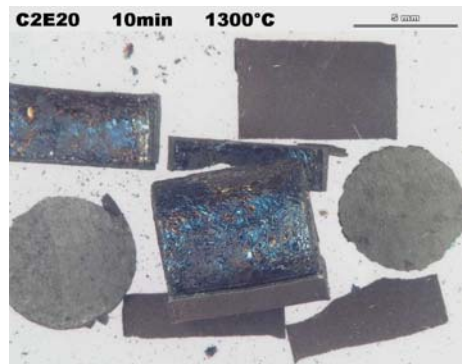
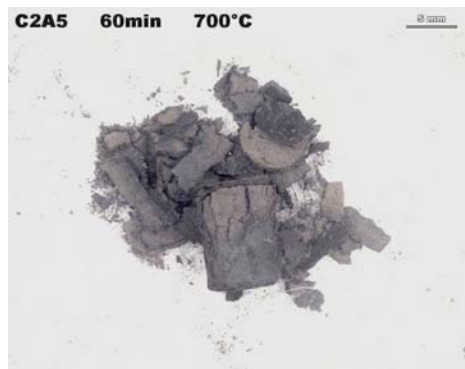
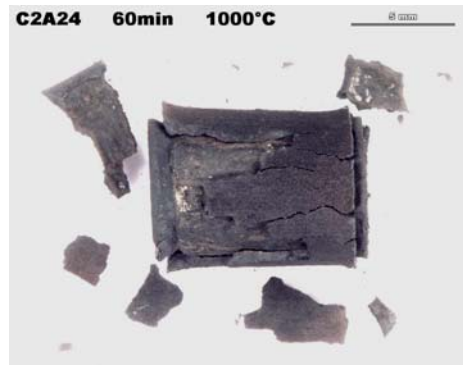
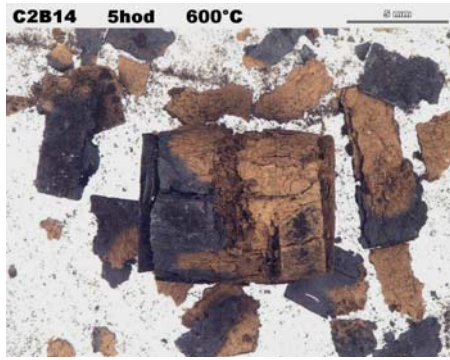


**Figure 38:** Alloy C2\* (30U-65Zr-5O): Visual appearance of the exposed specimens

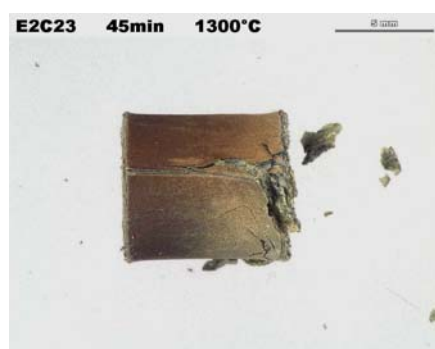
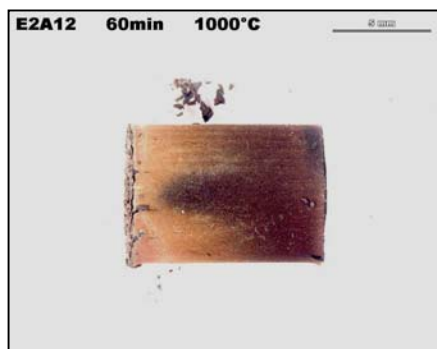
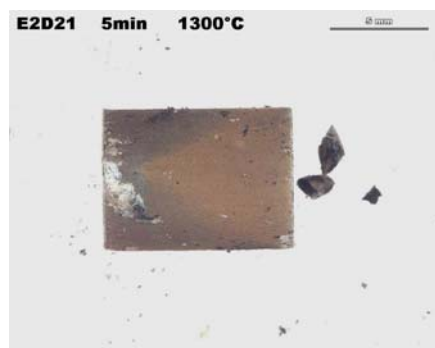
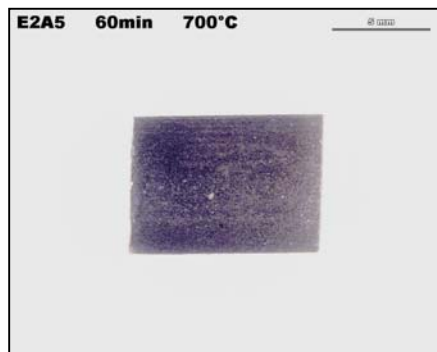


**Fig. 39:** Visual appearance of the exposed E2\* specimens.

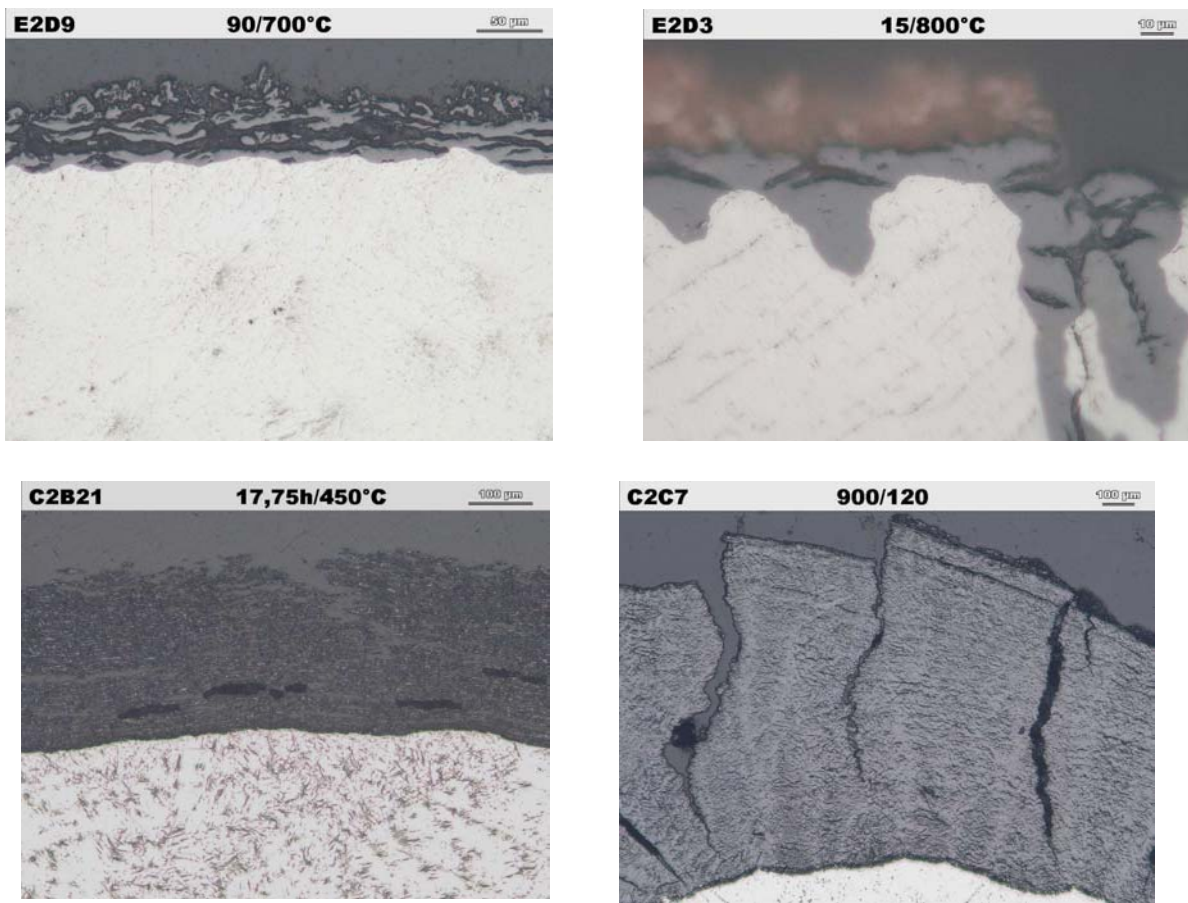


**Fig. 40:** Example of the oxide morphology grown on alloys E2\* and C2\*.

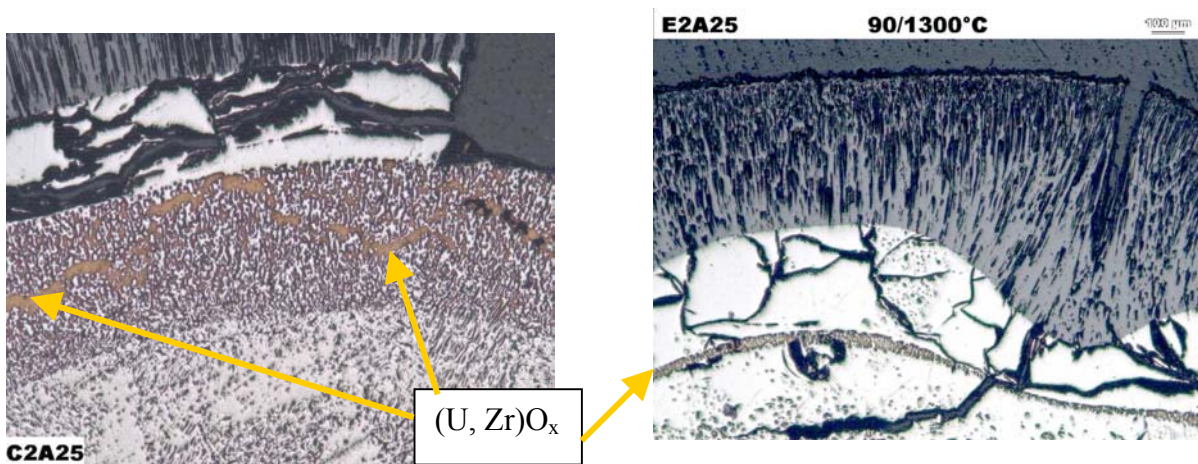


**Fig. 41:** Example of liquid phase (U, Zr)O<sub>x</sub> (in orange) that formed in the specimens near the oxide/metal interface.

### 3.7.2 ZrO<sub>2</sub> dissolution tests and oxidation of molten Zr-O mixtures (FZK)

#### Introduction

In order to facilitate the modelling of the oxidation of Zr-O and U-Zr-O melts planned in the WP7.2, it was agreed to use available FZK data on post-test examinations of molten materials oxidation in the CORA and QUENCH bundle tests, as well as to carry out new FZK tests on ZrO<sub>2</sub> crucible dissolution by molten Zry. These single-effect tests were specially designed for the investigation of long-term behaviour of the melt-ZrO<sub>2</sub> interaction considered representative of a melt oxidation process.

#### Thermal behaviour

Isothermal heating experiments at 2100 °C and 2200 °C and with annealing times up to 290 min were performed to study the dissolution of Y<sub>2</sub>O<sub>3</sub>-stabilised zirconia crucibles by molten Zircaloy-4 (Zry). The experiments should simulate the dissolution of steam-oxidised cladding surface layers by the molten Zry located between the ZrO<sub>2</sub> layer and the fuel pellet during a high-temperature transient of a severe fuel damage accident.

#### Materials

The tests were performed with crucibles of Y<sub>2</sub>O<sub>3</sub>-stabilised zirconia containing charges of as-received (oxygen-free) Zry. The crucibles were identical to those used in the AECL (Canada) tests (Ref.[12]) with yttria and wax binder contents of 7.9 wt% and 4.5 wt% respectively.

The tests were performed with two different values of surface to volume ( $S/V$ ) ratio ( $V$ : the melt volume,  $S$ : the ZrO<sub>2</sub> surface in contact with the melt). The initial weight of the Zry charge (cylindrical pellet of 6.2 mm diameter) was ~1.3 g for tests with  $S/V=770\text{ m}^{-1}$  and ~1.9 g for tests with  $S/V=720\text{ m}^{-1}$ .

#### Test procedure

The specimens were inductively heated by means of a tungsten susceptor in the LAVA furnace used also in the previous CIT project (Ref.[13]). In each test the furnace was evacuated several times and backfilled with high-purity argon. Then the specimen was slowly heated up (~1 K/s) to about 1650°C and kept at this temperature for about 3 min for thermal equilibrium. The specimen was then further heated to the desired test temperature with a heating rate of about 15 K/s. After the pre-determined annealing time the high-frequency generator was switched off and the specimen was rapidly cooled down.

The crucible temperatures were continuously recorded by a monochrome pyrometer and a W/Re thermocouple. The pyrometer, focused on the bottom of the tungsten susceptor through a quartz window in the furnace bottom, was also used as feedback device to a high frequency generator. A tungsten emissivity of 0.4 was used. The sheathed W/Re thermocouple was used for monitoring only. The distance between thermocouple and the upper edge of the crucible was about 10 mm. The thermocouple mainly heats because of radiation from the susceptor sidewall, therefore the thermocouple reading corresponds to the temperature of the outer side of the crucible wall.

The overpressure in the furnace was measured with a pressure transducer. The outputs of the temperature and pressure transducers as well as the generator power indication signal were fed into a computer-based data acquisition system and recorded at 0.3 s intervals. Plots of a temperature measurement are shown in Fig. 42. The test conditions are summarised in Table 14.

One can see from this table and the corresponding plots, that the temperature distribution in the furnace was inhomogeneous: the outer surface of the sidewall of the crucible was, for most tests, hotter than the crucible bottom. The inhomogeneity is due to the temperature gradient between the crucible wall and the melt losing heat by intensive heat radiation from the melt surface.

### Test results

The post-test crucibles were completely intact. There is the thin metallic coating on the outer surface of the crucible sidewall. The detailed SEM-EDX investigation shows the presence of  $\alpha$ -Zr(O) precipitates and many tungsten particles on the crucible surface. This is the result of the susceptor sublimation with the subsequent tungsten adsorption on the crucible surface.

A post-test metallography was performed. Three characteristic zones were observed across the crucible cross-section:

- a) the crucible wall with the  $\alpha$ -Zr(O) precipitates on the grain boundaries,
- b) the corrosion transition layer  $ZrO_{2-x}$  and,
- c) the refrozen melt.

The  $\alpha$ -Zr(O) precipitates along the grain boundaries indicates that oxygen diffuses to the melt mainly along the grain boundaries of  $ZrO_2$ . The transition layer between the melt and the wall crucible is formed after the cessation of the short-term wall dissolution phase and is the result of the boundary melt corrosion by the oxygen diffused from the crucible wall.

The tests can be divided into three characteristic groups: tests at 2100 °C, tests at 2200 °C with  $S/V=770\text{ m}^{-1}$  and tests at 2200 °C with  $S/V=720\text{ m}^{-1}$ . Figure 42 shows the cross-sections of some crucibles used with the measured values of the transition layer thickness. The group of tests at 2200 °C with  $S/V=720\text{ m}^{-1}$  includes the tests with a long time of annealing. The test FA10 of this group has a maximum test duration in isothermal conditions of 290 min and is characterised by the complete dissolution of the corrosion layer. Some cross-sections show the presence of relatively large voids in the melt. These voids can be interpreted as gas bubbles that formed at temperature with the tin vapour from Zr melt or with the oxygen not dissolved in the melt.

The quantitative image analysis of the melt region described in (Ref.[13]) was performed in order to determine the oxygen content in the melt. The corresponding results of this analysis as well as other post-test measurement results are summarised in Table 14. Individual measurement with the corresponding photographs of the melt structure are shown in Fig. 43. The comparison of the calculated oxygen content in the melt with the points of the liquidus line shows that all the test data lie in the two-phase region of the Zr-O phase diagram (melt with  $ZrO_{2-x}$  precipitates). With the oxygen gradient between solid state and melt, the oxygen content in the melt increases continuously and can reach the concentration that corresponds to a total melt oxidation. Ore information can be found in Ref.[14].

### Main outcomes

- Twelve experiments on the dissolution of  $ZrO_2$  crucibles by molten Zr have been performed
- Three stages of the process were observed:
  - the short-term phase of the crucible wall dissolution named “early dissolution” or “erosion”,
  - the medium-term named “corrosion phase” with oxide layer formation at the crucible-melt interface,

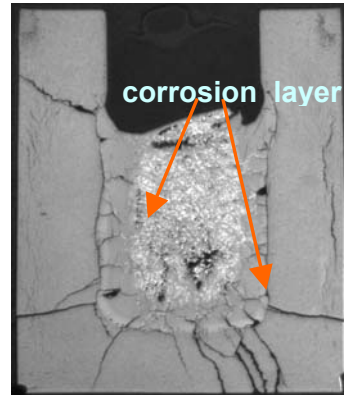
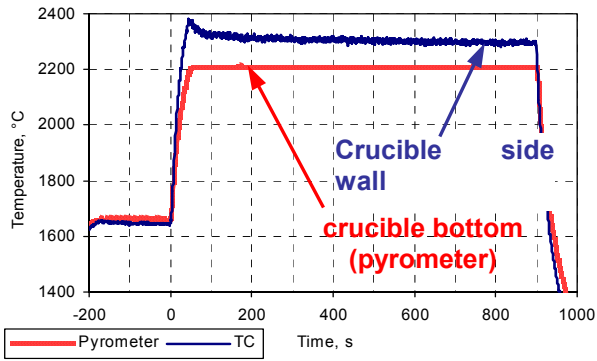
- the long-term phase of the repeated wall dissolution named “late dissolution” with the dissolution of the oxide layer formed in the previous phase.
- Two oxygen sources for the melt oxidation can be distinguished: the oxygen from the dissolved part of the crucible in the early dissolution phase and the oxygen continuously transported to the melt by diffusion from the surface of the grains of the ZrO<sub>2</sub> crucible matrix.
- The kinetics of the process was affected by an inhomogeneous temperature distribution in the system, i.e. the crucible walls were hotter than the crucible bottom and the melt.
- For all tests, the oxygen content in the melt at the annealing temperatures used corresponds to the two-phase region (liquid + ZrO<sub>2-x</sub> precipitates) of the Zr-O phase diagram.
- Some tests show the formation of gas bubbles in the melt. The formation of these bubbles was interpreted by the release of either the tin vapour from Zr melt or with the oxygen, which could not be dissolved in the melt.

This database was used for modelling the oxidation of molten Zr-rich mixtures in steam. (Task WP7.2) aimed at explaining the H<sub>2</sub> peak production during the quenching of degraded rods.

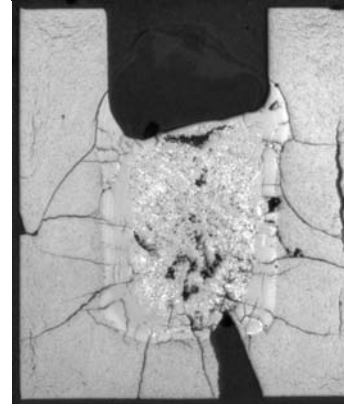
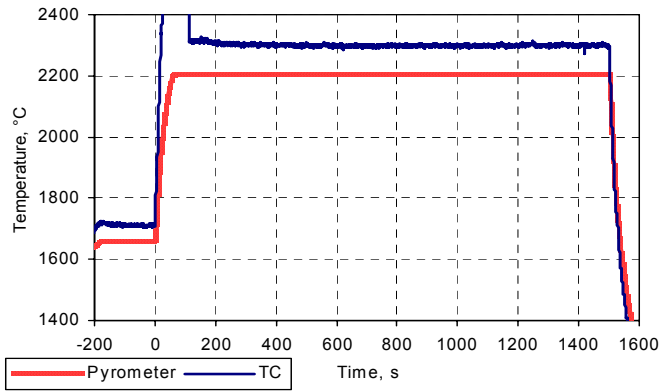
**Table 14:** Results of post-test analyses. (FA1-FA9: S/V ~ 770 m<sup>-1</sup>, FA10-FA12: S/V ~ 720 m<sup>-1</sup>)

Test No.	Pyromet. °C	TC °C	Time min	Probe weight change mg	Crucible wall dissolution, mm	Transition oxide layer mm	Image analysis of the melt					
							Ceramic %	Metal %	Pores %	Ceramic without pores, %	Oxygen wt %	Oxygen at %
FA2	2100	2100	10		0.22	0.97	38.9	49.5	11.6	44.0	14.5	49.1
FA8	2100	2100	15	-1	0.17	1.49	55.3	34.9	9.8	61.3	17.7	55.1
FA7	2100	2270	30	2	0.37	2.00	84.4	13.0	2.6	86.7	22.4	62.2
FA1	2100	2100	33		0.04	1.84	62.9	28.0	8.0	69.2	19.2	57.5
FA5	2200	2270	10	-4	0.32	0.99	70.2	21.1	8.7	76.9	20.6	58.3
FA9	2200	2290	15	-4	0.30	1.26	81.2	15.8	3.0	83.7	21.9	61.5
FA3	2200	2150	20		0.22	1.50	63.4	19.8	16.8	76.2	20.5	59.5
FA6	2200	2290	25	-2	0.24	1.01	86.8	5.7	7.5	93.8	23.7	63.4
FA4	2200	?	25	17	0.34	1.12	91.5	4.2	4.3	95.6	24.1	63.5
FA11	2200	?	75		0	1.69	81.0	11.2	7.8	87.9	22.6	62.5
FA12	2200	2200	200	-6	0.06	1.39	69.6	8.0	22.4	89.7	23.0	63.0
FA10	2200	2350	290	-37	0.71	0	85.9	2.1	12.0	97.6	24.4	63.1

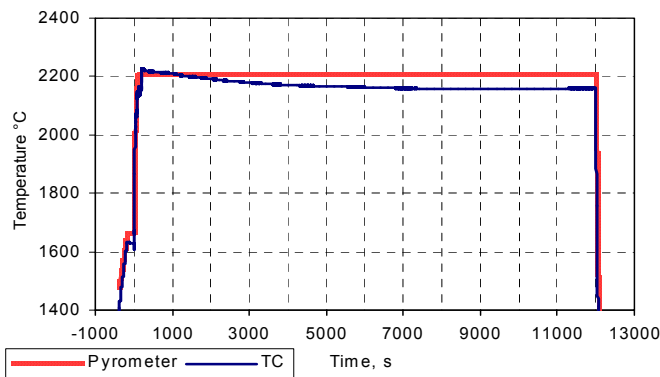
FA9:  $S/V=770 \text{ m}^{-1}$ , 15 min.  
Corrosion layer 1.26 mm



FA6:  $S/V=770 \text{ m}^{-1}$ , 25 min.  
Corrosion layer 1.01 mm



FA12:  $S/V=720 \text{ m}^{-1}$ , 200 min.  
Corrosion layer 1.39 mm



FA10:  $S/V=720 \text{ m}^{-1}$ , 290 min.  
Corrosion layer 0 mm

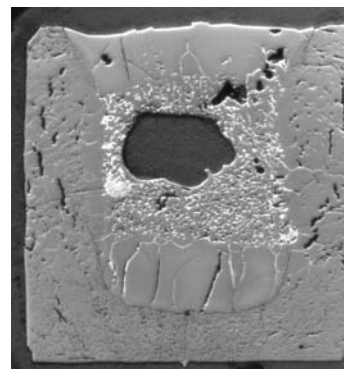
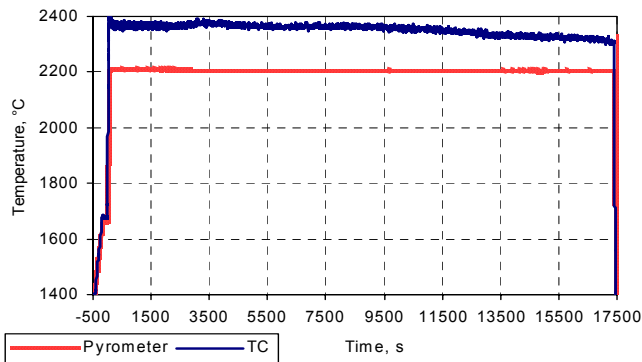
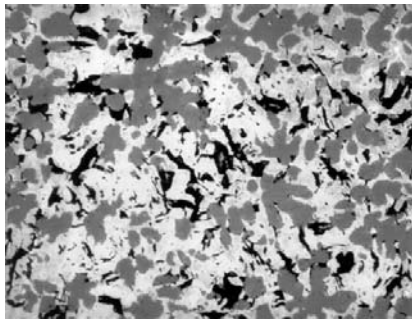
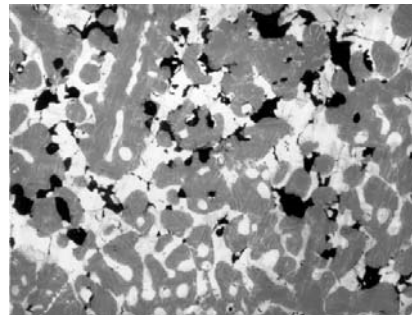


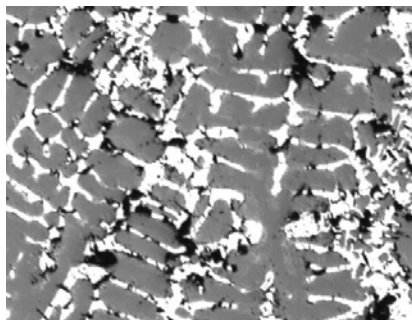
**Fig. 42:** Temperature tracing during the test at the crucible bottom temperature 2200 °C and cross sections of the post-test probes



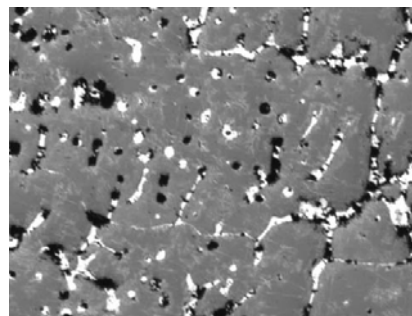
2100°C,  $S/V=770\text{ m}^{-1}$ , 10 min,  
oxygen 49.1 at%



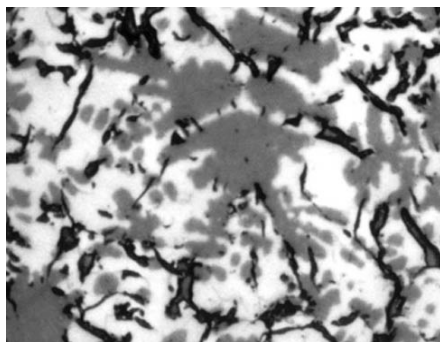
2100°C,  $S/V=770\text{ m}^{-1}$ , 33 min,  
oxygen 57.5 at%



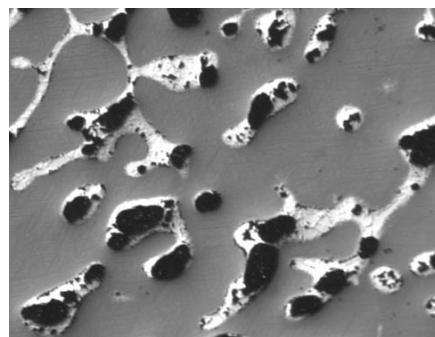
2200°C,  $S/V=770\text{ m}^{-1}$ , 10 min,  
oxygen 58.3 at%



2200°C,  $S/V=770\text{ m}^{-1}$ , 25 min,  
oxygen 63.4 at%



2200°C,  $S/V=720\text{ m}^{-1}$ , 10 min,  
oxygen 50 at%



2200°C,  $S/V=720\text{ m}^{-1}$ , 290 min,  
oxygen 63.1 at%

**Fig. 43:** Formation of precipitates in the melt. Results of image analysis for the oxygen content in the melt. Melt saturation conditions (content of the oxygen corresponding to the liquidus points): 45.3 at% at 2100 °C; 47 at% at 2200 °C.

### 3.8 WP3.2: Analytical support to tests on the oxidation of U-Zr-O mixtures

#### 3.8.1 Interpretation of the results with ICARE2 (IRSN - ALIAS CZ)

IRSN provided, in close cooperation with ALIAS CZ, support to ÚJP-PRAHA experiments on oxidation of U-Zr-O alloys (WP3.1) regarding both the experimental conditions and the composition of the tested alloys. ALIAS CZ carried out post-test calculations with the stand-alone ICARE2-V3mod1.2, compared the results with the existing database, improved the mixture oxidation model ZROX (see §4) and validated this improved model.

##### **Comparison of the U-Zr-O oxidation tests of ÚJP-PRAHA with the existing database**

The oxidation tests with U-Zr-O alloys below 1400 °C showed the following points:

- The oxidation kinetics in terms of weight gain (as well as the H<sub>2</sub> production) is always faster than that of pure cladding material.
- The oxidation obeys a parabolic law in those regimes where the oxide layer is adherent at temperature.
- The tendency to linear behaviour was observed below 900 °C mainly for the alloy rich in U and O due to pyrophoricity responsible of temperature escalations.

Tests were only carried out under isothermal conditions. No data were produced under controlled transient conditions.

The ÚJP-PRAHA weight gain data were approximated with both the parabolic and linear reaction rates and were compared with other available experimental data

Figure 44 shows that U-rich alloys oxidise significantly faster than the parabolic rates for Zr (Zircaloy-4) or Zr1Nb at temperatures below 1200 °C. Results are compared with the parabolic correlations available in ICARE2. At 1400 °C, the measured data for the U-rich 30U-65Zr-5O [wt%] alloy are in excellent agreement with the parabolic reaction rate for the 66U-30Zr-4O alloy measured by Prater-Courtright (Ref.[15]). However, the Prater correlation for mixtures cannot be extrapolated below 1400 °C. Figure 45 compares the linear behaviour of the 30U-65Zr-5O [wt%] alloy between 450-700 °C with the available data for U-Zr alloys and pure U in oxygen, air and CO<sub>2</sub>.

The Figure 46 shows that the original ZROX model underpredicts the oxidation of U-rich alloys (simulated in ICARE2 as the addition of Zr and UO<sub>2</sub> compounds), especially at temperatures below 1300 °C. The two options PROTECTI and EQUILIBR of this model gave the same results.

Figure 47 shows that with the ICARE2 model, the additional oxygen added in form of ZrO significantly reduces the further UZrO oxidation. The UO<sub>2</sub>-ZrO mixtures exhibit compared with UO<sub>2</sub>-Zr mixtures lower weight gain by a factor ~4.5 at 1300 °C to of ~250 at 700 °C. This calculated trend is obviously not correct.

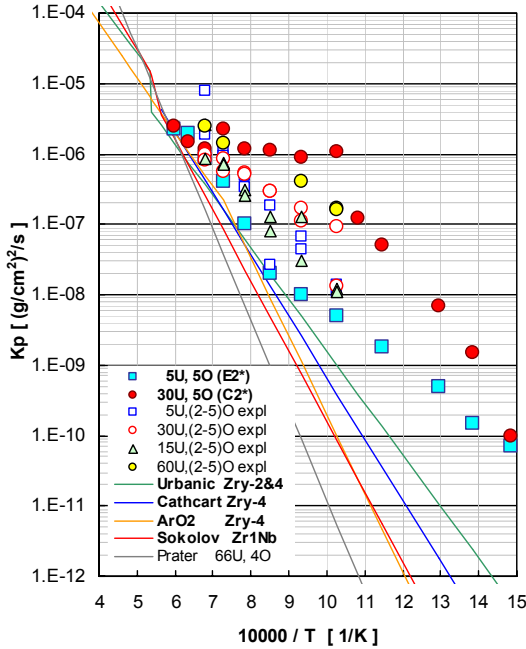


**Fig. 44:** Parabolic reaction rates: Comparison of the ÚJP-PRAHA data with Zry, Zr1Nb and the 66U-30Zr-4O alloy of Prater-Courtright.

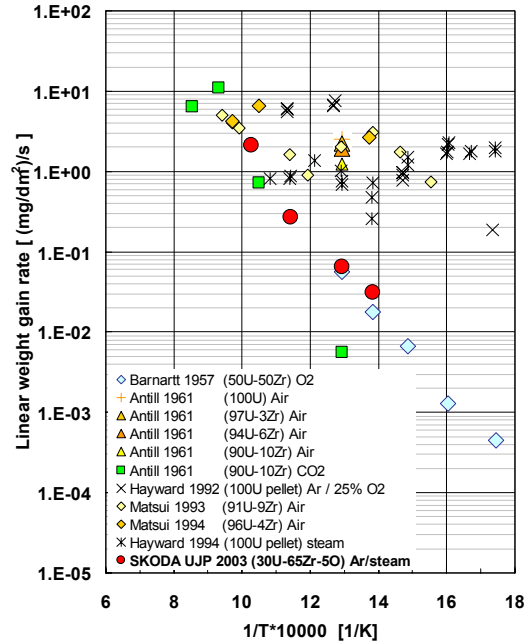


**Fig. 45:** Linear reaction rates: Comparison of the ÚJP-PRAHA data in Ar/steam with U-Zr and pure U oxidised in O<sub>2</sub>, air and CO<sub>2</sub>.

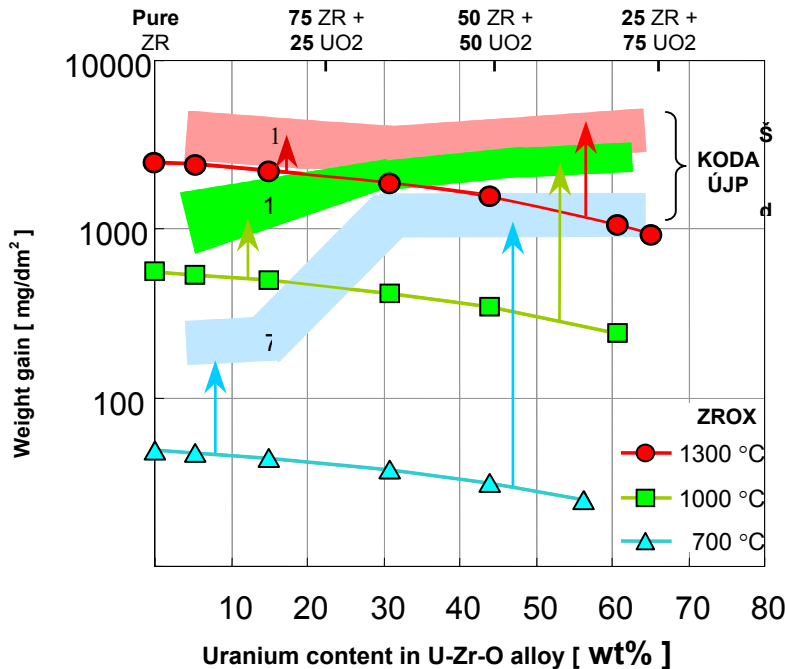


**Fig. 46:** Comparison between calculated oxidation of U-Zr-O alloys and experimental data after isothermal conditions during 600s.

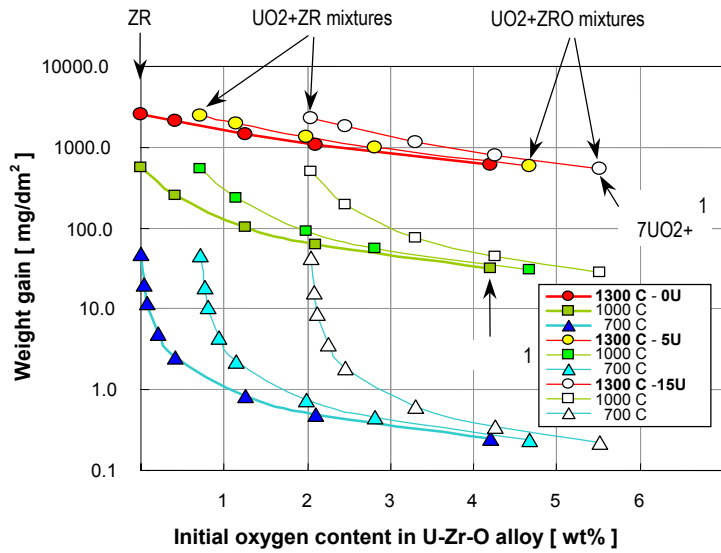


**Fig. 47:** Original ZROX model. Calculation of the weight gain versus oxygen content for three isothermal conditions (700, 1000 and 1300°C) during 600s

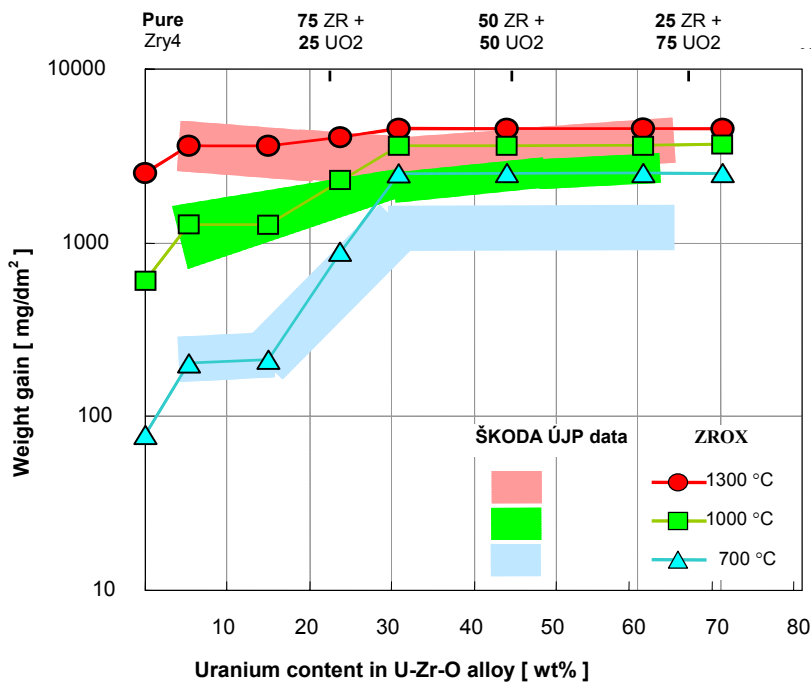


**Fig. 48:** Improved ZROX model. Comparison between calculated oxidation of U-Zr-O alloys and experimental data after three isothermal conditions during 600s.

The improved ZROX model (based on the ÚJP-PRAHA) data, see WP7.2 for details) considerably improved the code-to-data agreement (Figure 48). The improved model is conservative for U-rich alloys at exposure times  $< \sim 30$  min only.

### 3.8.2 Interpretation of the UJP-PHAHA results (RUB)

RUB/LEE provides an analytical support the experimental programme performed by SKODA-UJP (WP 3). A detail theoretical basis for high-temperature oxidation as well as for pyrophoricity has been provided for. Most important outcomes concern temperature escalation causes. The work is described in more details in Ref.[16].

#### Temperature escalation of U-Zr-O alloys

The temperature escalation can be understood as enhanced oxidation. In the Wagner theory, being the fundamental theory for high temperature oxidation, oxidation is mainly driven by transport of ions in a solid and compact oxide layer, which is enabled by defects in the solid structure, i. e. reactions at the surfaces are assumed to take place fast compared with the ions' movement. The transport can be described in terms of diffusion of charged particles. The driving force for transport by diffusion is the concentration gradient which is resulting from the reactions at the interface between the oxide and the atmosphere on the one side and between the oxide and the metal on the opposite side. The appropriate reactions are dissociation of molecular oxygen or steam and oxidation of the metal. Since oxidation is mainly determined by a diffusion process, the growth of the oxide layer ideally can be expressed by the common parabolic rate law. But for the U-Zr-O alloy, a deviation of the ideal law is likely to occur. This is mainly because the U-Zr alloy and the appropriate oxide most probably will not have a homogeneous structure as it is assumed following the Wagner theory for explaining the derivation of the parabolic rate law. Inhomogeneities are induced by the presence of two metals oxidising at different rates, hydrogen influencing the overall process, and different phases arising in the course of oxidation. Furthermore, the oxide is observed to have a porous structure influencing the mobility of the ions in it.

The oxidation processes described above do not necessarily lead to a temperature escalation. Here, it is reasonable to explain the latter with pyrophoric behaviour as it has been derived from post-test analysis. Accordingly, there are three necessary requirements for temperature escalation: Firstly, an ignitable material, referred to as the fuel, is needed. Secondly, an oxidiser has to be provided for as a reaction partner. Thirdly, a certain amount of heat is necessary for the reaction to start. Very often oxidation processes already can take place at very low temperatures. But since heat conduction or radiation lead to a heat transport away from the heat source, and this transport is increasing with increasing temperature, the temperature is not likely to rise above a certain level. Consequently, several additional conditions have to be fulfilled for temperature escalation.

The following factors have been proposed. First of all, the oxide phase is likely to contain the brittle species  $ZrO_2$ ,  $U_3O_8$ , and  $UH_3$ . Furthermore, a certain amount of gaseous hydrogen can be dissolved in  $\beta$ -Zr. If the surrounding temperature increases,  $\beta$ -Zr converts to  $\alpha$ -Zr and, thus, the hydrogen is released. The resulting pressure rise assisted by temperature gradients and phase changes in the solid is suspected to cause the embrittlement of the solid. Subsequently, metal and inflammable  $UH_3$  might come into contact with the oxidising gas, which in turn leads to further oxidation. Furthermore, heat transport by conduction is low because of the porous structure of the oxide. Looking at the experiments it can be assumed that the temperature escalation is closely related to the behaviour of uranium: In air the typical ignition temperature is just above  $500^\circ C$ , which corresponds to the temperature for which  $U_3O_8$  begins to powder at ( $535^\circ C$ ), while in steam the material starts to ignite between  $400^\circ C$  and  $500^\circ C$ , i. e. at the temperature, which  $UH_3$

decomposes to metal and hydrogen (435°C). As a first guess, it might be proposed that the decomposition of U<sub>3</sub>O<sub>8</sub> or UH<sub>3</sub> triggers the temperature escalation.

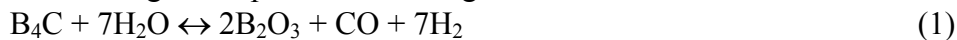
### **3.9 WP4: SETs on B<sub>4</sub>C and related analysis tasks (IRSN, FZK)**

Various types of nuclear power plants (high power PWRs, BWRs, Russian RBMKs and VVERs and the EPR) use boron carbide (B<sub>4</sub>C) as absorber material.

During a hypothetical severe accident the B<sub>4</sub>C reacts with the surrounding stainless steel cladding forming eutectic melts at temperatures above 1200 °C which is far below the melting temperatures of the single components. The remaining uncovered absorber pellets as well as the B<sub>4</sub>C-metal mixtures are exposed to the steam in the reactor core after failure of the control rod.

The oxidation of B<sub>4</sub>C by steam is highly exothermic and produces 6-7 times the amount of hydrogen as the oxidation of the same mass of Zircaloy. Furthermore, gaseous carbon- and boron-containing species are formed which may affect the fission product chemistry in the primary circuit, e.g. for the formation of organic iodine compounds from CH<sub>4</sub> formed in the cooler zones of the circuit.

The following chemical reactions are thought to play a role during oxidation of boron carbide according to the present knowledge:



Surplus steam then reacts with the liquid boron oxide to form volatile boric acids:



At the beginning of the project, it was recognised that the existing B<sub>4</sub>C database was not large enough for plant applications regarding effects on both corium behaviour and source term evaluation in case of a severe accident.

In particular, models in SA codes were either not validated or not available at all to evaluate the impact of B<sub>4</sub>C on, i) the degradation of the core, ii) the related production of H<sub>2</sub>, CO, CO<sub>2</sub>, CH<sub>4</sub>, B<sub>2</sub>O<sub>3</sub> and boric acids and iii) the effect of these gases or aerosols on the chemistry of FPs in the primary circuit. Especially for the temperature range above 1000°C -the temperature range relevant for SA conditions- the database was quite poor (Ref.[17, 18]).

To address this deficiency, two complementary programmes on B<sub>4</sub>C oxidation and B<sub>4</sub>C CR degradation were carried out by FZK and IRSN using different furnaces and conditions. FZK was using a thermo-balance (basic mechanistic studies using the mass signal) and the new BOX rig (furnace with a mass spectrometer to measure gas production) to carry out SETs on B<sub>4</sub>C oxidation. Additional tests on B<sub>4</sub>C CR degradation were also carried out in the QUENCH rig facility. IRSN did complementary tests on B<sub>4</sub>C oxidation using the VERDI inductive furnace. The initial experimental programme planned in the MADRAGUE facility with long B<sub>4</sub>C control rod tests could not be carried out due to unexpected difficulties and delays in the construction of a new furnace and was replaced by one additional FZK QUENCH test with a central B<sub>4</sub>C control rod (Ref.[19]).

### 3.9.1 SETs with VERDI on oxidation of B<sub>4</sub>C (IRSN)

Several B<sub>4</sub>C oxidation tests have been performed in the inductive furnace VERDI at Cadarache. Their objective was to provide data to validate and improve a boron carbide oxidation model which has been included in the ICARE 2 calculation code. These tests are also part of the preparation of the PHEBUS FPT3 experiment planned with a central B<sub>4</sub>C control rod. B<sub>4</sub>C samples studied are standard Framatome 1300/1450 PWR boron carbide pellets.

The experimental device has been designed in order to fulfil the following aspects:

- ensure a uniform oxidation of the lateral surface of vertical pellets,
- have a good control of the temperature and of the flowrate along the pellet,
- minimize the chemical interaction between B<sub>4</sub>C pellet and the ZrO<sub>2</sub> support.

The pellet is located between two fibrous ZrO<sub>2</sub> supports and is heated up using an iridium susceptor. One thermocouple located in the fluid channel at mid level of the lateral face of the pellet allowed the regulation the temperature (Fig. 49).

The experimental device was designed to minimise thermal gradients along the experimental section in order to avoid mechanical ruptures on the sample and surrounding structures and to have a good control of the power peak during the gas changes.

Experiments were carried out under isothermal conditions. All tests have been performed with the following scenario:

- a heat-up of ~15 K/min with argon flow up to the plateau temperature,
- a temperature plateau with a mixture of steam and argon,
- a cool-down of ~15 K/min in a argon flow.

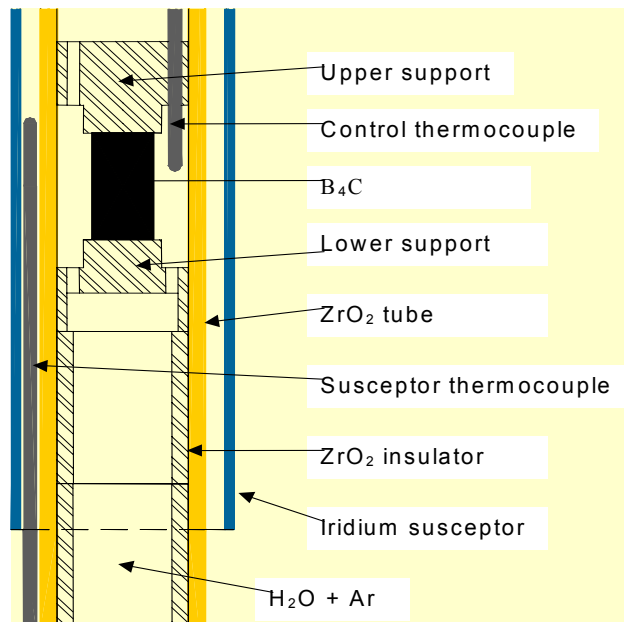


**Fig. 49:** Scheme of the VERDI inductive furnace

Tests have been realized with the following conditions:

- the range of temperature and the duration of tests are respectively 1200°C to 1800°C and 2.5 to 180 min,

- the total flow rates are in the range ~ 2 to 10 g/min and the steam partial pressure between 0.2 and 0.9 Pa.

**Table 16:** Test matrix with experimental conditions and main results. Hpp: high partial pressure, Lpp: low partial pressure

<i>Tests</i>	<i>Temperature (°C)</i>	<i>Time (mn)</i>	<i>Weight loss (%)</i>	<i>Argon flowrate (g/mn)</i>	<i>Steam flowrate (g/mn)</i>	<i>Partial pressure</i>
Hpp1	1200	20	22.84	1.25	5	0.9
Hpp2	1200	30	26.86	1.25	5	0.9
Hpp3	1200	10	1.47	3.57	6.43	0.8
Hpp4	1200	30	26.59	3.57	6.43	0.8
Hpp5	1200	60	43.81	3.57	6.43	0.8
Hpp6	1200	120	98.68	3.57	6.43	0.8
Hpp7	1200	90	46.62	0.89	1.61	0.8
Hpp8	1200	50	30.38	0.89	1.61	0.8
Hpp9	1200	20	11.48	0.89	1.61	0.8
Hpp10	1400	30	71.81	0.89	1.61	0.8
Hpp11	1400	20	47.34	0.89	1.61	0.8
Hpp12	1400	20	42.27	0.89	1.61	0.8
Hpp13	1400	10	26.74	0.89	1.61	0.8
Comparative test with FZK	1400	30	39.01	1.48	0.43	0.43
FZK test	1400	30	34-35	1.48	0.43	0.43
Hpp14	1600	15	94.28	0.89	1.61	0.8
Hpp15	1600	10	78.00	0.89	1.61	0.8
Hpp16	1600	5	44.44	0.89	1.61	0.8
Lpp1	1800	10	70	3.57	0.4	0.2
Lpp2	1800	5	37.9	3.57	0.4	0.2
Lpp3	1800	7.5	52.66	3.57	0.4	0.2
Lpp4	1800	2.5	22.06	3.57	0.4	0.2
Lpp5	1600	15	64.87	9	1.01	0.2
Lpp6	1600	10	55.02	9	1.01	0.2
Lpp7	1600	5	24.41	9	1.01	0.2
Lpp8	1400	60	84.1	9	1.01	0.2
Lpp9	1400	45	51.08	9	1.01	0.2
Lpp10	1400	30	25.62	9	1.01	0.2
Lpp11	1200	60	11.32	3.57	0.4	0.2
Lpp12	1200	60	9.70	3.57	0.4	0.2
Lpp13	1200	120	29.30	9	1.01	0.2
Lpp14	1200	120	19.58	3.57	0.4	0.2
Lpp15	1200	180	26.40	3.57	0.4	0.2

The Verdi experiments were mainly based on the measure of the mass change of the B<sub>4</sub>C pellet. Table 16 summarizes the test matrix and the experimental parameters. One test from the FZK programme is indicated for comparison purpose.

The mass loss of the B<sub>4</sub>C pellet is represented on Figure 50 versus time for different temperatures and partial pressures.

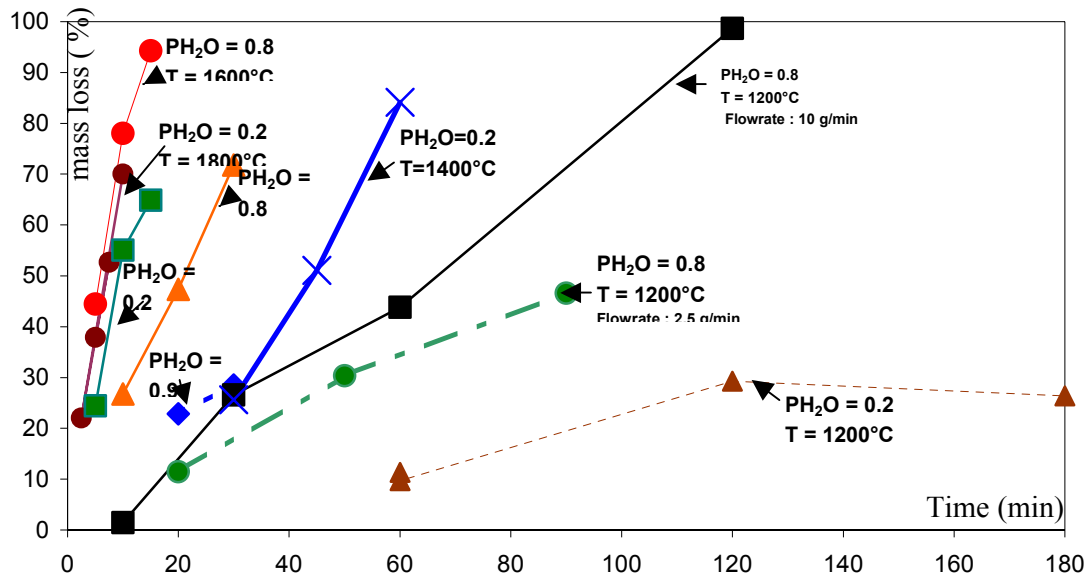


**Fig. 50:** B<sub>4</sub>C mass loss versus time for different temperature and partial pressure conditions

### Analysis of experimental results

Results indicated a large sensitivity of B<sub>4</sub>C oxidation to the temperature and to the thermal-hydraulic conditions as was evidenced also in the FZK tests (see next section on BOX rig and TG tests).

- In particular, for the same temperature and oxidised duration, the steam partial pressure effect was found to be a sensitive parameter whatever the temperature is as indicated on Figure 52.
- The influence of the total flowrate between 2.5g/mn and 10g/mn for the same temperature, steam partial pressure and oxidation duration was found to enhance the oxidation specially with tests performed at 1200°C and at the partial pressure of 0.8.

The boron carbide oxidation being a surface reaction, the oxidation rate depends on the formation of intermediate B<sub>2</sub>O<sub>3</sub> affected by two competing “formation and disappearing” processes. B<sub>2</sub>O<sub>3</sub> behaviour was found to be driven by mass transfer and consequently dependent on thermal hydraulic conditions. At temperature of 1600°C, the consumption kinetic (evaporation and chemical reaction with steam to form acid borid) of the boron oxide is very fast, so B<sub>2</sub>O<sub>3</sub> does not exist as a layer on the B<sub>4</sub>C pellet and cannot play a barrier to the B<sub>4</sub>C oxidation. On the contrary, at temperature of 1200°C, a liquid B<sub>2</sub>O<sub>3</sub> layer is expected to exist -in spite of evaporation and chemical reaction with steam- and can be a limiting factor of the B<sub>4</sub>C oxidation.

In the range between 1200°C - 1400°C it is more uncertain to evaluate the physical form of the boron oxide during the oxidation process. In this range of temperature, experimental results show that both the total flowrate and steam partial pressure have influence as indicated by tests at 1400°C,  $P_{H_2O}=0.2$ , total flowrate =10 g/mn and test at 1400°C,  $P_{H_2O}=0.8$ , total flowrate = 2.5 g/mn.

- From a material point of view, it would be interesting to model the physical way of evaporation of the  $B_2O_3$  compound. It has been observed  $B_2O_3$  drops on the surface of  $B_4C$  pellet after a cooling process but not a regular layer (Figure 51). The  $B_2O_3$  morphology on the  $B_4C$  pellet may influence the kinetic of boric oxide evaporation and reaction, the specific surface available for the oxidation being an important parameter during surface reactions.
- In SA conditions, the onset of  $B_4C$  oxidation occurs for temperatures greater than ~1300°C when the  $B_4C$  CR fails as evidenced by SETs and integral tests performed by FZK and AEKI. Main oxidation being expected above 1300°C, the liquid  $B_2O_3$  could then play a minor protective effect considering both its large vaporization and hydration -in particular for high steam partial pressure and total flowrate- and its downward relocation. This is of particular interest for modeling assumption purpose.

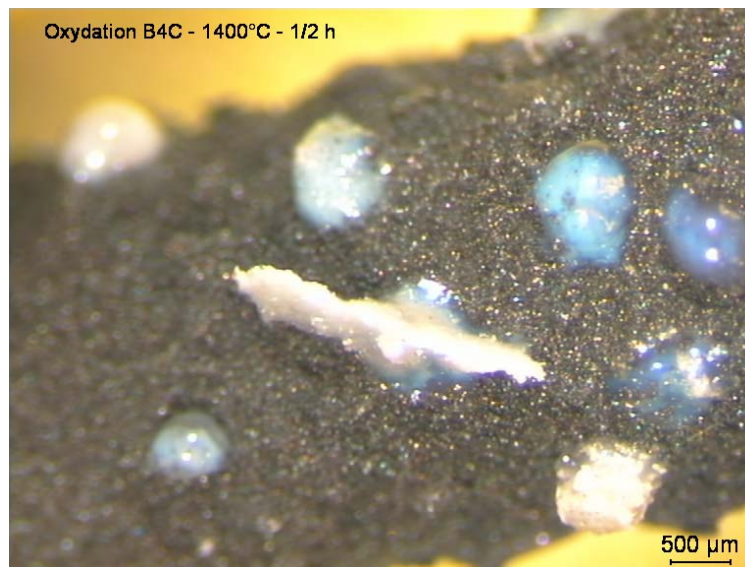


**Fig. 51:**  $B_2O_3$  drops on the  $B_4C$  surface after oxidation at 1400°C

At the end of the project, the Verdi experimental device was improved by the following new systems:

- a ventilation system to protect of the gas and boric aerosols product from the  $B_4C$  oxidation,
- a sampling system for the mass spectroscopy analyse.

Tests with these improvements were performed to calibrate the measurement of  $CO$ ,  $CO_2$ ,  $H_2$  and  $CH_4$  gases produced by the  $B_4C$  oxidation. In particular, conditions have been identified for measurements in good conditions. Future experiments are planned with these measurements.

## Main outcomes

A database was produced on the oxidation of Framatome B<sub>4</sub>C pellets bringing complementary results to the FZK database. The range of conditions was extended to higher temperatures and thermal-hydraulics conditions more representative of a power plant reactor (annular flow). In the common range of investigation results were found consistent with FZK results from the BOX rig tests (see comparison tests in Table 16).

- Results enable insights on the mechanisms of oxidation in particular in the temperature range of interest for severe accident conditions (after B<sub>4</sub>C control rod rupture above 1300°C).
- This database has been used for modelling and validation purposes regarding the B<sub>4</sub>C oxidation model of ICARE2 (see WP7). This analytical activity was performed in parallel with the VERDI programme enabling revised experimental and measurement conditions.
- Future experiments are planned after the project involving both pure B<sub>4</sub>C tests with the improved VERDI facility and long B<sub>4</sub>C-CR tests in the MADRAGUE furnace. In particular the spectrometer will be used to measure CO, CO<sub>2</sub>, H<sub>2</sub> and CH<sub>4</sub> gases produced by the oxidation of B<sub>4</sub>C.

### 3.9.2 SETs with BOX on oxidation of B<sub>4</sub>C (FZK)

#### Experimental set-up and specimens

An extensive test series on the oxidation kinetics of boron carbide was performed in the BOX rig. This experimental set-up, which was designed, constructed and put into operation within the first year of the project, consists of a sophisticated supply system for argon, hydrogen and steam, a tube furnace ( $T_{\max} = 1700\text{ °C}$ ) and a mass spectrometer for the analysis of the gaseous reaction products (Fig.52). The kinetics of the B<sub>4</sub>C oxidation is mainly evaluated using the hydrogen release rates. Further gases of interest are CO, CO<sub>2</sub>, CH<sub>4</sub>, and boric acids.

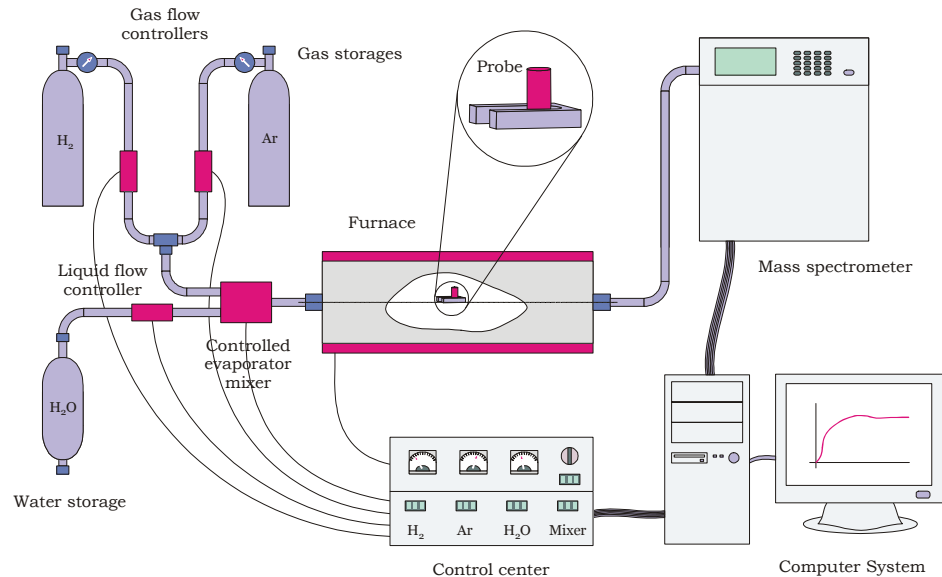


**Fig. 52:** BOX Rig for the investigation of the oxidation kinetics of B<sub>4</sub>C

Four types of B<sub>4</sub>C specimens with quite different microstructures were investigated:

- (1) Commercial pellets used in French 1300 and 1450 PWRs (Framatome),
- (2) Russian pellets used in the CODEX tests with B<sub>4</sub>C control rod (CODEX),
- (3) Dense pellets without open porosity obtained by Elektroschmelzwerk Kempten, Germany (ESK) and
- (4) B<sub>4</sub>C powder as formerly used in German BWRs and obtained by the same company (ESK powder).

### Transient tests

A series of transient tests with Framatome pellets was performed in order to get an idea on the reaction behaviour of B<sub>4</sub>C in Ar/steam and Ar/steam/H<sub>2</sub> in the temperature range between 800 and 1500 °C. Figure 53 shows a typical example of the gas release during a transient test.

The main gaseous reaction products from oxidation are hydrogen, carbon dioxide and carbon monoxide, as it is expected from equations 1 and 2. Methane was produced only to a very low extent at the beginning of the oxidation phase at the lowest oxidation temperatures. Taking the hydrogen release rate as a measure of the oxidation rate, one could recognise from Figure 53 a strong oxidation peak immediately after steam inlet. Then, the oxidation rate remains roughly constant during heat-up of the pellet up to temperatures of about 1200 °C. At higher temperatures the rate increases again. The first peak will be discussed later in the next section.

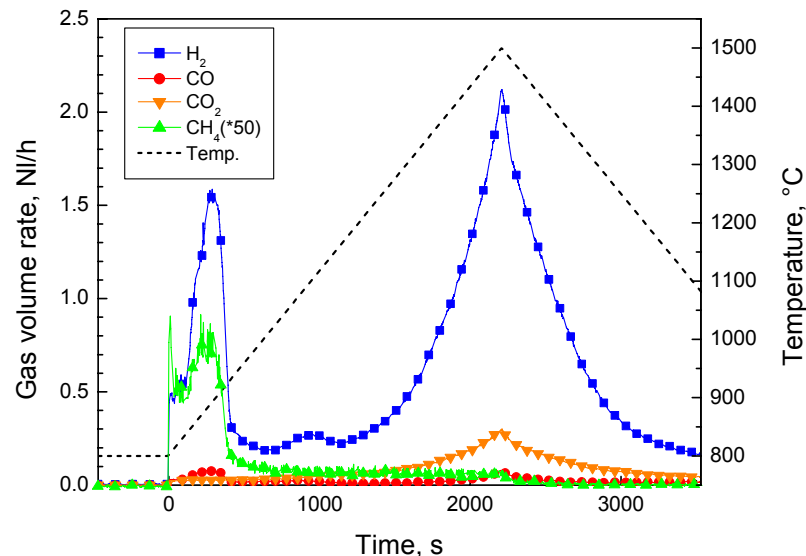


**Fig. 53:** Gas release during transient oxidation of a B<sub>4</sub>C pellet in flowing argon/steam atmosphere

Figure 54 illustrates the dependence of the oxidation rate on temperature in an Arrhenius diagram. This shows a complex behaviour caused by at least two independent mechanisms with the initial peak due to steam injection and an intermediate peak at about 1100 °C. An exponential Arrhenius type temperature dependence indicating thermal activation of the oxidation reaction is only established above ~1270 °C.

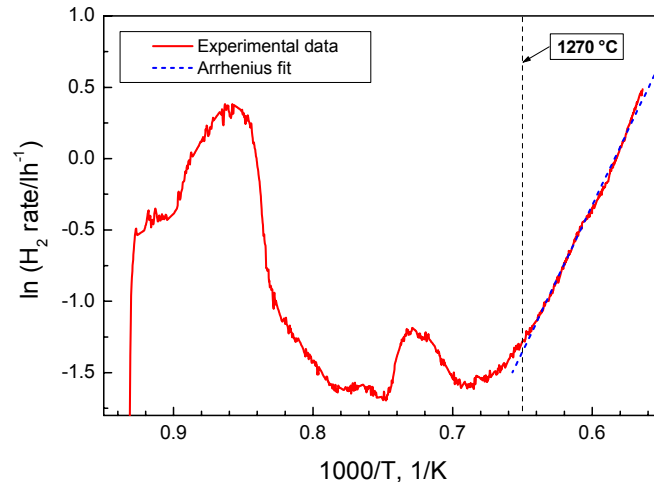


**Fig. 54:** Dependence of hydrogen release rate on temperature. Arrhenius plot

### Isothermal tests

More than 40 isothermal tests on the oxidation of  $\text{B}_4\text{C}$  were performed with different species under various boundary conditions. Most tests were performed for 30 minutes at temperatures between 800 and 1400 °C with a flowing argon/steam mixture resulting in a steam partial pressure of 42755 Pa (total pressure:  $10^5$  Pa). An automated procedure allowed comparing various tests with each other.

A clear tendency was seen for an increasing release of  $\text{H}_2$ ,  $\text{CO}_2$  and (to a less degree)  $\text{CO}$  with increasing temperature. On the other hand, the highest, but nevertheless very low  $\text{CH}_4$  production was measured at the lowest oxidation temperature. Besides the non-condensable gases some masses assigned to boric acids were measured by the mass spectrometer. Boric acids are products by the reaction of  $\text{B}_2\text{O}_3$  with steam believed to play a significant role in the overall oxidation kinetics.

The comparison of results obtained with the different  $\text{B}_4\text{C}$  samples offers interesting insights into the oxidation mechanisms at 1200°C. Figure 55 demonstrates that the initial  $\text{H}_2$  peak production is tightly correlated with the porosity of the sample. Large initial  $\text{H}_2$  rates are only observed for the porous pellets and the powder. A more or less constant oxidation rate is established soon and is, at least for the pellets, only dependent on the steam flow rate or more generally on the thermal hydraulic boundary conditions. Obviously, the porous specimens and the powder initially have a higher active surface leading to increased oxidation rates. The formed liquid  $\text{B}_2\text{O}_3$  fills or clogs up pores and afterwards only the geometric surface is available for steam access during the constant phase. For the powder it seems that the pores are not completely filled. During that phase, the oxidation rate is controlled by gas phase transport of the boric acids formed by the reaction of  $\text{B}_2\text{O}_3$  and steam or at higher temperatures ( $>1500^\circ\text{C}$ ) by direct evaporation of boron oxide.

These suspected mechanisms are also supported by the integral mass changes measured for all specimens shown in Fig. 56.

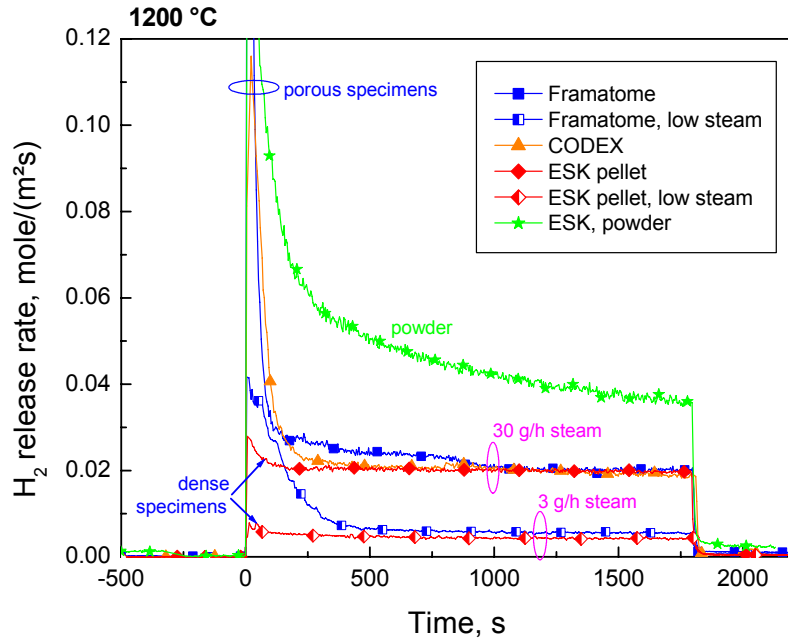


**Fig. 55:** Specific hydrogen release rates (\*) during isothermal oxidation of the various B<sub>4</sub>C specimens. Influence of porosity and steam flow rate.  
 (\*): referred to the geometric surface of the specimen

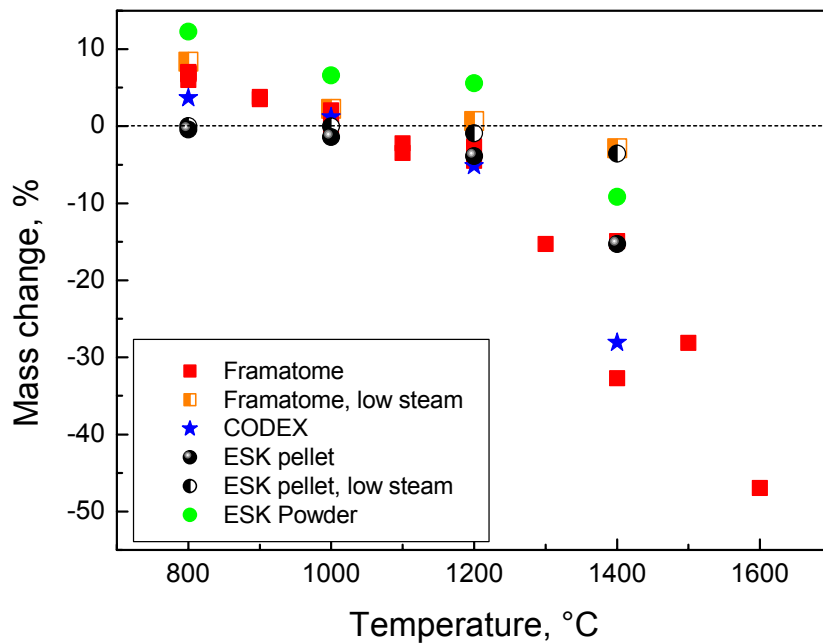


**Fig. 56:** Integral B<sub>4</sub>C mass change after 30 min oxidation in a flowing steam/argon mixture versus temperature. Time of tests with low steam flow was 60 min and 30 min in all other cases

### Tests under varying atmospheres

Some tests were performed under varying atmospheres to quantify the effect of gas/steam flow rates and composition on the oxidation kinetics and to investigate its influence on the off-gas composition. In particular, it was of interest to check whether the production of methane can be forced by atmospheres with a high content of hydrogen and thus low oxygen potential. Two tests were conducted with stepwise changes from pure steam (+Ar) to almost pure hydrogen (+Ar) atmosphere at 800 and at 1200 °C. The reduction of the steam flow rate led to a decrease of the carbon containing species CO, CO<sub>2</sub>, and CH<sub>4</sub>, thus indicating a decrease in the oxidation rate. The change in the oxygen potential did not significantly influence the relative composition of the off-gas, only the CO/CO<sub>2</sub> ratio increased initially with the hydrogen injection.

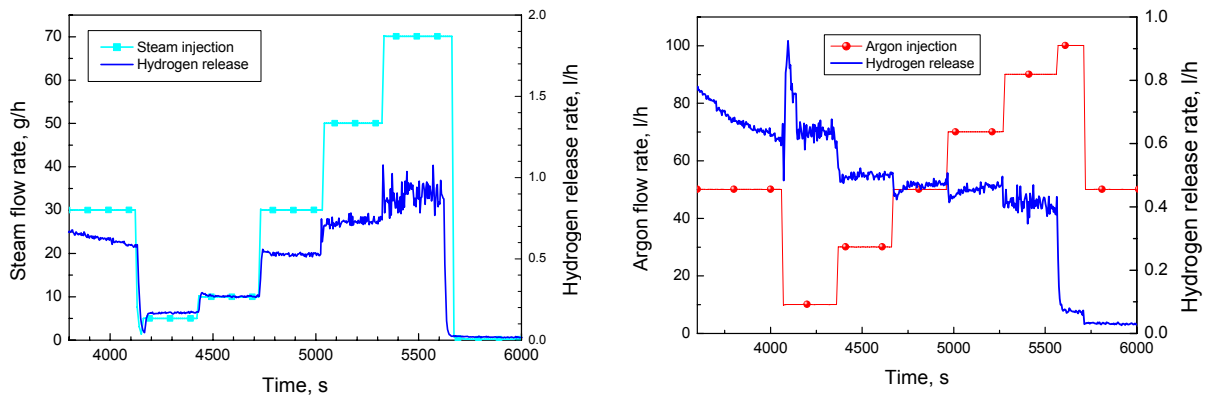


**Fig. 57:** Influence of steam (left) and argon (right) flow rate on the oxidation kinetics of B<sub>4</sub>C at 1200 °C

Figure 57 shows the results of two tests with stepwise changing steam and argon atmosphere. The increase of the steam flow rate by one order of magnitude (steam partial pressure 0.11→0.64 bar) enhances the oxidation rate by a factor of five. On the other hand, the increase of the argon flow rate by an order of magnitude (steam partial pressure 0.79→0.27 bar) causes a decrease of the oxidation rate by about 30 %. These results demonstrate that the oxidation rate of boron carbide is strongly influenced by the steam flow rate and by the steam partial pressure of the inlet gas mixture. These two parameters determine the local steam partial pressure at the surface of the specimen and therefore the oxidation rate.

### Comparison with literature data

Because of the strong dependence of the oxidation rate on the thermal-hydraulic boundary conditions the literature data on the oxidation of B<sub>4</sub>C considerably scatter and allow no direct comparison with each other. Figure 58 compares oxidation rates obtained in BOX tests based on the hydrogen release data during the plateau phase and referring to the geometric surface of the pellets with literature data. The FZK data usually were obtained at higher steam partial pressures and rates and are therefore above the mainstream of the data known from literature. The FZK data obtained at lower steam flow rates are more comparable with Sato's and Liljenzin's results. The equation for the dependence of the oxidation rate on temperature given in Figure 58 is only valid for the conditions of this test series (Framatome pellets in BOX rig) and must not be generalised.

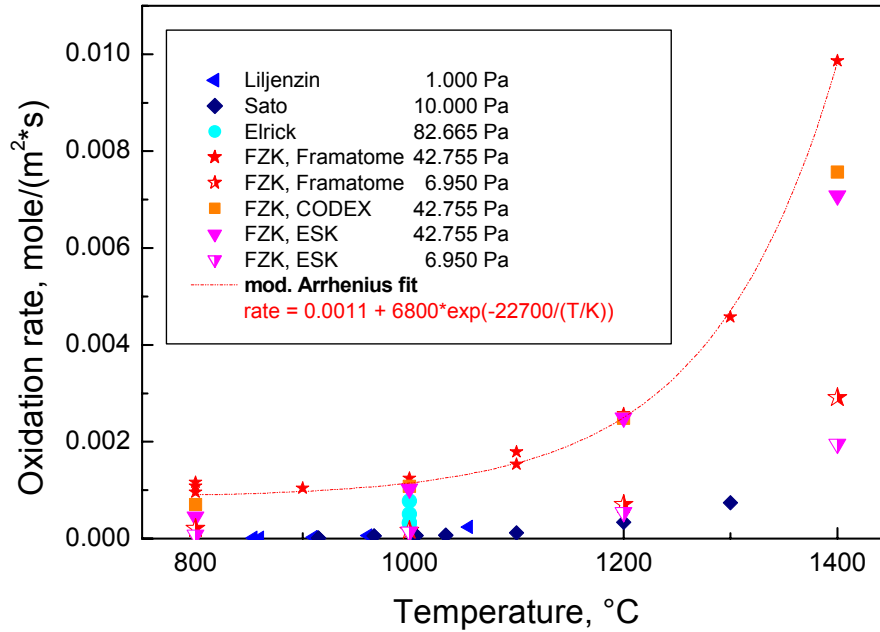


**Fig. 58:** Oxidation of B<sub>4</sub>C at high temperatures: comparison of recent FZK results with literature data obtained under different boundary conditions

### Main outcome

During the COLOSS program the understanding of the mechanism of the B<sub>4</sub>C oxidation has been considerably improved. A large amount of data is now available for model development and validation.

- The oxidation rate is strongly influenced by the thermal-hydraulic boundary conditions, especially by the steam flow rate and the steam partial pressure due to their effect on the formation of volatile boric acids and the transport of the reaction products.
- The properties of the B<sub>4</sub>C specimens have only a minor influence on the overall oxidation kinetics. The porosity of the specimen affects the oxidation rate at lower temperatures and at the initiation of the process by providing a larger surface.
- Surface reaction and gas phase diffusion determine the kinetics at higher temperatures relevant for severe accident conditions (T > 1300°C).
- Only negligible amounts of methane are released during high temperature oxidation of boron carbide. This has been confirmed by thermodynamic equilibrium calculations which gave considerable methane production only below 700 °C.

An open question is to which extent methane can be produced in the downward primary circuit by the gas mixture produced in the core by oxidation of B<sub>4</sub>C.

### 3.9.3 SETs on degradation of B<sub>4</sub>C control rod segments and oxidation of B<sub>4</sub>C-rich mixtures (FZK)

#### Specimens, experimental set-ups and procedure

Different kinds of samples were investigated:

- short, i.e. one-pellet-size control rod segments,
- longer 10 cm control rod segments and
- B<sub>4</sub>C/SS/Zry-4 absorber melts of different composition.

All materials investigated were commercial control rod materials used in French 1300 and 1450 PWRs. The tests with the small specimens were performed in the BOX rig and the longer control rod specimens were inductively heated in the single rod QUENCH rig. Transient and isothermal tests were performed. The specimens were heated up to 800 °C in inert atmosphere, then steam was injected at a predefined rate, and the temperature program was run either as a transient (20 K/min to 1500 °C) or as an isothermal plateau (usually 1 hour). The tests were terminated by changing the atmosphere from oxidising to inert before the final cool-down of the specimens. Post-test examinations were performed using light microscopy, SEM/EDX and Auger spectroscopy.

#### Pellet-size control rod segments

The degradation of the control rod is strongly dependent on the atmosphere. This was seen in two transient tests with short CR specimens between 800 and 1500 °C; one in inert and one in oxidising atmosphere. The specimen completely degraded in inert gas due to the eutectic interactions between B<sub>4</sub>C and stainless steel cladding as well as between stainless steel and Zircaloy-4 guide tube (Fig. 59) whereas the specimen heated up in steam/Ar atmosphere did not fail due to the formation of an external ZrO<sub>2</sub> scale. More information can be found in Ref.[20].



**Fig. 59:** B<sub>4</sub>C control rod segments after transient tests between 800 and 1500 °C. Left: in steam/Ar, right: in pure Argon atmosphere

In an isothermal test series the same kind of specimens were kept at temperatures from 800 to 1600 °C for one hour in steam/argon atmosphere. Up to 1000 °C, no interaction at all took place between the components. At 1200 °C, small interactions between B<sub>4</sub>C and SS as well as between SS and Zircaloy were observed. Significant melt formation was seen at 1300 °C and at

higher temperatures (Fig. 60). The steel cladding was completely dissolved during these tests and the  $B_4C$  consumption increased with temperature.

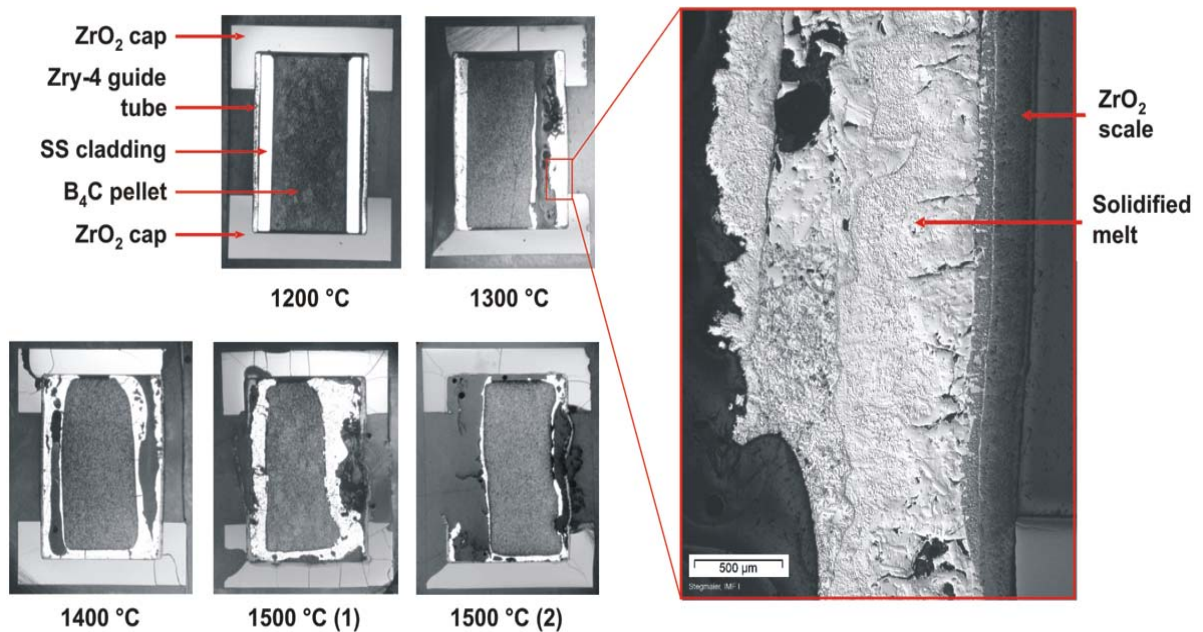


**Fig. 60:** Cross sections of short  $B_4C$  control rod segments after isothermal tests for one hour at the specified temperature

The formation of an outer  $ZrO_2$  scale prevented the specimens from early failure. During the tests at 1500 and 1600 °C the oxide shell failed accompanied by a strong formation of  $CO$  and  $CO_2$  and additional  $H_2$  release which increased by a factor of 30 (Fig. 61). The oxidation of the absorber melt and/or the remaining  $B_4C$  pellet was very rapid and even led to splashing of melts in the reaction tube.

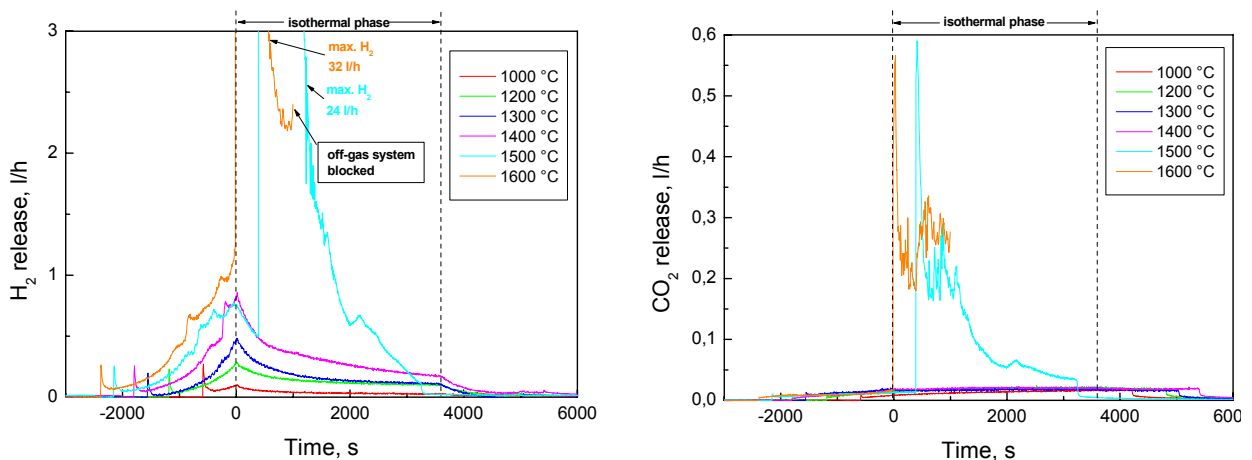


**Fig. 61:** Gas release during isothermal oxidation of short  $B_4C$  control rod segments

### 10 cm control rod segments

The longer specimens showed a similar behaviour. Additionally, axial relocation of the melt in the gap between boron carbide pellet and external oxide shell and local consumption of

the B<sub>4</sub>C pellets near the failure position was observed. The failure temperatures (when considerable amounts of B<sub>4</sub>C oxidation products were measured) were determined to be in the range between 1350 and 1500 °C.

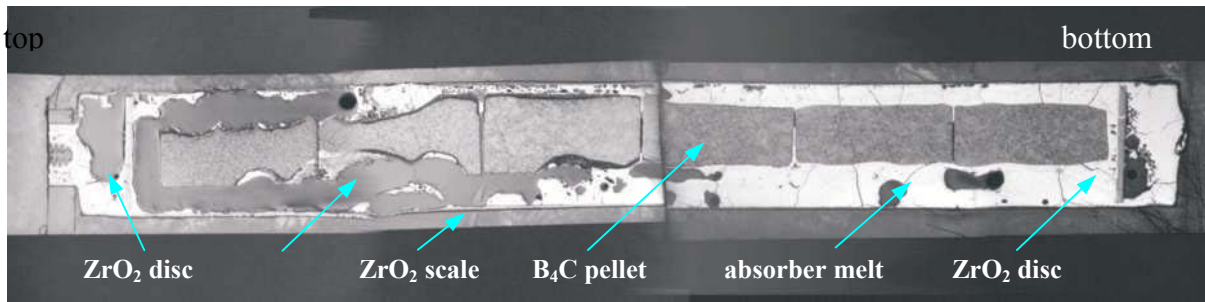


**Fig. 62:** Cross section of a control rod segment after transient oxidation up to 1580 °C in steam showing melt formation and relocation as well as local consumption of the B<sub>4</sub>C pellets near the position of the failure (left: top of the vertically tested specimen)

### B<sub>4</sub>C/SS/Zry-4 melts

Absorber SS/B<sub>4</sub>C and SS/B<sub>4</sub>C/Zry-4 melts of different compositions were produced in an inductive furnace at temperatures between 1800 and 2000 °C and oxidised in the BOX Rig. Figures 63 and 64 present typical results of these melt oxidation experiments. Separate-effects tests on the oxidation of melts confirmed the results obtained in the CR tests. Strong gas release was measured starting at temperatures below 1200 °C. The oxidation rate rapidly increased by more than one order of magnitude after (partial) melting of the samples. Oxidation rates are significantly larger than for pure materials and show strong scattering.

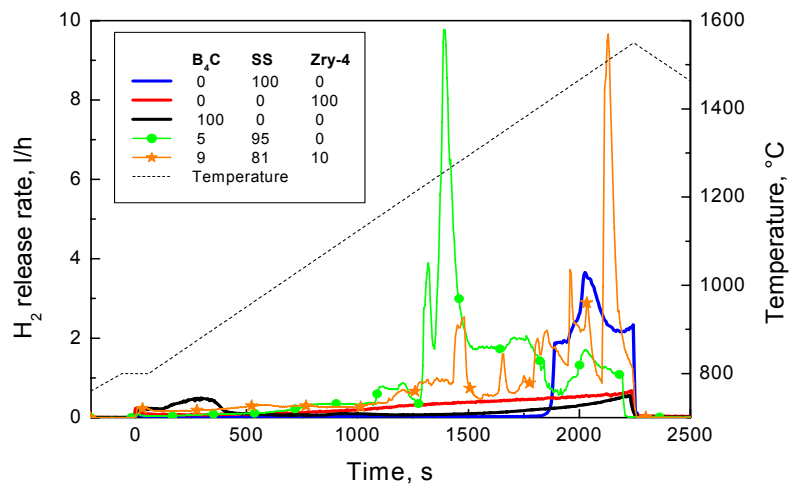


**Fig. 63:** Hydrogen release during oxidation of absorber melts in comparison with the pure components (compositions in wt%)

The post-test appearance of the crucibles and the reaction tube revealed splashing and fragmentation of the melts probably due to local reactions. Figure 63 shows the formation of loose, non-protecting oxide scales. B<sub>4</sub>C-rich melts involving Zr induced a chemical interaction

with the  $ZrO_2$  crucible. The aggressiveness of the melt towards the  $ZrO_2$  crucible under oxidising conditions increases with increasing complexity of the melt.

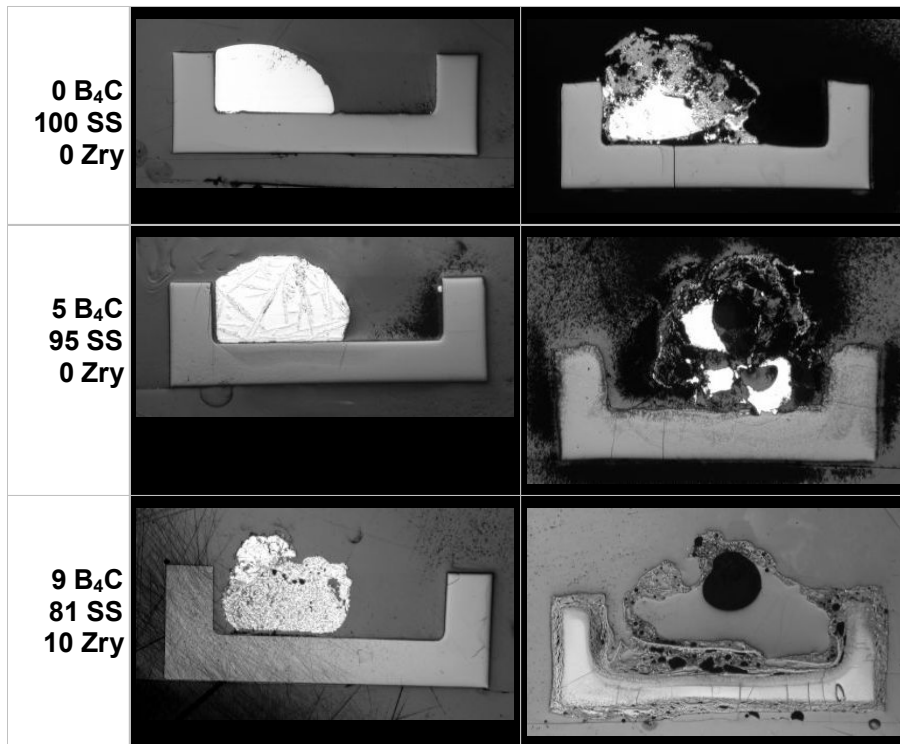


**Fig. 64:** Cross sections of selected absorber melts in  $ZrO_2$  crucibles after preparation (left) and after oxidation (right) stage

#### Main outcomes

The degradation of boron carbide control rods is strongly dependent on the atmosphere. In oxidising atmosphere, as expected to exist during a severe accident sequence, an external  $ZrO_2$  oxide scale at the guide tube prevents the control rod from early failure. Consequently, axial melt relocation initially occurs only inside the guide tube and the release of carbon and boron containing oxidation products is deferred.

- Rapid oxidation of both  $B_4C$  and absorber melt was observed after failure of the oxide scale at high temperatures.
- The oxidation kinetics of the  $B_4C$ -metal melts is significantly higher than that of the pure components and is a very stochastic process.
- The absorber melts are very corrosive towards the  $ZrO_2$  crucibles under oxidising conditions.

These results suggest that a  $B_4C$  control rod failure in a fuel element may cause early failure of surrounding fuel rods connected with release of fission products and relocation of  $UO_2$  containing melts.

### 3.9.4 Thermogravimetric SETs on $B_4C$ oxidation and analytical evaluation (FZK)

#### Context and objective

This complementary program of FZK based on thermogravimetric SETs consisted of both analytical experiments aimed at analysing the  $B_4C$  oxidation mechanisms and parallel modelling

work of the B<sub>4</sub>C oxidation based on detailed evaluation of test data concerning reaction kinetics. This experimental programme was well suited to understand the complex mechanisms of B<sub>4</sub>C oxidation and satisfy modelling needs (Ref.[21]).

The parameters for the TG test series were oriented on the requirements of the COLOSS project and on the demands for interpretation of the complex oxidation behaviour of B<sub>4</sub>C and evaluation of the test results by modelling. The test series included, besides the examination of B<sub>4</sub>C reactions in wet atmospheres (steam partial pressure up to 0.2 bar), tests in non-prototypical Ar/O<sub>2</sub> atmosphere as well as the examination of basic components as e.g. B<sub>2</sub>O<sub>3</sub> under different environment conditions. The advantage of the use of the thermal balance technique is the simultaneous measurement of sample temperature and mass changes in time dependence under transient as well as under isothermal conditions. The used atmospheres were pure Ar, Ar/O<sub>2</sub> and “wet” Ar (Ar/H<sub>2</sub>O). The TG-tests were performed in the temperature range 700 to 1300 °C. Planned tests at higher temperatures had to be withdrawn caused by technical restrictions resulting from necessary system modifications to prevent the TG unit from the highly corrosive B<sub>4</sub>C reaction products.

The parallel activity on modelling was launched to achieve a better understanding of the ongoing processes, to evaluate the produced TG oxidation data and to help comparing different and complementary tests, as TG and BOX tests. The benefit was a common interpretation and evaluation of the B<sub>4</sub>C oxidation.

### TG-tests conditions

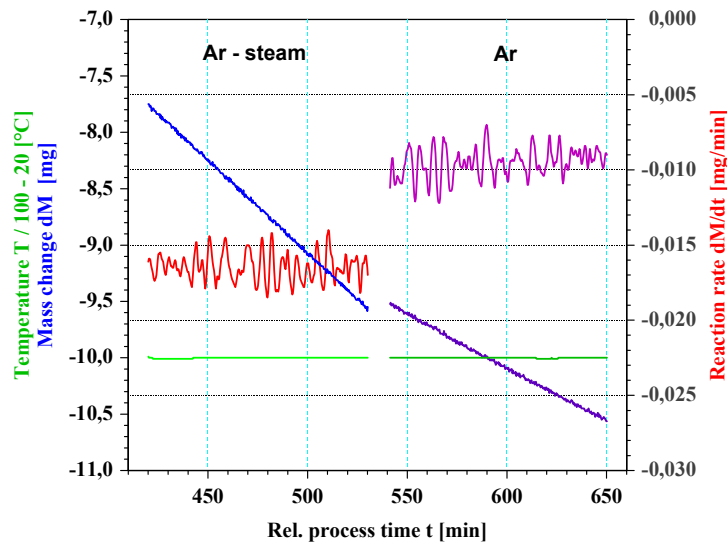


**Fig. 65:** Evaporation behaviour of B<sub>2</sub>O<sub>3</sub> for Ar-steam (evaporation in a wet Ar flow of 10 l/h p<sub>H<sub>2</sub>O</sub> = 12 mbar) and pure Ar atmosphere at 1000 °C (Ar flow of 10 l/h).

The TG test series included, besides the examination of B<sub>4</sub>C reactions in wet atmospheres (steam partial pressure up to 0.2 bar), tests in non-prototypical Ar/O<sub>2</sub> atmosphere as well as the examination of basic components as e.g. B<sub>2</sub>O<sub>3</sub> under different environment conditions. Most of the tests were performed with a heating rate of 20 K/min. The used atmospheres were pure Ar,

Ar/O<sub>2</sub> with a volume ratio of 80 to 20, and 'wet' Ar, realised by saturation in a water bath at temperatures between 20 and 60 °C.

### Basic reactions

Tests on the evaporation behaviour of B<sub>2</sub>O<sub>3</sub> were performed in the temperature range between 500 and 1300 °C under different flow rate conditions and steam concentrations. Tests were carried out using a thermal balance system (TG) with a direct recording of mass losses. Dried B<sub>2</sub>O<sub>3</sub> powder was used located into a Y<sub>2</sub>O<sub>3</sub> crucible with 1.11 cm<sup>2</sup> cross section. The investigations on B<sub>2</sub>O<sub>3</sub> evaporation were started using non-prototypical test conditions in Ar/O<sub>2</sub> atmosphere and then extended to experiments with Ar-steam atmospheres. In dry Ar atmospheres significant evaporation rates for B<sub>2</sub>O<sub>3</sub> were observed for temperatures higher than 800 °C. At the same temperature and same flow rates (e.g. 1000 °C, Fig. 65) evaporation rate is higher in wet atmospheres compared to dry ones.

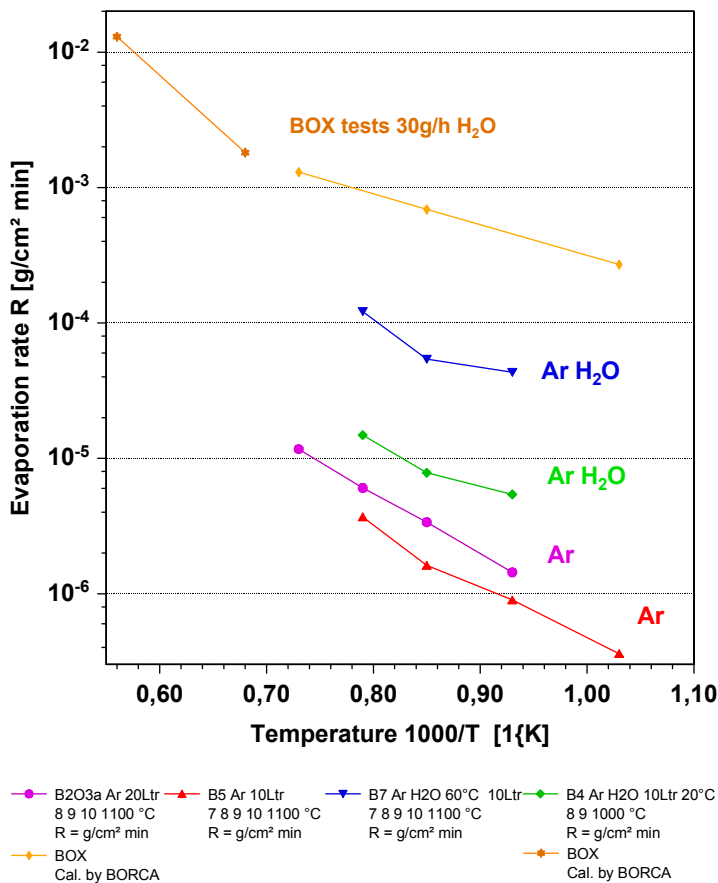


**Fig. 66:** Comparison of B<sub>2</sub>O<sub>3</sub> evaporation rates for TG and BOX tests.

The TG data were determined by direct mass-loss measurement whereas the BOX values were calculated from H<sub>2</sub> release rates. The TG data show clear dependencies on flow rate and steam concentration.

The temperature dependency is given in Figure 66. Additionally it can be seen, that evaporation rate of B<sub>2</sub>O<sub>3</sub> increases with Ar flow rate and H<sub>2</sub>O concentration. For comparison purposes evaporation rates of BOX tests, which were calculated from the measured gas release data but performed with much higher flow rates, are included in this figure. The global information of this comparison is that the slopes of the test series in the Arrhenius plot (at least in the low temperature region) are similar and higher flow rates and/or steam concentrations lead to stronger evaporation of B<sub>2</sub>O<sub>3</sub> or oxidation of B<sub>4</sub>C.

## Oxidation of B<sub>4</sub>C

Compared to Zr-steam oxidation reaction, the B<sub>4</sub>C oxidation behaviour is much more complex. The first B<sub>4</sub>C oxidation tests showed, that several oxidation mechanisms and phenomena occur at different regimes and exhibit various temperature, time and atmosphere dependencies. In order to facilitate the understanding of B<sub>4</sub>C oxidation the TG work-program was divided into the following separate topics:

- B<sub>4</sub>C oxidation tests with dense pellets,
- B<sub>4</sub>C oxidation tests with porous reactor-type pellets,
- Tests with the non prototypical Ar/O<sub>2</sub> dry atmosphere,
- Tests with Ar-steam mixture atmosphere.

The Ar-steam mixture was realized by passing Ar through a temperature controlled water bath.

Oxidation tests of dense (ESK) and porous (Framatome) B<sub>4</sub>C pellets were performed in the temperature range 800 °C to 1300 °C. At low temperature of 800 °C, the evaporation in Ar-O<sub>2</sub> is negligible, and the registered mass increase corresponds to the formation of B<sub>2</sub>O<sub>3</sub> reduced by C loss. The reaction rate was found to decrease with time due to the formation of B<sub>2</sub>O<sub>3</sub> as shown in Fig. 67. This behaviour indicates that a passivating scale is formed. Detailed analysis showed that the reaction kinetics is of parabolic type. In general, a similar qualitative behaviour was observed for porous pellets. However additional effects, which led to a double humped reaction rate curve (see Fig. 68), appeared in the short time test period. A possible explanation may be that a rearrangement of the liquid B<sub>2</sub>O<sub>3</sub> scale takes place due to pore filling processes.

At much higher temperatures (e.g. 1300 °C) it was detected that B<sub>2</sub>O<sub>3</sub> scales are flowing down and that the mass gain rate is constant. This means that after a certain test time a scale with constant thickness covers the pellet.

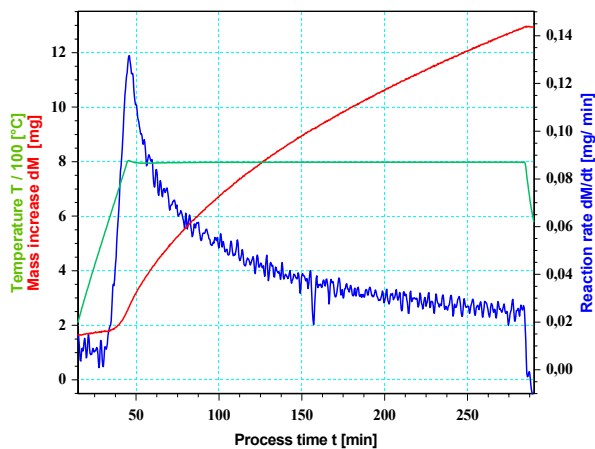


**Fig. 67:** Oxidation of a dense B<sub>4</sub>C pellet at 800 °C in Ar-O<sub>2</sub> atmosphere with an active surface of 5.7 cm<sup>2</sup>

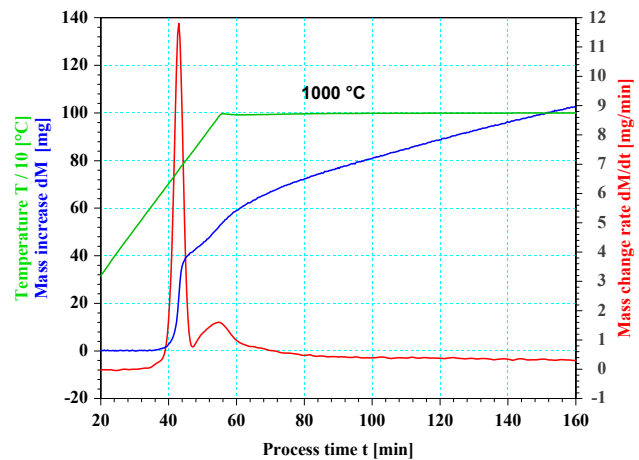


**Fig. 68:** Oxidation of a porous B<sub>4</sub>C pellet at 1000 °C in Ar-O<sub>2</sub>

As can be seen from Fig. 66 evaporation of B<sub>2</sub>O<sub>3</sub> in wet atmospheres is much higher than in dry atmospheres. By this fact a pronounced change in reaction behaviour was expected by switching over from dry to wet atmospheres.

At low temperatures (800 °C) for both types of dense and porous B<sub>4</sub>C pellets, a continuous mass increase was detected for several hours of test duration together with a decrease in reaction rate. At that test conditions, scale growth is dominating the oxidation process. Porous samples show a faster mass increase compared to dense samples. In the early stage of oxidation differences are very strong with reaction rate of porous pellets several times the rate of dense pellets as can be seen from Fig. 69. Afterwards reaction rates are similar. During the early stage, internal oxidation, oxidation of rough surfaces (= increased active surfaces) and pore filling by melt are responsible for faster oxidation.

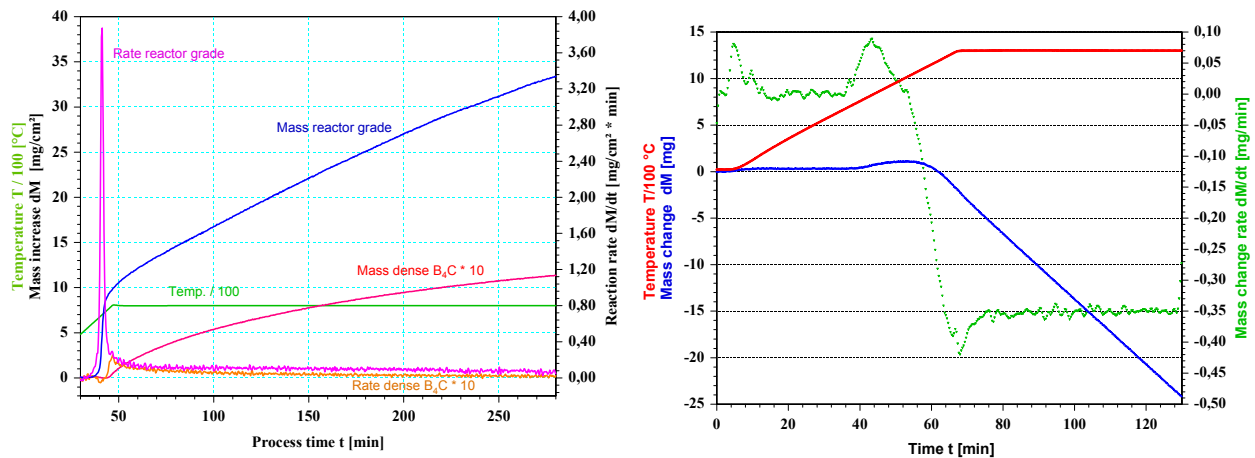


**Fig. 69:** Comparison of reaction behaviour for dense and reactor grade B<sub>4</sub>C at 800°C in Ar-steam (steam partial pressure 100 mbar) **Fig. 70:** Oxidation of B<sub>4</sub>C at 1300 °C in Ar-steam, flow rate 20 l/h, p(H<sub>2</sub>O)= 100 mbar

At higher temperatures and for intermediate times the general shape of mass curves change. In the beginning of the oxidation the mass increase is found corresponding with the formation of a protective B<sub>2</sub>O<sub>3</sub> oxide scale. Later, the total mass change decrease is due to mass losses by evaporation of B<sub>2</sub>O<sub>3</sub> scale. As can be seen in Fig. 70 the mass loss is constant under unchanged environment conditions (flow rate, temperature, gas composition). This is indicating that an equilibrium between B<sub>2</sub>O<sub>3</sub> formation and evaporation is reached.

The shape of TG curves imply that two main processes dominate the B<sub>4</sub>C oxidation. The first is formation of an oxide scale with parabolic kinetics and the second is evaporation of B<sub>2</sub>O<sub>3</sub> with a linear time dependence.

In further TG tests performed with varied flow rates and steam saturation levels of the carrier gas Ar it was found that reaction rate increases with higher flow rates and steam partial pressure.

## Model development

The aim of the TG tests on basic  $B_2O_3$  and  $B_4C$  oxidation interactions was to provide precise information which can be used to identify and separate  $B_4C$  typical reaction parameters and to introduce complementary test results (e.g. BOX-tests) into the data evaluation process.

Based on the TG observations a mechanistic model (Ref.[22]) was developed, which uses in the first approximation step a parabolic scale growth correlation for the formation of  $B_2O_3$  and a linear time dependence for the evaporation of  $B_2O_3$  or formation of boric acids under constant environment conditions. The total mass increase and/or decrease evolution observed in TG tests could be simulated by this model (Fig. 71).

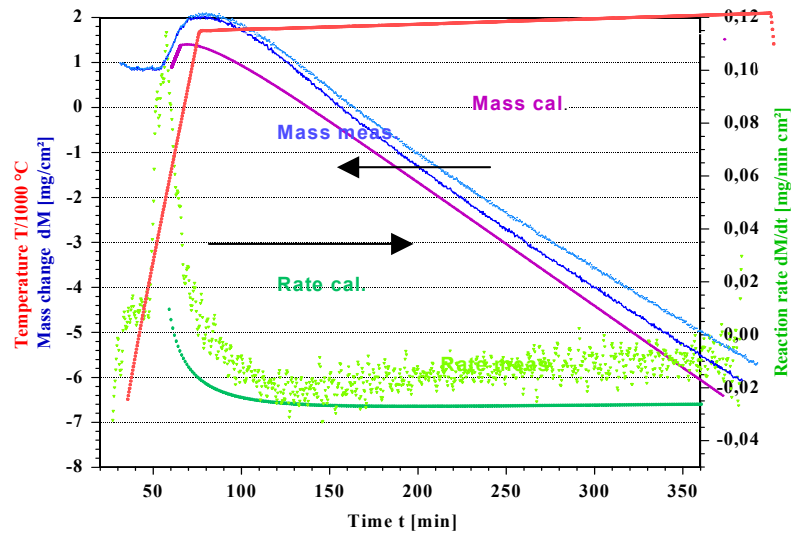


**Fig. 71:** Oxidation of dense  $B_4C$  at 1000 °C in  $H_2O$  saturated Ar at 60 °C. Comparison between test results and modelling.

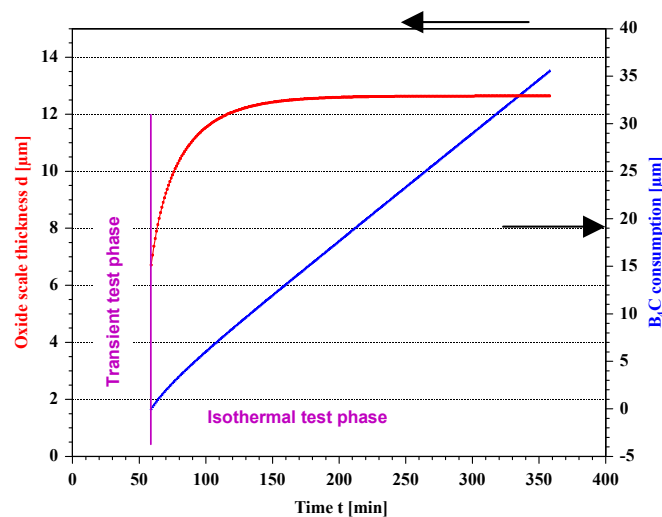


**Fig. 72:** Calculation of  $B_2O_3$  scale growth and  $B_4C$  consumption for  $B_4C$  oxidation of a dense pellet after transient heating in wet Ar atmosphere at 1000 °C. TG test are performed with a flow rate of 10 ltr/h Ar saturated by passing through a water bath of 60 °C.

Furthermore, the scale growth evolution and the B<sub>4</sub>C consumption (Fig. 72) can be predicted. By application of this model on BOX-test results it can be shown, that the assumed mechanisms are of general origin and are not test-equipment specific. From the H<sub>2</sub> release measured in BOX-test the B<sub>2</sub>O<sub>3</sub> evaporation rates could be calculated. The calculated values (inserted into Fig. 71 for comparison) are in good agreement with the measured TG values considering the higher flow rates and steam concentrations.

### **Main outcomes and future work**

The TG tests provided a database for interpretation of mechanisms occurring during B<sub>4</sub>C oxidation. Furthermore, thermo-dynamical reaction parameters (e.g. parabolic rate coefficient or activation energies) could be determined and different kinds of tests (TG or BOX tests) deliver a consistent picture. However, the quantification of the effects and parameters have to be seen as preliminary.

An extended verification process has to follow beyond the COLOSS project in order to define parameter values with sufficient accuracy. Additional modelling efforts are necessary to support data evaluation and to quantify effects of B<sub>4</sub>C oxidation as well as to integrate this knowledge into bundle test interpretation, code development and severe accident risk assessment.

### **3.10 WP5.1: VVER bundle test with a central B<sub>4</sub>C control rod (AEKI)**

The CODEX-B<sub>4</sub>C experiment was completed in May 2001 using an electrically heated VVER-1000 type bundle with a central B<sub>4</sub>C control rod. The experimental parameters were defined to simulate a severe accident conditions in a VVER-1000 type reactor. The main objectives of the test were to provide experimental data on the following points:

- the impact of B<sub>4</sub>C on the gas production (in particular H<sub>2</sub>, CO, CO<sub>2</sub> and CH<sub>4</sub>) and aerosols in conditions as representative as possible for a VVER-1000 reactor core under severe accident conditions,
- the impact of B<sub>4</sub>C on the degradation of surrounding fuel rods and structures.

### **The CODEX facility**

The current configuration of the CODEX (COre Degradation EXperiment) integral test facility represented the geometrical arrangement of a VVER-1000 reactor fuel assembly and has been constructed with VVER materials. The basic part of the facility was the test section comprising a bundle with seven rods of 600 mm heated length. The rods were arranged in hexagonal geometry (Fig. 73), the external diameter of the cladding being 9,13 mm. The six peripheral rods were electrically heated by tungsten bars. The 3,0 mm diameter bars in the heated rods were surrounded with ring-shaped UO<sub>2</sub> pellets - 3,6% enrichment of U<sup>235</sup> - and enclosed in prototypic Zr1%Nb alloy cladding. The central rod was a B<sub>4</sub>C control rod in steel cladding with Zr guide tube and was not heated.

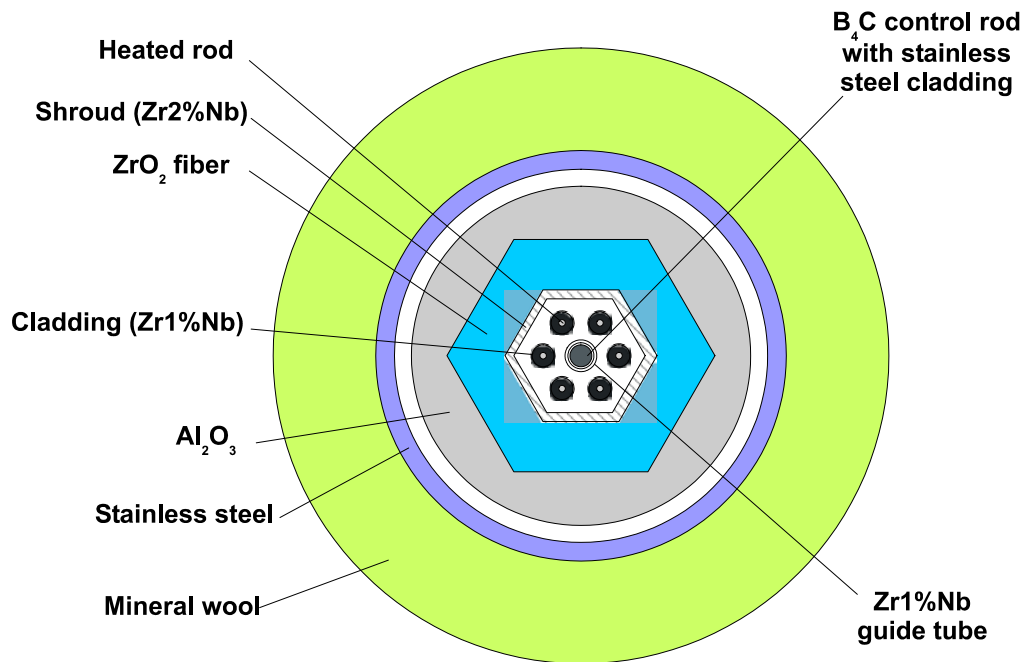


**Fig. 73:** Horizontal cross section of the CODEX-B<sub>4</sub>C bundle

In the standard configuration of the facility the steam generator and superheater section of the facility provide argon and steam inlet flow for the test section during heating-up and cooling-down phases. In the CODEX-B<sub>4</sub>C test very low steam flow rate was foreseen and for this reason direct injection of room temperature water into the superheater was applied with manual regulation. The steam generator was not used for steam supply. The coolant gas leaving the upper part of the test section flows through a steam condenser and enters the off-gas system with filters. The coolant cools down, the steam condenses and the water is collected at the bottom of cooler-condenser unit.

The gas concentration was measured in the off-gas system - behind the filters - using a mass spectrometer. The system was calibrated before the test and prepared for the on-line acquisition of H<sub>2</sub>, CH<sub>4</sub>, CO, CO<sub>2</sub> concentration in the Ar flow with 30 s scanning time.

In the CODEX-B<sub>4</sub>C experiment two laser airborne particle counters were applied. The aerosol sampling head of the nearer instrument was connected to the top of the facility using a ~0.5 m long copper tube. The outer sampling instrument was connected to the same point of the facility using a ~1.5m long copper tube. The sampling sites were connected to the top of the cooler, before the outlet gas entered the cooler tube section. Impactors for elemental analysis of aerosols were also connected to the upper part of the cooler.

*In-situ radiography* was applied in the test making use of X-ray source and imaging plates. The plates were moved into the view position at selected time periods in order to indicate the structural changes of the bundle during the test.

### **The CODEX-B<sub>4</sub>C test**

The commissioning test with the CODEX-B<sub>4</sub>C bundle showed the operability of the main technological systems and data acquisition. It included a stepwise increase of power up to a final peak value of 4 kW in inert gas atmosphere. The fuel rod temperature rose above 1100°C. The measured data were collected and used for the evaluation of heat losses.

The test conditions of CODEX-B<sub>4</sub>C experiment were selected on the basis of pre-test calculations to emphasize the role of the B<sub>4</sub>C control rod in the degradation process. The test included five main phases as indicated in Figure 74 and indicated below:

I. 0-13646 s: The preheating period to establish a stable temperature distribution (~600°C) in the bundle and in the test section without chemical interactions and core degradation.

II. 13640-15600 s: The power ramp period to simulate the heat-up of the bundle as a consequence of loss of heat removal from the reactor core and power production due to decay heat.

III. 15600-16830 s: The control rod degradation period with a temperature stabilization through the regulation of steam flow rate. Steam-starvation conditions were established in this period in order to create hydrogen-rich atmosphere and facilitate methane formation.

IV. 16830-17050 s: The bundle degradation period characterized by a temperature escalation was initiated without further power increase, only the coolant parameters were changed. Conditions at ~2000°C were reached in the upper part of the bundle for 2 minutes..

V. 17050-21705 s: The cool-down period was carried out with a slow cooling down in steam atmosphere during ~30 min. This last phase covered a wide temperature range and provided possibility for the investigation of gas production.

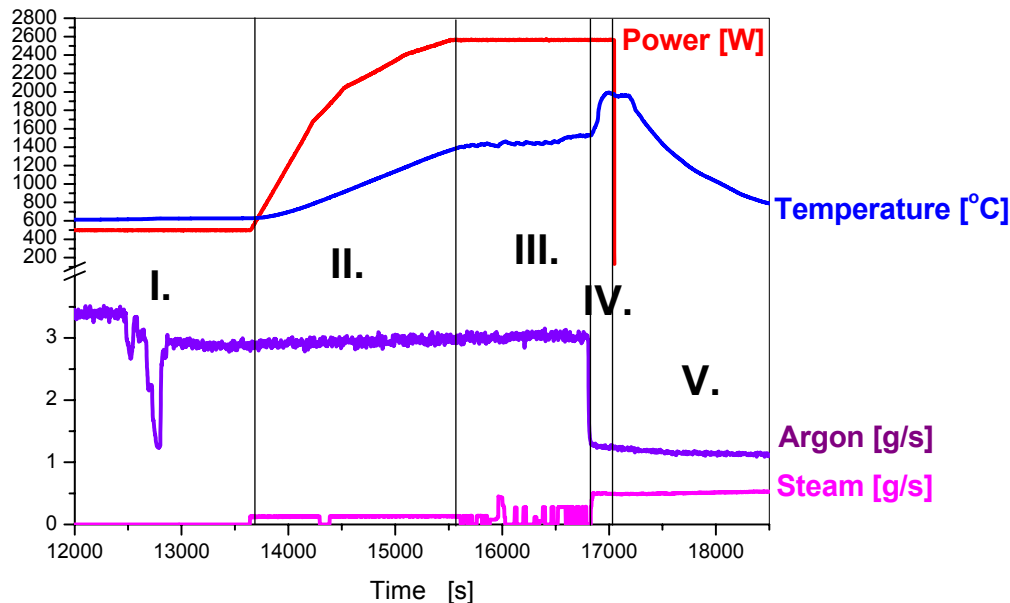


**Fig. 74** : Main phases of the CODEX-B<sub>4</sub>C test and power, temperature, steam and argon flow rate versus time.

The B<sub>4</sub>C CR steel-cladding started to melt and interact with the Zr1%Nb guide tube during phase III. The onset of B<sub>4</sub>C oxidation was detected at the end of this period. The gas measurement with mass spectrometer indicated hydrogen, methane, carbon monoxide and carbon-dioxide (Fig. 75).

Significant hydrogen production was seen as a common result of Zr and B<sub>4</sub>C oxidation in steam. The peak of hydrogen generation was related to the temperature escalation, the maximum H<sub>2</sub> production being ~40 mg/s and the total H<sub>2</sub> mass ~25 g.

A temporary heat-up was observed in the cool-down phase as a result of local oxidation in the upper part of the bundle.

The methane measurement showed very low values, practically below the detection limit. Both CO and CO<sub>2</sub> production was measured, the maximum production rate was 16 mg/s for CO and 4 mg/s for CO<sub>2</sub>. The integrated mass of CO and CO<sub>2</sub> showed that ~40% of the original B<sub>4</sub>C was oxidized during the test.

The two particle counters indicated high release of aerosols when steam was available in the coolant. The typical concentration of particles in each measured range was close to 10<sup>6</sup> particle/l. The oscillating behavior of the measured values was in direct correlation with the steam supply, which was in manual regulation mode (Fig. 76).

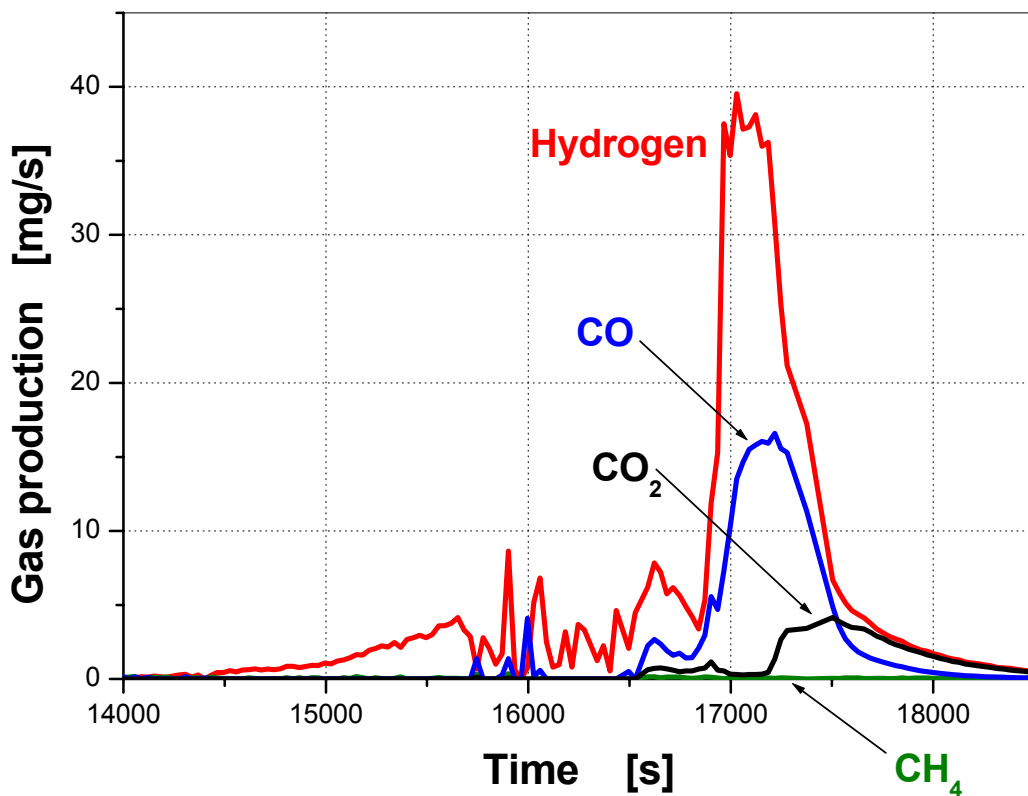
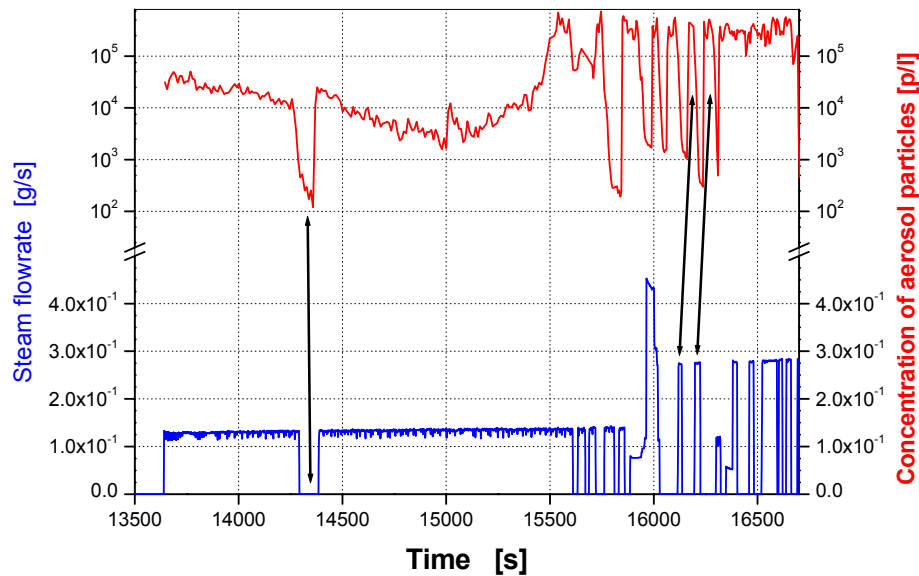
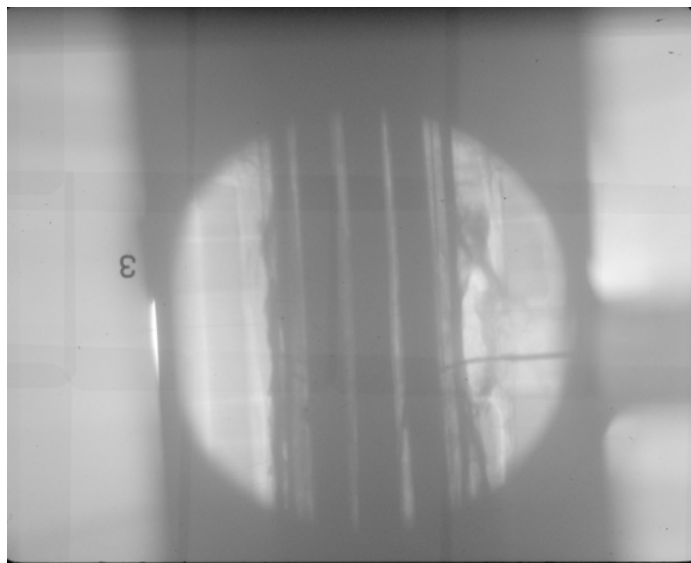


Fig. 75 : Gas flow rates in the CODEX-B<sub>4</sub>C test



**Fig. 76 :** Correlation between steam flowrate and aerosol particle concentration



**Fig. 77 :** In-situ X-ray view of the CODEX-B<sub>4</sub>C bundle at ~2000°C

### **Examination of the bundle**

The in-situ X-ray radiography during the test did not show structural changes up to 1530°C. The first degradation event observed at 1600°C was a small droplet of molten material moving down on a fuel rod side. The step by step degradation could be followed above 1800°C. At higher temperatures the heavy oxidation of Zr shroud was observed, the oxide scale was peeling off from its original position and a multi-layer structure was formed on the surface (Fig. 77)

The visual observation of the bundle after the experiment indicated strong degradation. In the upper part of the bundle the melting of the central rod produced some chemical compounds, which stuck together the rods. The external surface of the shroud was affected by heavy oxidation. The rods in the lower part were also oxidized and fragmented. In spite of being brittle

in the upper half the shroud could be removed easily from the bundle. After visual observation of the rods the shroud was put back to its original position and the structure was fixed with epoxy.

The post-test examination of the bundle started with X-ray radiography of the total bundle length. Horizontal cross sections were prepared and metallographic analysis was performed. Photos were made from the polished surfaces for studying the bundle degradation. The last step of examinations was the SEM analysis of samples taken from the melt in the central rod of the bundle.

Different bundle cross sections were made at 50, 75, 100, 125, 150, 175, 200, 235, 335, 410, 460, 535 and 555 mm from the bottom of the rods. As an example, the polished cross section at 335 mm elevation is shown in Figure 78. The cladding of heated rods is strongly oxidized and in some places fragmented. As regard the control rod it can be clearly seen, that the steel cladding has disappeared and the boron carbide pellet diameter has been substantially reduced.

The  $\text{UO}_2$  rods were kept roughly in their original position by the tungsten heater bars in the lower part of the bundle, while strong  $\text{B}_4\text{C}$  CR degradation took place in the central zone of the bundle. The guide tube of the control rod was completely oxidized in the upper part of the bundle, part of the failed guide tube showed internal and external oxide layers (Figure 79). In the upper part of the bundle the fuel rods were heavily oxidized and fragmented and some molten material could be observed between the rods keeping together the bundle (Fig. 80).

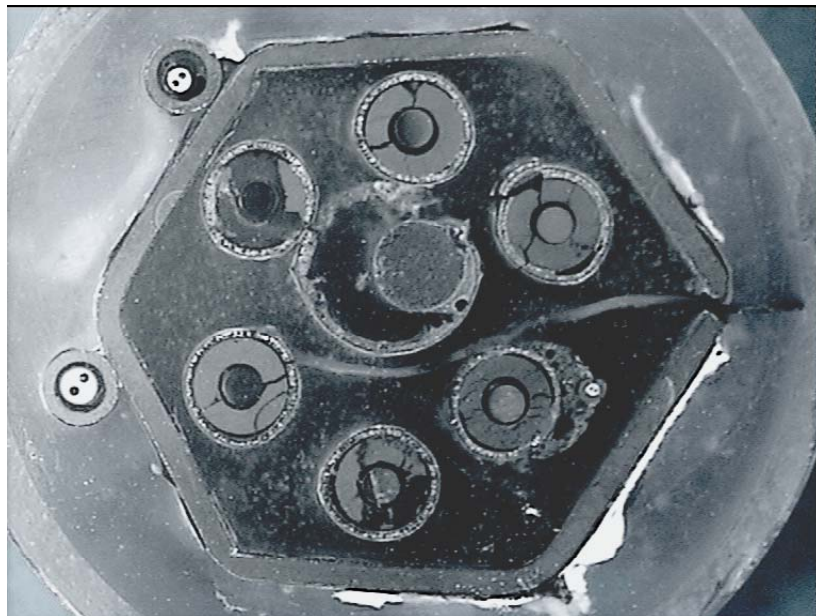


**Fig. 78 :** CODEX- $\text{B}_4\text{C}$  bundle cross section at 335 mm elevation

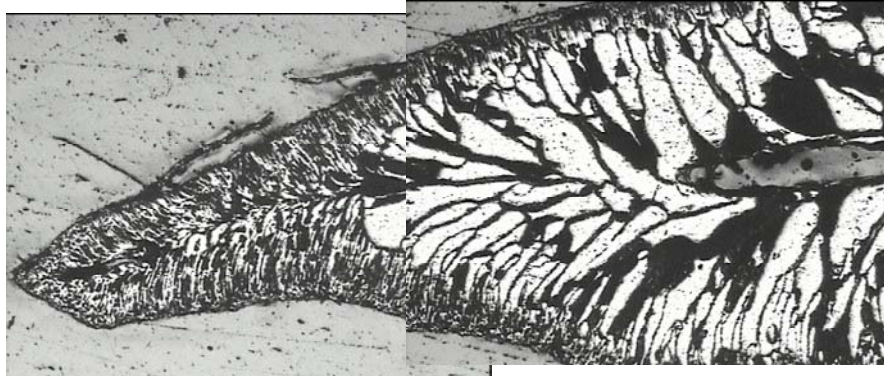


**Fig. 79** : Oxidized control rod guide tube at 410 mm elevation.

The oxide layer thickness on Zr alloy tubes has been determined by optical microscopy. Separate measurements were taken on each rod. Full oxidation of claddings has been found above the 410 mm level (Fig. 79).

The boron carbide remained in its original position below 335 mm. No boron carbide pellets can be seen in the elevations above this position, so ~45% of the original  $B_4C$  rod disappeared during the test. It is in good agreement with the results calculated from the released CO and  $CO_2$  content, which showed that ~40 % of  $B_4C$  inventory has been oxidized by steam. The volume of the melt in the lower part of the control rod was estimated on the basis of metallographic examinations as  $\sim 3.5 \text{ cm}^3$ . At 235 mm the melt almost completely closed the gap between the  $B_4C$  CR and the guide tube.

Iron-oxide containing red melt was seen between the fuel rods, forming blockage in the channels and fixing the rods to each other. This *sticking effect* was not observed in earlier CODEX tests without large steel components in the bundle and in which more intense fragmentation was seen.



**Fig. 80** : Oxidized control rod guide tube at 535 mm elevation.

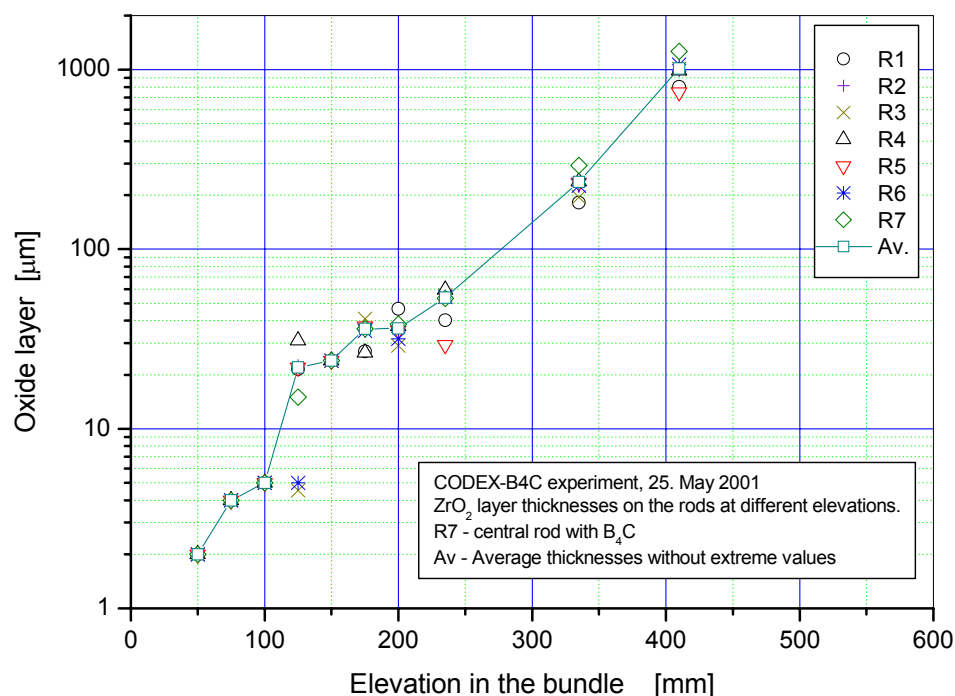


**Fig. 81:** Rod average oxide layer thickness on zirconium cladding as function of bundle elevation

Small size samples (filings) were taken from the gap between the control rod and guide tube, where molten material was observed at lower elevations. The results of control rod melt measurements, showed that the melt in the gap between the guide tube and control rod contained mainly Zr and some stainless steel components. High content of steel components was found in the sample taken from the upper part of the bundle. No boron content was detected in the melt.

#### Examination of aerosol samples

Aerosol samples were taken during the test using 10 impactors. Two-stage impactors were used in the experiment, which had two collector plates and one quartz fiber filter. The two plates were analysed by scanning electron microscope, while the fiber filter was used for spark source mass spectrometry. Besides the impactors an impaction plate made of nickel was also applied for aerosol collection. After the experiment about 10 g light blue deposits was found on the top plate of the outlet gas cooler. Therefore the following types of aerosol samples were studied:

- collector samples,
- filters,
- Ni impaction plate,
- deposits on the top of the cooler.

Mass spectrometer analysis of deposits on top of cooler indicated that it contained mainly boron (75 % boric acid, 1 % Zr, 0.7% Fe, 0.5 % Al, 0.2 % Si, and 0.2 % W). Large part of deposits on the impactor filters was boron compounds, certainly  $\text{HBO}_2$ .

40 mg U was measured in the precipitate and 0.1 mg U on the Ni plate. The integrated values of the U content in the outlet gas was estimated as 0.008 mg, considering the U content on

the impactors, the total flowrate and the operating period of impactors No. 7-8-9. According to the above values most of the released U deposited on the cooler surface (~500 °C) and only very small amount reached the room temperature impactors and the environment.

Uranium was found on collectors by scanning electron microscopy. U deposits are characterized by individual particles with a size varying between 1 and 10 µm. The smaller U-rich particles had globular shape, while the larger ones were elongated. Their length was in the range of 5-10 µm, while the width was about 3-5 µm. Typical U-rich particles are shown in Fig. 81.

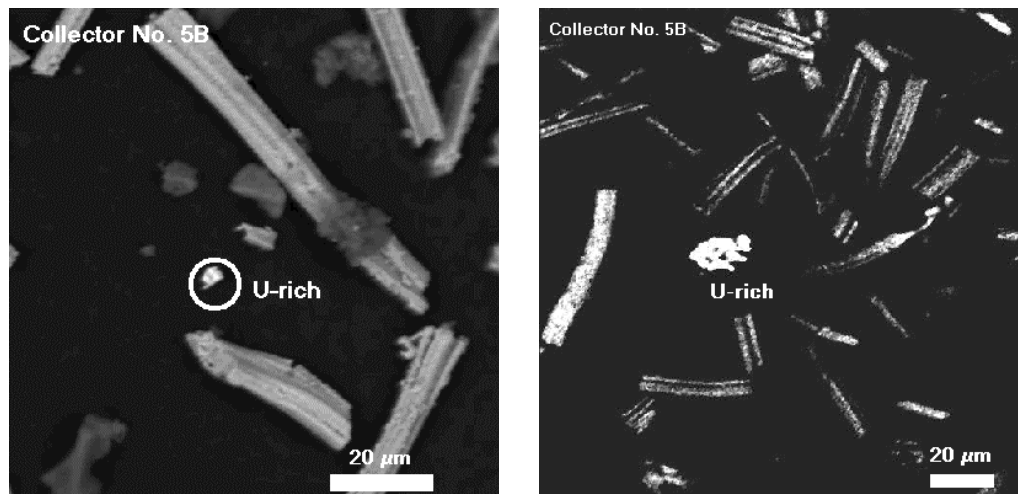


**Fig. 82 :** U-rich particles detected on collector plates

### **Main outcomes**

The CODEX-B<sub>4</sub>C experiment provided important information on the behavior of VVER-1000 fuel and control rods under severe accident conditions. The low temperature control rod degradation period was extended in order to produce more details on the degradation process.

The B<sub>4</sub>C CR steel-cladding started to melt and interact with the Zr1%Nb guide tube during phase III. The onset of B<sub>4</sub>C oxidation was detected at the end of this period (T~1500°C).

The test indicated no CH<sub>4</sub> formation from the oxidation of B<sub>4</sub>C pellets. The loss of geometry started with the liquefaction of the steel cladding of the control rod and it accelerated the fuel rod degradation process.

The control rod completely disappeared above 335 mm elevation, which means that ~45% of the B<sub>4</sub>C was missing. Most of the B<sub>4</sub>C was oxidized, as ~40% of equivalent carbon was indicated by the release of CO and CO<sub>2</sub>. Part of the stainless steel cladding melted and dissolved part of the Zr guide tube. The total volume of the relocated melt in the lower part of the control rod was ~3,5 cm<sup>3</sup> and contained steel and cladding components. The mass of dissolved Zr at ~1500 °C was estimated as 1-2 times of molten steel. No boron was found in the melt.

High release of aerosols was observed during the oxidation of core components in steam, the aerosol release correlated with steam flow rate.

The in-situ radiography application indicated that the degradation of the bundle took place mainly in the high temperature ( $\sim 2000^{\circ}\text{C}$ ) period of the test. However the fuel rods remained in their original position.

The recorded on-line data have been collected into an experimental database and are available for model development and code validation. The database includes the commissioning test results as well, which could be used for estimation of system heat losses. More than 250 pictures of metallographic investigations have been collected into the post-test examination database available in electronic form (individual *pdf* file for each cross section). The database includes the macro view of each cross section, the enlarged view of each rod and some interesting parts of the fuel and control rods, showing important details of bundle degradation.

The post-test examination of the CODEX-B<sub>4</sub>C experiment focused on two items:

- detailed investigation of the bundle, including radiography, metallography of 13 horizontal cross sections, analysis of the control rod degradation,
- study of released aerosol samples analysis.

According to metallographic examination, the Zr cladding and shroud in the upper part of the bundle were completely oxidized. This observation is consistent with the temperature escalation during the cool-down phase: the temperature started to decrease only after the complete oxidation of the high temperature zone.

Detailed studies were performed on various aerosol samples collected in the experiment. Large amount of blue precipitates was observed on the top of the cooler, containing mainly boron released as a result of control rod oxidation. Uranium containing particles were found on impactors activated during the high temperature phase of the test. Uranium was found on the surface of the Ni impaction plate as well. U release was proportional to partial pressure of UO<sub>3</sub>, the total U release was about 40 mg. Beside uranium a lot of tungsten, zirconium furthermore iron, chromium, nickel, tantalum, molybdenum, niobium, yttrium, hafnium were detected in form of small particles and/or aggregates of them.

### **3.11 WP5.2: Analytical support to the VVER-B<sub>4</sub>C control rod (KI, AEKI)**

Different partners were involved on the analytical support of the CODEX-B<sub>4</sub>C test. This section summarises main contributions.

#### **3.11.1 Calculations with ICARE/CATHARE (KI)**

Following the main topics studied in the COLOSS project, most attention was put on the B<sub>4</sub>C oxidation reaction in steam on the basis of ICARE/CATHARE V1 code version which involves the recent B<sub>4</sub>C oxidation model. This V1 version was provided by IRSN to partners during the project. In parallel to calculations of the VVER-B<sub>4</sub>C test, comparable calculations of the CORA-W2 test, also carried out with a VVER bundle containing a central B<sub>4</sub>C control rod,

has been re-examined to provide a more general assessment of the B<sub>4</sub>C effects on a bundle degradation. The work was performing in 4 stages:

- Post-test calculation of the CODEX-2 test carried out earlier by AEKI,
- Pre-test calculation of the CODEX-B<sub>4</sub>C test using current version of ICARE/CATHARE,
- Post-test calculation of the CODEX-B<sub>4</sub>C commissioning test. The main objective of this work was an adjustment of input deck on the bundle temperature behaviour,
- Post-test calculation of the CODEX-B<sub>4</sub>C test and re-examination of the CORA-W2 test using the improved version V1 of the ICARE/CATHARE code with the B<sub>4</sub>C oxidation model.

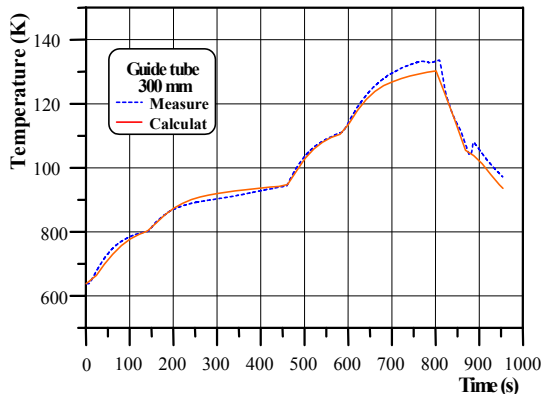


**Fig. 83:** CODEX-B<sub>4</sub>C commissioning test. Guide tube temp. at elevation 300 mm.

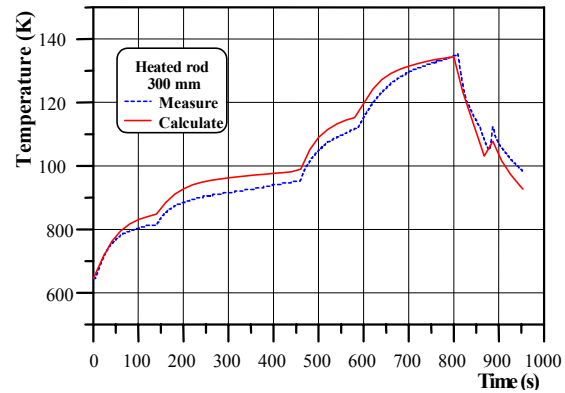


**Fig. 84:** CODEX-B<sub>4</sub>C commissioning test. Heated rod temp. at elevation of 300 mm.

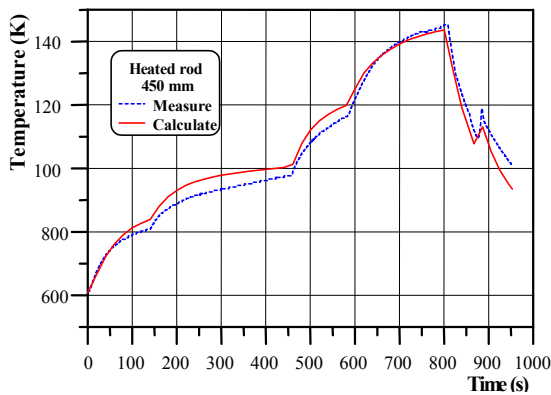


**Fig. 85:** CODEX-B<sub>4</sub>C commissioning test. Heated rod Temp. at elevation 450 mm.

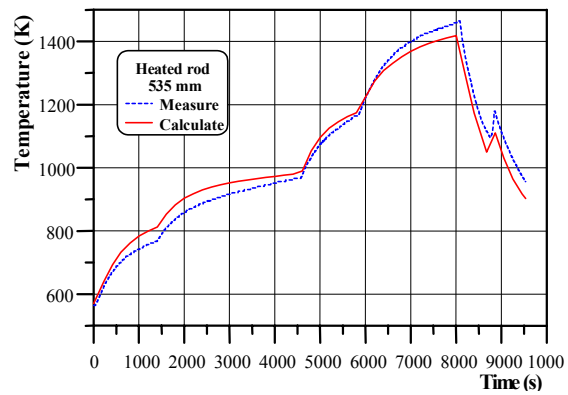


**Fig. 86:** CODEX-B<sub>4</sub>C Commissioning Test. Heated Rod Temp. at elevation 535 mm.

At the first stage of the work a preliminary input deck describing the CODEX facility was developed and tested. Then it was used for pre-test calculation of the CODEX-B<sub>4</sub>C. Results of this calculation were used by the experimental team for preparation of the test.

At the third stage of the work the post-test calculation of the CODEX-B<sub>4</sub>C commissioning test was performed. The main objective of the work at this stage was an adjustment of input deck on the base of experimental data on the bundle temperature behaviour. Figures 83 to 86 illustrate a satisfactory agreement between measurements from the CODEX-B<sub>4</sub>C commissioning test and calculated fuel rod and guide tube temperature evolutions at different bundle elevations.

**Table 17:** Main features of modelling approach for CODEX-B<sub>4</sub>C and CORA-W2 base case calculations.

Physical model	Modelling approach
Thermalhydraulics	1-D gaseous flow in two fluid channels: steam – non-condensable gas mixture, change of geometry due to relocation.
Heat transfer	Radiation in participative gas with updating of view factors, convection, conduction in radial and axial directions
Chemical interactions UO <sub>2</sub> /Zr/H <sub>2</sub> O	Urbanic-Heidricks' parabolic correlations for Zr oxidation, Kim-Olander convective model for UO <sub>2</sub> dissolution without ZrO <sub>2</sub> dissolution, option EXTRA for solubility limit
Relocation of melts	Use of the generalized 2D melt movement model MAGMA
B <sub>4</sub> C oxidation	Default options of current model
B <sub>4</sub> C/SS interaction	JAERI parabolic correlations for B <sub>4</sub> C powder
B <sub>4</sub> C/Fe eutectic	Simulated by low liquefaction temperature of B <sub>4</sub> C (1500 K)
Loss of integrity	Main criteria: failure temperature at 2400 K Absorber cladding and guide tube: failure temperature at 1500 K

Results from the first three stages confirmed a good enough quality of the ICARE2 input deck for CODEX facility modelling. That allowed also good conditions for the last post-test calculation of the CODEX-B<sub>4</sub>C test with the improved version of ICARE/CATHARE. In parallel, the CORA-W2 was also re-examined using the same user choice options. The performed work described bundle temperature behaviour, chemical interactions, hydrogen release, melt relocation and final bundle damage. The particular attention was given to the analysis of the impact of the B<sub>4</sub>C oxidation model on bundle degradation process. The analysis has been performed on the basis of specific ICARE2 modules:

- B<sub>4</sub>C oxidation module;
- B<sub>4</sub>C interaction with stainless steel;
- Generalized material movement model with MAGMA components, taking into account U-Zr-O mixture oxidation during relocation.

A common modelling approach was used in both tests simulations. Table 17 gives a short description of the models and their parameters used for base case calculations.

Figures 87 – 89 illustrate the results of comparisons between measured and calculated values on temperature evolutions, axial mass distribution and hydrogen generated for CODEX-B<sub>4</sub>C and CORA-W2 tests. Investigation of B<sub>4</sub>C impact on CODEX-B<sub>4</sub>C and CORA-W2 transients is completed with application of B<sub>4</sub>C oxidation model. It operated correctly during all runs and additional power and hydrogen, induced by the reaction B<sub>4</sub>C/H<sub>2</sub>O, was obtained considering B<sub>4</sub>C in absorber rod and B<sub>4</sub>C trapped in the melt. The impact of this phenomenon was studied in the modelling by simple elimination of BCOX block-data from ICARE2 input deck in sensitivity study and cross-comparisons of calculations with and without B<sub>4</sub>C.

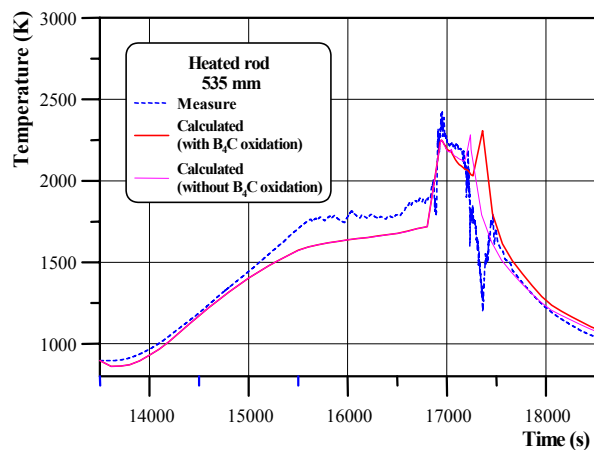


**Figure 87:** CODEX-B<sub>4</sub>C base case. Temp. of heated rod at elevation 535 mm.

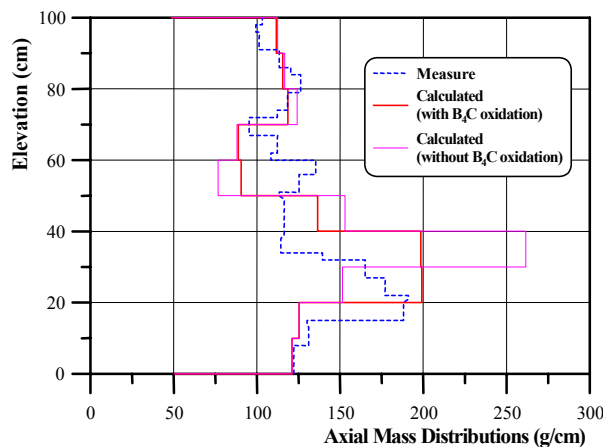
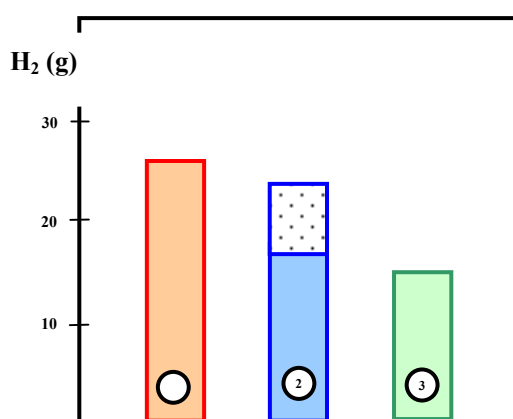
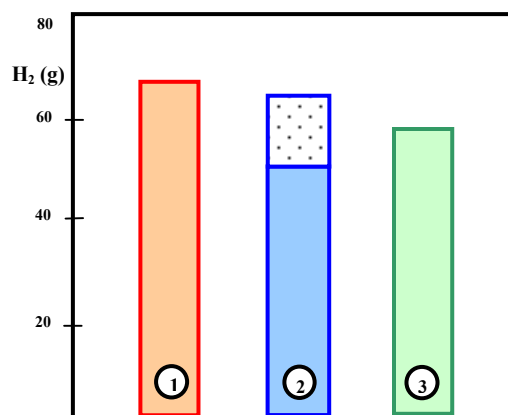


**Figure 88:** CORA-W2 base case. Axial mass distributions.



a) CODEX-B<sub>4</sub>C test



b) CORA-W2 test

**Figure 89:** Total Hydrogen Generated due to Zr and B<sub>4</sub>C Oxidation.

1 - experiment, 2 - calculation with B<sub>4</sub>C oxidation (upper rectangle shows H<sub>2</sub> generated from B<sub>4</sub>C), 3 - calculation without B<sub>4</sub>C oxidation.

The comparison of the separate hydrogen source with total production shows that hydrogen from direct oxidation of B<sub>4</sub>C can reach up to 20% of total value (CODEX-B<sub>4</sub>C simulation). CORA-W2 calculations demonstrate lower relative quantity that is about 15%. Possibly, the decrease of this relative hydrogen source is connected with less number of absorber rods with respect to fuel ones: in CODEX-B<sub>4</sub>C bundle the ratio is 1: 6, while in CORA-W2 it is 1: 18.

Another effect was observed in calculations with elimination of the B<sub>4</sub>C model. Namely, total amount of hydrogen is decreased for both tests as illustrated in Figures 89 a) and b). The exclusion of B<sub>4</sub>C oxidation led to a general reduction of H<sub>2</sub> release but the reduction is not exactly equal to the amount of H<sub>2</sub> coming directly from the B<sub>4</sub>C oxidation. This effect can be connected to complex mutual influence of different physical processes during transients such as melt relocation and melt oxidation. Possibly, elimination of B<sub>4</sub>C oxidation source results in different melt behaviour and composition with higher ceramic compounds in the melts. This has direct influence on melt progression downward (viscosity of the MAGMA component depends

on melt composition). Final bundle damage and axial mass distributions in Figure 88 are different with relocation at higher elevations in the case without B<sub>4</sub>C oxidation reaction. Then, the H<sub>2</sub> source from the melt oxidation is different.

The performed examination provides a set of recommendations for further model application and development. In particular, correct results were obtained using realistic simulation of earlier failure of B<sub>4</sub>C absorber rod (1500K eutectic temperature in B<sub>4</sub>C/Stainless steel reaction) and modelling of the spreading of absorber material throughout the bundle with the 2D MAGMA model.

An important feature in simulations of the CODEX-B<sub>4</sub>C and CORA-W2 tests was connected with the substantial influence of B<sub>4</sub>C absorber rod on the transient. This influence was detected experimentally in CORA-VVER tests and was also evidenced by these calculations as follows:

- B<sub>4</sub>C material starts to relocate earlier than the fuel rod cladding (about 50-100 seconds);
- B<sub>4</sub>C-rich melts flow down before the bundle temperature escalation and step-by-step preheated the lower part of the bundle up to 1500 K;
- During melt relocation mixtures accumulate in preheated region where the bundle damage is accelerated.

The hydrogen production agrees in timing and total amount with measurements. Current calculations show that in bundle experiments, H<sub>2</sub> can be substantially influenced by B<sub>4</sub>C oxidation with the following peculiarities.

- Increase of total hydrogen release (up to 30% in CODEX-B<sub>4</sub>C case and 10% in CORA-W2 case) due to direct and indirect effects;
- Relatively large specific hydrogen source term from direct B<sub>4</sub>C oxidation reaction (up to 20% in the CODEX-B<sub>4</sub>C and 15% in the CORA-W2 cases);
- Most of additional simulated hydrogen is released during relocation phase from relocated mixtures.

In a whole the results obtained for CODEX-B<sub>4</sub>C and CORA-W2 tests indicate a successful common operation of new models of the ICARE2 code (B<sub>4</sub>C and MAGMA melt relocation) that allowed adequate description of quite different physical phenomena.

The oxidation of B<sub>4</sub>C trapped in melt is calculated in the ICARE/CATHARE model using the B<sub>4</sub>C oxidation kinetics derived from pure B<sub>4</sub>C oxidation. This approach is not validated. Recent FZK experimental results on oxidation of B<sub>4</sub>C-SS-Zr mixtures show greater kinetics compared to that of pure materials. Further investigations are needed to improve this aspect.

### **3.11.2 Calculations with ICARE/CATHARE (AEKI)**

The objectives of the work were to support the test preparation, the definition of experimental scenario and post-test analysis of the CODEX-B<sub>4</sub>C test. Code versions ICARE/CATHARE V1-mod1.0, mod1.1, mod1.2 and mod 1.3 were used in this project.

### **Input model**

The input model was based on the CODEX-2 input developed earlier for the post-test analysis of the CODEX-2 experiment. The CODEX-B<sub>4</sub>C test bundle was modeled in cylindrical co-ordinate system. The outer boundary of the computational domain in radial direction was the external diameter of the shroud isolation. The length of the domain was the length of the CODEX test-vessel. The representation of the CODEX-B<sub>4</sub>C test section was modeled as a set of initially solid macro-components capable to participate to chemical interactions, to melt, to flow down and to resolidify depending on the temperature conditions. All macro-components of the test section were defined in one vertical flow channel. The hexagonal form shroud liner was converted to cylindrical form preserving the internal cross section and the material thickness. The structures around the shroud liner were divided in radial direction to simulate the heat losses through the isolating layers.

The inlet and outlet boundaries were defined at the bottom and the top of the domain. Argon and steam flows and temperatures were defined as inlet boundary conditions inside the test section. Pressure boundary condition was prescribed at the outlet. The axial power distribution was calculated by the ICARE code according to the computed temperature distribution and heater resistance. To simulate the heat losses through the shroud an outer flow channel were defined. The cross section of this channel was prescribed on the basis of engineering judgment.. The heat losses were also calculated at the bottom and at the top of the test section.

Zirconium oxidation by steam was defined on the external surfaces of the cladding surfaces of the heated rods and on the internal surface of the shroud liner. Double-side oxidation was assumed on the guide tube. The inner part can oxidize up to the degradation of the absorber cladding. The external surface oxidation of the absorber cladding was calculated by the standard options of the FEOX module. B<sub>4</sub>C oxidation was calculated by the new model of ICARE2.

### **Commissioning test**

In the commissioning test only argon flow was used instead of the argon-steam mixture planned in the experiment. Electrical heat source changed in stepwise manner during the test. The measured outside shield temperatures were applied to the peripheral temperature distribution of the shroud. The calculated results followed the trends of the temperature measurements. Up to 1.2 kW electrical power, the calculated and measured temperatures were in good agreement. After the last power increase up to 1.8 kW the calculated bundle temperatures were lower than the measured values.

### **Pre-test calculation**

The first pre-test calculations for the CODEX-B<sub>4</sub>C experiment were carried out by RRC KI (previous section). Making use of their conclusions additional work was done at AEKI in order to produce further results and precise the experimental conditions. Peripheral boundary conditions were established based on the results of the calculation of commissioning test. The inlet flow and electric power supply were chosen according to the planned experimental program.

The pre-test simulation showed that in the case of the planned experimental scenario it was possible to achieve the following trends:

- a local temperature plateau in the higher region of the experimental bundle by keeping the inlet steam flow rate in a low level,
- a temperature escalation by increasing the inlet steam flow and decreasing argon flow without additional power increase,
- early relocation of the SS cladding together with some dissolved B<sub>4</sub>C pellets,
- relocated B<sub>4</sub>C mixtures in the vicinity of the original structure,
- small effect of the B<sub>4</sub>C pellet oxidation on the hydrogen generation.

### Post-test calculation

The post-test analysis of the CODEX-B<sub>4</sub>C test was performed with the input data set developed for the pre-test calculations. Argon and steam flows and temperatures were defined as inlet boundary conditions inside the test section. The values were the same as in the experiment with the exception of the manually controlled region where the average steam mass flow rate was prescribed. Pressure boundary condition was prescribed at the outlet. The total integrated electric power was defined in the input file as function of time. The axial power distribution was calculated by the ICARE code according to the computed temperature distribution and heater resistance. The main events and actions during the test and their timing in the calculation are presented in Table 18.

**Table 18:** Main events and actions of CODEX-B<sub>4</sub>C test

Events	Experiment [s]	Calculation [s]
Start of Ar injection, 2,3 g/s	0	0.
Increase of electric power up to 500 W	1200	1200.
Start of steam injection, 0,1 g/s	13640	13640
Start of power increase with 2 W/s	13646	13646
Start of H <sub>2</sub> production(>1 %)	14000	14200
1750 K reached in the upper part of the bundle	15600	15350
2560 W power constant	15600	15600
Start of steam starvation region	15610	15610
Control rod failure	16600	16400
Argon flow-rate reduction to 1,3 g/s	16830	16830
Steam flow-rate increase to 0,5 g/s and end of steam flow-rate regulation	16850	16850
2373 K reached in the upper part of the bundle	16908	17100
Switch off power	17050	17050
End of simulation	21705	18000

Figure 90 illustrates the top part of the heated section. The simulation predicts an early temperature escalation at ~ 15500 s not observed in the test. This can be explained by the overestimation of the Zr oxidation in the transition period during the recrystallization of the cladding material. The final escalation process however was well represented.

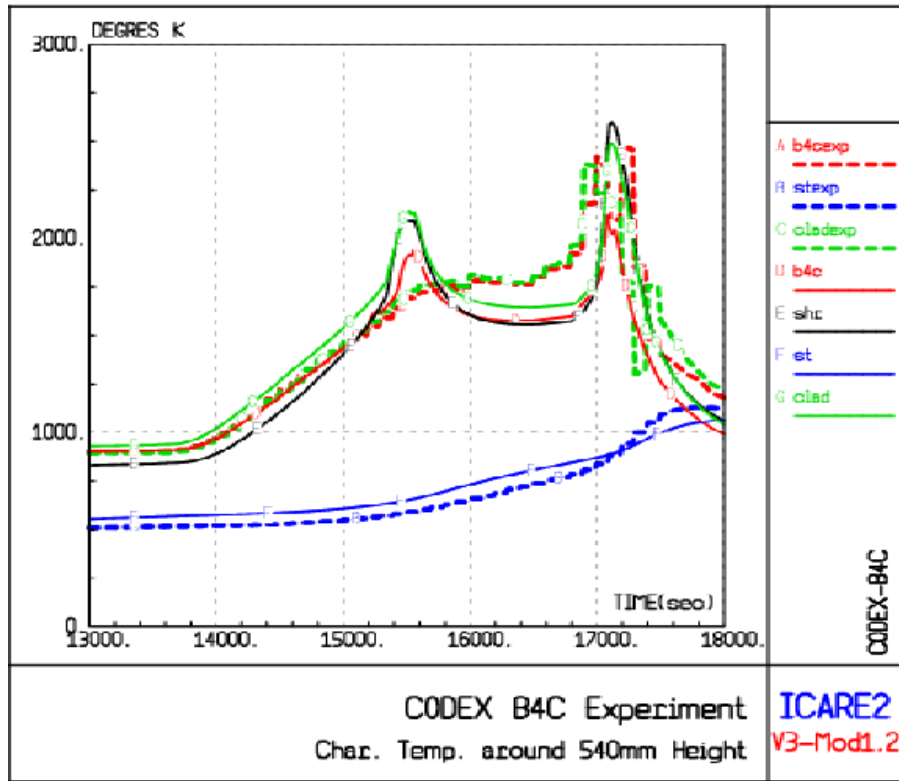


**Fig. 90:** Calculated and measured temperatures in the upper part of the bundle  
Dotted lines: measurements, solid lines: calculation of control rod and shroud

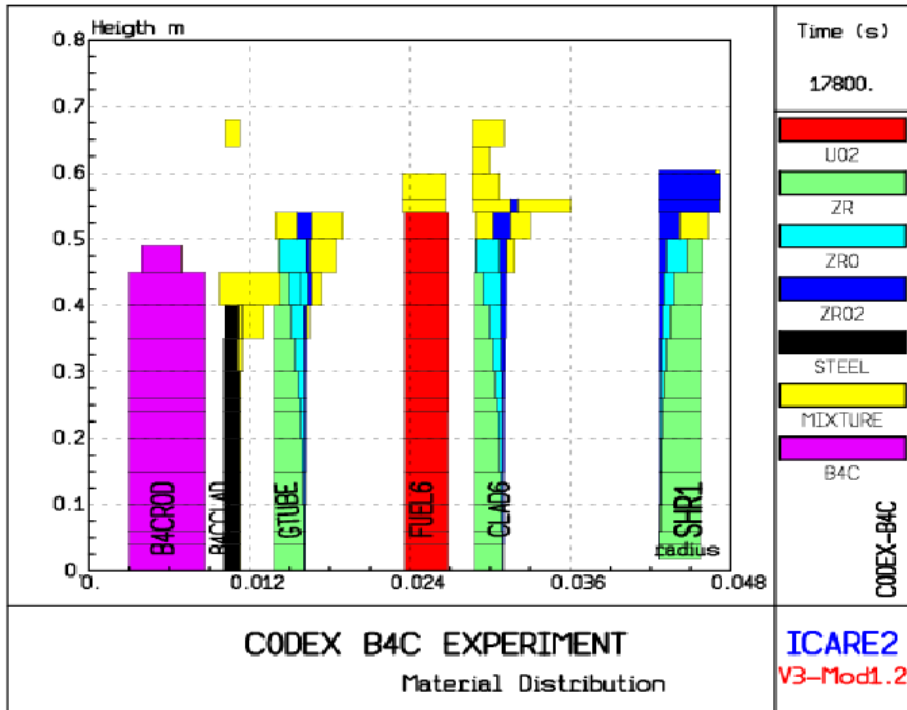


**Fig. 91:** Final state of the CODEX-B<sub>4</sub>C bundle degradation

The overall hydrogen generation was underestimated in the final escalation period and as it was for the B<sub>4</sub>C oxidation (total H<sub>2</sub> measured: 24.5 g, total H<sub>2</sub> calculated: 15.5 g).

The steel cladding remained intact up 16800 s. No significant oxidation took place at the steam starvation period, but 10% of the total cladding mass reacts with the B<sub>4</sub>C pellets.

The final state of calculation is illustrated in Figure 91. Strong degradation is predicted in the upper part of the bundle. The control rod pellets disappeared at the upper part. The SS cladding was dissolved in this position with guide tube and the shroud in the upper part was fully oxidized.

The reduction of B<sub>4</sub>C was underestimated by the code.

### **Main outcome**

In spite of the difficulties in the simulation of bundle oxidation, the simulated temperature behavior was close to the experimental one. The oxidation heat gave high contribution only at the end of power ramp (1<sup>st</sup> escalation) and during the bundle degradation period (2<sup>nd</sup> escalation). The electrical resistance heat of the simulator rod controlled the other part of the heat source.

During the frame of the post-test analysis of the CODEX-B<sub>4</sub>C experiment sensitivity studies were done up to 18000 s to investigate the Zr and B<sub>4</sub>C oxidation. The numerical simulation with ICARE code with fitted input parameters described the main experiment results of the CODEX-B<sub>4</sub>C test successfully.

The analysis called the necessity of the further improvements of the current B<sub>4</sub>C oxidation model of ICARE2. It was found that the simulation of the VVER-1000 control rod design is a complex task and needs further efforts for the proper simulation.

## **3.12 WP6.1: PWR bundle tests with a central B<sub>4</sub>C control rod (FZK)**

QUENCH-07 and QUENCH-09 tests were to fulfil two aims. Firstly they should provide experimental data on degradation of B<sub>4</sub>C control rods, its impact on surrounding fuel rods, and the production of gas (in particular H<sub>2</sub> and CH<sub>4</sub>) before and during reflood in conditions as representative as possible of commercial 1300/1450 MW PWR and BWR. Secondly, it should provide a useful database for the preparation of the future PHEBUS FPT3 experiment (Ref.[<sup>23</sup>]).

### **3.12.1 Quench facility**

The main component of the QUENCH test facility is the test section with the test bundle. Superheated steam from the steam generator and superheater together with argon as a carrier gas enter the test bundle at the bottom. The argon, the steam not consumed, and the hydrogen produced in the zirconium-steam reaction flow from the bundle outlet at the top through a water-cooled off-gas pipe to the condenser where the steam is separated from the non-condensable gases argon and hydrogen. The system pressure in the test section is around 0.2 MPa. QUENCH experiments can be terminated either by quenching with water from the bottom or from the top or by the injection of cold steam. The test section has a separate inlet at the bottom to inject water for quenching whereas the steam for cooldown enters the test section through the same line that is used for the superheated steam during the previous phases.

The test bundle is made up of 20 fuel rod simulators approximately 2.5 m long and a B<sub>4</sub>C absorber rod in the centre. Stainless steel clad B<sub>4</sub>C absorber rod is identical in configuration

to that specified for the next PHEBUS experiment, FPT-3. Control rod parameters are shown in Table 19.

**Table 19:** B<sub>4</sub>C control rod characteristics in QUENCH tests

Total rod length	2842 mm
B <sub>4</sub> C pellets	∅7.48x14 over 1000 mm length in heated zone
cladding	SS material, ∅10.24/∅7.72
SS to B <sub>4</sub> C mass ratio	3.5
guide tube	Zircaloy, ∅12.1/∅11.3 holes in both ends for steam access into the gap
filling gas	Helium, 0.02 MPa overpressure, to detect absorber rod failure by mass spectrometer
instrumentation	three NiCr/Ni thermocouples located at the cladding surface at elevations 750, 850 and 950 mm

Fuel rod simulators are heated over a length of 1024 mm. Heating is electric by 6 mm diameter tungsten heaters installed in the rod centre. Electrodes of molybdenum and copper connect the heaters with the cable leading to the DC electric power supply. The total heating power available is 70 kW distributed between two groups of heated rods. The distribution of the electric power within the two groups is as follows: 40 % of the power is released in the eight inner fuel rod simulators, 60 % in the twelve outer fuel rod simulators. The fuel rod simulators are held in position by five grid spacers, four are made of Zircaloy and the one at the bottom of Inconel. The tungsten heaters are surrounded by annular ZrO<sub>2</sub> pellets. The rod cladding of the heated fuel rod simulator is identical to that used in LWRs with respect to material and dimensions (Zircaloy-4, 10.75 mm outside diameter, 0.725 mm wall thickness). The heated rods are filled with Ar-5%Kr at a pressure of approx. 0.22 MPa. The krypton additive allows test rod failure to be detected by the mass spectrometer.

Four Zircaloy corner rods are installed in the bundle. Three of them are used for thermocouple instrumentation (solid Zry rod at the top, Zry tube at the bottom) whereas the fourth rod (solid Zry rod, position B, 6 mm diameter) can be withdrawn from the bundle to check the amount of oxidation.

The test bundle is surrounded by a shroud of Zircaloy with a 37 mm thick ZrO<sub>2</sub> fiber insulation up to the upper end of the heated zone and a double-walled cooling jacket of stainless steel up to the upper end of the test section.

The 6.7 mm annulus of the cooling jacket is cooled by water from the upper end of the test section to the upper end of the heated zone and by argon from the upper end of the heated zone to the bottom of the bundle. Both the absence of a ZrO<sub>2</sub> insulation above the heated region and the water cooling are to avoid too high temperatures of the bundle in that region.

Hydrogen is analyzed by three different measurement systems: (1) a state-of-the-art mass spectrometer GAM300 located at the off-gas pipe about 2.7 m behind the test section, (2) a commercial-type H<sub>2</sub> detection system "Caldos 7G" located behind the off-gas pipe and condenser, and (3) a second, simpler mass spectrometer "Prisma" installed close to the Caldos device.

The test bundle and the shroud are instrumented with 30 double-sheathed high temperature WRe thermocouples above the elevation 650 mm and with 20 sheathed NiCr-Ni thermocouples below the elevation 650 mm.

### 3.12.2 Main Results of QUENCH-07 Test

The major objective of QUENCH-07 was to provide information on the B<sub>4</sub>C/SS interactions (absorber rod failure), on the formation of gaseous reaction products during the absorber rod degradation and B<sub>4</sub>C oxidation, in particular of H<sub>2</sub>, CO, CO<sub>2</sub> and CH<sub>4</sub>, and on the impact of control rod degradation on surrounding fuel rods. The test conduct was broadly similar to previous QUENCH experiments, but with the inclusion of a phase of B<sub>4</sub>C absorber rod degradation and oxidation. Main test phases are summarized in Table 20 and Figure 92.

**Table 20:** QUENCH-07 phases

Phase I	Heat-up to ~873 K. Facility checks.
Phase II	Heat-up with 0.3 – 0.5 K/s to ~1720 K. Failure of B <sub>4</sub> C control rod leading to B <sub>4</sub> C-SS-Zry melt formation
Phase III	Oxidation of the test bundle and of B <sub>4</sub> C at a temperature of ~1720 K for ~15 min
Phase IV	Heat-up with a rate of 0.35 – 0.45 K/s to a maximum temperature of ~2300 K. Delayed oxidation of B, C - containing compounds at high temperature
Phase V	Cooldown of partially degraded bundle. Exposure of still non-oxidized B, C-containing materials to steam

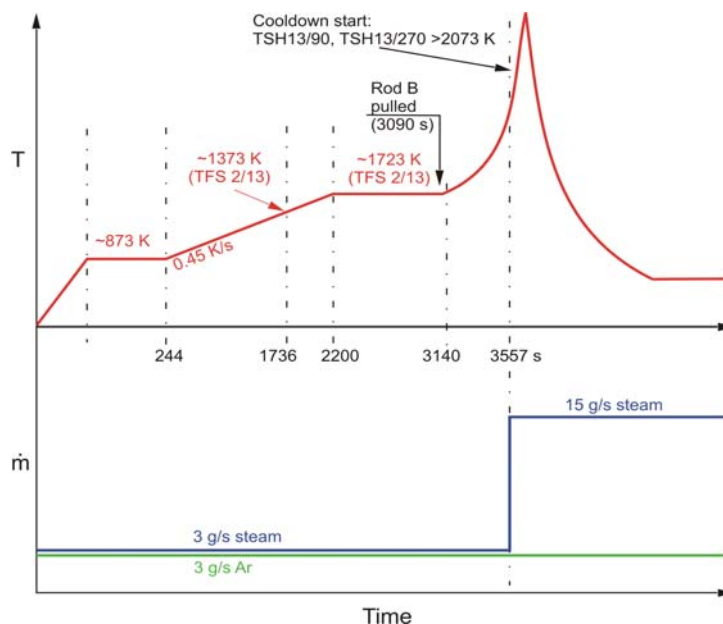


**Figure 90:** QUENCH-7 scenario

Already during the **Phase II**, before the target temperature of 1720 K was reached, helium was detected in the off-gas, in conjunction with a local perturbation of the control rod temperature, thus indicating control rod cladding failure at ~1600 K (Fig. 93). Formation of CO and CO<sub>2</sub> was observed shortly afterwards.

During **Phase III** ( $T_{\max} \sim 1720$  K) the production rates of  $\text{CO}$ ,  $\text{CO}_2$  and  $\text{H}_2$  were approximately constant. Some methane was observed but in a much smaller quantity. Metaboric and orthoboric acids were also detected by the mass spectrometer (Fig. 94). At the end of Phase III one of the corner rods was removed from the bundle to check the extent of oxidation. The oxidation was strongest in the region between 900 and 1000 mm with a maximum oxide layer thickness of  $\sim 230$   $\mu\text{m}$  at 950 mm elevation.

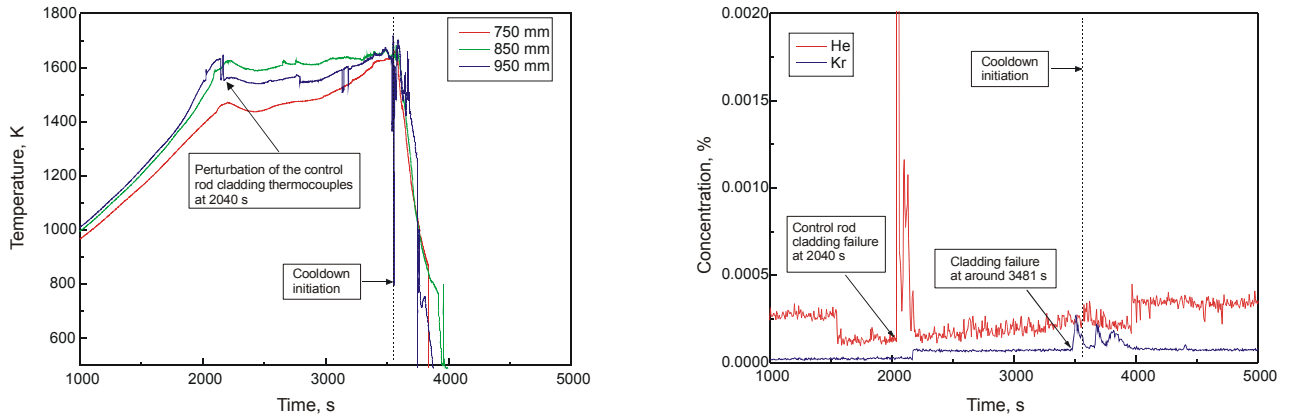


**Fig. 93:** Control rod temperatures at elevations 750, 850 and 950 mm (left). He and Kr concentration measured by mass spectrometer indicating failures of control rod and fuel rod simulators (right).

**Phase IV** was started by ramping the power at 6 W/s. During this phase most of the surface-mounted thermocouples located in the hot zone failed. The increase in temperature was accompanied by a significant increase of all gaseous reaction products except methane. Up to the end of test phase IV the atmosphere consisted of flowing argon (3 g/s) and steam (3 g/s).

**Phase V** (cooldown) was initiated when the two shroud thermocouples at 950 mm had exceeded 2073 K by switching the injection to saturated steam at a rate of 15 g/s, while argon flow was kept unchanged. Power ramp was continued for  $\sim 20$  s and then was reduced from 18.5 to 4 kW in 15 s and kept constant for  $\sim 150$  s to simulate decay heat level. The electrical power was then shut off but the steam injection continued until cooldown to  $\sim 473$  K had been achieved.

Within the heated zone immediate cooling was detected by all thermocouples up to the center of the heated zone (however, it is noted that several thermocouples failed), as shown in Fig. 95. A very different behavior was observed at elevations above the top of the heated zone during the period shortly after beginning of the cooldown phase. Temperature escalation started there, heatup rates of more than 40 K/s were exhibited and temperatures up to  $\sim 2300$  K were reached (Fig. 96). Associated with these high temperatures an increased release of gaseous reaction products was observed. In addition to large increases in generation of  $\text{H}_2$ ,  $\text{CO}$ ,  $\text{CO}_2$ , and boric acids, small amount of methane was detected (Fig. 94). Despite the absence of thermocouple measurements that could indicate a temperature escalation within the heated zone, there is positive evidence from the observed gases that a temperature escalation occurred there.

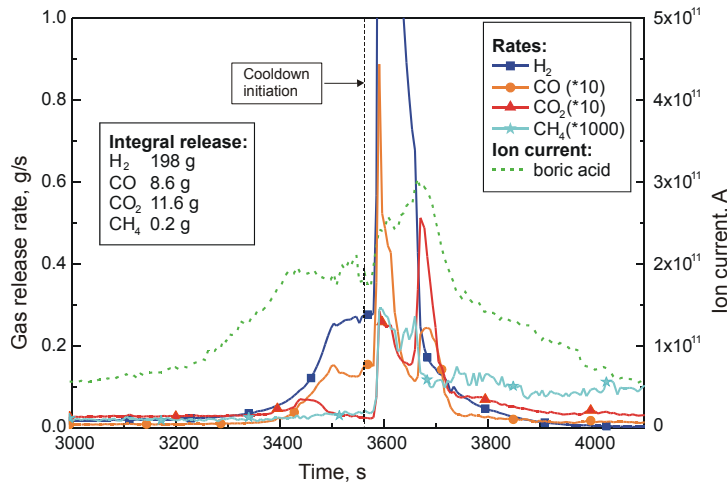


**Figure 94:** Release rates of H<sub>2</sub>, CO, CO<sub>2</sub>, and CH<sub>4</sub> measured during the cooldown phase.

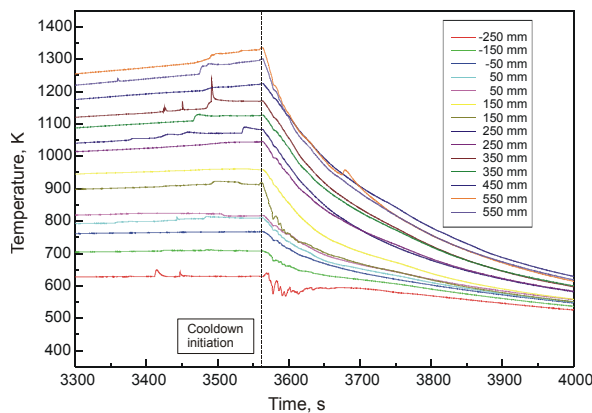


**Figure 95:** Surface temperature of the fuel rod simulators at lower elevations (-250 mm to 550 mm) during the cooldown phase.

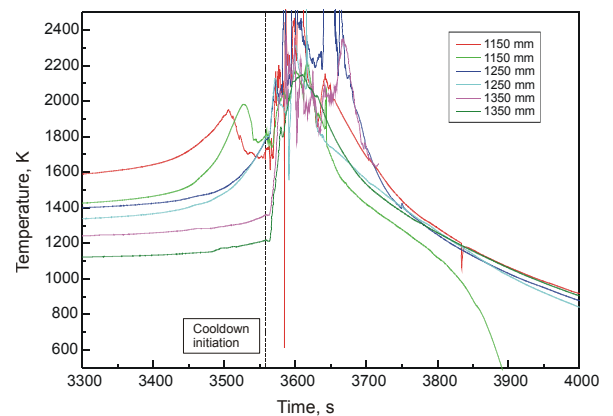


**Figure 96:** Surface temperature of the fuel rod simulators at higher elevations (1150 mm to 1350 mm) during the cooldown phase.

The evaluation of the mass spectrometer data resulted in 198 g of H<sub>2</sub> release in total, most of which (137 g) was produced during the cooldown. The evaluation of the CO and CO<sub>2</sub> release indicates that about 40 % of the B<sub>4</sub>C in the central rod was oxidized during the whole test.

During the test condensate was collected at the sampling point for the mass spectrometer. Analysis of the chemical composition performed after the test shows a good correlation between the boron content in the condensate and release rate of boric acids detected by the mass spectrometer at atomic mass 45 (Fig. 97).

Test bundle and shroud appear severely damaged in the region from ~750 mm elevation upwards (Fig. 98). In this region the shroud and the bundle were partially molten. The major part of the shroud above the heated zone relocated to the region below 1000 mm. Another damage zone is apparent at the level of the topmost grid spacer, i.e. at 1450 – 1500 mm.

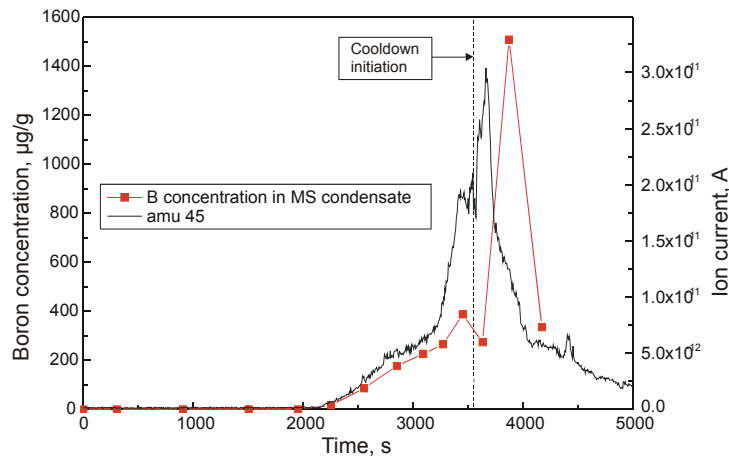


**Figure 97** Boron concentration in the condensate.



The control rod region is shown and interpreted in more detail in Fig. 7. On the lower side the B<sub>4</sub>C pellet stack is essentially intact, the pellets being glued together and surrounded by melt. The absorber pellet stack is essentially intact up to ~800 mm elevation. Above this level an obliquely fixed pellet residue, also melt-infiltrated, shows items of ongoing dissolution under formation of an interaction zone. Thin ceramic structures are identified as guide tube scale. At the elevation of the separate B<sub>4</sub>C pellet CR interaction with the adjacent fuel rod is seen to begin by dissolution of the guide tube scale, after getting embedded into melt from both sides.

**Fig. 90:** View of the bundle after removing of the fragmented shroud.

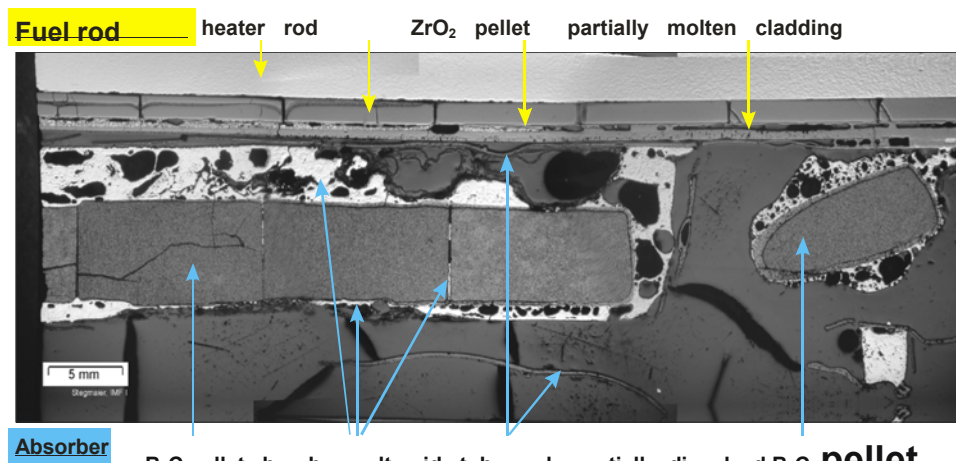


**Figure 99:** Longitudinal section from 760 to ~ 822 mm bundle elevation (left to right); transition zone from intact B<sub>4</sub>C pellet stack towards absorber rod destruction.

### 3.12.3 Main Results of QUENCH-09 Test

QUENCH-09 experiment concentrated on the effects of a B<sub>4</sub>C absorber rod. Major objectives of the test were the investigation of the impact of B<sub>4</sub>C and stainless steel on bundle degradation and composition of the gaseous reaction products formed during oxidation of the B<sub>4</sub>C and B, C-containing melts in steam-starved conditions.

Test conduct was planned to be as for QUENCH-07, but after the temperature plateau steam flow should be reduced to 0.3 g/s to reach steam starvation in the bundle, and cooldown should be achieved with 50 g/s of saturated steam. The investigation of steam starvation conditions was to widen the database and to provide closer comparison with PHEBUS FPT3; the high steam mass flow rate was to cool down the bundle as fast as possible and so to preserve the bundle status before cooldown initiation. Main test phases are summarized in Table 21 and Figure 100.

**Table 21:** QUENCH-09 phases

Phase I	Heat-up to ~873 K. Facility checks
Phase II	Heat-up with 0.3 – 0.5 K/s to ~1770 K. Failure of B <sub>4</sub> C control rod leading to B <sub>4</sub> C-SS-Zry melt formation
Phase III	Oxidation of the test bundle in steam-starved conditions for ~15 min
Phase IV	Cooldown of partially degraded bundle. Exposure of still non-oxidized B <sub>4</sub> C and B, C-containing materials to steam

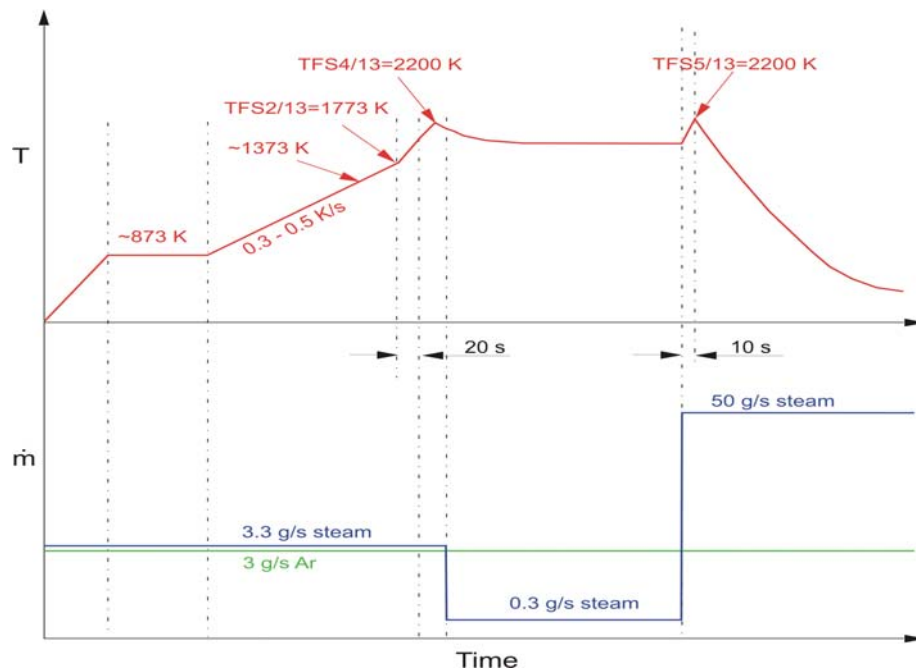


**Figure 100:** QUENCH-09 scenario planned before the tests

The bundle was heated by a series of stepwise increases of electrical power from room temperature to  $\sim 873$  K in an atmosphere of flowing argon (3 g/s) and preheated steam (3 g/s). The bundle was stabilized at this temperature, the electrical power being 4 kW. During this time the operation of the various systems was checked. Afterwards the power was ramped smoothly to 13.3 kW, corresponding to a maximum temperature of  $\sim 1340$  K, and then kept constant in order to reach the target temperature of 1770 K at the hottest location.

Local perturbation of the control rod temperature was first detected during Phase II indicating initial degradation of the control rod at  $\sim 1550$  K. Helium was detected in the off-gas a few seconds afterwards, confirming failure of the control rod cladding (Fig. 101). Despite the test conduct being identical to QUENCH-07 test at this stage, no significant CO, CO<sub>2</sub> or CH<sub>4</sub> generation was observed.

When the target temperature of 1770 K at the hottest location (950 mm above the bottom of the heated length) was reached, power reduction manoeuvre was initiated. Simultaneously, an unexpected temperature escalation occurred at the same elevation, possibly triggered by local degradation of the heater rods. Increases in temperature were observed during the next few seconds at elevations 850 and 750 mm.

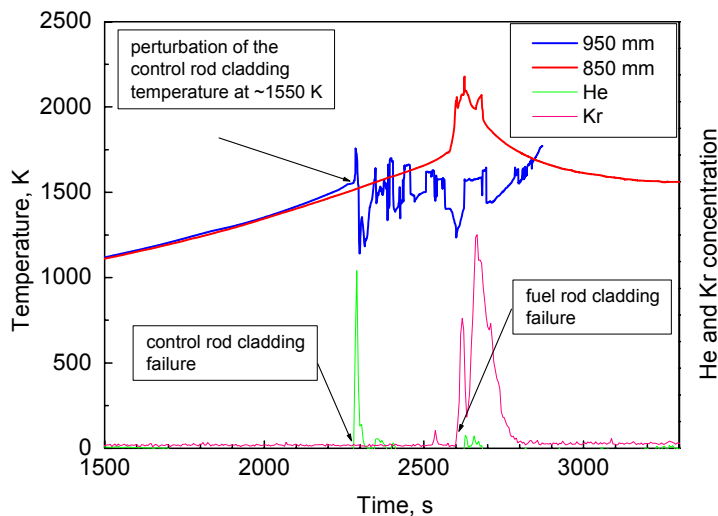


**Figure 101:** Control rod and fuel rod simulator temperatures at elevations 850 and 950 mm; helium and krypton concentration measured by mass spectrometer indicating failures of control rod and fuel rod simulators.

This early escalation did not occur during QUENCH-07 and, indeed, had not been observed at such temperatures in any previous QUENCH experiment.

Due to the temperature excursion and possible melt formation corner rod was not withdrawn as was planned prior to the test so that there are no oxidation data available before the start of the cooldown phase.

When the power reduction was completed, krypton was detected in the off-gas pipe, indicating failure of at least one of the fuel rod simulators (Fig. 101). Also at this time the maximum temperature was  $\sim 2050$  K, and despite the lower power the temperature escalation continued, reaching a peak of  $\sim 2280$  K. At about the same time the shroud failed.

Steam flow was reduced to 0.3 g/s to limit the oxidation power and hence to stabilize the bundle temperatures. At that time some temperatures at higher elevations began already to decrease. During the next eleven minutes the conditions in the bundle were essentially steam-starved, as indicated by the mass spectrometer measurements. In this period of time the power was increased in a stepwise manner to stabilize the maximum bundle temperature at 2073 K. The location of the

escalation moved downward, and at the upper elevations the bundle temperature generally decreased (Fig. 102). Thermocouple failures began with the first temperature excursions, so that the maximum bundle temperature cannot be determined. The maximum measured test rod temperature amounts to 2473 K during the steam-starvation phase at the 750 mm bundle elevation. The shroud temperatures had their maximum around cooldown initiation.

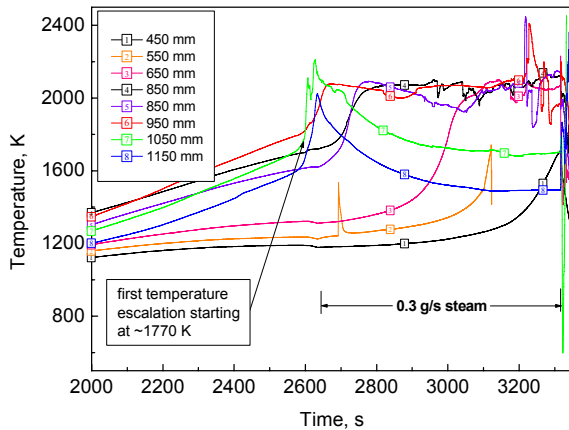


**Figure 102:** Surface temperature of the fuel rod simulators during the heat-up and steam-starved phases.

The cooldown was initiated by switching the injection to cold steam at a rate of 50 g/s. The power was kept at 15 kW for ~20 s, reduced to 4 kW in 15 s and kept constant for ~70 s. The electrical power was then shut off, but the steam injection continued until cooldown to ~470 K.

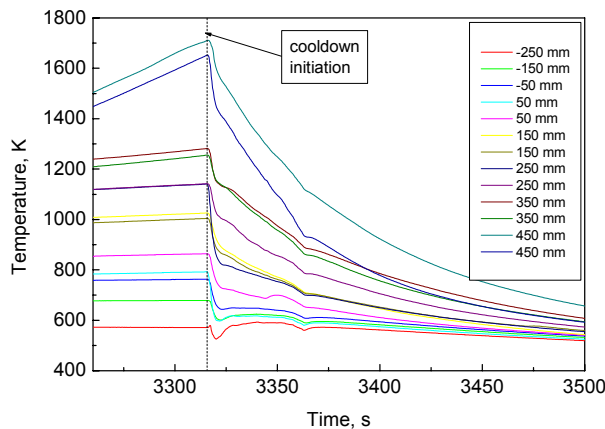


**Figure 103:** Surface temperature of the fuel rod simulators at lower elevations during the cooldown phase.

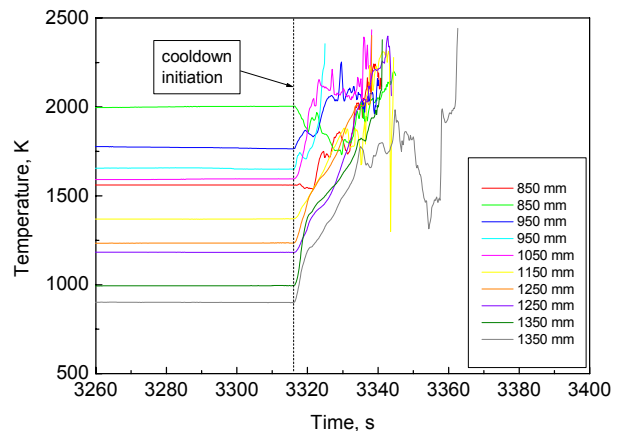


**Figure 104:** Surface temperature of the fuel rod simulators at higher elevations during the cooldown phase.

The temperature escalation that meanwhile had moved into the lower half of the bundle during steam starvation period was immediately terminated at the beginning of the cooldown phase, as shown in Fig. 103. However, several locations toward the top and above the heated zone which had exhibited stable or even decreasing temperatures prior to the initiation of cooldown experienced a strong escalation immediately after increase of the steam flow (Fig. 104).

The high value of 50 g/s steam flow rate, as used in all steam cooldown tests before Q-07, was intended to conserve the bundle condition at the time of cooldown initiation. However, the high hydrogen release during cooldown leads to the conjecture that the long period of steam starvation caused regions of the bundle to be particularly susceptible to further oxidation.

Associated with the first temperature escalation in the bundle during the heat-up phase an increased release of hydrogen was observed. In addition there were only small increases in generation of CO and CO<sub>2</sub> (Fig. 105).

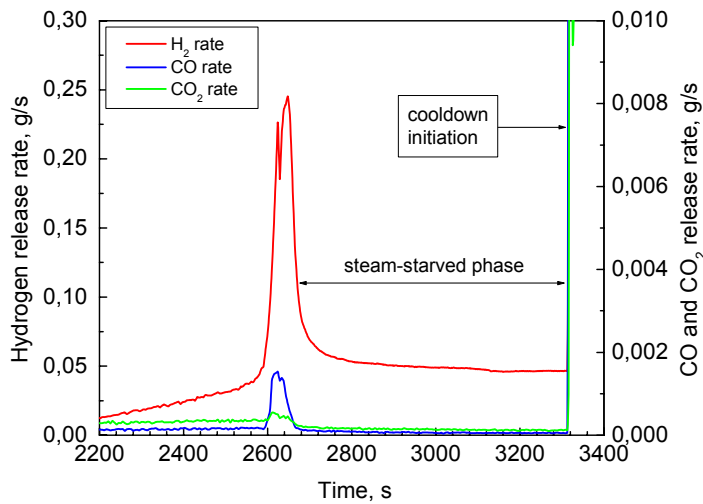


**Figure 105:** Release rates of H<sub>2</sub>, CO and CO<sub>2</sub> measured during the heat-up and steam-starved phases.

Generation rate of hydrogen was approximately constant at a rate of ~0.4 g/s during the steam-starved phase, corresponding to complete steam consumption, as also shown in Fig. 105. The total hydrogen generation up to the begin of the cooldown phase is estimated to ~60 g. Surprisingly no B<sub>4</sub>C oxidation products were detected during this phase.

Strong temperature escalations in the cooldown phase led to an increased release of all gaseous species. A large amount of hydrogen and significant quantities of CO and CO<sub>2</sub> were produced during the cooldown phase for a period of about two minutes (Fig. 106), i.e. even after electrical power shut down. The detection of boric acids persisted for a further two minutes. Methane production was much smaller and for a shorter period.

Approximately 30 s after cooldown initiation a failure of the inner cooling jacket wall was detected (post-test examination showed damage on the elevation ~ 850 mm), probably caused by interaction between the Zr-cladding of shroud thermocouples and SS cooling jacket at high temperatures (~950°C) of cooling steam flowing through the damaged shroud. As a consequence, argon, used for the cooling, entered the bundle, perhaps near the upper end of the heated zone. This argon flow was determined posttest with help of a mockup of the annulus of the cooling jacket.

For the gas measurements by the mass spectrometer the values for all gas species are reliable up to the end of the steam starvation phase, i.e. up to 3315 s. After the initiation of the cooldown phase the argon concentration was analyzed to be almost zero for a period of about 30 s. Since the Ar mass flow rate is used for quantitative evaluation of mass spectrometer data, the steam flow rate is used for this purpose, when the argon concentration is too small, giving ~400 g of hydrogen release during cooldown phase. This was found to be a source of uncertainty on the gas measurement. Total amounts of CO and CO<sub>2</sub> were estimated to 33 g and 22 g, respectively. Hydrogen resulting from the B<sub>4</sub>C oxidation was analyzed to be ~33 g, i.e. about 7% of the total H<sub>2</sub> produced. The data obtained indicate almost complete oxidation of the Zircaloy as well as the B<sub>4</sub>C inventory of the bundle. Additionally, molybdenum and tungsten used as electrodes/heaters could have been oxidized as seen from post-test examination.

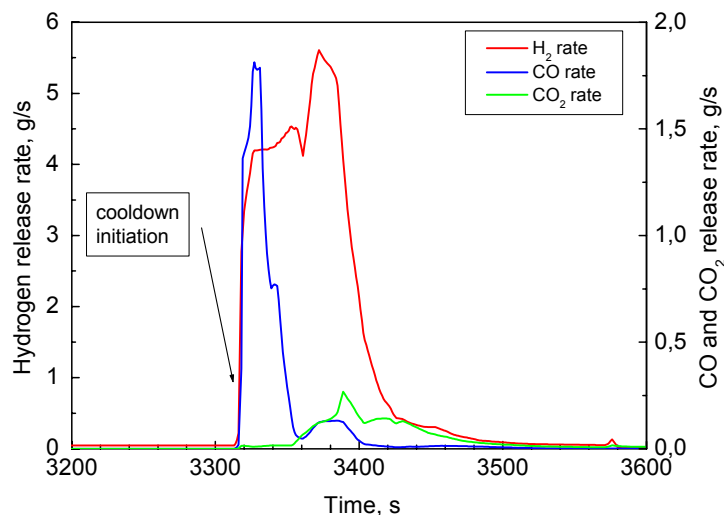


**Figure 106:** Release rates of H<sub>2</sub>, CO and CO<sub>2</sub> measured during the cooldown phase.

During the test condensate was collected at the sampling point for the mass spectrometer. Analysis of the chemical composition performed after the test shows a good correlation between the boron content in the condensate and release rate of boric acids detected by the mass spectrometer at atomic mass 45 (Fig. 107).

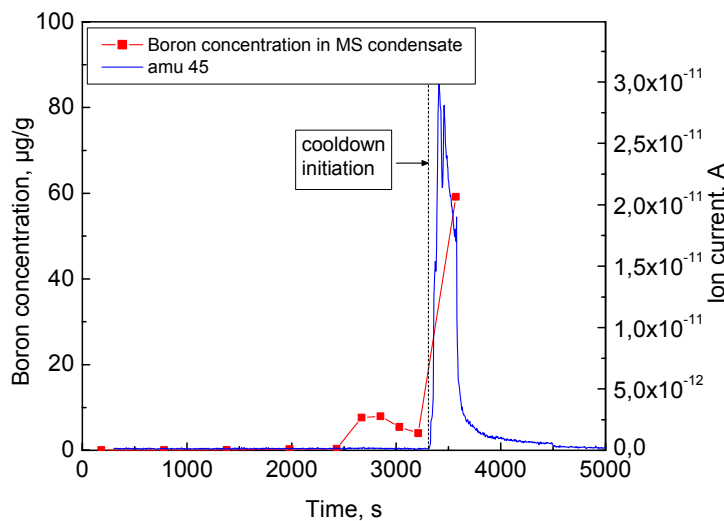


**Figure 107:** Boron concentration in the condensate.

Test bundle and shroud appear severely damaged in the region from ~500 mm elevation upwards, as shown in Fig. 108. In the region between ~520 and 840 mm the shroud and the bundle were partially molten, and the shroud was shaped to a large “bubble”, similar to the QUENCH-07 bundle. The major part of the shroud above the heated zone relocated to the region below 800 mm.

A large number of once-molten debris (Fig. 109) were found at the opening and were seen to have been transported for more than one meter into the off-gas pipe. A more detailed description requires supporting information from SEM-EDX analyses at different positions.



**Figure 108:** Post-test appearance of the QUENCH-09 bundle after removing of the fragmented shroud.

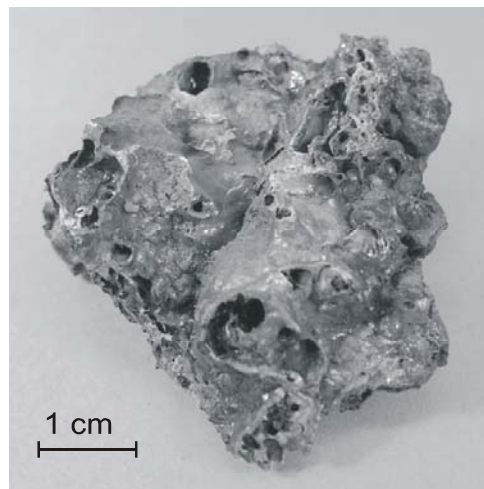


**Figure 109:** Debris taken post-test from the QUENCH-09 bundle.

### 3.12.4 Main outcomes from QUENCH-07 and QUENCH-09 tests

The tests QUENCH-07 and QUENCH-09 provided an extensive database for the model development and code verification. For the first time B<sub>4</sub>C oxidation with related gas production and degradation of the B<sub>4</sub>C control rods was quantitatively assessed in integral experiments.

The tests are regarded as a significant support for the preparation of PHEBUS FPT3 (information related with the B<sub>4</sub>C effects such as control rod failure, gas release, core degradation etc.) during the early phase of the bundle degradation.

The differences in the behavior of the QUENCH-09 bundle compared to previous experiments were unexpected. It is expected that fuel element quenching in a starvation scenario will require efforts beyond the COLOSS project.

### 3.13 WP6.2: Analytical support for QUENCH-07 and -09 tests (FZK, EDF, PSI, IKE, UPM, ENEA and IRSN)

#### 3.13.1 Analytical support for QUENCH-07 (FZK)

The aims of the pre-test calculations were twofold: they should give a sufficient confidence that the integrity of the QUENCH facility would be maintained in the test, and they should help to optimize the test conduct, so that as much benefit as possible could be drawn from the experiment. For the calculations presented here, the in-house version of SCDAP/RELAP5 (S/R5) mod 3.2 has been used; the new code version, mod 3.3 being inoperable. Among others, the current in-house version contains an improved model for heat transfer in the transition boiling region (Ref.[24]), an adaptation of the CORA heater rod model to the conditions of the QUENCH facility, and the material property data for ZrO<sub>2</sub> instead of those for UO<sub>2</sub> to model the

pellets (Ref.[25]). Between PSI and FZK, a close cooperation was initiated, because in both institutions S/R5 mod 3.2 was used. In this context, FZK delivered FZK programme changes (Ref.[25]) and a current input deck to PSI.

First pre-test calculations showed that the test protocol had to be modified, because the original ideas could not be realized. In the following the large computational effort is described, which was necessary to perform test QUENCH-07. It also gives a first insight of the quality of this work by comparing results, calculated according to the real experimental conditions, with the measured data and identifying open points and needs for further interpretation of the test. More details about FZK analytical support are given in (Ref.[26]).

### **Modelling of the QUENCH Facility**

The modelling of the QUENCH facility with S/R5 is the same for all QUENCH tests. In the radial direction, the whole facility including the containment is modelled (Fig 109), because the radial heat losses out of the bundle depend ultimately on the ambient room temperature.

The central rod, the two rings of rods to be heated independently, the four Zircaloy corner rods, the inner and outer cooling jacket, and the containment are modelled as SCDAP components. In this way two-dimensional heat conduction within the structures and radiation between adjacent structures are taken into account. As a central rod, an unheated fuel rod is modelled for nearly all calculations, the original code model of B<sub>4</sub>C absorber rods being rather poor or even inappropriate. Meanwhile, however, the SCDAP model for the PWR control rod was extended for the correct B<sub>4</sub>C material property data. B<sub>4</sub>C oxidation is not yet taken into account, because further interpretation of separate effect tests at FZK is necessary for completion of the B<sub>4</sub>C modelling. The corner rods are modelled as fuel rods. The ZrO<sub>2</sub> fibre insulation is modelled to end at the upper end of the heated zone. With this exception, all structures must be modelled to have the same length because of limitations in the code. Therefore, the upper and lower head cannot be modelled in all details.

The bundle flow and the gas atmospheres outside the outer cooling jacket, i.e. in the containment and the laboratory, are represented by a single channel each.

The off-gas pipe is taken into account with its whole length of 3 m, including the orifice at the position where the gas sample for the mass spectrometer is taken and the orifice at the outlet of the off-gas pipe to simulate correctly the pressure boundary conditions during reflood phase. The mass flows in the off-gas pipe and the adjacent cooling jacket are modelled to be one-dimensional, the structures are modelled as RELAP heat structures, thus taking into account radial heat transfer within the structures.

For most calculations, the region of the heated part is axially modelled with ten 0.1 m long mesh cells. In the lower and upper electrode zones 0.45 and 0.6 m, respectively, of the test section are considered, each by three mesh cells. For the lowermost node in the lower electrode zone copper as electrode material is assumed and molybdenum elsewhere. In addition to this 16 nodes facility (16f) model, a 32 nodes facility (32f) model is now available, where the whole facility is modelled as in the 16f model, but all axial mesh lengths as well in the heated zone as well as the electrode zones are halved.

### **Original Test Protocol**

Since test QUENCH-07 was also intended to support preparation of the planned PHEBUS test FPT3, a first proposal for the test conduct, the original test protocol, was derived as outlined in the following. As usual in QUENCH tests, the experiment begins with a stabilisation phase with a constant maximum bundle temperature of about 800 K. To be as close to FPT3 as possible, a power transient similar to previous QUENCH experiments is applied afterwards. When a maximum bundle temperature of 1500 K is reached, the nominal steam mass flow of

3 g/s is reduced to such a low value that steam starvation occurs in the bundle. As a first guess, “steam starvation” means a steam mass flow of not more than 10 mg/s at the end of the heated zone. The test is continued at a constant maximum bundle temperature of about 2000 K for 15 to 20 minutes (plateau phase) before initiating the cool-down phase. During the steam-starved phase, electrical power is assumed still to increase linearly for a certain time as in the projected FPT3 test. Some more details of the test conduct were to be derived from the results of pre-test calculations.

### **First Pre-Test Calculations**

Pre-test calculations show that the original test protocol is not adequate for the QUENCH test. Firstly the electrical power transient should be continued for some time after steam flow reduction only to reach elevated temperatures as soon as possible, but then be reduced to a much lower value and be kept constant. Besides, the argon flow must be increased for a sufficient heat removal. Otherwise, too high temperatures occur, and even clad melting must be faced before the end of the envisaged duration of the high temperature test phase.

In subsequent calculations, electrical power input, steam, and mass flow rates were therefore varied. The results show that for a modified test protocol the bundle reacts sensitively to changes of physical parameters during the plateau phase because of the low convective heat transfer: the two cases shown in Figure 111 differ only by the argon mass flow rate as a test parameter. For a value of 8 g/s, the bundle temperatures in the upper half of the heated zone have a maximum somewhat above 1600 K, whereas temperatures increase steadily for an argon mass flow of 6 g/s. This leads to clad melting, when the low steam flow phase is longer, and anyway constant temperatures as desired do not occur. To give an impression of this sensitivity, results for all calculations, done up to this time, are given in Figure 112.

Figure 111 also shows that just after power reduction chemical power due to oxidation has about the same value as electrical power. In contrast to electrical power, which is released into the whole bundle, chemical power release is mainly constrained to a small region in the upper half of the heated zone, and hence local chemical power input exceeds local electrical power input by far. Since maximum temperature depends strongly on local power input, these results demonstrate the limits to influence the behaviour of the bundle by varying global electrical power input.

### **Final Test Protocol**

Consequently, a new test conduct, the final test protocol as indicated in Figure 113, was proposed closer to previous QUENCH tests. The main difference is the phase after reaching elevated temperatures, which shall now be performed with nominal steam mass flow. Clad temperature increase is limited to 0.3 – 0.5 K/s during test phase II to guarantee a benign temperature increase and so to minimize the risk of temperature escalations and premature rod damage.

To finalise this protocol, it was agreed to perform three sets of pre-test calculations. The first one should be performed exactly according to Figure 113; test phase IV being achieved by increase of electrical power input at constant steam mass flow rate of 3 g/s. The second one should be done with test phase III to be extended to 15 to 20 minutes. The third one should be performed with constant electrical power and reduced steam flow during phase IV to obtain steam starvation in the bundle at least before cool-down initiation.

Maintaining the high temperature plateau over a sufficiently long time, but keeping maximum temperature below clad melting point, proved to be difficult mainly due to the high temperature level and hence the small safety margin for the facility. Figure 114 illustrates the sensitivity of the facility with respect to changes of electrical power input showing that even minor changes can induce either a clad melting or an acceptable temperature range during phase III.

The calculation labelled “final” shows that a temperature plateau of about 1800 K can be maintained for 20 minutes without difficulties except for a careful tuning of electrical power input. A maximum oxide layer thickness of 400  $\mu\text{m}$  at the end of test phase III was considered reasonable in the sense that effects expected in the following oxidation should be sufficiently large. Therefore, phase III was restricted to 15 minutes being completed at 4000 s.

Results for the first alternative for phase IV (power ramp at constant steam and argon mass flow rates) show that temperature increase is rather small in the beginning of the power transient. A maximum temperature of 2150 K, i.e. shortly below clad melting temperature, is reached at  $t = 4579$  s, i.e. nearly 10 min after the beginning of test phase IV.

For the alternative phase IV with steam mass flow reduction at constant electrical power input, this maximum temperature of 2150 K is reached at  $t = 4160$  s, i.e. only 2.5 min after the beginning of phase IV. Steam consumption is somewhat more pronounced than predicted for the first alternative and the temperature increase is much faster. Therefore, temperature levels are generally higher in this case and  $\text{H}_2$  production rate and oxide layer thickness are also higher.

Due to the fast temperature increase in case of steam mass flow reduction, the transient is very short and much faster than in the case of electrical power increase. Hence time for measurements as well as for operator intervention is very limited in the first case.

The duration of the transient might be increased, when the electrical power is reduced at the time of steam mass flow reduction. This procedure had been proposed by UPM to avoid an undesired temperature escalation. This variant was not investigated because such a test conduct is considered rather difficult to realize: an inappropriate change of electrical power might either jeopardize the integrity of the bundle or cool it down unintentionally.

Furthermore, the results of the CODEX  $\text{B}_4\text{C}$  test suggested that not much  $\text{CH}_4$  formation can be expected for a steam mass flow of 1 g/s. For these reasons, a test conduct with a power transient instead of a steam mass flow reduction was favoured at FZK. Cool-down was calculated to occur without temperature escalation.

### **Post-Test Calculations**

Post-test calculations are based on the real test conduct with the same modelling as for the pre-test calculations. Results are given in Fig. 115 and Fig. 116. Long-dashed lines refer to the 16f model. During phase II, calculated temperatures are underestimated (Fig. 115) in the upper zone, whereas during oxidation (phase III) a temperature stabilisation is measured which has not been calculated. As a consequence, hydrogen production is overestimated. With the 32f model, results for phase II are not improved, but there is a better agreement with the experiment for higher temperatures in phase III. This leads to a later calculated onset of temperature escalation, giving better agreement of oxide layer thickness and a smoother profile of linear electrical rod power at the time when the corner rod is withdrawn.

The difference of the results for the two axial discretizations is very pronounced for the oxide layer thickness and hydrogen production rate (Fig. 116), because for the fine axial discretization an escalation is calculated just to have started, whereas for the coarse discretization it is calculated to begin about 120 s earlier. For this reason, the peak value of hydrogen production rate is calculated to be one order of magnitude larger for the coarse axial

discretization. As can also be seen from the axial temperature profiles (Fig. 116), the fine axial discretization generally improves the agreement in the upper electrode zone. During cool-down differences between experiment and calculation mainly seem to rise from different temperatures at the initiation of cool-down.

Calculations carried out later for test QUENCH-09, suggest that a decrease of thermal conductivity of the shroud insulation material might improve the agreement in phase II. This item needs some more work to be done, because it is an aim of the analytical support at FZK to perform the calculations for all QUENCH tests with the same modelling.

No further investigation of that sort was made because the oxidation model in S/R5 was being improved according to suggestions made in the COLOSS WP8 (Schanz recommendations (Ref.[50])). First results with this oxidation model suggest that the calculated hydrogen production agrees somewhat better with experimental data for lower temperatures. In the high temperature regime (Prater law), however, a large over-estimation is calculated, even though the steam available for oxidation is assumed limited. This limitation is calculated according to the model already implemented in S/R5 and this model is also used for the other calculations. It is based on an analogy of heat and mass transfer and, because dimensionless numbers are used, it should essentially be applicable irrespective of the oxidation model. However, this new oxidation modelling requires more verification to be applied successfully.

### **Conclusions**

The conduct of test QUENCH-07 was originally planned to be similar to the planned PHEBUS test FPT3. Since it differed in more than one aspect from previous tests in the QUENCH facility at FZK, more attention than for other QUENCH tests had to be paid to define the test conduct. In particular, other institutions as PSI and UPM participated with other SA codes to identify and to solve problems in the preparation of the test.

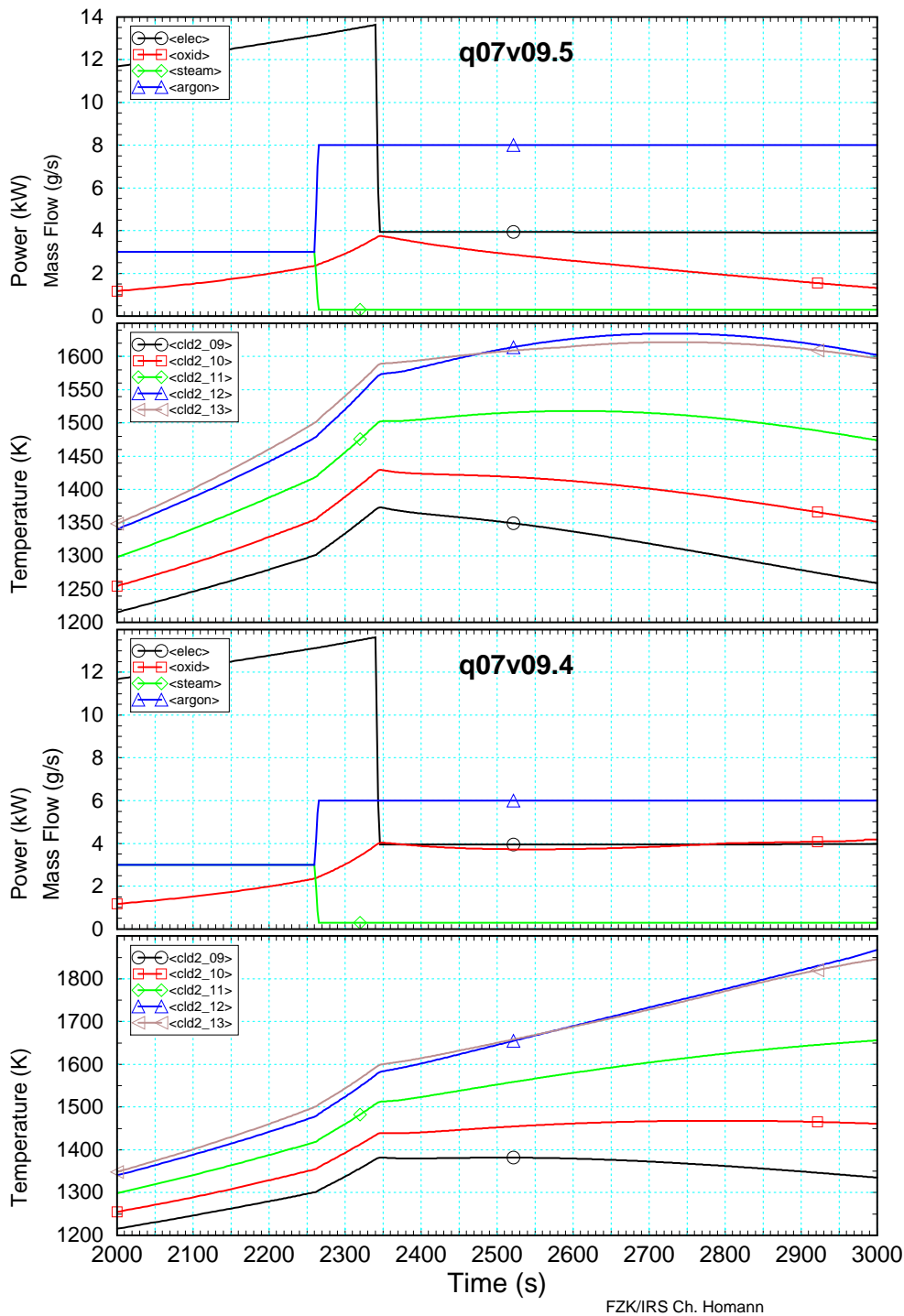
FZK pre-test calculations with in-house version S/R5 mod 3.2 showed that for the original test protocol the various aims of the test cannot be fulfilled in the QUENCH facility at the same time. Even for a modified test protocol, pre-test calculations predicted that due to the elevated temperatures to be maintained for a long time the QUENCH facility would be rather sensitive to changes of experimental parameters as electrical power input and that the facility might even be damaged during the test. With a steam mass flow reduced, this sensitivity was enhanced because of the lower conductive heat removal. Sensitivity studies showed that a power transient to reach very high temperatures in the bundle was more advantageous than a steam mass flow reduction. The other participants engaged in these analyses calculated the same trends.

Post-test calculations show deviations to measured temperatures in the first transient (phase II) already, but further work is needed using code improvements to conclude. This modelling work also depends on further interpretation of experimental results obtained in the 5<sup>th</sup> FWP. The post-test results also showed the necessity of a sufficiently fine spatial resolution of the computational domain.

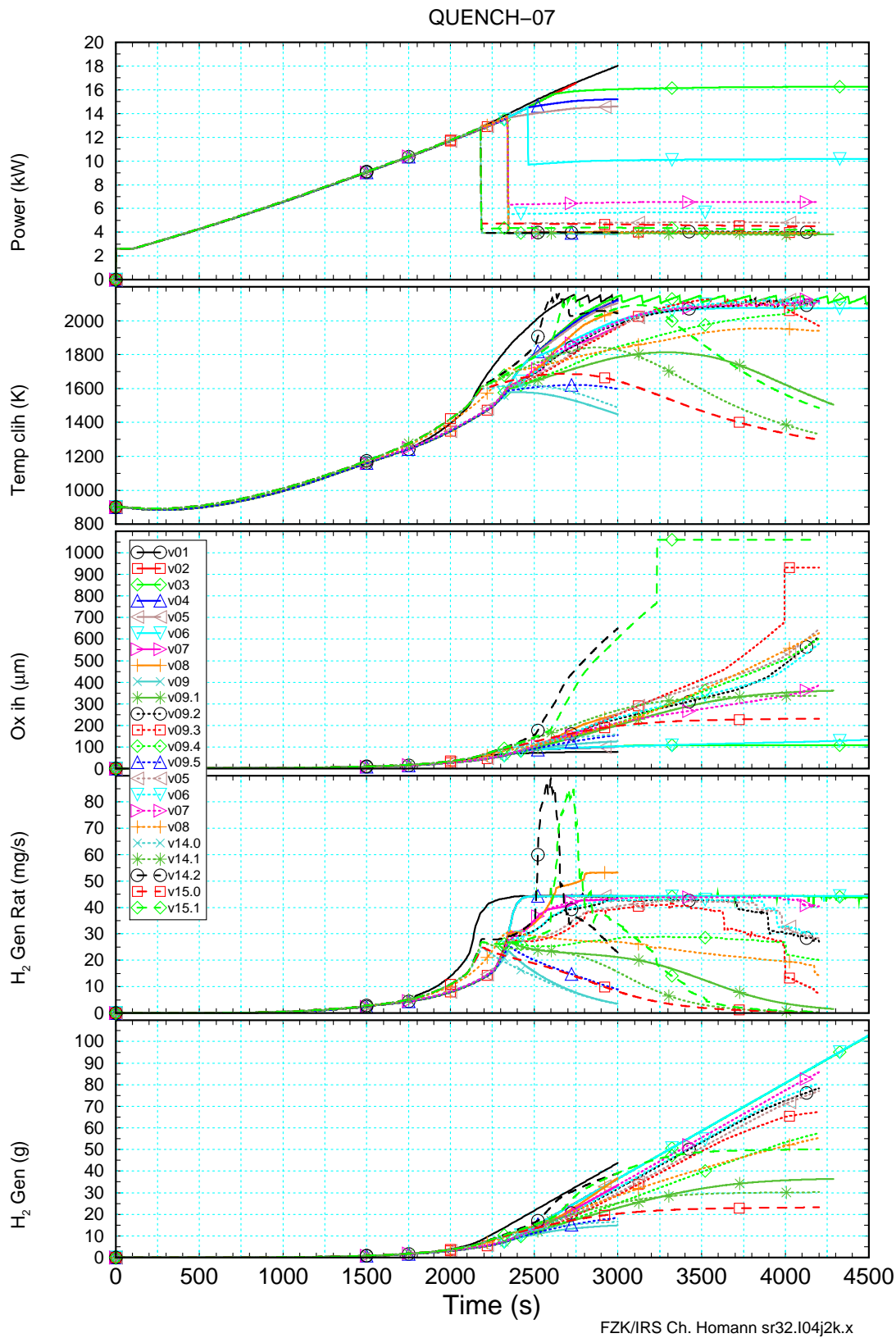
Finally, a large computational effort was necessary to define an appropriate test conduct, but the post-test calculations and the subsequent QUENCH-09 test justified this work and the insight gained during its course.



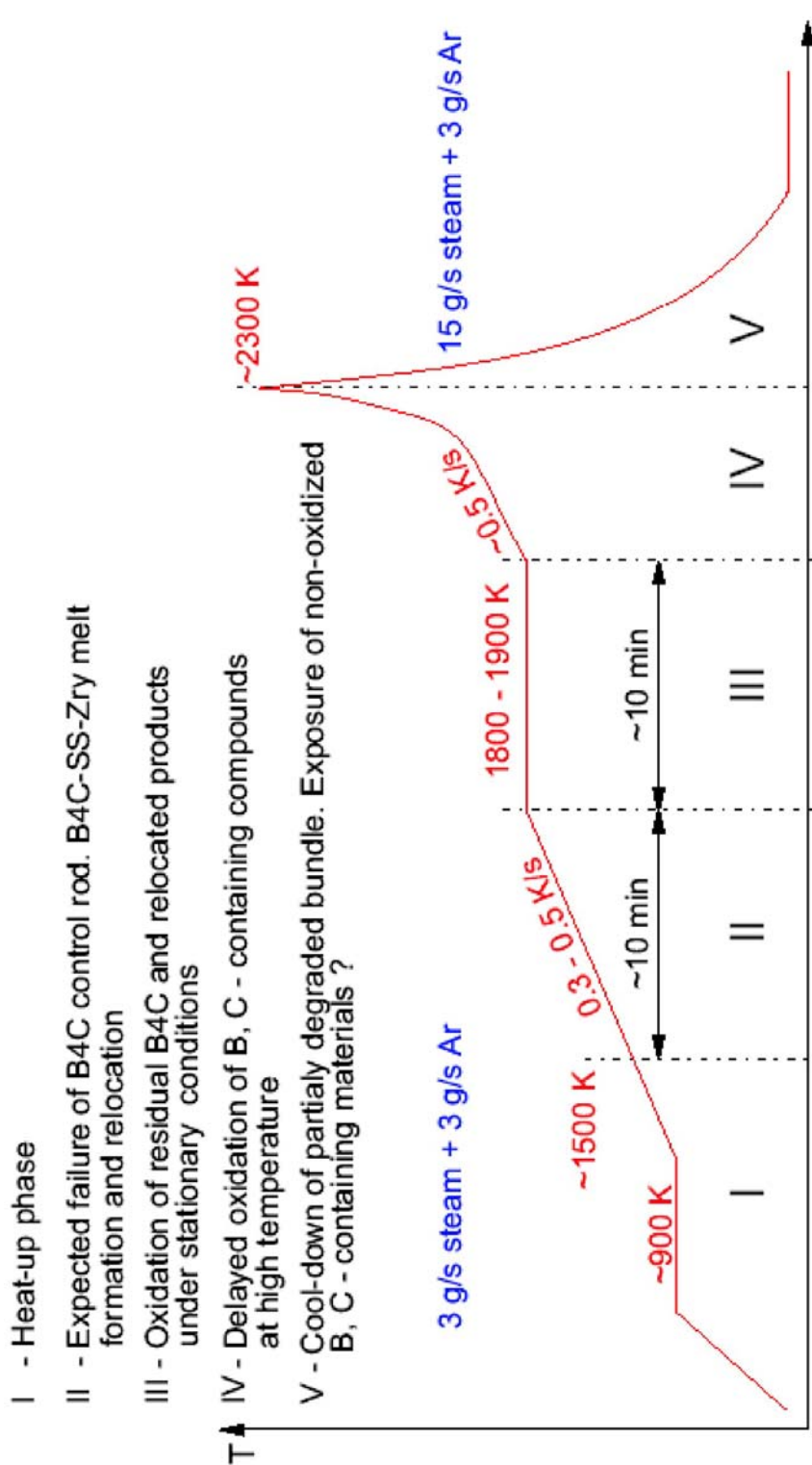
QUENCH-07



**Fig. 111:** Selected variables for two different argon flow rates as a function of time (first pre-test calculations): power, mass flow rates, and clad surface temperature of inner heated rods at axial levels 9 to 13 (elevations 0.55 to 0.95 m) for two different runs.

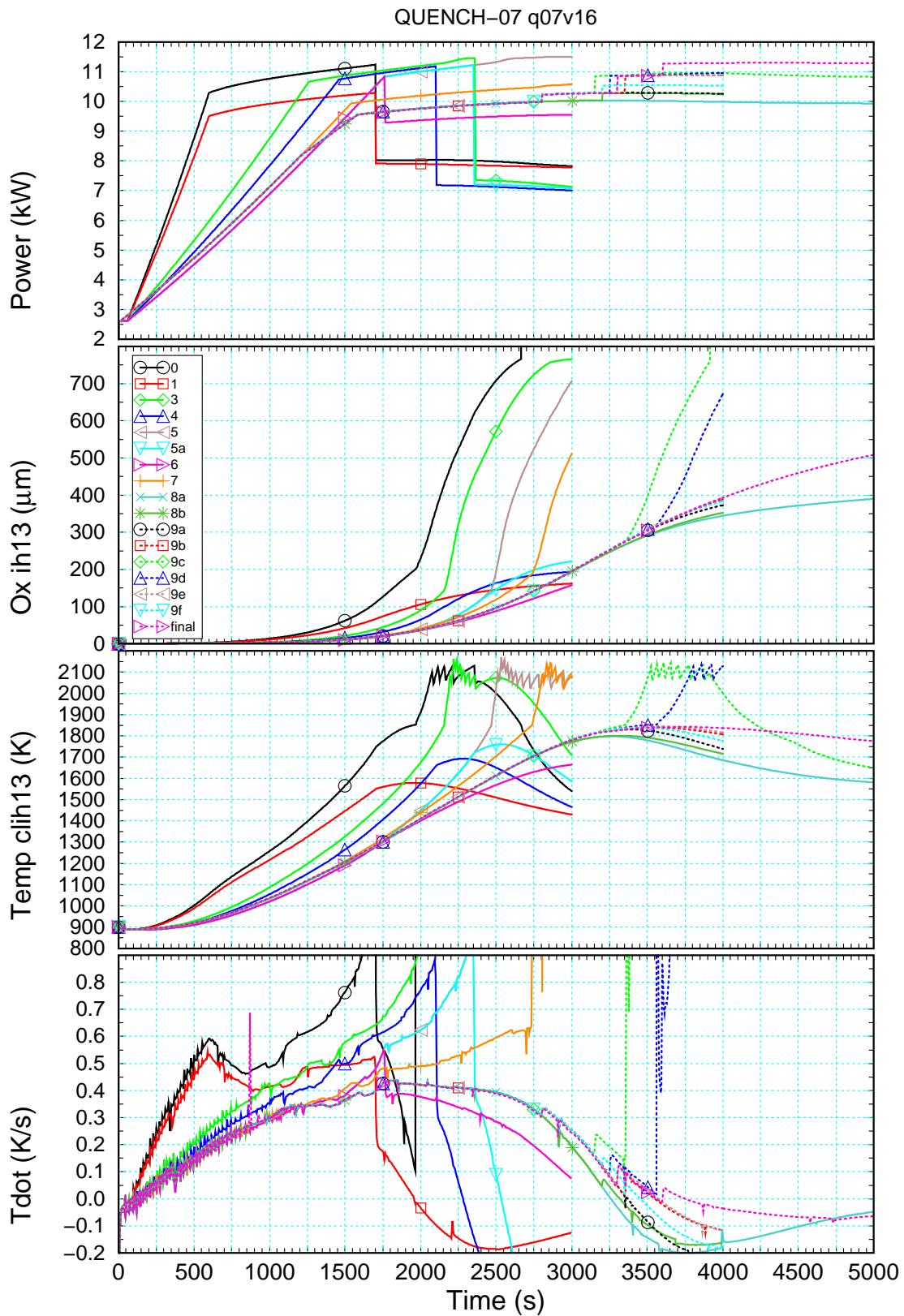


**Fig. 112:** Survey of first pre-test calculations. From top to bottom, electrical power, oxide layer thickness and clad temperature for the inner heated rods at axial level 13 (elevation 0.95 m), H<sub>2</sub> production rate and cumulated hydrogen mass as a function of time.



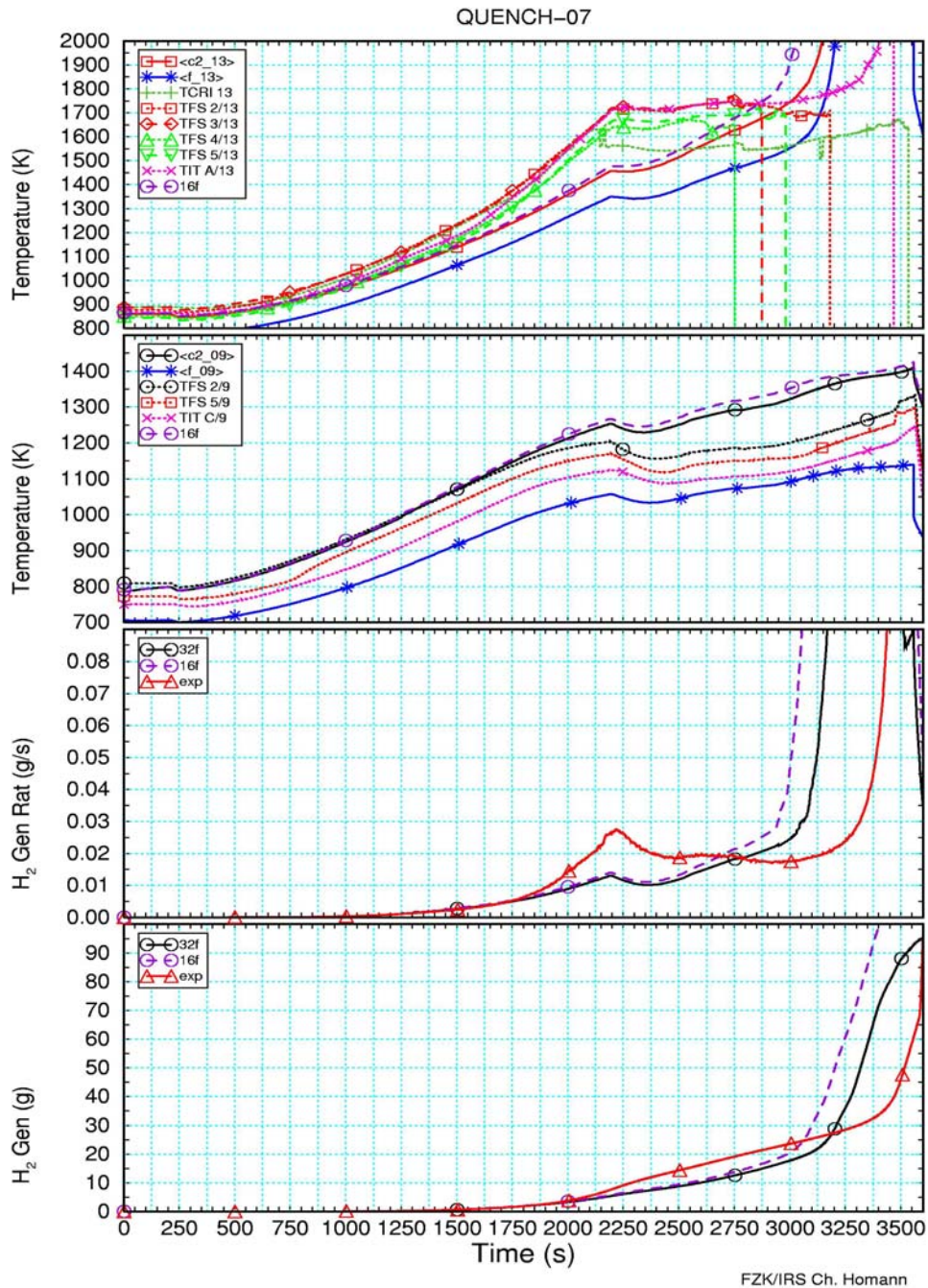
A. Miassoedov, IMF III

Fig. 113: Final test protocol for QUENCH-07



FZK/IRS Ch. Homann sr32.l036g.x

**Fig. 114:** Survey of calculations for final test protocol. From top to bottom electrical power release into the bundle, oxide layer thickness, clad temperature for the inner heated rods and its time derivative at axial level 13 (elevation 0.95 m) as a function of time.



**Fig. 115:** Comparison of selected measured and calculated variables for QUENCH-07. From top to bottom: bundle temperatures at axial levels 13 and 9, and measured and calculated H<sub>2</sub> production rate and cumulated H<sub>2</sub> mass.

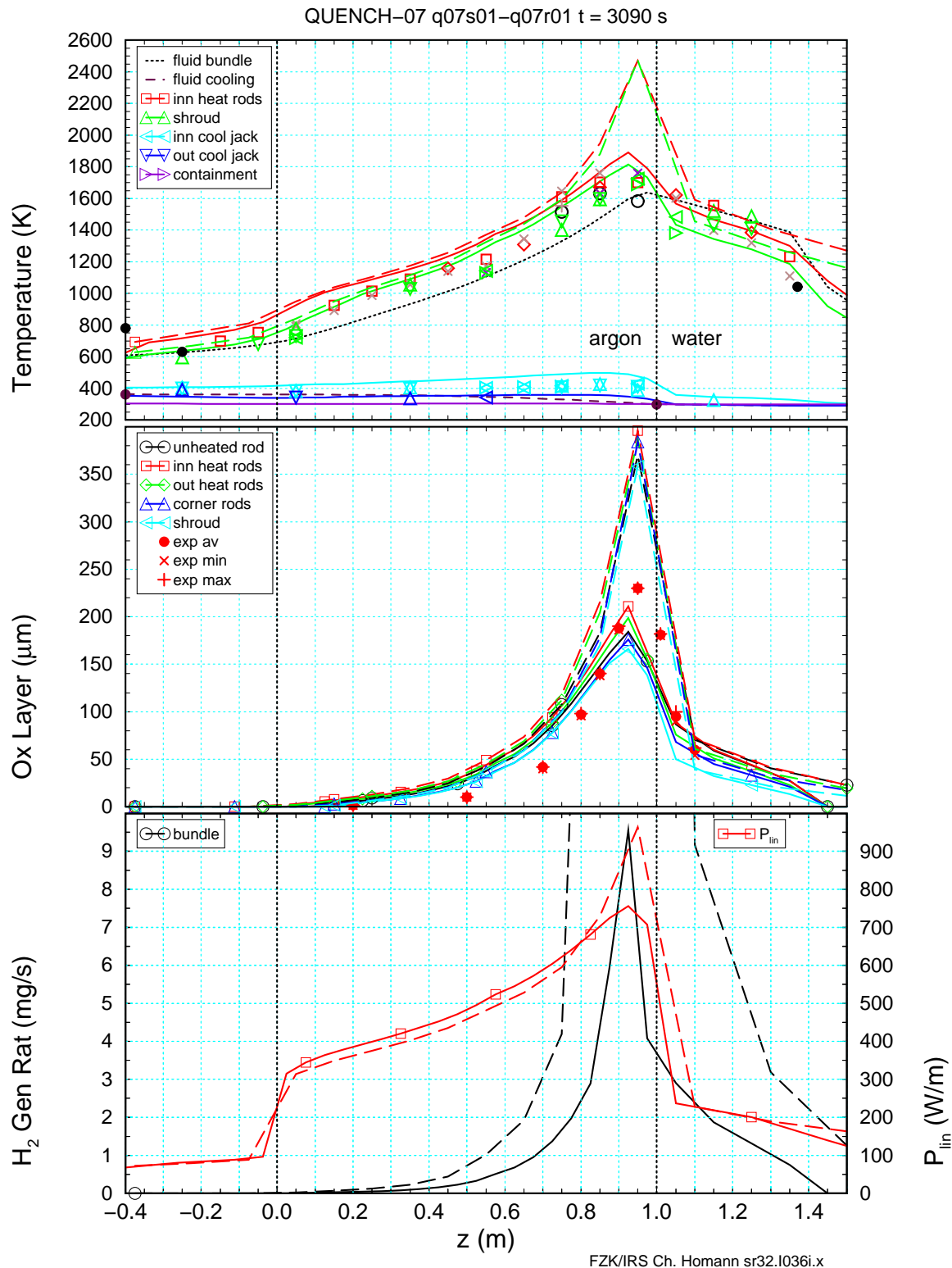


**Fig. 116:** Axial profiles of selected variables at the time of withdrawal of a corner rod (post test calculation). From top to bottom: measured and calculated axial profiles of temperatures, oxide layer thickness, hydrogen production rate, and linear electrical rod power.

### 3.13.2 Post-test calculations of QUENCH-07 (EDF)

The purpose of the QUENCH07 global test was to investigate the impact of a B<sub>4</sub>C absorber rod on a pre-oxidized LWR fuel rod bundle at high temperature and during the cool-down by steam. The test was characterized by steam-rich conditions. The central rod was a control rod simulator consisting of an absorber rod with B<sub>4</sub>C pellets in a stainless steel clad and a Zircaloy-4 guide tube prototypic of that used in the current design of French PWRs. This experiment has provided notably information on the impact of B<sub>4</sub>C on core liquefaction plus some measurements related to non-condensable gases production.

The calculation of such an integral experiment provides a unique opportunity to assess the ability of the EDF MAAP4.04 code version to predict the absorber rod degradation and B<sub>4</sub>C oxidation and its impact on surrounding fuel rods. Previous sensitivity studies to fuel rod clad degradation and oxidation parameters have provided relatively good results in terms of temperature history up to the initiation of the cooling phase. The analysis of a 2<sup>nd</sup> set of sensitivity calculations focused on the B<sub>4</sub>C model developed by EDF.

Sensitivity calculations were carried out to check the three B<sub>4</sub>C oxidation kinetics available: ICARE2, Steinbrück and MELCOR oxidation laws. The gas partitioning resulting from the B<sub>4</sub>C oxidation was calculated using the GEMINI/COACH equilibrium model. The B<sub>4</sub>C results obtained by the different correlations are illustrated in Table 22. The Figure 117 gives the the rate and the total H<sub>2</sub> production.

In conclusion, the ICARE2 oxidation model coupled to the GEMINI-COACH equilibrium model for the production of non-condensable gases, provided valuable results regarding all risk relevant issues such as core degradation, non-condensable gases production and hydrogen generation up to the end of the test. The specificity of this model regarding the steam partial pressure effect seems consistent. As observed in the test the CH<sub>4</sub> production during B<sub>4</sub>C oxidation is negligible. Regarding the B<sub>4</sub>C modeling, there is a lack on the oxidation of B<sub>4</sub>C-rich metallic mixtures.

In summary, limitations identified in the MAAP4 code at the beginning of the COLOSS project regarding B<sub>4</sub>C effects have been strongly reduced. This situation is a real improvement for the French 1300 MWe plants.

**Table 22:** MAAP4 calculations with assessment of hydrogen and non-condensable gases mass at the end of the QUENCH-07 test.

Case	CO mass (g)		CO <sub>2</sub> mass (g)		CH <sub>4</sub> mass (g)	H <sub>2</sub> mass (g)	
<b>REFERENCE (no B<sub>4</sub>C model)</b>	0,0	-	0,0	-	0,0	152	-23%
<b>ICARE</b>	4,4	-49%	11,7	+1%	4,0 10 <sup>-12</sup>	189	-4%
<b>MELCOR</b>	10,4	+20%	18,9	+63%	1,6 10 <sup>-9</sup>	153	-23%
<b>STEINBRÜCK</b>	2,8	-67%	6,4	-45%	5,2 10 <sup>-11</sup>	106	-46%
<b>EXPERIMENT</b>	8,6		11,6		2,0 10 <sup>-4</sup>	198	

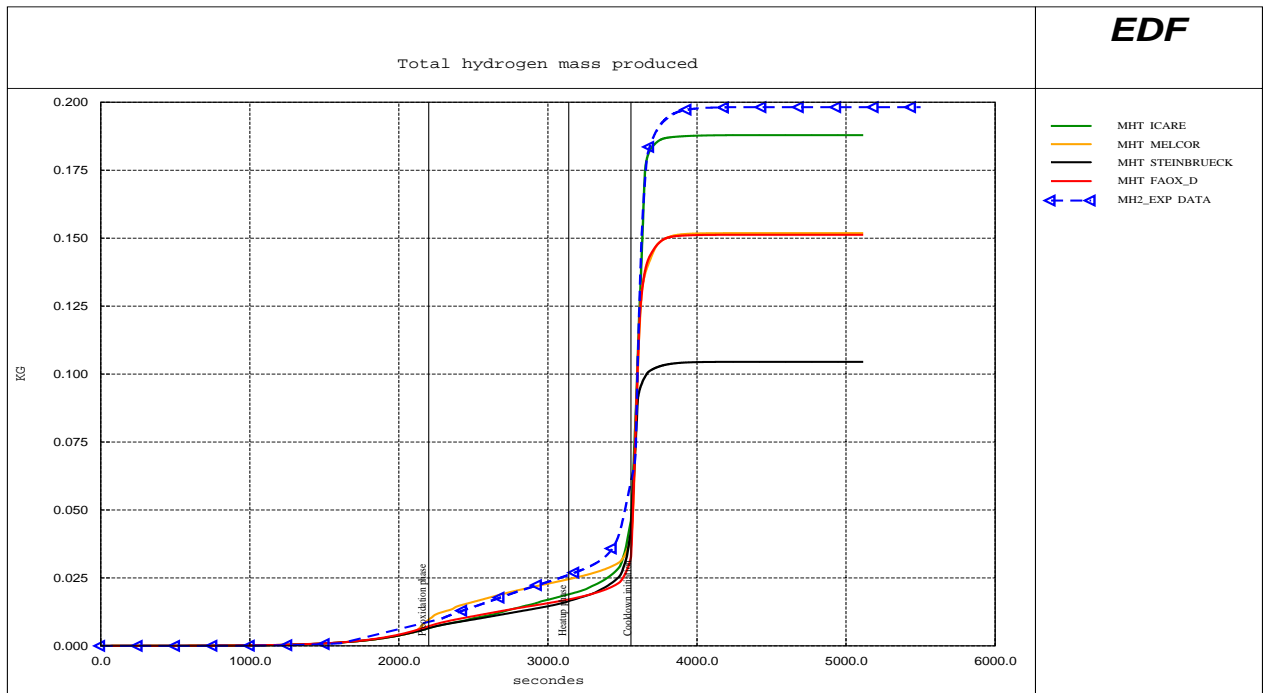
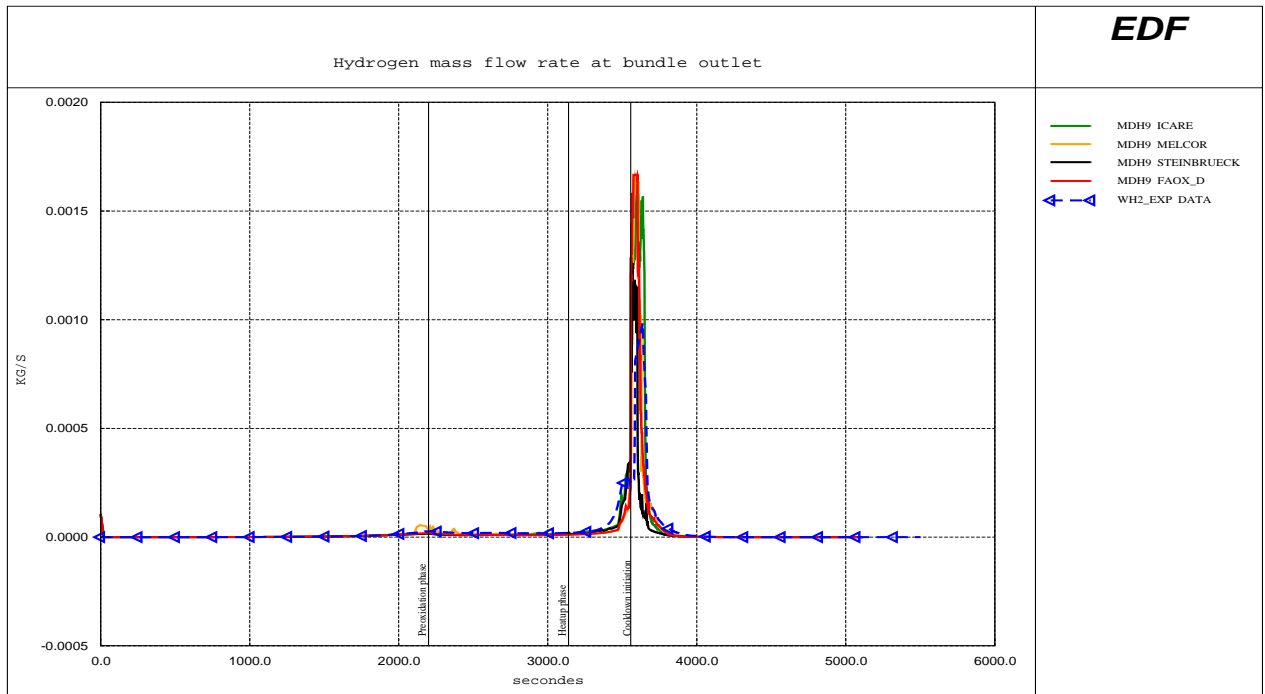


**Fig. 117 :** MAAP4 calculations showing the effect of different B<sub>4</sub>C oxidation kinetics on H<sub>2</sub> production in the QUENCH-07 test (H<sub>2</sub> rate in the upper part and total H<sub>2</sub> production in the lower part).

### 3.13.3 Analytical support for QUENCH-09 test (FZK)

Test overall objectives of the QUENCH-09 and QUENCH-07 tests are the same regarding the study of the B<sub>4</sub>C effects on core degradation. QUENCH-09 was carried out to extend the database to different core degradation conditions and provide more information for the preparation of the future PHEBUS FPT3 test.

The preparation of the QUENCH-09 test was performed in the same context as for the test QUENCH-07, using the same tool SCDAP/RELAP5 (S/R5) mod 3.2 and in close cooperation with PSI. The various calculations also rely on the experience gained from calculations and experimental results from QUENCH-07.

In the following FZK work for pre- and post-test analysis is summarized, showing crucial points in the preparation of the test and the status of the work with open questions for further analysis. More details about FZK analytical support are given in Ref.[27].

#### Test Protocol

After discussions in several COLOSS meetings (Ref.[28, 29]) about the test conduct, a test protocol was set up, which should be the same as in QUENCH-07 up to and including the plateau phase at a maximum bundle temperature of more than 1700 K. If no reaction products from the degradation of the absorber rod are detected, the plateau phase before the second transient should last 5 minutes, otherwise 15 minutes to facilitate the detection of the reaction products as in QUENCH-07. However, the subsequent temperature increase (second transient) was planned at constant electrical power input and steam mass flow reduced to 0.3 g/s in order to have steam-starvation conditions as planned in the FPT3 test. Cool-down was planned from the same maximum temperature as in QUENCH-07 but with a steam mass flow rate of 50 g/s instead of 15 g/s, intended to conserve the status of the bundle before final cooling.

#### Pre-Test Calculations

The modelling of the test facility with SCDAP/R5 is as for QUENCH-07. Because of the similarity of the two tests, pre-test calculations for QUENCH-09 were based on post-test analysis of QUENCH-07 (Ref.[26]). These post-test calculations gave, however, too large deviations between calculated and measured temperatures and hydrogen production rates, in the initial period with the same scenario in the two tests. The differences were mainly in the hot zone and too large to be acceptable for reliable pre-test calculations for QUENCH-09, because the hot zone is the most important and the most critical issue for the test conduct.

As a first step, the electrical power has been modified with respect to QUENCH-07 experimental data so that measured temperatures are sufficiently well met in the calculation for the phases up to and including the temperature plateau, above all in the hot zone. Representative results, obtained with the coarse axial discretization, the 16f model, are given in Fig. 118. Experimental values from QUENCH-07 are included for comparison on all figures. Similarly to the findings for QUENCH-07, it gives the sensitivity of the facility, when experimental parameters are changed. Since the convective heat removal is smaller when the steam mass flow rate is decreased, this sensitivity is enhanced during that phase. In these conditions, the reaction time for operators is more limited.

Representative results for the 32f model are given in Fig. 119 and Fig. 120, the current preliminary absorber model being used for run q09w08. The time dependant results as well as the

axial profiles show that during the second transient (Phase IV) (before *steal cool\_down*) practically the *whole steam supply is consumed in the bundle as it was intended*. The peculiar oxide layer profile for the absorber rod may be attributed to rod degradation. Differences to the present results are limited, when an unheated fuel rod is simulated (run q09w06) or when the 16f model is used (run q09v05).

During the second part of the transient, the axial temperature profile becomes broader. The maximum of hydrogen production rate shifts markedly to lower axial elevations, but for temperature and oxide layer thickness, this shift is less pronounced. Larger shifts of the maximum temperature and eventually even a second maximum in the lower bundle half, calculated by other participants occur mainly at later times than considered in FZK calculations. The effect is an essential issue for an appropriate instrumentation.

During steam cool-down, some limited temperature escalation was predicted to occur due to local shattering of the oxide layer, but problems for the test conduct were not identified.

### **Post-Test Calculations**

Post-test calculations are based on the real test conduct with the same modelling as for the pre-test calculations. Results are given in Fig. 121 as a function of time using the 16f coarse core model. In the first part of the transient, calculated temperatures are underestimated at the top of the heated zone (axial level 13), and in the plateau phase temperatures are calculated to increase continuously. Before steam mass flow reduction, hydrogen production is hence underestimated. No significant difference between the coarse and the fine axial discretization of the facility was found except near the bundle exit and furthermore near the upper end of the heated zone during cool-down. This result is in contrast to that for QUENCH-07 (Ref.[26]); it may depend on details of the test conduct; therefore, it cannot be generalized.

For standard calculations, the thermal conductivity for the shroud ZrO<sub>2</sub> fibre insulation, delivered by the manufacturer, was increased by 80 %, based on experience from QUENCH-01. This physical parameter was changed to better meet the measured data in the first transient and hence get better-calculated initial conditions for the plateau phase. The temperature escalation and the hydrogen production during the heat-up phase could only be calculated using the manufacturer's data (Fig. 122), and the temperature escalation at the time of absorber rod failure agrees quite well with measured temperatures. The calculated time of control rod failure shifts from 2343 s to 2280 s as detected in the experiment. However, in the following plateau phase deviations with respect to experimental data were larger than in the first post-test calculation.

Since the axial temperature profile during the second part of the transient was a concern in the preparation of the test, measured and calculated data were analysed in more detail. In Fig. 123, their values are compared at different times; the readings of the questionable thermocouples are not included. As a rough estimate for the bundle behaviour, the shroud thermocouples can also be included. At about 2800 s the maximum temperature shifts somewhat to the bundle centre, then the profile becomes flatter, and eventually extends down to elevation 10 (0.65 m). Calculated values overestimate measured ones except in the beginning of the second part of the transient, but the change of the axial profile with time is correctly calculated.

In a further calculation, the recommendations for Zr oxidation, made during the COLOSS project (see Part 2 of this report), have been applied instead of the standard correlations in S/R5 (Cathcart and Urbanic-Heidrick for low and high temperatures, respectively). Discussions during COLOSS meetings showed that a steam supply limitation in the boundary layer of the cladding is mandatory for the new oxidation model with Prater law for high temperatures. For the calculations presented here the model, already implemented in S/R5 is used as for the other calculations of QUENCH-07. The agreement with experimental data is improved during steam rich periods (Fig. 124, label Schanz) and during cool-down. Preliminary results for QUENCH-

07, however, gave with recommended oxidation laws a drastic overestimation of oxidation at high temperatures. Therefore, more work is necessary to apply the new oxidation correlation successfully.

The comparison of test QUENCH-07 and QUENCH-09 shows tremendous differences after the failure of the absorber rods, though experimental conditions differ only marginally, if any. The reasons for these differences are not yet clear and probably need more investigations. Consequently, further model development for absorber rod behaviour should not be done before the experimental differences are better understood.

**Table 23:** Sequence of phenomena during B<sub>4</sub>C degradation and observed effects on QUENCH tests

Temperature		Phenomena	Significance	Quench		Consequences	Parameters
[K]	[°C]			07	09		
		Clad rupture (depressurization)	No	No	Limited steam access to B <sub>4</sub> C		
1250	977	Onset of Zr-SS Interaction (Guide tube - Absorber sheath)	Y	Y	Initiation of guide tube weakening	Protective: ZrO <sub>2</sub> layer > 50µm	
1470	1197	Enhanced Zr-B <sub>4</sub> C dissolution rate	---	---	After failure	no	
1473	1200	Liquefaction of the B <sub>4</sub> C-SS system	Y	Y	Liquid layer of B <sub>4</sub> C-SS (kept within ZrO <sub>2</sub> shell)	Limitation: max. 9% wt of B <sub>4</sub> C in SS	
1550	1277	Perforation of SS and Zr layers by Zr-B <sub>4</sub> C/SS interaction	Y	VL	Release of gases + liquified MeB, increase of breach size, access of steam	Steam concentration, pressure difference	
		Lateral relocation/spreading of absorber/steel alloy	Onset of propagation	---	No	Triggers ZrO <sub>2</sub> scale failure in adjacent rods	No large relevance compared to AgInCd - CR
		<b>B<sub>4</sub>C Oxidation</b>	<b>Localized</b>	<b>Y</b>	<b>VL</b>	B <sub>4</sub> C oxidation limited? release of oxidation products (B <sub>2</sub> O <sub>3</sub> )	Access of steam through breach
1573	1300	Axially spreading of zone with T>1500K	?	No	Increases area for oxidation, compensates the effect of ZrO <sub>2</sub>	Electrical and chemical power protection	
1723	1450	Melting temperature of SS	no	---	---	Liquid column kept within outer ZrO <sub>2</sub> shell; No longer metallic β-Zry available	no
		Limitation of oxidation?	Chemical thinning of ZrO <sub>2</sub>	No	Y	Less protective ZrO <sub>2</sub> layers on fuel rods and absorber rod guide tube	Steam supply
1870	1597	Zr-B <sub>4</sub> C reaction rate jumps (app. 2 orders of Mag)	Protective oxide layer inhibits interaction?	?	?	Inhibited by ZrO <sub>2</sub> layer in case of QUENCH-09	wetted surface, mass
2033	1760	Melting temperature of β-Zry		---	---	Enhanced U-Zr-O interaction starts (similar for Zr-ZrO <sub>2</sub> )	
2330	2057	Lowest reasonable clad failure temperature (α-Zr(O))	Formation of B <sub>4</sub> C-Zr-SS mixture, release possible	Y	Y	Fuel rod: melt release (U-Zr-O), influence of CR behavior?	Limitation: max. 9% wt of B <sub>4</sub> C in SS+Zry
?	?	Cool down initiation: high steam supply		---	Y	QUENCH-09: Steam starvation favours uncontrolled temperature escalation	Cool-down in Q-07 faster than in Q-09
		Amount of B <sub>4</sub> C reacted		40	>40	% of 1 m bundle fraction (consider only T>1500K !)	

Notes: Some temperatures are lower limits for reaction

Status: based on present knowledge (Jan 2003)

CR: control rod

VL: localized and very limited interaction

### First analysis of control rod failure

For a better understanding of the respective QUENCH tests and as a general basis for code developments, the sequence of phenomena related to absorber rod degradation is investigated in two QUENCH tests, based on present knowledge. Further insight is expected, when results of the destructive post-test analyses for QUENCH-09 are available. A list of phenomena is given in

Table 23, focusing on the explanation of the different B<sub>4</sub>C-CR behaviours observed in QUENCH-07 and QUENCH-09.

As can be seen, no difference between the two QUENCH tests is noticeable up to 1550 K. In both tests, the stainless steel tube was penetrated, but in QUENCH-09 no significant amount of reaction products of B<sub>4</sub>C degradation was detected before cool-down initiation. This behaviour was quite unexpected. For a better understanding of the test, the following scenario is presently supposed for QUENCH-09. From this finding it is deduced that no direct steam access to the B<sub>4</sub>C was possible at that time and hence the melt remained localized either due to a protective ZrO<sub>2</sub> scale or, more likely, because the melt blocked the breach, even after exceeding 1700 K, the melting temperature of SS. Between 2700 s and 3300 s, measured temperatures exceed 2040 K. This indicates that the  $\alpha$ -Zr(O) is liquid, forming a liquid alloy column, composed of B<sub>4</sub>C, SS, and Zr. With the failure of the oxide scale on the guide tube, which occurred during reflood, this liquid is released and oxidized immediately.

Such a scenario would explain the observed rapid increase of CO<sub>2</sub> and CO release, which is favoured by the steam excess during the final fast cool-down. The ideas mentioned above have to be checked by the results of the destructive post-test analyses.

### **Main outcomes**

#### Pre-test calculations

Due to the similarity of the first part of the two tests, calculations of QUENCH-09 could be based on post-test analysis of QUENCH-07.

The electrical power input was modified with respect to QUENCH-07 to improve the agreement between calculated and measured data up to the start of steam mass flow reduction.

The preliminary modelling of the absorber rod did not change results appreciably with respect to former calculations, where an unheated fuel rod was modelled instead of the central B<sub>4</sub>C CR.

The major difference of axial mesh refinement was only in the upper electrode zone and around the upper end of the heated zone during cool-down. The axial temperature profile became broader with time. The maximum of temperature and oxide layer and, to a larger extent, of hydrogen production shift somewhat to lower elevations during the transient.

Some limited temperature escalation was predicted to occur during steam cool-down, but no difficulties were predicted in the cool-down phase.

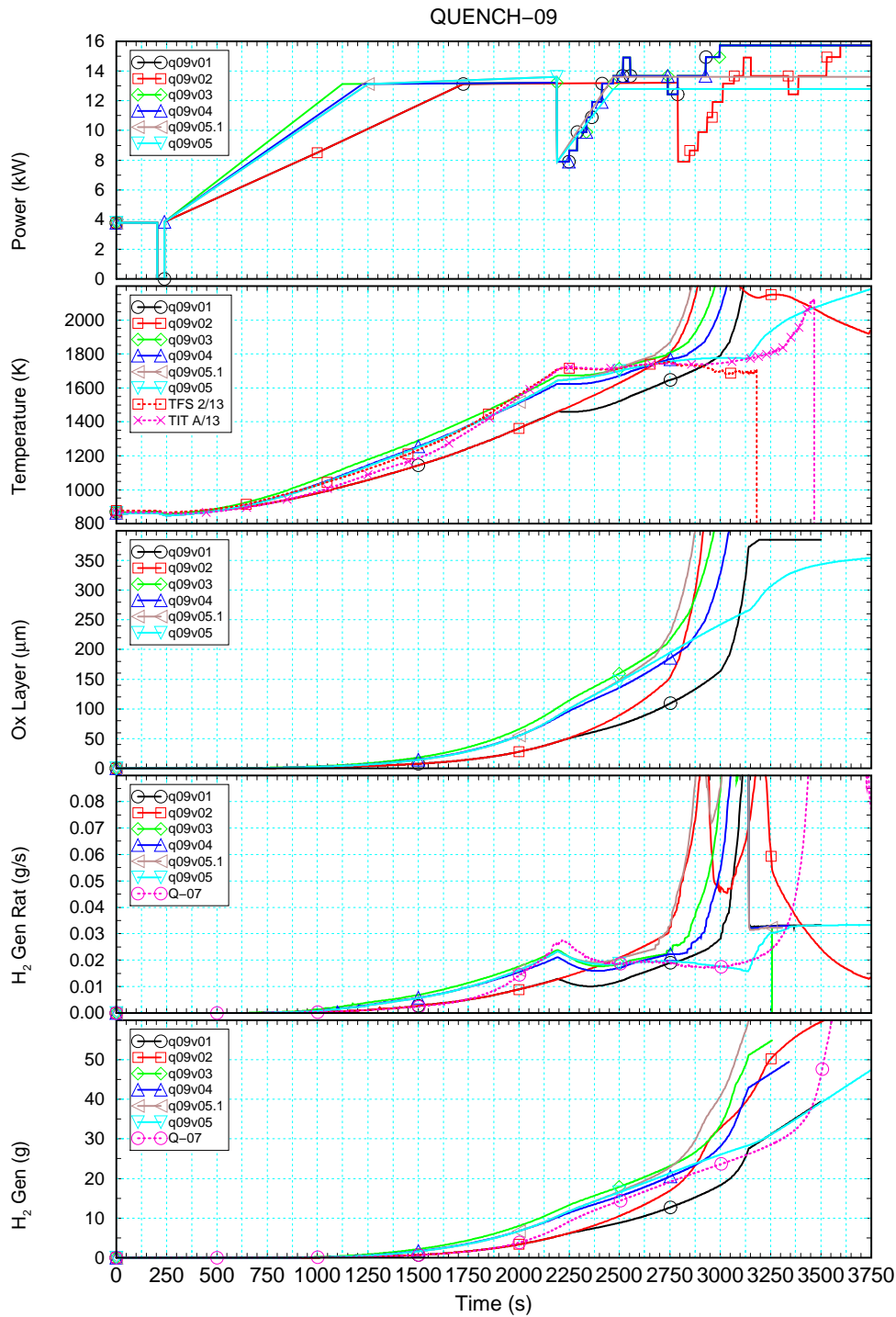
With the experimental conditions chosen, calculations confirmed that the QUENCH facility would be rather sensitive to changes of experimental parameters as electrical power input and that the facility might even be damaged during the test.

#### Post-test calculations

Preliminary studies showed deviations from experimental data. A parameter study to improve the agreement at the time of the steam mass flow reduction gave no better results in the subsequent test phase. The calculated broadening of the temperature profile was in agreement with experimental data. The recommendations on the choice of Zircaloy oxidation correlations gave some improvement, but this choice remains to be confirmed.

Further work is needed to finalise the interpretation taking into account post-test measurements and the analysis of accompanying SET on B<sub>4</sub>C oxidation.

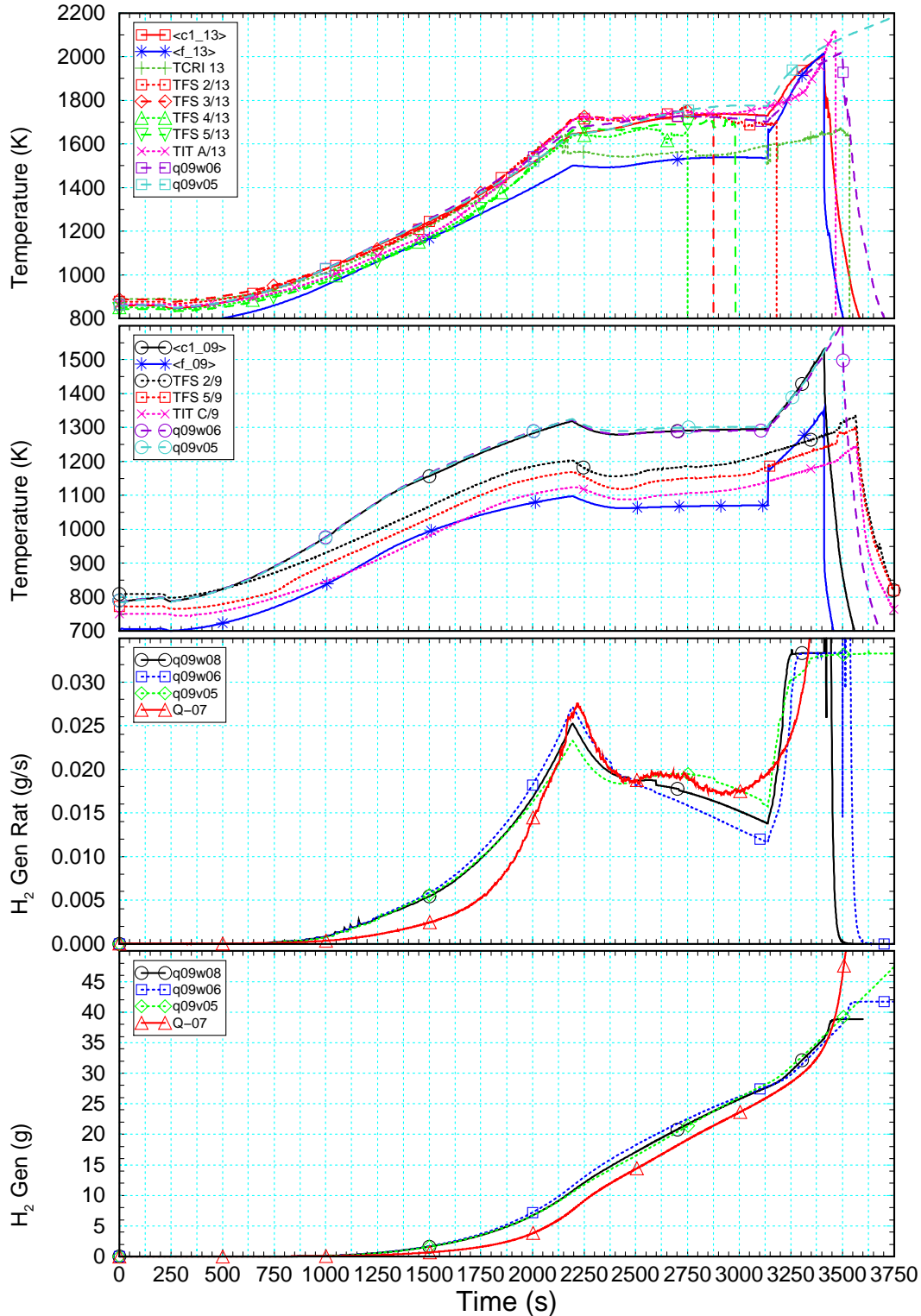
The sensitivity of the facility, when experimental parameters are changed, and the small safety margin for the given experimental conditions, predicted in the pre-test calculations, was confirmed during the course of the test. This result justifies the large effort, done by several institutions, engaged in the COLOSS project to define an appropriate test conduct for both QUENCH tests with a central B<sub>4</sub>C absorber rod.



FZK/IRS Ch. Homann sr32.1036i.x

**Fig. 118:** Pre-test calculations with S/R5 using the coarse ‘16f core model’. From top to bottom: electrical power input, temperatures and  $\text{ZrO}_2$  layer thickness at axial level 13 (elevation 0.05 m),  $\text{H}_2$  production rate, and total  $\text{H}_2$  mass. In the legends experimental values (TFS 2/13, TIT A/13, and Q-07) refer to QUENCH-07, the other labels refer to identifiers for the computational runs.

QUENCH-09 q09w08



FZK/IRS Ch. Homann sr32.i036i.x

**Fig. 118:** Pre-test calculations with S/R5 using the fine ‘32f core model’. From top to bottom: clad temperatures for the inner heated rods at axial levels 13 and 9, and hydrogen production rate, and cumulated hydrogen mass in comparison to experimental values for QUENCH-07.

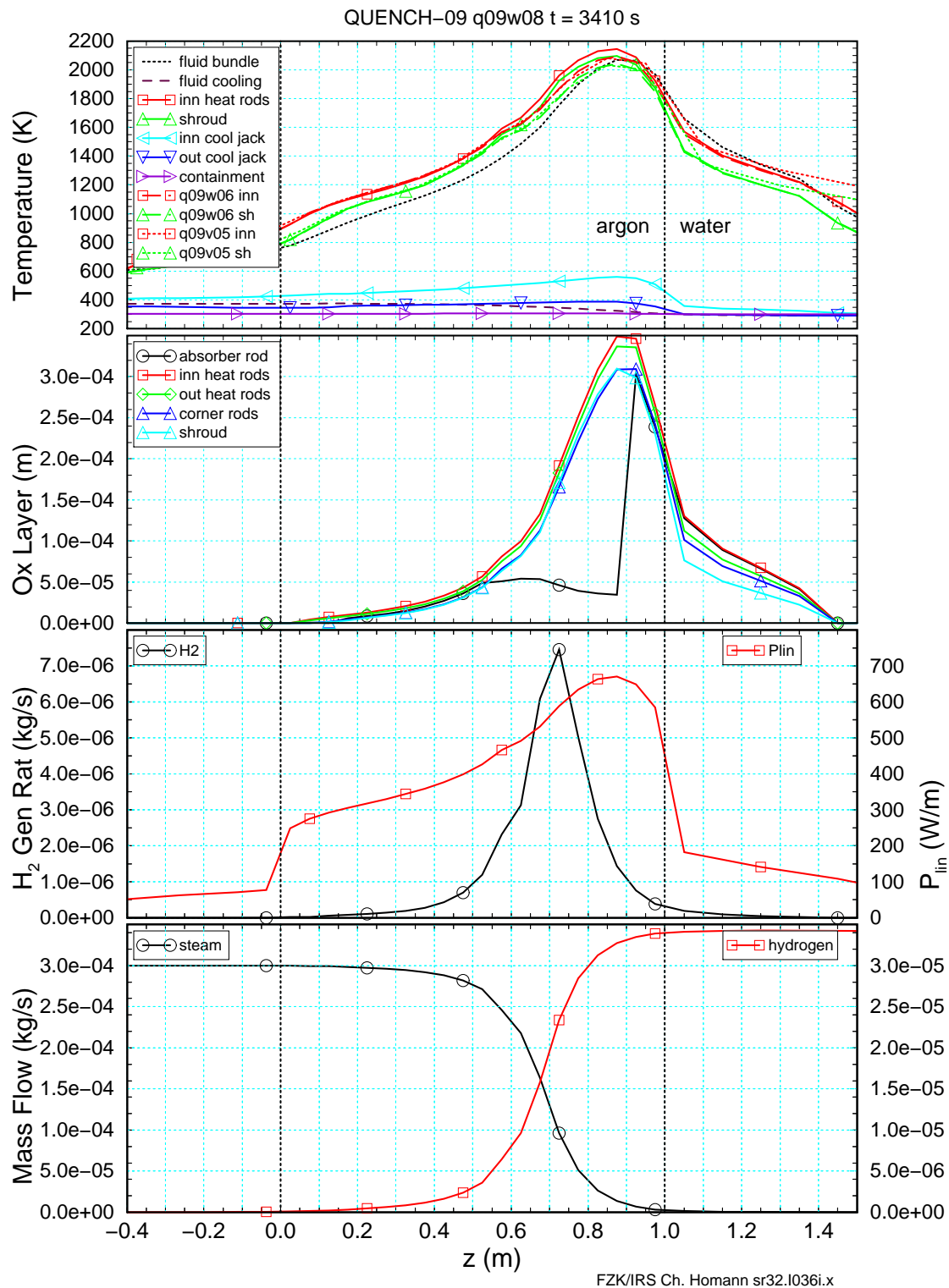
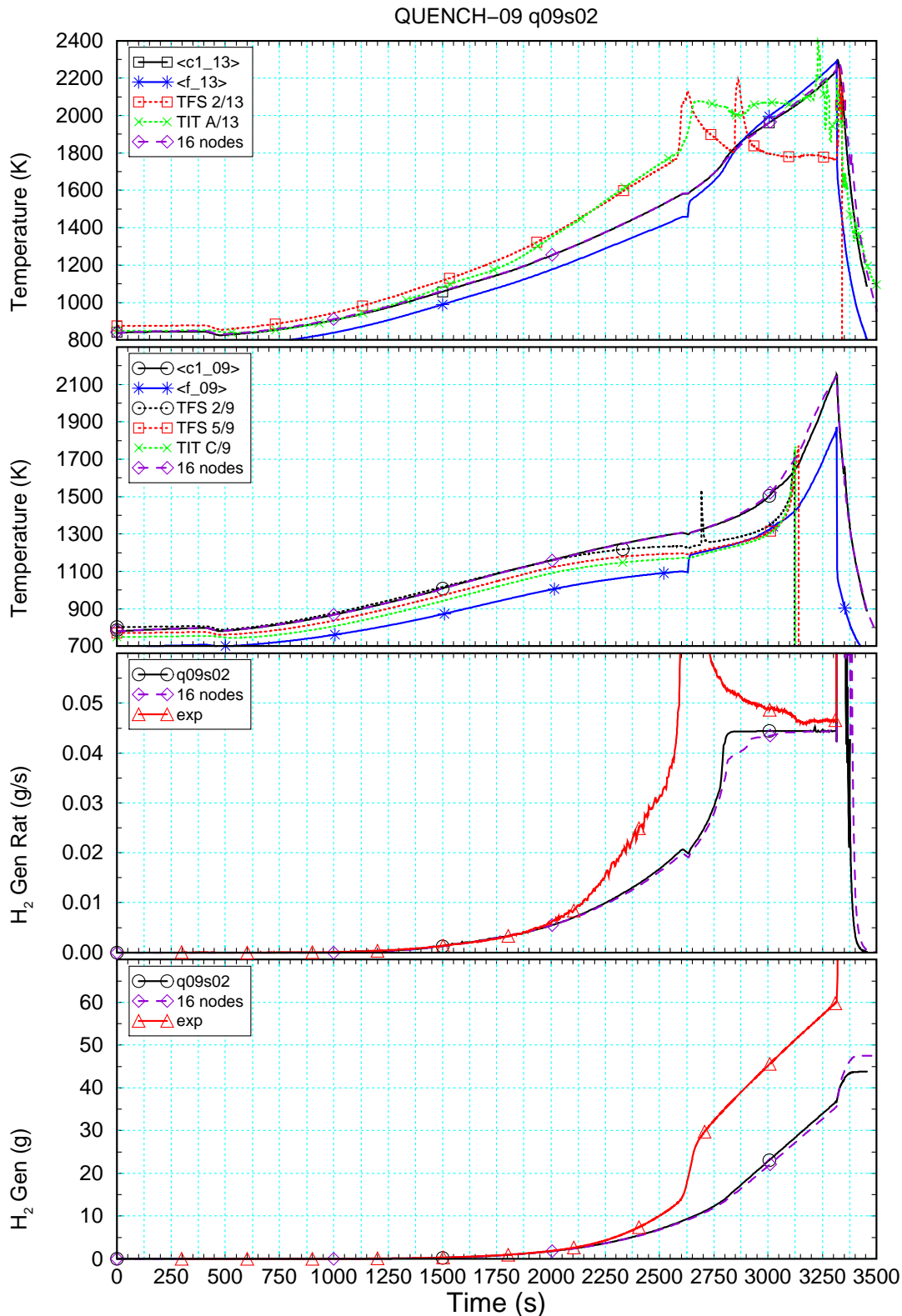
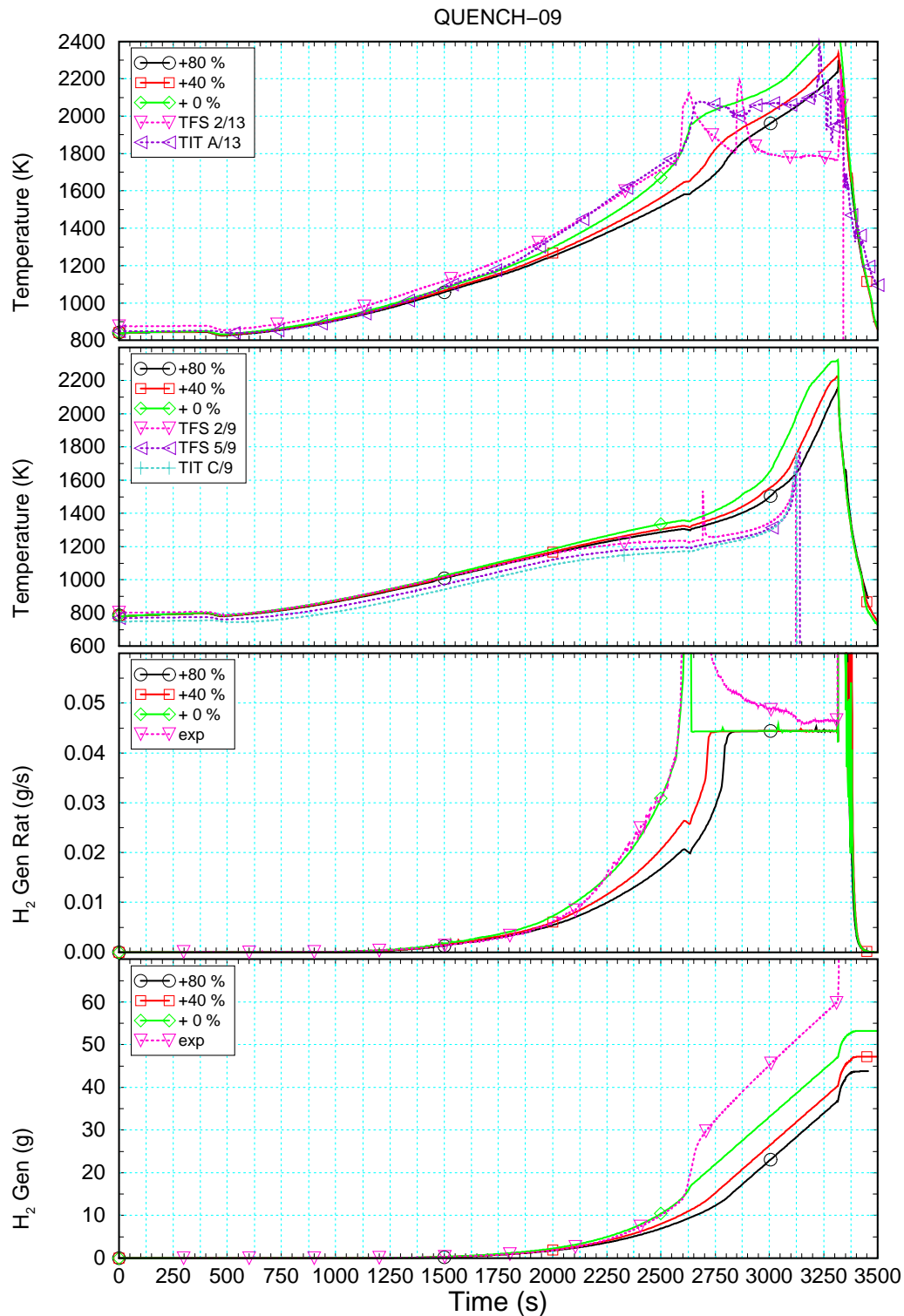


**Fig. 120:** Pre-test calculations with S/R5 using the fine ‘32f core model’. Axial profiles of selected variables at the end of the second transient (pre-test calculations). From top to bottom temperatures, oxide layer thickness, H<sub>2</sub> production rate, linear electrical rod power, steam, and H<sub>2</sub> mass flow rates at the end of the second transient.



FZK/IRS Ch. Homann sr32.i036j.x

**Fig. 121:** Post-test calculations with S/R5 using the coarse '16f core model'. From top to bottom calculated and measured values for temperatures at axial levels 13 and 9 (elevations 0.95 and 0.55 m), H<sub>2</sub> production rate, and cumulated H<sub>2</sub> mass for calculated and measured results.



FZK/IRS Ch. Homann sr32.i036j.x

**Fig. 122 :** Selected variables as a function of time (parameter study). From top to bottom calculated and measured temperatures at axial levels 13 and 9 (elevations 0.95 and 0.55 m), H<sub>2</sub> production rate, and cumulated H<sub>2</sub> mass for the three increases (80, 40, and 0 %, respectively) of thermal conductivity of shroud insulation with respect to manufacturer's data.

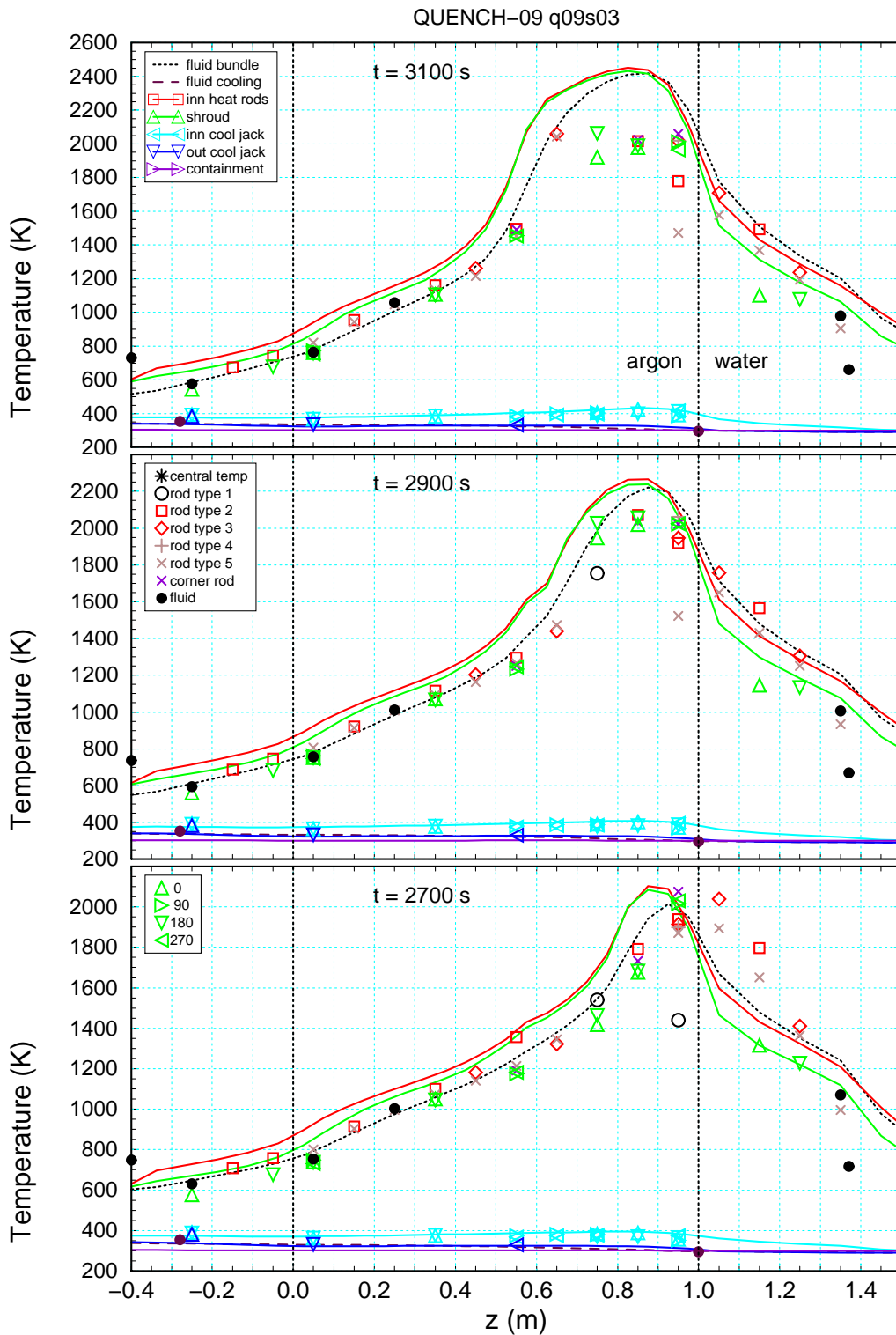
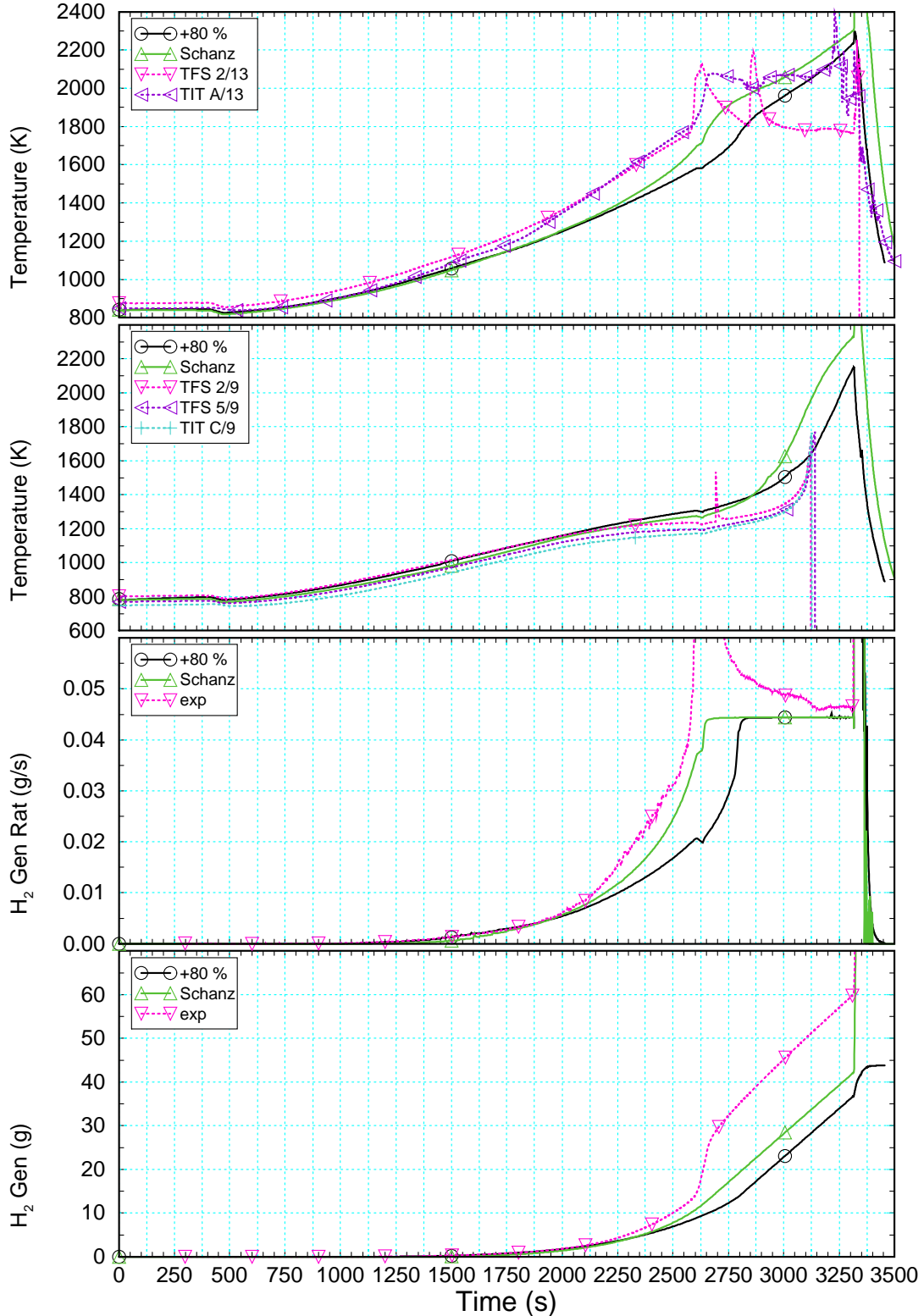


**Fig. 123:** Axial temperature profiles in the second transient. Calculated and measured temperatures for inner heated rods, the shroud, inner and outer cooling jacket, the containment and for the fluid in bundle and cooling at three times during the second transient. Manufacturer's data for shroud insulation are used in the calculation.

QUENCH-09



FZK/IRS Ch. Homann sr32.1036j.x

**Fig. 124:** Selected variables as a function of time (oxidation correlation). From top to bottom calculated and measured temperatures at axial levels 13 and 9 (elevations 0.95 and 0.55 m), H<sub>2</sub> production rate, and cumulated H<sub>2</sub> mass for the standard and the oxidation correlation recommended by Schanz.

### 3.13.4 Analytical support for QUENCH-07 and QUENCH-09 (PSI)

#### Pre-test calculations of QUENCH-07

PSI collaborated closely with FZK to support the planning of QUENCH-07 and provided calculated results for inclusion in the pre-test prediction report (Ref.[26]). The calculations were performed with SCDAP/RELAP5 using two alternative models:

- A 'fuelrod' model using the same unheated fuel rod component as in QUENCH-01 to simulate the central absorber rod, but with the dimensions and cladding thickness corresponding to the guide tube.

- A 'bladebox' model using the SCDAP BWR blade-box component, which nominally comprises the B<sub>4</sub>C rods, stainless steel sheath and blade, and the Zry channel box. The geometries were defined to reproduce the dimensions of the single absorber rod, its cladding and guide tube in the QUENCH-07 bundle. This arrangement, although a distortion of the SCDAP blade-box, provided the best simulation achievable with SCDAP.

The 'bladebox model' attempted to investigate the effect of B<sub>4</sub>C and steel on the degradation and oxidation offgas composition. The model predicted significant movement of generated melts to the lower part of the bundle and some local blockage, but limitations in the SCDAP code and in the way the model is implemented in the code meant that these estimates were very uncertain and no information could be gained about offgas CO, CO<sub>2</sub>, CH<sub>4</sub> and B compounds production.

The 'fuelrod model' proved more reliable and was used for estimates of the thermal and oxidation transients. The model predicted a gradual increase in temperatures to the target of 1700 K for the plateau, followed by a transient driven by electrical heating to ca. 2300 K. The oxidation rate increased during the transient but the bundle outlet conditions remained steam rich. A rapid cooldown was predicted with no suggestion of an oxidation excursion.

#### Pre-test calculations of QUENCH-09

Planning calculations for QUENCH-09 were performed using SCDAP/RELAP5 with the same input model and test conditions as for QUENCH-07 for the phases up to the start of the second heat-up, at which point the steam flow was reduced with the power kept constant. Four cases were run with different reduced flow rates between 0.2 and 1.0 g/s. The results indicated a temperature escalation driven by the oxidation but limited by the steam availability (steam-starvation conditions), so that the escalation was slowest at the low steam flow and fastest at the higher flow. A mild cooldown excursion was calculated with 12 g H<sub>2</sub> generated.

#### Post-test analyses of experiments QUENCH-07 and -09

Preliminary calculations were performed for QUENCH-07 using SCDAP/RELAP5 with the actual transient test conditions (q07post02). Attainment of the plateau temperature was delayed and the hydrogen generation was underestimated during all phases of the experiment, suggesting that the model overestimated the bundle heat losses. In particular the oxidation excursion during cooldown was not calculated. Modifying the boundary conditions to mimic the operator control (q07post03) enabled the temperature plateau to be calculated correctly but made no difference to the calculation during cooldown. Delaying the initiation of cooldown resulted in higher peak temperatures, but again with no affect on cooldown behaviour. In a further sensitivity study, the global shattering model was invoked at the start of cooldown in order to simulate enhanced exposure of metallic. Close agreement was achieved for the total hydrogen

mass but there was a gross overestimate of the bundle temperatures and a distortion of oxidation axial profile. The comparisons suggest that degradation events during the experiment exposed the metallic and made it more susceptible to oxidation. Some results are shown in Figure 125 and 126. The SCDAP/RELAP5 post-test calculations of QUENCH-07 are reported in (Ref. [30]).

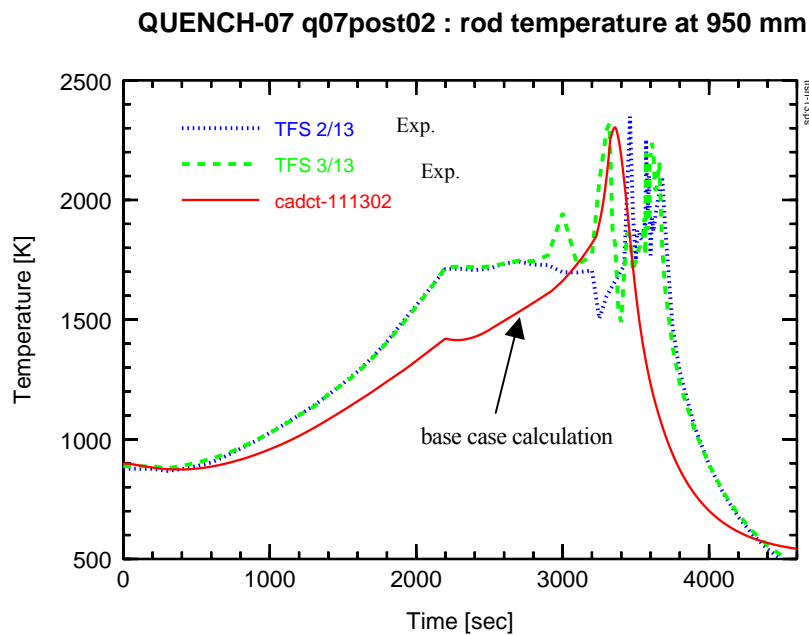


**Figure 125:** Post-test calculation of heater rod temperatures

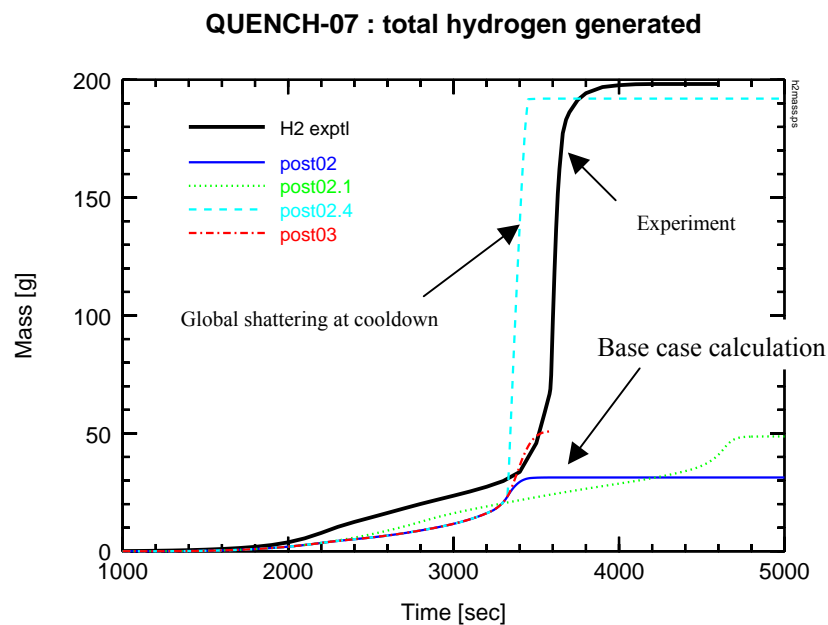


**Figure 126:** Comparison of H<sub>2</sub> generation (expt; base case calculation; modified power history; global shattering at cooldown; delayed cooldown)

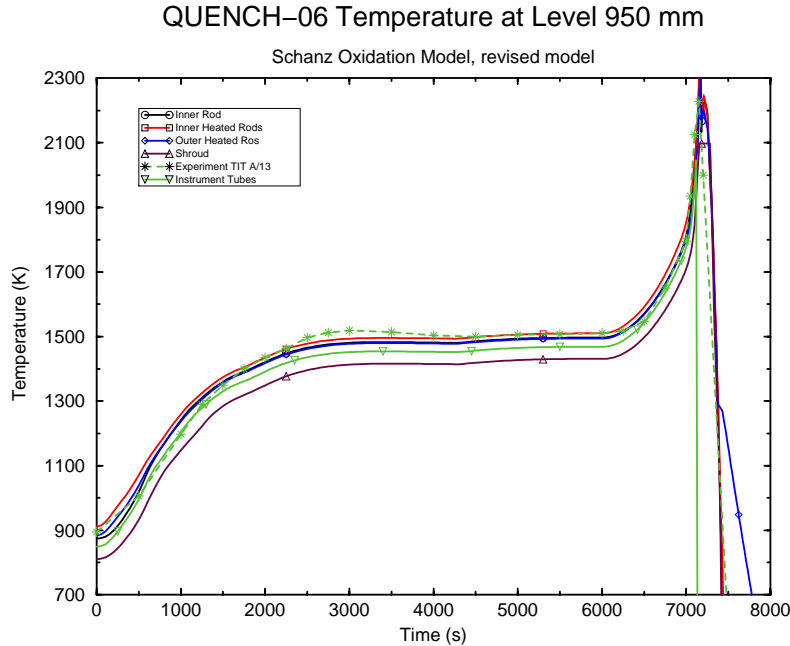


**Figure 127:** Temperatures in radial zones at 950 mm, and experimental temperature on corner rod TIT A/13: Revised model, Schanz recommendations.

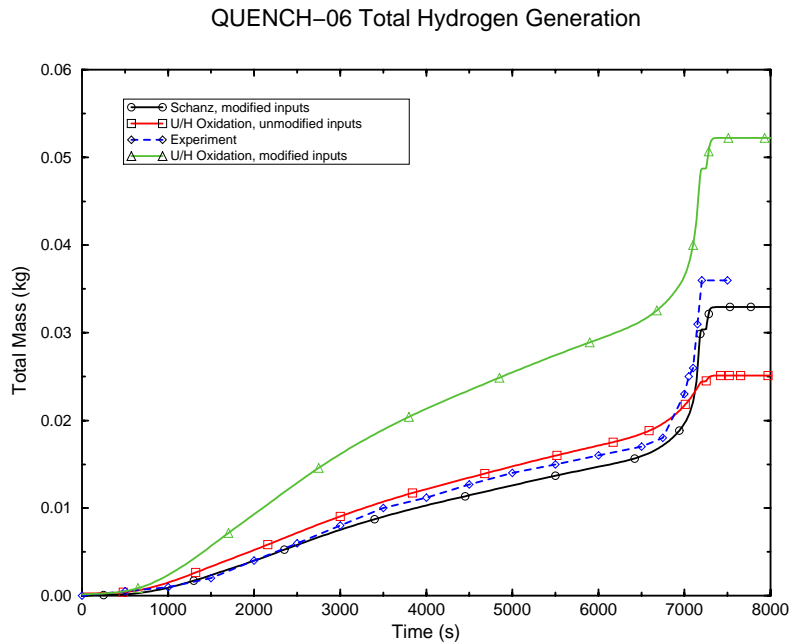


**Figure 128:** Comparison of total hydrogen generation between experiment, original and revised models (U-H and Schanz recommendations)

Deficiencies in the models for B<sub>4</sub>C absorber rods, in particular the lack of representation of oxidation offgas composition motivated the adoption of MELCOR 1.8.5 (release RD) for further

post-test analyses. The switch is in line with the choice of MELCOR for plant applications at PSI, and the fact that it was used in the plant calculations performed in COLOSS WP8 (see Part 2 of the report).

Analyses of the QUENCH experiments are reported in (Ref.[31]). Preliminary benchmarking calculations were performed against QUENCH-06, after some changes to the input. A feature of the input was the use of a BWR-type geometry in order to represent the Zircaloy shroud by a canister component for which MELCOR models the oxidation. This non-standard treatment is specific to the QUENCH facility. However, it did not appear to compromise the calculation of QUENCH-06 - indeed, the model gave very satisfactory agreement for temperature (Figure 127). Introduction of the Leistikow/Prater-Courtright correlations for Zircaloy oxidation (Schanz recommendations) gave much better results for hydrogen generation than the default Urbanic-Heidrick model (Figure 128) and was therefore adopted in the base model for QUENCH-07 and -09.

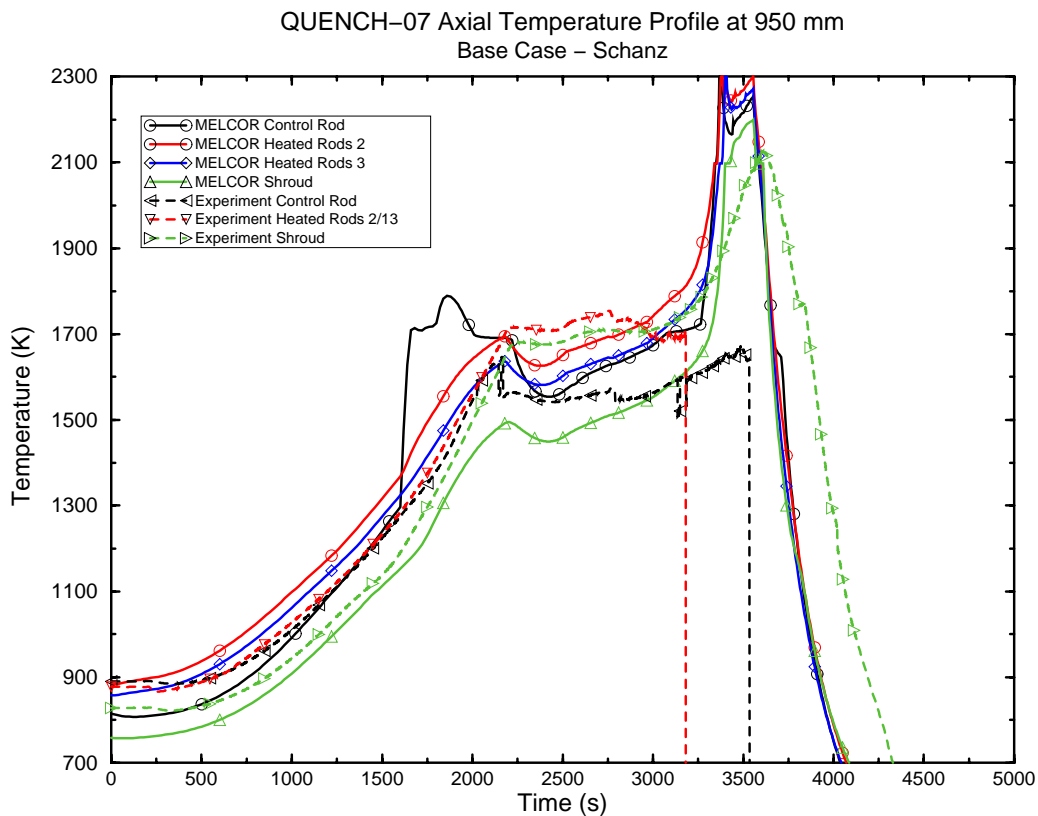


**Figure 129:** Comparison of temperatures at elevation 950 mm MELCOR and experimental data, various radial locations.

The input was modified further to include the B<sub>4</sub>C absorber rod. The QUENCH-07 experiment proved more challenging to reproduce. The initial heat-up was, again, in good agreement but the thermal response became increasingly sensitive as the temperatures increased to and beyond 1700 K. It appears that the thermal response was driven by the cladding oxidation at these higher temperatures so that small differences in temperature became magnified. The oxidation of B<sub>4</sub>C was more problematic in that the rate was grossly overestimated during the initial phase just after failure of the steel cladding. Adjusting the input parameters that control the oxidation gave some improvement but the MELCOR B<sub>4</sub>C model is designed primarily for a

BWR configuration and is not well-suited to the rod geometry of a PWR. In particular the assumption that the  $B_4C$  is in powder form grossly overstates the kinetics with the result that the rate and total  $B_4C$  oxidation was overestimated. Despite these difficulties the model gave an otherwise good representation of the thermal response, oxidation and degradation up to the initiation of cooldown. The offgas composition was calculated with at least acceptable accuracy. In common with the SCDAP analyses, the cooldown excursion was calculated only by artificially enhancing the oxidation kinetics. Some results are shown in Figure 129.

The initial phase of QUENCH-09 was conducted in a similar manner to QUENCH-07 but the temperature ramp was continued slightly further, approaching 1800 K, so the oxidation had an even stronger effect in driving the thermal behaviour. The temperatures during the initial heat-up were underestimated slightly, but sufficiently so that the first oxidation excursion was not calculated with the base model (use of Leistikov-Schanz oxidation correlation). Use of Urbanic-Heidrick instead of the Leistikov/Prater-Courtright model gave more rapid oxidation and overestimated the initial excursion. Thus the two cases bracketed the experimental behaviour during this first heat-up period. Both models correctly calculated the steam starvation following the reduction in steam flow as well as the degradation in the upper part of the bundle. Again, however, the large excursion during cooldown was not calculated so that the extent of degradation and the total  $B_4C$  oxidation were underestimated. A curious difference between the tests was the oxidation of  $B_4C$  observed during the main phase of the QUENCH-07, but not in – 09. The onset of  $B_4C$  oxidation can be controlled by suitable choice of model input parameters, but the difference between the tests cannot be predicted in any MELCOR calculation. The treatment of  $B_4C$  oxidation must be considered as somewhat uncertain in MELCOR analyses. Some results are shown in Figures 130 to 134.

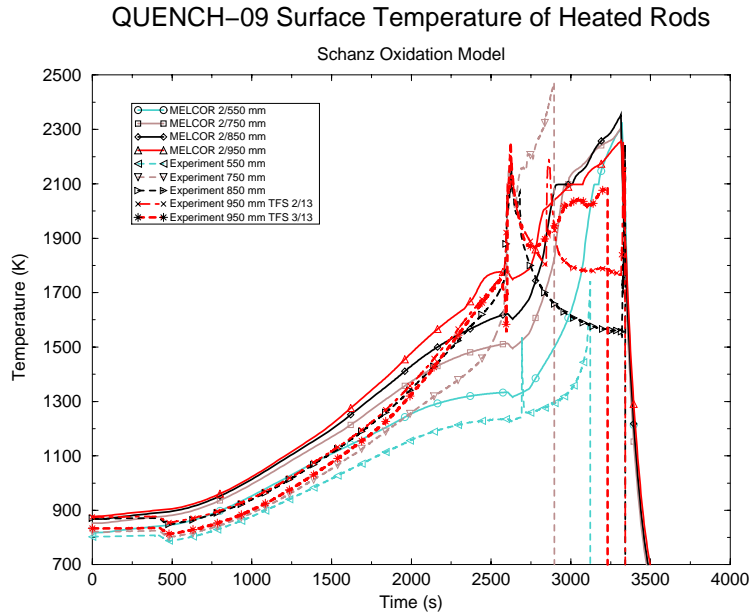


**Figure 130:** QUENCH-09 test: Comparison of MELCOR calculation using the Schanz oxidation model with measured heated rods surface temperature

### QUENCH-09 Surface Temperatures of Heated Rods

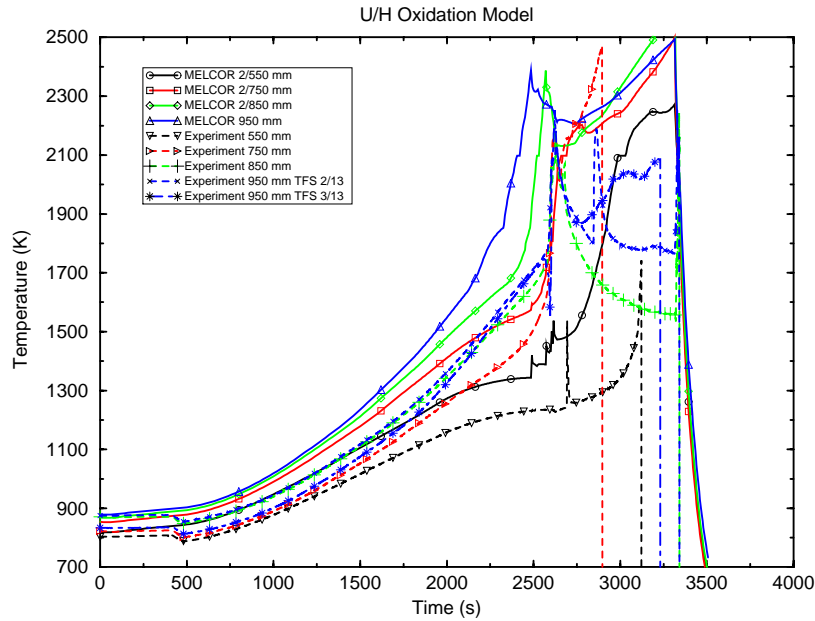


**Figure 131:** QUENCH-09 test: Comparison of MELCOR calculation using U/H oxidation model with measured heated rods surface temperature

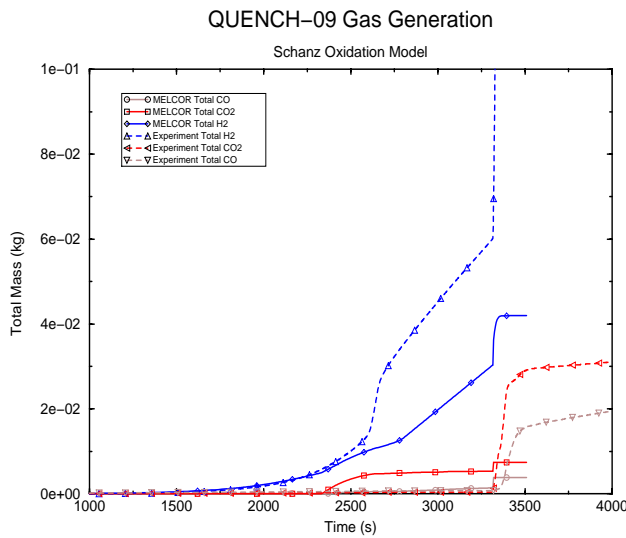


**Figure 132:** Generation of H<sub>2</sub> using the Schanz oxidation model

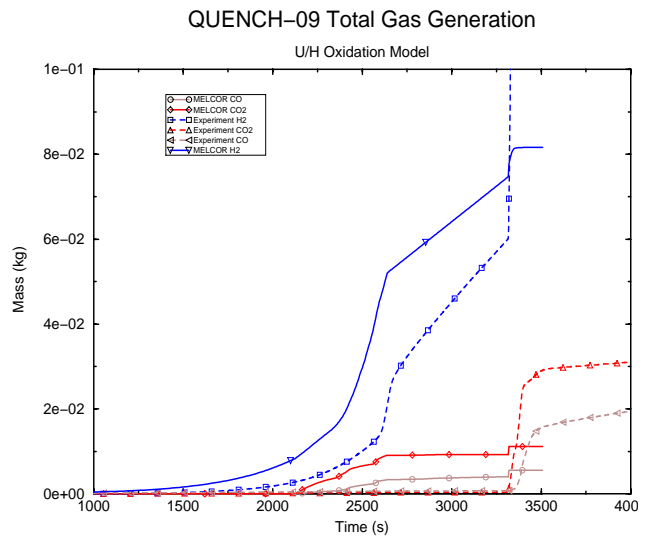


**Figure 133:** Generation of H<sub>2</sub> using the U/H oxidation model

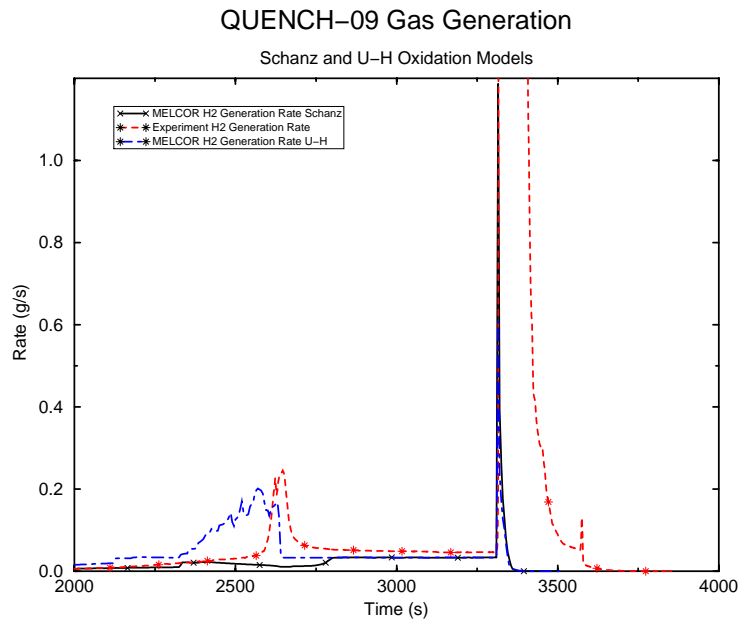


**Figure 134:** Hydrogen generation rates

### Main outcomes

Despite the difficulties concerned with modelling QUENCH facility specific features, MELCOR gave a satisfactorily description of most aspects of the experiments. The main limitations concern  $B_4C$  oxidation and offgas composition, which should be investigated more fully with data from separate effects experiments, for example from the BOX rig tests carried out in WP4.

- The present study concurs with the conclusions given by FZK with S/R5. The “ $B_4C$  oxidation needs more interpretation of the available experimental data”. An appropriate correlation should be pursued, through analysis of the recent and current experiments conducted by FZK and IRSN, and applied to QUENCH-07 and -09. Oxidation of  $B_4C$ /metallic mixtures should also be included.
- The temperature transient is highly sensitive to the conditions at conditions close to the low-high oxidation transition ( $\sim 1800K$ ). The onset of escalation is a knife edge effect at temperatures close to 1800K.
- Uncertainties on the modelling of electric power and shroud heat transfer make difficult to conclude on the best Zr oxidation laws. In the low temperature range, the Schanz recommendation reproduces correctly the Zr oxidation and the  $H_2$  generation for QUENCH-06 test. Nevertheless, there was an underestimation of the initial oxidation stage in the QUENCH 09 test.
- The oxidation of relocating debris and melts can lead to extensive and rapid generation of hydrogen under steam rich conditions. The current models in the code are insufficient and should be thus extended. Account should be taken of possible enhanced oxidation rate of pure metallic due to increased exposure or modified morphology of the debris.

### 3.13.5 Analytical support for QUENCH-07 and QUENCH-09 (IKE)

IKE contributed the preparation and analysis of the QUENCH-07 and QUENCH-09 tests using the ATHLET-CD code.

#### Pre-test and post-test calculations of QUENCH-07

These calculations were carried out with ATHLET-CD using a version without B<sub>4</sub>C modelling. The objectives were:

- to investigate the feasibility of a temperature plateau around 1800-1900°C enabling to study the B<sub>4</sub>C control rod degradation during a sufficient time,
- to investigate the steam and power scenarios (respectively one and two calculations) enabling the temperature increase during Phase IV.

The reduction of the flow rate was found to induce a too large escalation of rod temperatures. The 2<sup>nd</sup> case with a power ramp of 6 W/s induced a maximum temperature of ~ 2000°K and a total H<sub>2</sub> production of ~ 70 g.

First post-test calculations indicate a continuous temperature escalation in the upper zone instead of the 1700K temperature stabilization observed in the test even when the input deck is improved with a finer meshing. The 1700K temperature plateau could only be obtained when the power history was adjusted. Therefore, the input data deck used for simulation of the QUENCH-07 test has been thoroughly revised and inconsistencies regarding the experimental boundary conditions have been eliminated. New calculations were in good agreement with the experimental results, at least up to the initiation of the cool-down phase.

A relatively strong sensitivity has been observed with respect to the Zr oxidation model applied. Using the standard model using the Cathcart correlation up to 1853 K and the switching to the Urbanic/Heidrick model at temperatures above, the maximum temperature of ~ 2200 K and no escalation after cool-down initiation was predicted. The total hydrogen mass of ~ 50 g was slightly underestimated. Following the recommendation of G. Schanz for Zirconium oxidation models using the Cathcart correlation with a transition to the Prater/Courtright correlation above 1800 K, on the other hand yielded a stronger temperature escalation in the upper part of the bundle, continuing after cool-down initiation. The total hydrogen mass of ~ 80 g produced in the calculation nevertheless was still below the ~ 200 g observed in the test (Fig. 135).

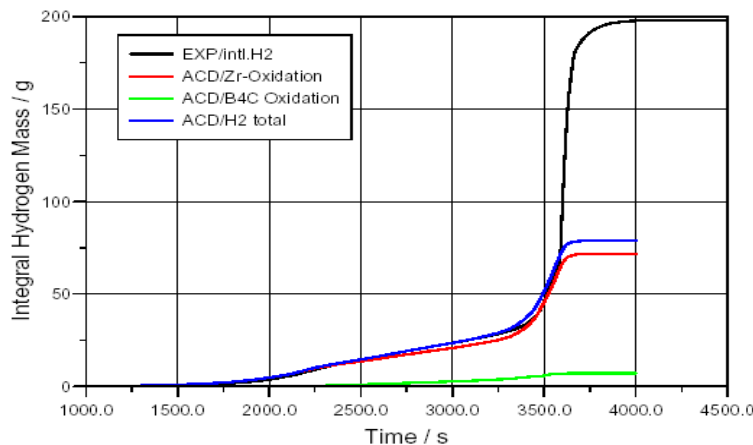


**Fig. 135:** H<sub>2</sub> production measured and calculated by ATHLET-CD in QUENCH 07

The new degradation and oxidation of the central B<sub>4</sub>C control rod has been used, applying the revised B<sub>4</sub>C oxidation model developed and implemented in ATHLET-CD in the frame of the COLOSS project. The B<sub>4</sub>C oxidation was however underestimated in the calculations, giving a maximum total amount of 20% B<sub>4</sub>C consumed by oxidation applying the Liljenzin correlation in the case with Schanz recommendation for Zirconium oxidation.

#### Pre-test and post-test calculations of QUENCH-09

First pre-test calculations have also been performed assuming as boundary conditions the bundle power and the steam flow rate as in QUENCH-07 up to the end of the pre-oxidation phase at 3140 s. Then the bundle power was kept constant at 15.7 kW, with the steam flow rate reduced to 0.3 g/s. Cooldown was assumed to be initiated at 3750 s with a mass flow rate of 50 g/s of saturated steam. During the heatup under steam-starved conditions in the transient phase, maximum temperatures remained below 2300 K, applying both the Urbanic/Heidrick and Prater/Coutright correlations at elevated temperatures. Also, no further temperature escalation has been obtained after cooldown initiation in both cases.

Post-test calculations could not be produced during the project but are planned in the validation matrix of the ATHLET-CD code.

### **3.13.6 Analytical support for QUENCH-07 and QUENCH-09 (UPM)**

UPM contributed the preparation and analysis of the QUENCH-07 and QUENCH-09 tests using the SCDAP/RELAP5 and ICARE/CATHARE codes.

#### Pre-test and post-test calculations of QUENCH-07

Initially, the scenario of QUENCH-07 was planned to be as PHEBUS FPT3 test in order to favour CH<sub>4</sub> production during the degradation/oxidation of the B<sub>4</sub>C control rod. Preliminary pre-test calculations have been carried out with ICARE2 V3mod1 (version with the preliminary model on B<sub>4</sub>C oxidation) using the test scenario similar with that planned for the PHEBUS FPT3; initial steam and argon flow rates of 3 g/s, power increase of 0.3 W/s per rod, steam flow reduced to 0.4 g/s when T<sub>max</sub> ~ 1200 °C, stabilisation phase at low power (Pelec=4000 W) before complete steam starvation and finally completion of the test by a final cool-down phase in steam conditions when T<sub>max</sub>=1900 °C.

The ICARE2 modelling of the QUENCH-07 involved the central B<sub>4</sub>C control rod, a first ring with eight heater rods, a second ring with twelve heater rods and surrounding structures with a Zry shroud, a fibre insulation of ZrO<sub>2</sub> and a Stainless Steel cooling jacket with Ar.

A step-by-step process involving several calculations have been carried out to define a test protocol enabling the test objectives to be fulfilled. Additional sensitivity studies have also been carried out. From the results of these preliminary calculations, it has been concluded that ICARE2 V3mod1 simulations present high sensitivity to main parameters such as electrical power, argon and steam flow rates. Small variation of argon flow determines if cladding melting occurs or not. A 50% increase of the Ar mass flow rate seems to lead to limited bundle temperatures while no modifications in the Ar flow leads to an early temperature escalation.

Differences have been found between SCDAP/RELAP5 and ICARE2 results regarding the prediction of rod temperatures. For instance, a parallel SCDAP/RELAP5 simulation with the

same parameters as in the ICARE2 V3mod1 reference calculation showed a rapid temperature rise up to clad melting and steam starvation at the end of the heated zone. The corresponding ICARE2 calculation predicted lower temperatures and consequently no steam starvation.

The above-mentioned pre-test calculation and the comparison with experimental results revealed some deficiencies in the simulation according to the phenomena observed. A detailed study of the different test phases showed that some discrepancies were due to the differences between the proposed scenario and the actual test conduct. A revised calculation was carried out using “adjusted boundary conditions” enabling a good prediction of the temperature and oxidation behaviour. Main characteristics of this calculation were the following:

- A decrease of the electrical power during the initial stationary and heat-up phases, for a better prediction of the bundle maximum temperatures;
- A reduction of the oxidation phase duration, a little bit less than in the test, in order to better account for the integral H<sub>2</sub> mass flow measured and to get a thinner oxidation layer;
- No modification regarding the fast transient heat-up phase conditions. In that way, the experimentally observed total cumulative H<sub>2</sub> mass flow could be well reproduced;
- Modification of the chronology of events for the quenching phase in order to reproduce the test scenario. However, this did not lead to a better description of the fast oxidation transient experimentally observed. Due to the lack of corresponding model, the oxidation escalation observed was not predicted. This highlighted the need in ICARE/CATHARE to develop quenching models with the related oxidation effects.

Regarding the B<sub>4</sub>C oxidation phenomena, it was not possible to compare predictions with experimental data because of the difference of information received from the experiment and from the code regarding the gas releases. ICARE2 distinguishes the H<sub>2</sub> coming from Zr oxidation and H<sub>2</sub> coming from B<sub>4</sub>C oxidation. This obviously cannot be distinguished experimentally. On the opposite, the CO, CO<sub>2</sub> and CH<sub>4</sub> gas productions were measured but not predicted by ICARE2 which cannot support more than two non-condensable gases at the same time (Hydrogen and Argon are used in this case). Figure 135 illustrates the cladding temperature and H<sub>2</sub> production predicted by ICARE/CATHARE in the revised pre-test calculation of QUENCH-07 test.

A revised post-test calculation has been realized with boundary conditions that closely reproduced those used in the test. In summary, it can be said that all the stages are adequately reproduced. In particular the total hydrogen production just before the final quench phase is correct (Figure 136) again with exception of the quenching phase, for which the oxidation excursion and the associated H<sub>2</sub> release are not predicted due to the lack of quench models.

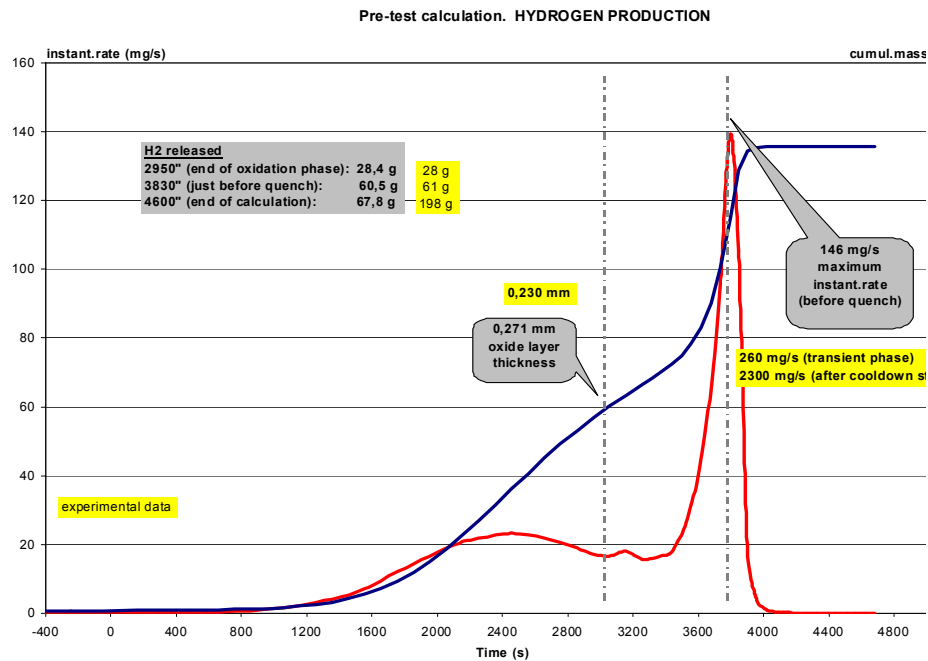
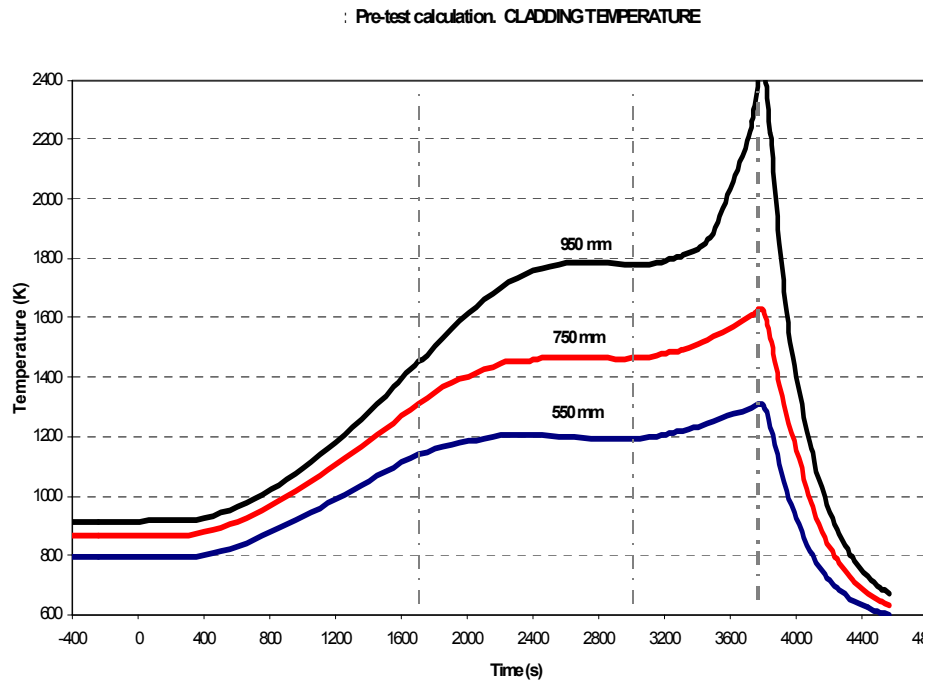


**Fig. 136:** Cladding temperature (top) and H<sub>2</sub> production (bottom) predicted by I/C in the revised pre-test calculation using “adjusted boundary conditions”.

Figure 5: Post-test calculation. CLADDING TEMPERATURE

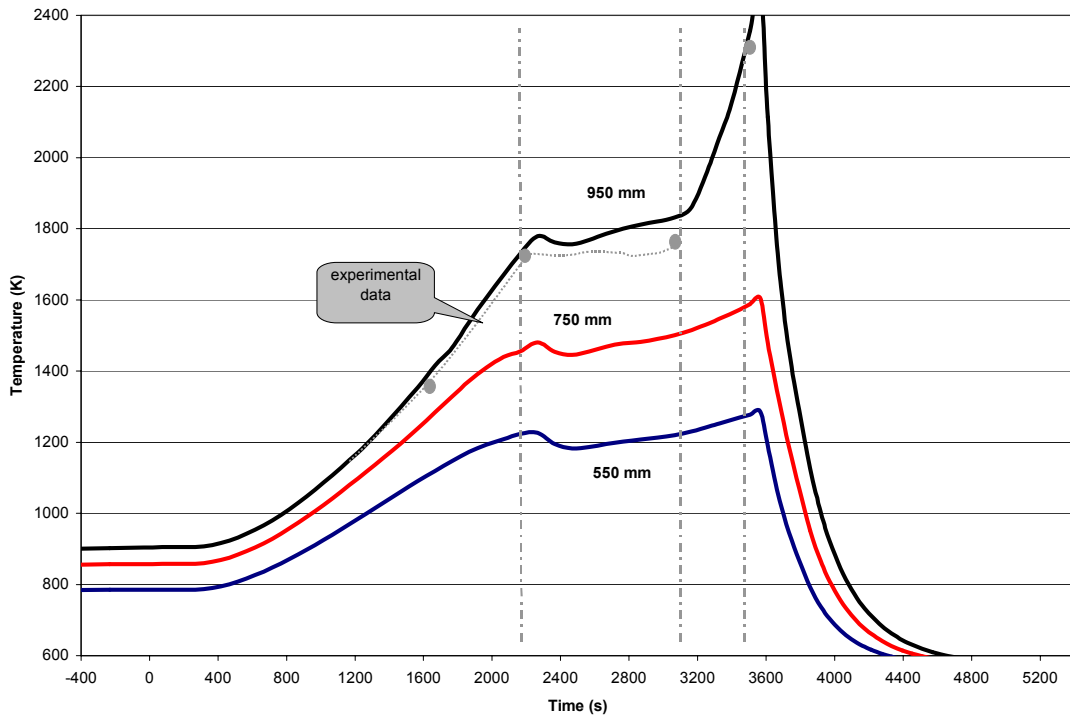


Figure 6: Post-test calculation. HYDROGEN PRODUCTION

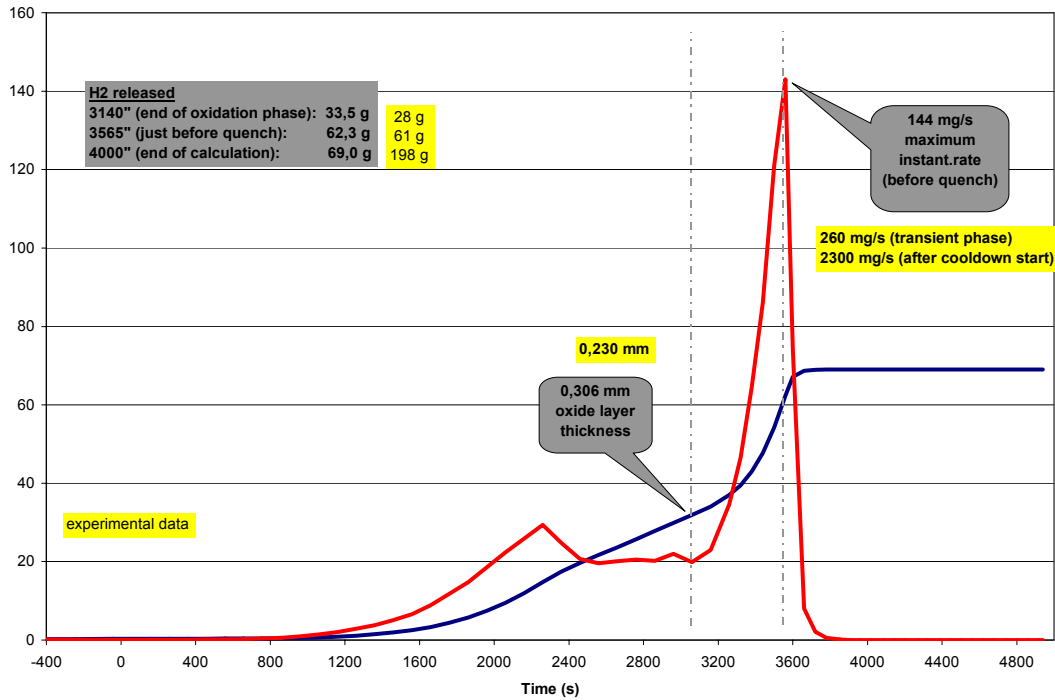


Fig. 137: Cladding temperature (top) and H<sub>2</sub> production (bottom) predicted by I/C in the revised post-test calculation using the QUENCH-07 boundary conditions

## Pre-test calculations of QUENCH-09

Once the basic test conditions were known and after a close collaboration with ENEA enabling comparison and optimisation of the UPM ICARE2 input desk, a reference calculation was performed with some sensitivity calculations.

In a preliminary calculation, Phases I & II (heatup and oxidation, respectively) were the same as those in QUENCH-07 (Fig 138). During the transient phase, steam starvation conditions were obtained by steam mass flow reduction together with a constant electrical power supply (at 15 kW). The temperature behaviour calculated showed a well-controlled temperature transient (probably more stable than for the previous QUENCH-07 test). The final cooling phase was still characterised by the same uncertainties as in the QUENCH-07 calculation for which the code prediction was far from the experimental results. In addition, a higher coolant mass flow rate planned in QUENCH-09 (50g/s instead of 15g/s in QUENCH-07) led to more uncertainty in the estimation of the final H<sub>2</sub> production excursion.

Results, as expected, do not differ sensibly in both QUENCH-07 and QUENCH-09 calculations. Time evolution is faster in QUENCH-07 during the transient phase due to the mentioned differences in the test conduction. Obviously, a lower total H<sub>2</sub> production (57.5 g) was estimated for QUENCH-09 due to steam starvation conditions reached (Fig. 131). As expected, no quenching effect was captured in terms of enhanced oxidation (only 10 g of H<sub>2</sub> was generated during this phase).

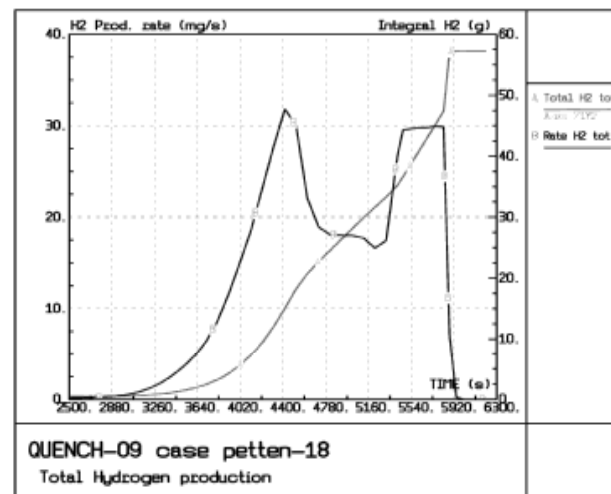
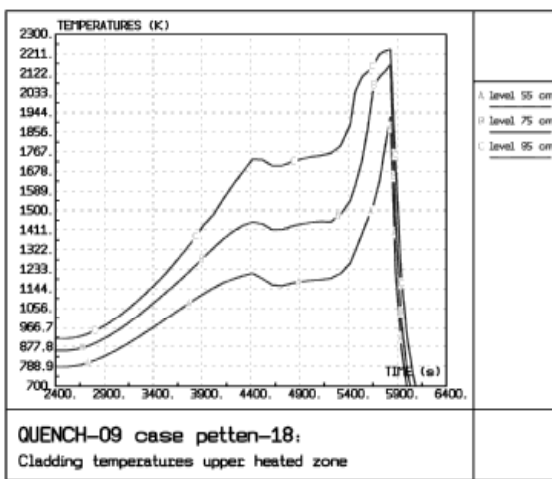


**Fig. 138:** Pre-test calculation of the temperature evolution in the upper part **Fig. 139:** Pre-test calculation of H<sub>2</sub> production

Oxidation of B<sub>4</sub>C was evaluated with the initial simple model existing in ICARE2 V3mod1.1. A negligible B<sub>4</sub>C oxidation and related H<sub>2</sub> production (<1.5g) was found. It was pointed out that output information concerning CO, CO<sub>2</sub>, CH<sub>4</sub> emissions is not available in the calculation.

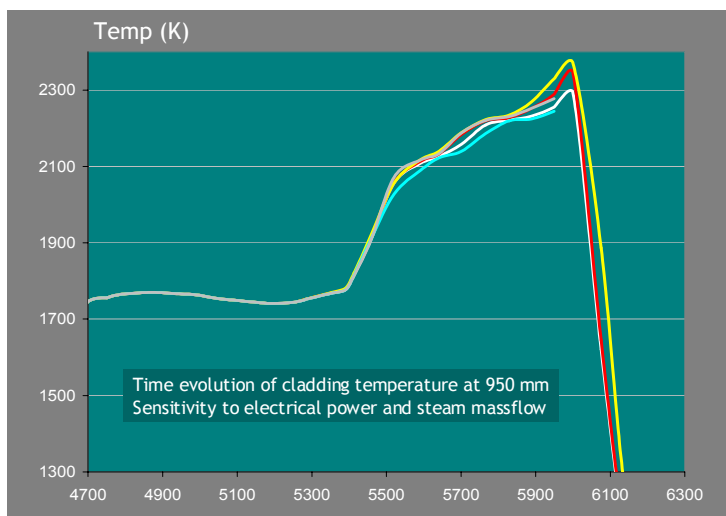


**Figure 140:** Sensitivity studies and base case pre-test calculation

Lessons learned from the analysis of the pre-test and post-test calculations of QUENCH-07 were applied on QUENCH-09 simulation, in particular regarding the estimation of the outer circuit resistance (OCR) that should be could temperature dependant. Therefore, an optimisation of the reference case was attempted by variation of the OCR from the recommended value, which resulted in a better evaluation of the cladding temperature during the oxidation phase.

In addition, some sensitivity calculations were carried out from the reference case regarding:

- the electrical power supply during the temperature plateau with a deviation up to 20% from the constant level of 15.7 kW,
- steam flow mass deviation from the 3g/s during the transient ( $\pm 10\%$ ).

All the results obtained from these calculations show small differences compared with the reference case (Fig. 140). This indicated a stable and consistent scenario and a safe performance of the test (always with the necessary reserve).

Following the PAG recommendations on the choice of Zr oxidation correlations (G. Schanz, FZK) an additional sensitivity calculation was performed using Prater-Courtright instead of Urbanic-Heidrick correlations. In ICARE2 code, Cathcart-Pawel and Prater-Courtright correlations are similar for lower temperatures (under 1800K) and differ only above 1800K, where the latter shows a sudden increase in the kinetics rate near the ZrO<sub>2</sub> phase transition temperature. The choice of the oxidation correlations was small. In fact, the QUENCH-09 test conditions were not very adequate for revealing differences when changing the oxidation model because oxidation behaviour was mainly imposed by starvation conditions (steam supply) and slightly by the choice of the oxidation kinetics under 1800K.

In summary, the ICARE2 pre-test calculation and sensitivity analysis indicated that the proposed scenario for QUENCH-09 was stable enough for a successfully performance of the test even in case of small deviations from the expected experimental conditions. Code limitations concerning B<sub>4</sub>C oxidation (lack of CO, CO<sub>2</sub> and CH<sub>4</sub> calculation) and oxidation enhancement

during cool-down did not enable a complete simulation of the test for comparison with experimental data.

### Post-test calculations of QUENCH-09

Post-test calculations were also carried out with ICARE2. The cladding temperatures were sensitive to the power reduction time because the bundle conditions were near oxidation escalation conditions as evidenced in sensitivity studies carried out for the previous QUENCH-07 test.

At each level, the clad temperature after the temperature escalation phase was not maintained at a stabilised level before the final heat-up phase. The continuous increase of calculated temperatures could only be reduced by reducing the final electric power increase. The H<sub>2</sub> production up to the end of the steam starvation phase was acceptable (50 g instead of 60g in the test due to the under-prediction of the early clad temperature excursion near 2600s). The steam starvation condition was correctly calculated during the low steam flow phase. The H<sub>2</sub> coming from the B<sub>4</sub>C oxidation remained unexpectedly very low (1 g) compared with calculations carried out by other partners of the project.

As expected, the oxidation escalation observed during the final cooling phase is not calculated due to the lack of an adequate oxidation model. Consequently, the total H<sub>2</sub> production was significantly underestimated (120 g) compared with 468 g measured even if there is a large over-estimation of H<sub>2</sub> produced in the experiment.

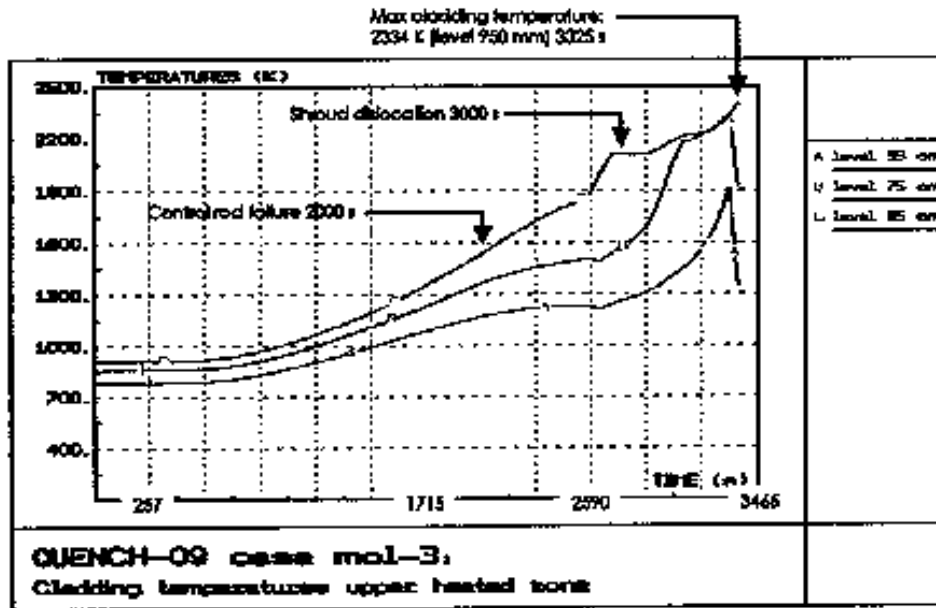


Figure 141: Temperature behaviours and degradation events calculated by ICARE2 for the QUENCH-06 test.

Concerning core degradation, the control rod failure took place near 2000s when the bundle temperature was about 1550K (Figure 141).

Due to high temperatures reached at the top of the bundle during the escalation phase, the structures in the upper part of the bundle were predicted very damaged (as in the test). The thickness of the ZrO<sub>2</sub> layer on the shroud was too low when the Zr melting point was reached and the shroud was predicted dislocated at ~3000 s enabling the relocation of molten Zr (Figure 141). The oxidation of this molten mixture has not been taken into account in the calculation. This factor would have increase significantly the calculated total H<sub>2</sub> release reducing the discrepancy with the test.

### 3.13.7 Analytical support for QUENCH-09 (ENEA)

Pre-test analysis of QUENCH-09 have been performed by ENEA using the ICARE/CATHARE V1 Mod1 code to verify the adequacy of boundary conditions to achieve the test objectives and help FZK in test conduct. Some sensitivity calculations have been performed to evaluate the influence of some important parameters during the transient phase.

Pre-test and post-test analysis have been performed with an improved version of ICARE/CATHARE code.

#### Pre-test analysis

Boundary conditions for the test were the same as in QUENCH-07 experiment up to the end of pre-oxidation phase. The following transient phase was characterised by a reduction of the inlet steam flow rate in order to get reducing conditions in the upper part of the bundle. The influence of residual steam flow rate and power ramp during the transient phase on test conduct has been investigated by sensitivity analysis.

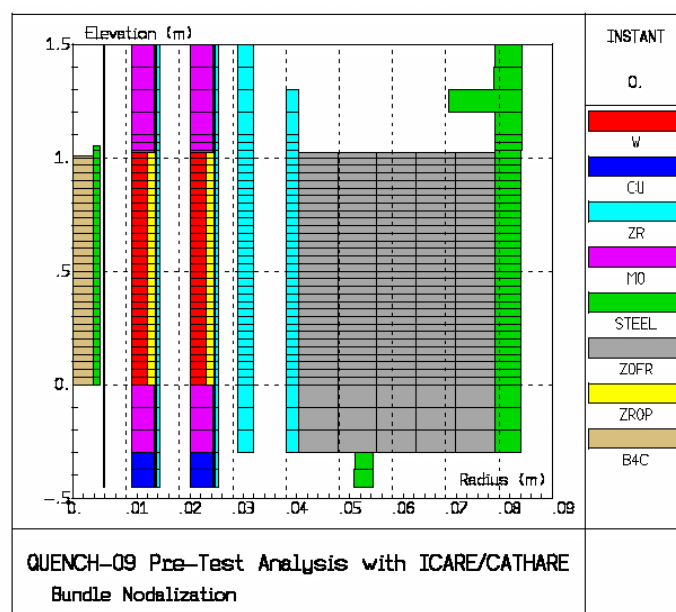


**Fig. 142:** QUENCH-09 test section modelling

## Test section modelling

Modelling of the QUENCH-09 test section with ICARE/CATHARE is shown in Fig. 142. Three representative rods are used to model the central B<sub>4</sub>C control rod, the 8 inner ring heated rods and the 12 outer ring heated rods. The surrounding Zircaloy shroud liner, the Zirconia insulation and the inner cooling jacket made of inconel are also represented.

The validity of this model has been confirmed by a preliminary post-test analysis of QUENCH-07 experiment. Bundle temperature and hydrogen release calculated by the code are compared with experimental data in Figs. 143 and 144. The code is adequate to calculate bundle thermal behaviour and hydrogen release during the oxidation and transient phases. Large uncertainties remain in the evaluation of hydrogen release during cooldown due to the lack of a quench model.

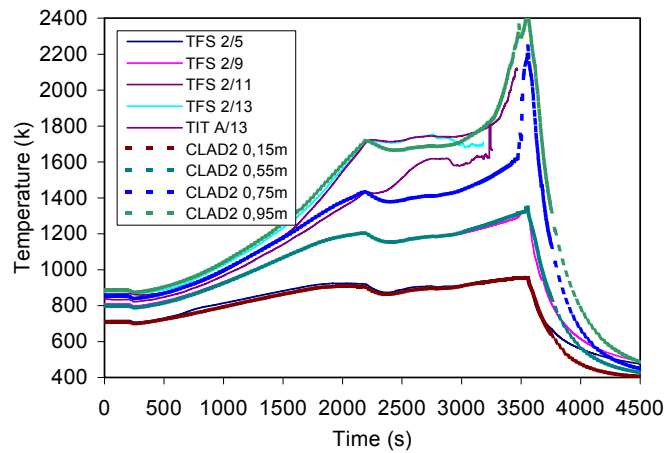


**Fig. 143:** QUENCH-07 inner heated rod Temp.

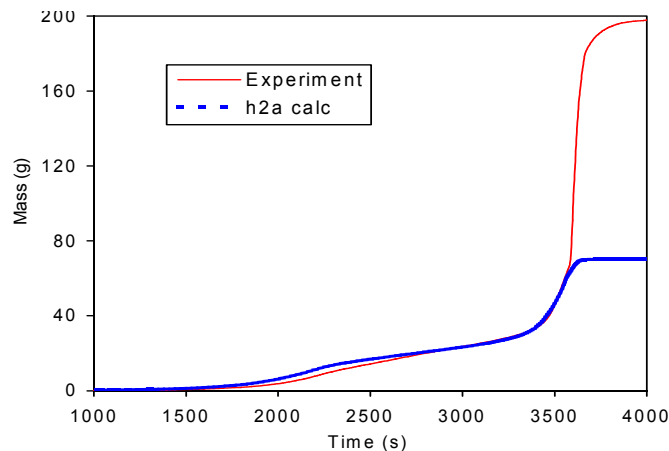


**Fig. 144:** QUENCH-07 hydrogen release

### Reference case results

In pre-test analysis of QUENCH-09 experiment, the inlet steam mass flow rate to the bundle was reduced to 0.3 g/s at the end of pre-oxidation phase to initiate the transient phase. In the reference case, a constant electrical power supply was assumed during the transient phase. The transient phase was terminated by a very fast cooldown, with a steam flow rate of 50 g/s, as soon as the maximum bundle temperature calculated by the code exceeded 2273 K.

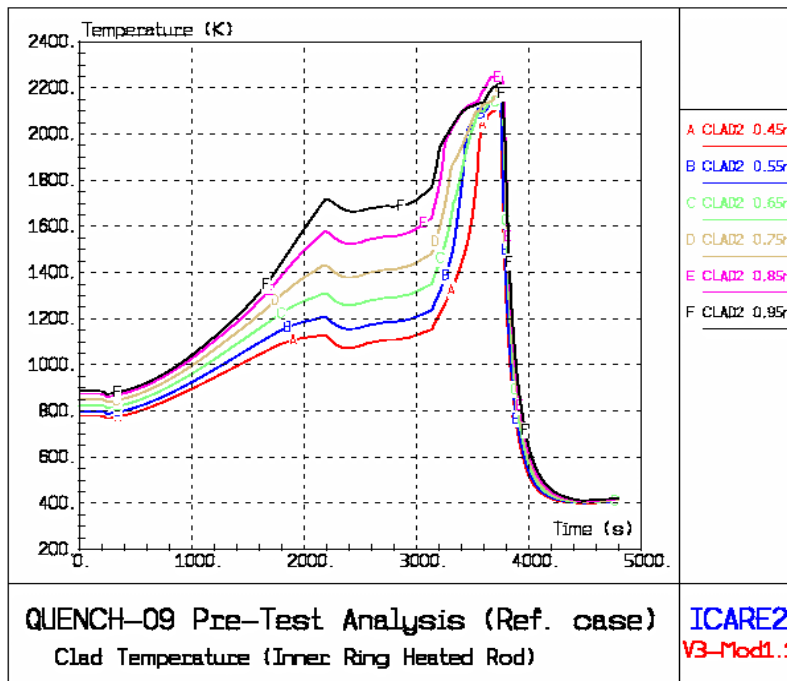


Fig. 145: Inner ring heated rod clad temperature

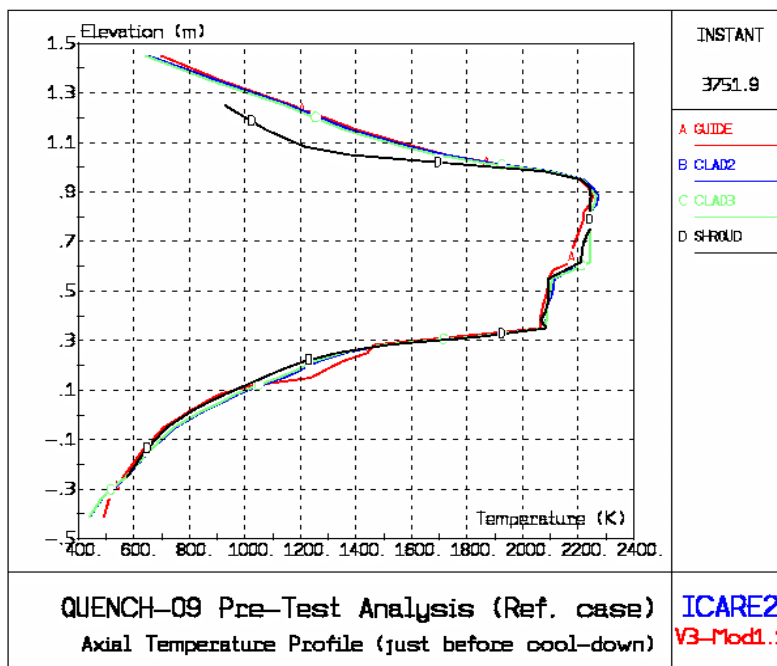


Fig. 146: Axial temperature profile in the bundle

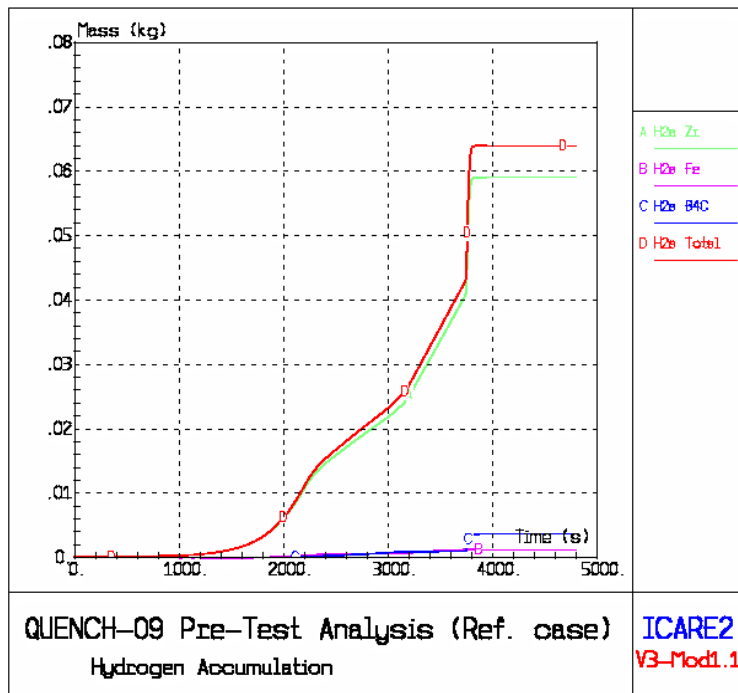


Fig. 147: Hydrogen release

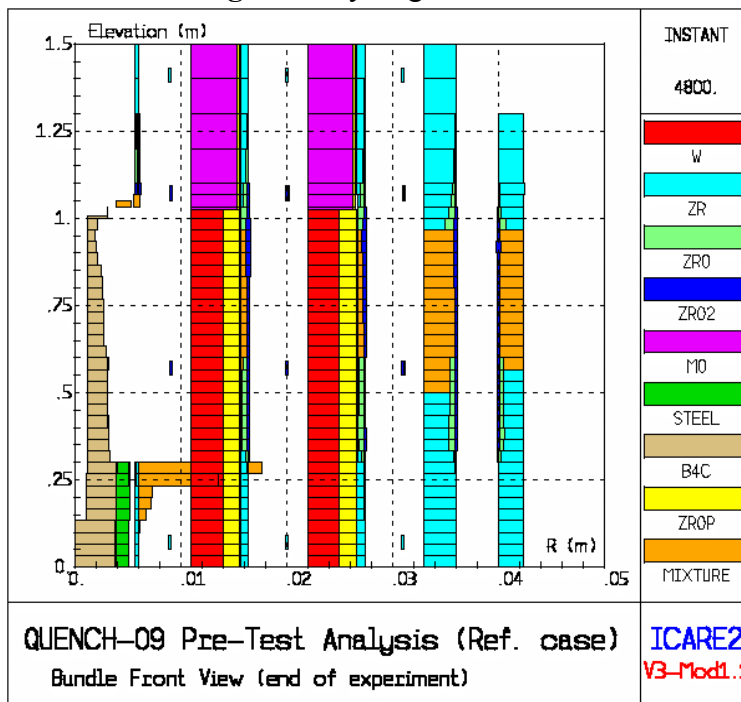


Fig. 148: Bundle degradation at the end of experiment

Fig. 145 shows the inner heated rod clad temperature history in the upper half of the heated bundle. Bundle temperature reached the maximum foreseen value at 0.85 m elevation at about 3750 s. No electrical power ramp was needed to get the transient phase within a reasonable time. Fig. 146 shows the axial temperature profile in the bundle at the end of transient phase just before cooldown. Because of steam starvation conditions predicted in the bundle, the oxidation front moves downwards from the top of the heated bundle towards the middle of the bundle during the

transient phase, resulting in an almost flat temperature profile above 0.35 m elevation. This shift was really observed in the test. Fig. 147 shows the predicted hydrogen release which increases linearly during the transient phase as expected. No heated rod bundle degradation was predicted at the end of experimental transient (Fig. 148). The B<sub>4</sub>C control rod was significantly damaged and absorber material oxidation contributed by about 6% to hydrogen source.

### **Sensitivity studies**

Some sensitivity studies have been performed to evaluate the influence of residual steam flow rate and bundle power ramp during the transient phase.

In a first calculation, the steam flow rate was reduced to 0.4 g/s (instead of 0.3 g/s) during the transient phase. With respect to the reference case, the hydrogen release during the starvation phase increased according to steam flow rate increase. No very significant difference was found in bundle thermal behaviour and bundle degradation at the end of transient phase. The duration of the transient phase reduced by about 60 s.

In a second calculation, the electrical bundle power supply was increased during the transient phase by a ramp of 0.32 W/s per heated rod as in QUENCH-07 experiment. The duration of the transient phase was reduced by about 70 s, and large rod degradation was calculated during the cooldown phase. In fact, at the very beginning of bundle cooldown; initiated at 2273 K, an even small temperature peak, caused by the enhanced oxidation produced by large steam supply just after the starvation conditions (before cooldown becomes effective) is sufficient to overcome the clad failure limit imposed in input (2300 K).

### Post-test analysis

Due to an unexpected bundle temperature excursion observed in the test at the end of heatup phase, the QUENCH-09 pre-oxidation phase was different from QUENCH-07 while experimental conditions during heat-up were similar. In the test, the steam flow rate was reduced as expected to 0.3 g/s as soon as temperature excursion occurred, to try to limit bundle temperature escalation during this early oxidation phase. The bundle power was also reduced for the same reason while it was initially planned to stay constant. Later the bundle power was increased to initiate the transient phase ended with a final fast cooldown by 50 g/s steam mass flow rate. A second temperature excursion was observed in the upper part of the bundle during the final cooldown, resulting in large bundle oxidation and degradation above the heated length.

Post-test analysis of QUENCH-09 has been carried out with the ICARE/CATHARE V1 Mod1.3p code including an improved model for B<sub>4</sub>C oxidation developed within the COLOSS project. The test section modelling used in pre-test analysis was slightly modified to obtain a best-estimate calculation. In particular, the candling velocity of relocating material was reduced to 0.01 m/s according to PHEBUS FPT2 analysis by IRSN, to better predict material relocation according to PHEBUS experimental observations. Boundary conditions of the test have been revised according to actual test conduct.

### **Results of Best-Estimate Calculation**

Inner ring heated rod clad temperatures at different elevations are compared with experimental data in Figs. 149 and 150. Clad temperatures are well calculated during the heatup phase. First temperature escalation at the top of the bundle is well predicted at the end of heatup phase (Fig. 150). The large discrepancy in temperature escalation at 0.75 m (Fig. 149) is due to a

measurement error (TFS 2/11). The overall clad temperatures behaviour is correct but in general overestimated during the steam starvation phase. As expected, the final temperature escalation during cooldown was not calculated.

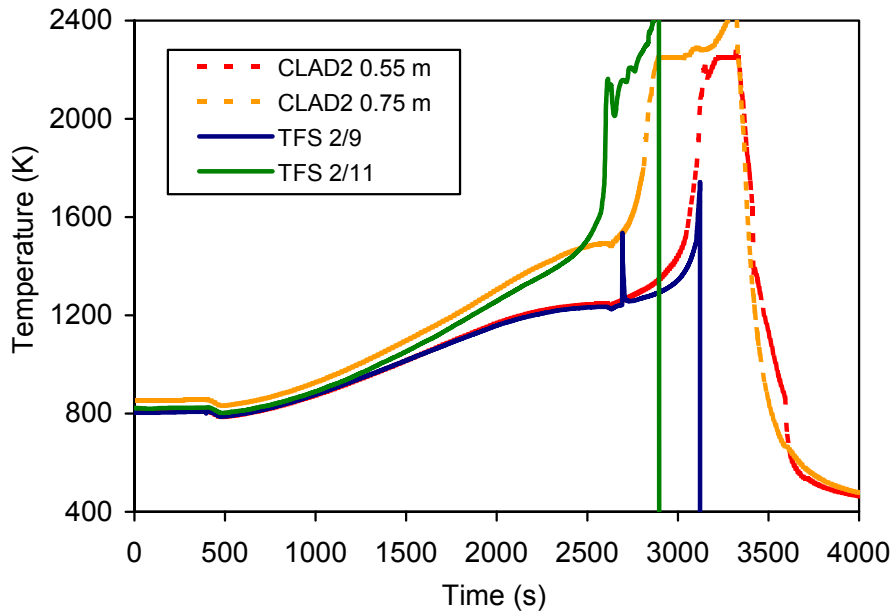


**Fig. 149:** Clad temperature in the centre of bundle

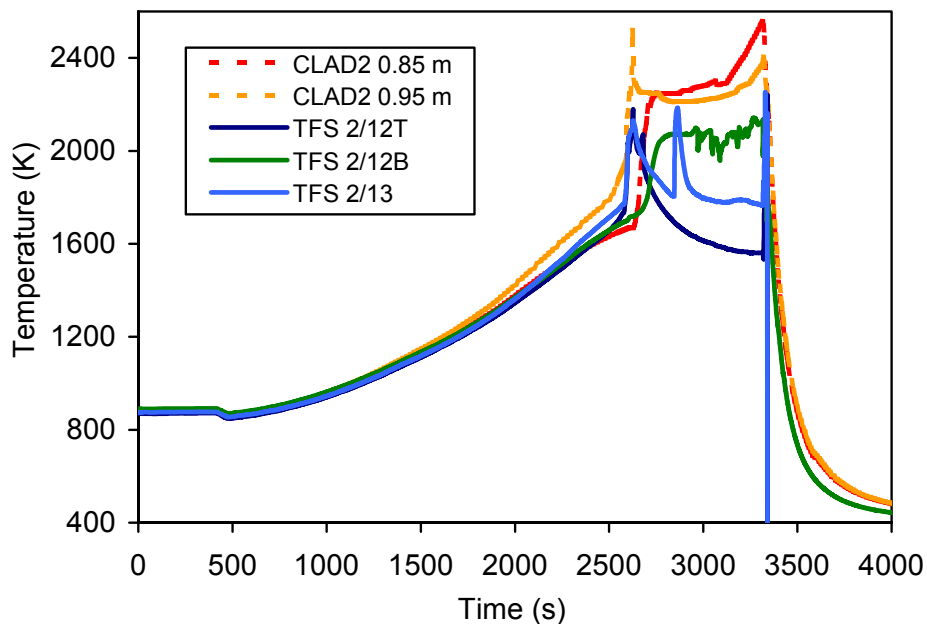


**Fig. 150:** Clad temperature in the upper part of bundle

The hydrogen release calculated is compared with experimental data in Figs. 151 and 152. The steam starvation conditions and hydrogen generation before cooldown are correctly calculated. The large amount of H<sub>2</sub> released during final cooldown is not predicted due to the

lack of a adequate quench model. B<sub>4</sub>C oxidation contributes directly by about 7% to the total amount of H<sub>2</sub> release.

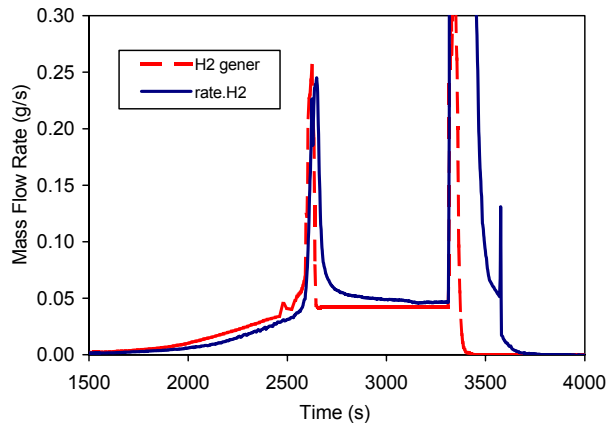


**Fig. 151:** Hydrogen generation

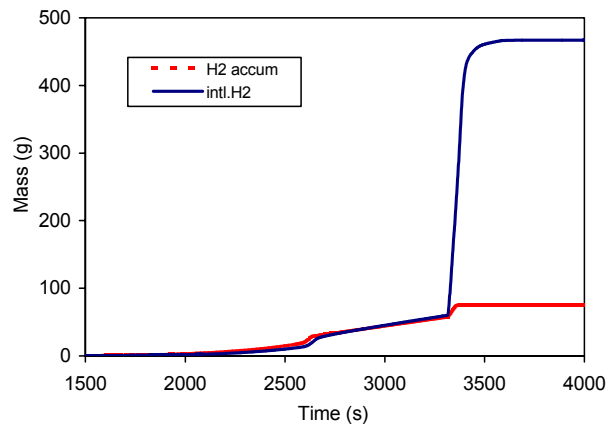


**Fig. 152:** Total hydrogen release

Bundle degradation calculated at the end of experiment is shown in Fig. 153. The whole bundle is largely degraded in the upper part of heated length and molten material relocated near the middle of the bundle in quite good agreement with experimental observations. Control rod failure is calculated with some delay, because no chemical interaction between stainless steel absorber cladding and Zr guide tube is taken into account by the code.

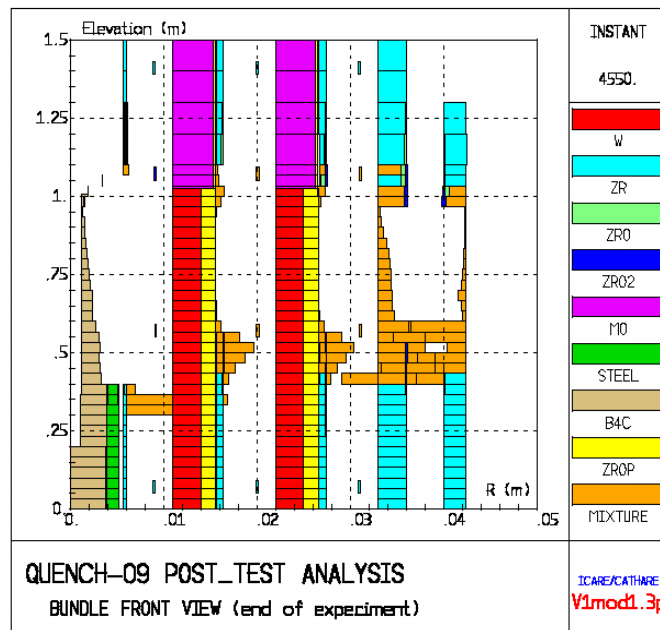


**Fig. 153:** Bundle degradation at the end of experiment

The control rod failure is observed at 2280s in the test at the temperature of 1580 K; while it is calculated by the code at about 2450s, when the absorber cladding temperature reaches the melting

During cooldown, no bundle degradation was calculated in the upper part of bundle above the heated length as it was observed in the test.

## **Main outcomes**

In spite of the difficulties in carrying out the QUENCH-09 experiment according to test specifications, significant data have been obtained regarding core degradation and B<sub>4</sub>C effects under steam starved conditions.

- Because of an unexpected bundle temperature excursion at the beginning of pre-oxidation phase, the experimental transient was different from what it was foreseen in pre-test analysis.
- The analysis of the experiment with ICARE/CATHARE has demonstrated the validity of the new model implemented in the code to compute control rod material oxidation and degradation.
- In general the code is able to simulate quite well the experiment up to the final cooldown phase in spite of the difficulty of such a calculation with other codes. The general trend of the thermal behaviour was correctly calculated in pre-test and post-test calculations.
- As already known, large uncertainties still exist in the evaluation of bundle behaviour during cooldown due to the lack of an appropriate oxidation model during quench conditions. In particular oxidation could have been enhanced during cooldown by a large oxidation of B<sub>4</sub>C-SS-Zr mixtures in addition of the oxidation of existing U-O-Zr mixtures and partially oxidised structures.

### **3.13.8 Post-test calculations of QUENCH-09 (IRSN)**

Post-test calculations of the QUENCH-09 experiment were performed with ICARE2 V3 mod1. A reference case calculation has been performed and sensitivity calculations have been added to understand the behaviour of the test section observed during the transient.

#### **Test conditions and preliminary comments**

The boundary conditions of the test are represented on the Figure 154. The test transient consists of a power ramp followed by a plateau stabilising the power near 13 kW. During this period, the argon and steam flow rate are kept constant, respectively equal to 3 and 3.4 g/s. Due to an unexpected temperature escalation in the upper part of the bundle, the power and the steam flow rate were reduced at 2636 seconds, the steam flow rate being thus decreased to 0.3 g/s. The following period with an increase of the power is called the steam starvation phase. Finally, around 3300 seconds the cool down phase was initiated characterised by a power shut down and a switch of the steam flow rate to 50 g/s.

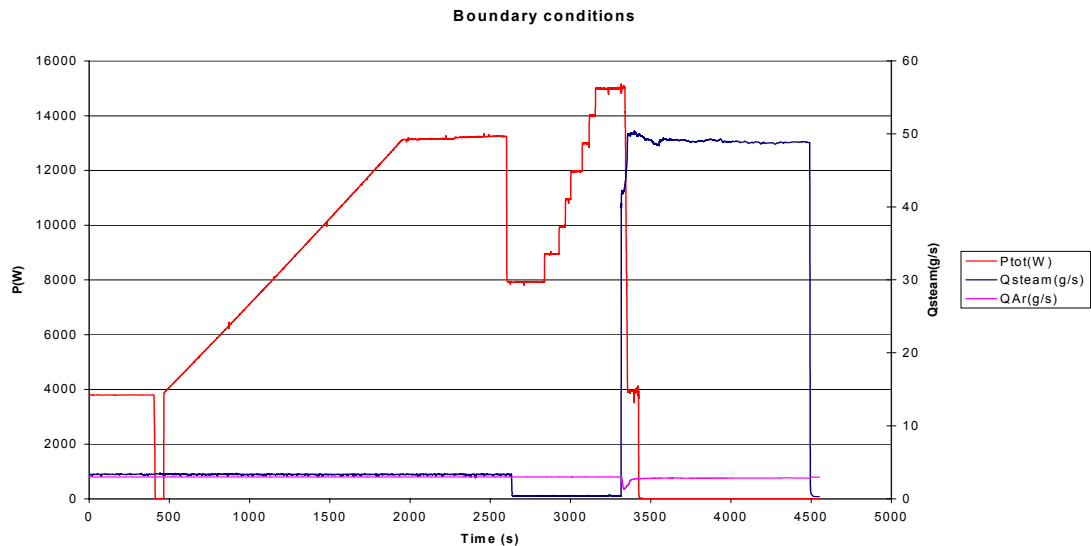


**Figure 154:** Boundary condition in QUENCH-09 test

Preliminary comments regarding the experimental conditions of the test are needed to correctly analyse and evaluate the thermal behaviour of the test section up to the cool-down phase and to underline the limitations of the calculations due to the extreme high steam flow conditions during the cool-down phase.

The first comment deals with the TC shunting effect, suspected to induce an artificial temperature escalation at 750 and 850 mm high. This effect, which was latter confirmed by the experimental team, was derived from the following results. The calculation of the oxidation runaway as indicated by thermocouples at 750 and 850 mm just before the steam flow rate decrease was found impossible to predict, neither the hydrogen measured during the whole heat-up phase that would have produced more than 50 g of  $H_2$  (at 2636 s) while this value was only measured at the end of the starvation phase ( $\sim 3300$  s). The measured total amount of  $H_2$  released is believed to be a valuable parameter to assess the extent of the oxidation up to the end of the starvation phase. At these levels, there is also an unphysical temporal shift between the temperature escalation measured in the bundle and those observed in the shroud, the two kinds of thermocouples having different wires way configurations. In other terms, these upper bundle thermocouples are affected by a thermal shunting effect giving an erroneous indication of the temperature escalation while the escalation actually occurred only at the hottest level (950 mm). The shroud thermocouples are believe to indicated more correct temperatures behaviour, wire way of corresponding thermocouples being different.

The second comment is related with the high steam flow rate (50 g/s) during the cool down phase, the flow velocity being very large compared to usual ICARE2 validation domain and to the associated nodalization. The corresponding velocities, enhanced by the test section flow blockages due to shroud and claddings liquefaction and relocation, have been estimated to almost 400 m/s. Such a high velocity could have induced very strong drag forces, able to exhaust the debris observed downstream of the bundle. This explanation is consistent with the pressure evolution within the test section (pressure increased up to 4 bars followed by a decrease to 2 bars, possibly due to the expulsion of the debris). With such a velocity, which is not representative of plant conditions, models are probably used out of the validation domain.

## ICARE2 modelling of the QUENCH test section

The ICARE2 nodalization of the test section is presented on the Figure 155.

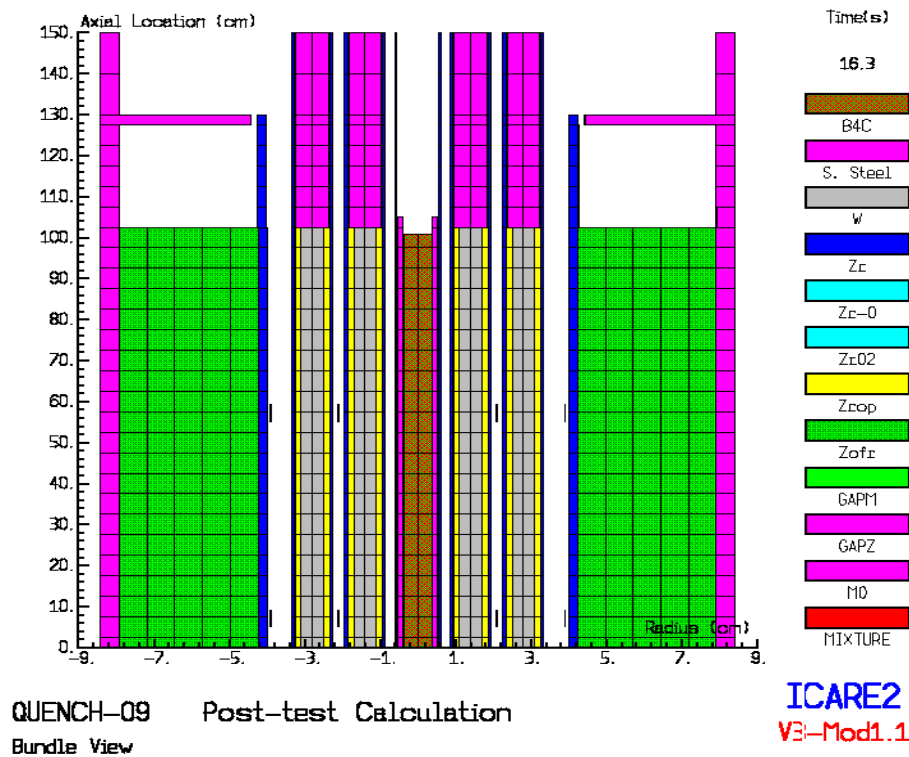


**Figure 155:** ICARE2 nodalization of the Quench test section

The monodimensional hydraulic model has been used, taking into account one channel only. Moreover, the temperature of the steam injected in the bundle has been set to 718 K to match the measurement available at -250 mm elevation. In ICARE2, the SS/B<sub>4</sub>C solid/solid interaction begins as soon as the temperature exceeds 1073 K leading to a liquefaction when the temperature exceeds 1473 K. Once this SS/B<sub>4</sub>C interaction is achieved, that is when the SS is completely liquefied, the guide tube is declared failed. This hypothesis enable to overcome the lack of model simulating the interaction between the SS-B<sub>4</sub>C mixture the Zr guide tube.

The new B<sub>4</sub>C oxidation model developed by IRSN and the Prater correlation for the claddings oxidation have been used. The fuel rod relocation criterion has been chosen at the melting point of ZrO<sub>2</sub> and the candling relocation model was used with a low melt velocity (1 cm/s) corresponding to a thermally controlled flow down. The oxidation of B<sub>4</sub>C-rich mixtures was considered taking into account the oxidation kinetics law valid for pure B<sub>4</sub>C.

## Reference case calculation results and sensitivity studies

### Heat up and starvation phases

Figures 156 and 157 exhibit a good agreement between the temperature evolution measured and calculated, taken into account the shroud temperature evolution at the elevation 750 and 850 mm. This feature indicates that the modelling of the zircaloy oxidation, using the *Prater* correlation and considering that the Zr-rich mixture is able to flow down only once the outer zirconia layer began to melt, permitted to predict fairly well the thermal behaviour up to the cool down phase.

The guide tube, the claddings and the shroud failure were rather well predicted also. As in the test, the failure of the shroud and of the rod claddings occurs at the hot spot of the bundle (at 950 mm high) around 2600 seconds. Furthermore, the control rod failure is observed at 2280 s in the test, whereas it is calculated at 2350 s. The corresponding temperature of the rod is 1580 K in the calculation, against 1560 K in the experiment.

Finally, the control rod degradation is rather well predicted up to the cool down phase during which the experimental evidences regarding this point are not quite clear. However, the early phase of this QUENCH-09 calculation provided a good validation exercise for the B<sub>4</sub>C oxidation model of the ICARE2 code. In particular, the influence of the steam partial pressure on the oxidation process is correctly taken into account by ICARE2. Consequently, though the guide tube failed 150s before the starvation phase, the B<sub>4</sub>C has been slightly oxidized during this short period in a limited small zone in the upper part of the bundle as illustrated on the Figure 158 (left side).

During the following steam starvation period, the steam was mainly consumed by Zr oxidation as shown by the temporal shift of the successive temperature escalations. Due to the too low steam partial pressure provided after the flow rate reduction (near 2600 seconds), the control rod was almost no more oxidized up to 3300 seconds but dissolved by its cladding and partly relocated (right side of Figure 158).

According to the experimental result, the B<sub>4</sub>C seems to have been oxidized, even when the control rod is not yet broken. This behaviour is not reproduced by the code modelling, since it is assumed that the B<sub>4</sub>C oxidation begins only after the failure of the control rod cladding and of the guide tube. Despite this discrepancy, the order of magnitude of the B<sub>4</sub>C oxidized at the end of the cool down (based on gas measurements) is correctly predicted by the ICARE2 calculation.

This ICARE2 calculation illustrates the ability of the code modelling, to take correctly into account, the effect of the partial pressure on the B<sub>4</sub>C oxidation process as well as the coupling of this process with the Zircaloy oxidation and with the thermal-hydraulics phenomena.

The hydrogen release up to the onset of the final cool down is represented on the Figure 159. The agreement between the calculated and measured H<sub>2</sub> release is fairly good, even though in the calculation the steam starvation is obtained just before the steam flow reduction, which is not the case in the test. At the end of the starvation phase there is a slight under-prediction of the H<sub>2</sub> release.

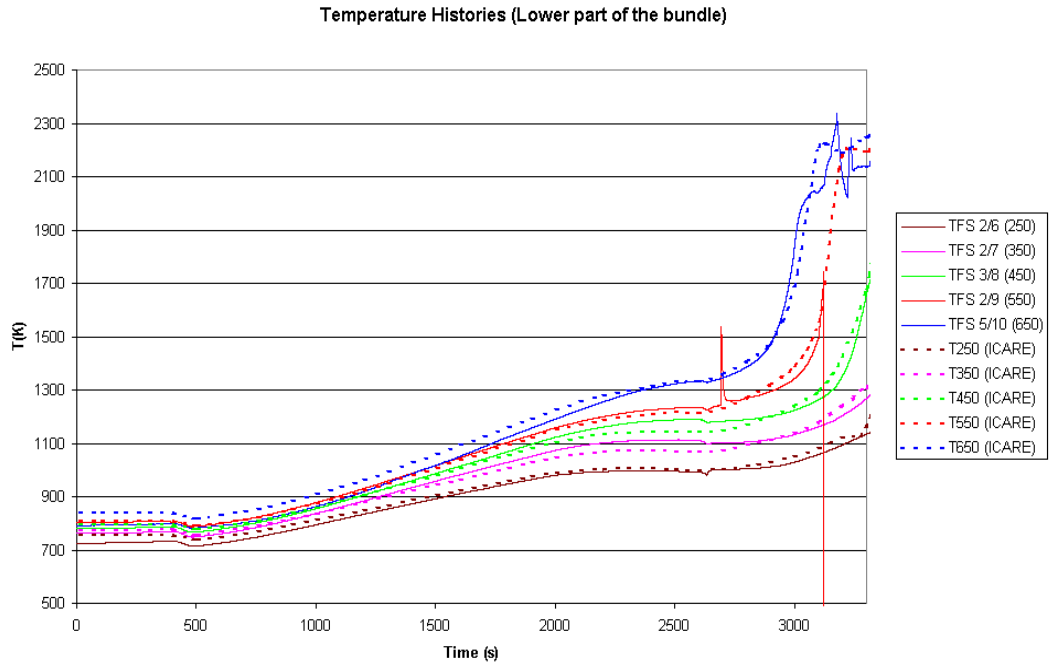


**Figure 156:** Bottom temperature evolution calculated and measured up to the cool down

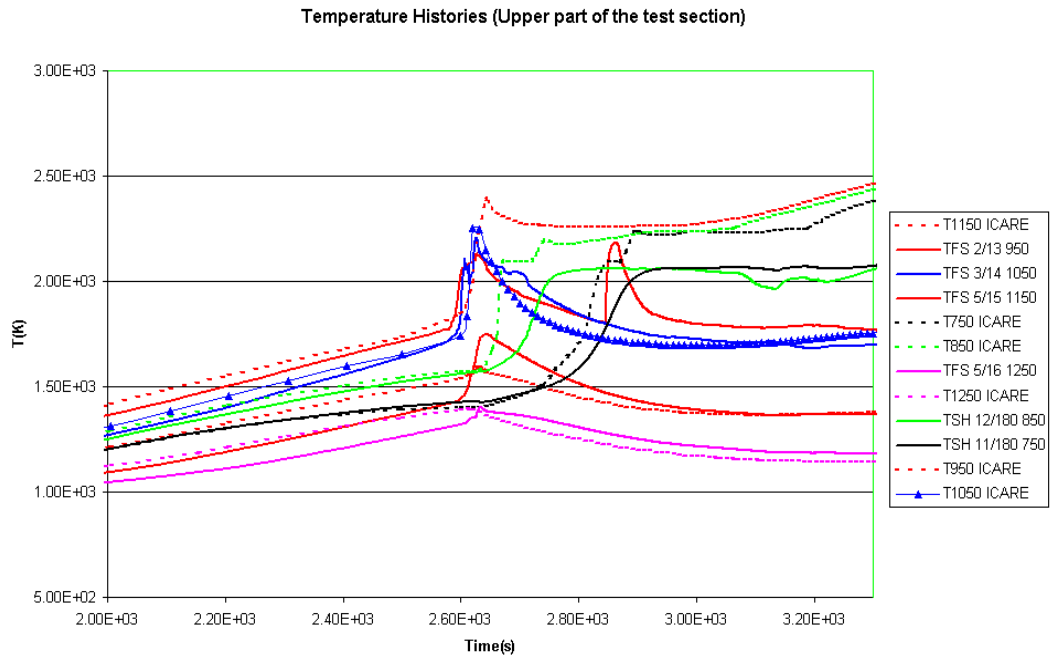


**Figure 157:** Top temperature evolution calculated and measured up to the cool down

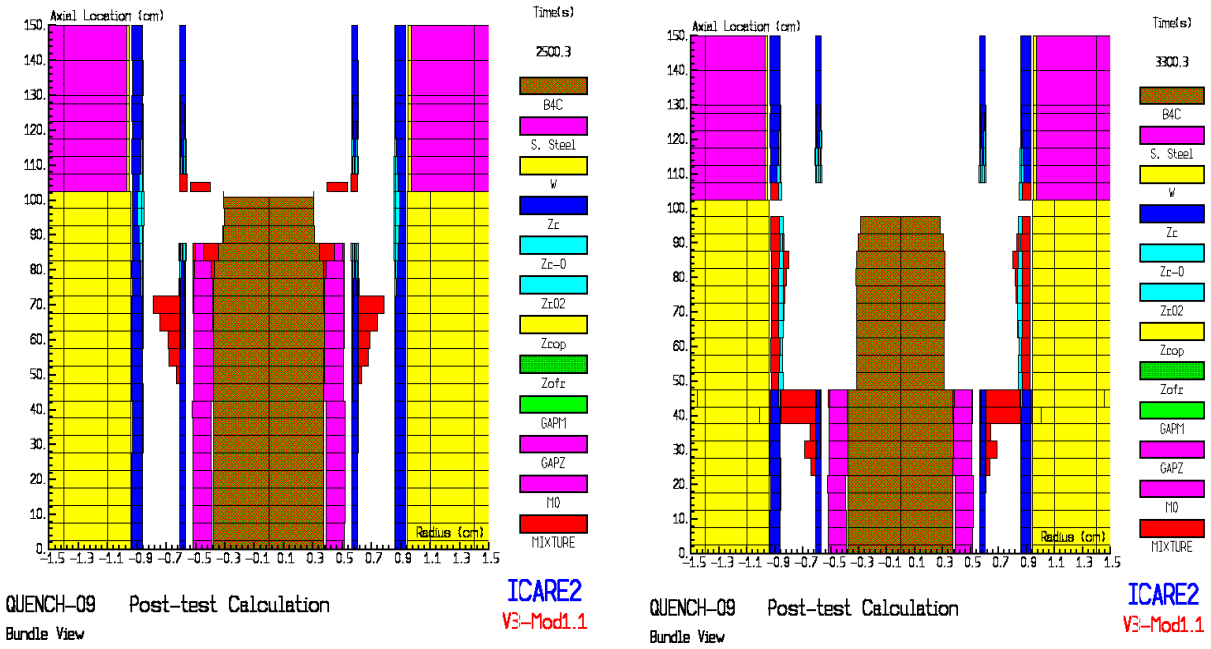


**Figure 158:** Views of the control rod at the end of the heat-up and during the steam starvation just before the cool down

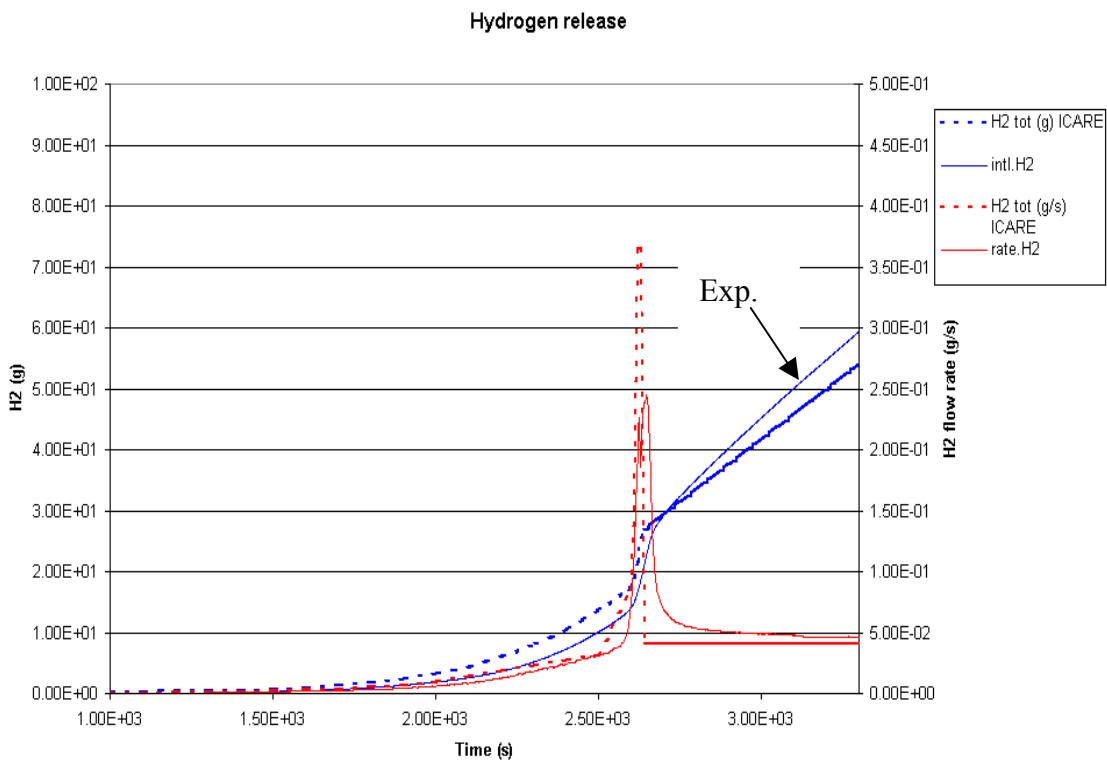


**Figure 159:** Instantaneous and total hydrogen release

## Sensitivity calculations on the thermal behaviour

The Figure 160 shows the temperature evolution calculated in the bundle and the hydrogen production up to the onset of the final cool down, corresponding to a calculation assuming a 15 % increase of the thermal conductivity of the insulating Zirconia shroud. Conversely to the reference case, the runaway measured above 950 mm at the end of the power plateau is not reproduced by the code.

The oxidation runaway is only obtained after the steam flow reduction because of the decrease of the convective power extracted from the bundle. On the other hand, the hydrogen release is lower than in the base case and underestimated.

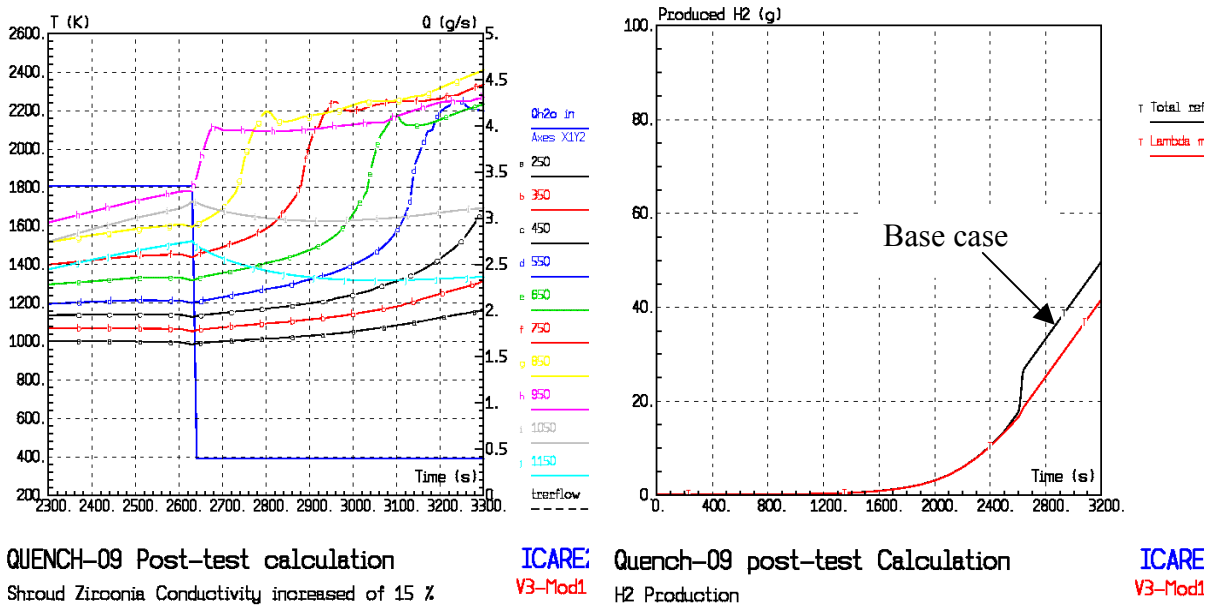


**Figure 160:** Sensitivity calculation assuming a shroud thermal conductivity increased of 15 %

Moreover, the Figure 161 represents the thermal behaviour and the hydrogen production, considering a 10 K increase of the steam inlet temperature. This temperature increase induces an extended oxidation runaway including an overestimation of the hydrogen production.

This calculation showed that the thermal behaviour of the quench test section is very sensitive to a small variation of the convective boundary condition. This is due to the large part of the electric power extracted by convection, the shroud being a very good insulating layer. This high sensitivity of the bundle to small boundary conditions could explain why in the QUENCH-07 test the temperature stabilisation was achieved while it was not in QUENCH-09. Conversely, a large variation of the shroud conductivity had a smaller impact in the hydrogen production.

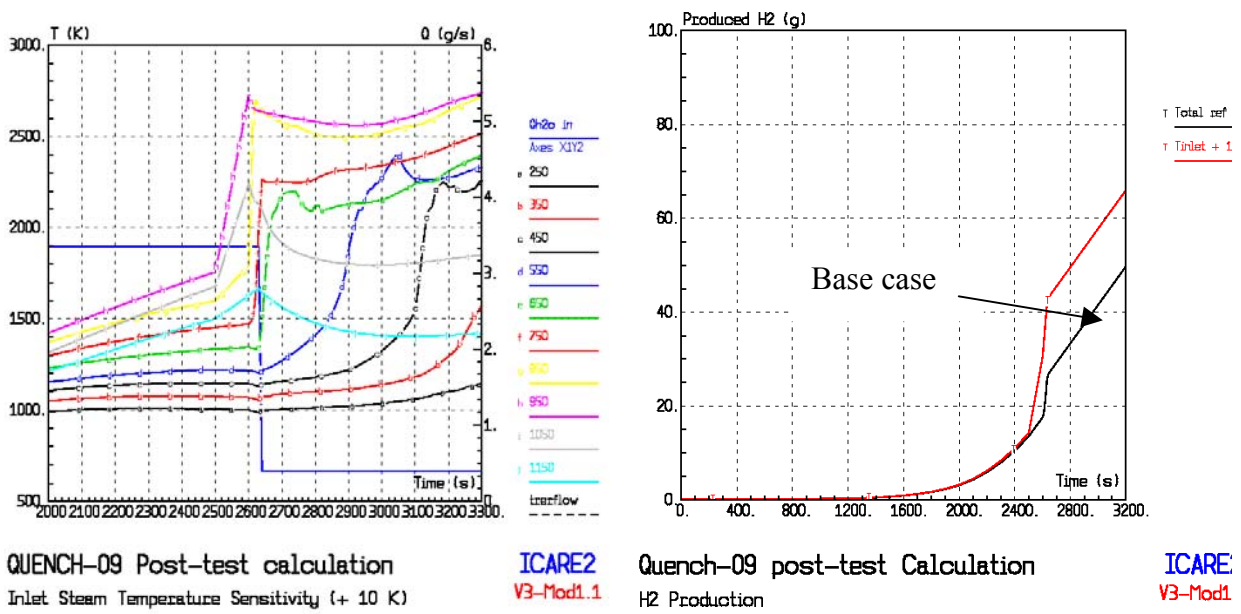


**Figure 161** : Sensitivity calculation assuming a steam inlet temperature increase of 10 K.

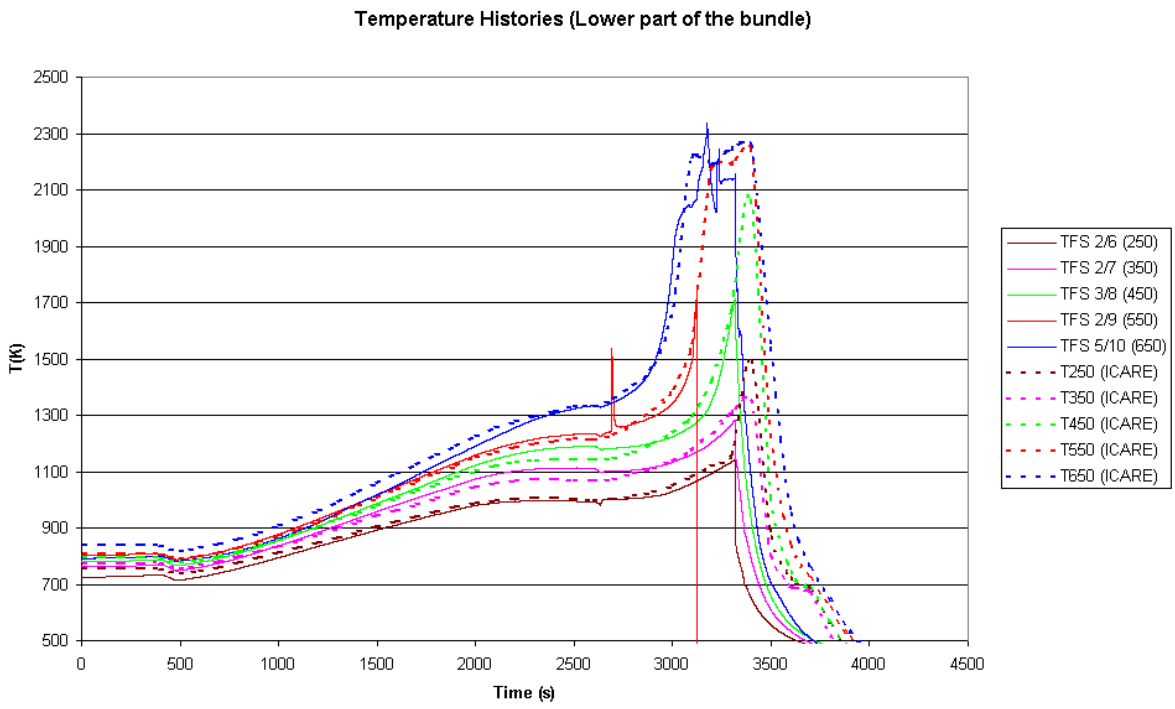


**Figure 162**: Comparison between the temperature measured and calculated

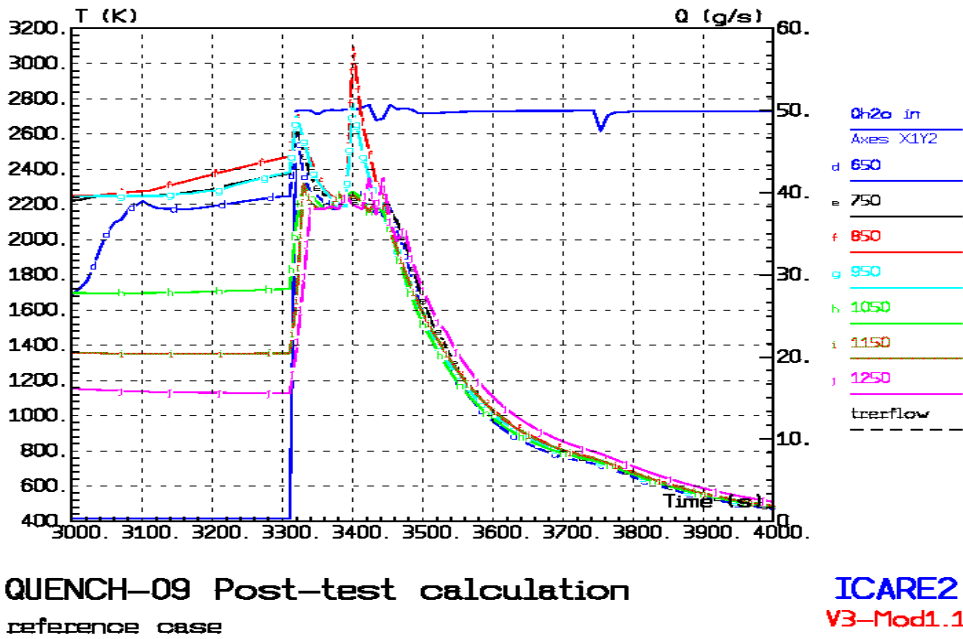


Figure 163: Temperature evolution calculated in the upper zone of the bundle

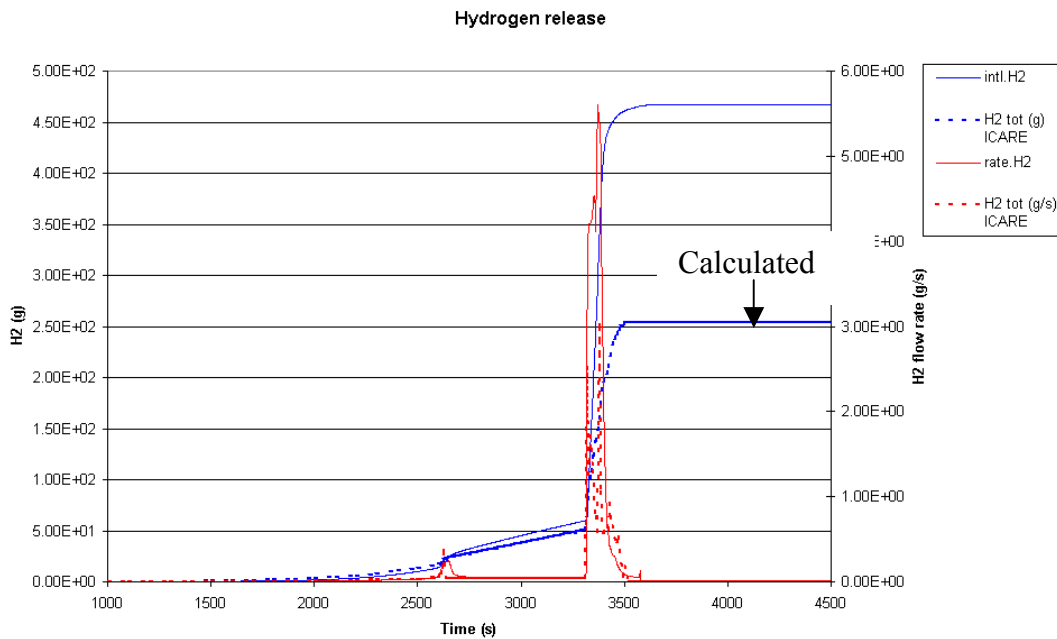


Figure 164: Hydrogen release measured and calculated

## **Reference case calculation results regarding the cool-down phase**

The temperature recorded during the test showed that during the cool down phase, the lower part of the test section did not experience oxidation after the onset of the cooling. Conversely, the upper part of the test section experienced a very violent oxidation runaway which destroyed the major part of the thermocouples. The so-called best-estimate calculation permitted to reproduce correctly the thermal behaviour observed up to 650 mm (Figure 162). Above this elevation, the comparison to the experiment is very difficult because the major part of the thermocouples failed at the beginning of the cool down. During cool-down, a massive oxidation was calculated due to an efficient convective energy transfer from the lower part to the upper part of the test section (Figure 163). Nevertheless, the hydrogen generation calculated during the final cooling phase is significantly lower: 250 g calculated instead of 468 g measured for the whole transient (Figure 164). The hydrogen mass flow rate released in the experiment at the onset of the cool-down indicated that the steam starvation was reached. In this condition, the steam flow rate injected in the bundle (50 g/s) induces a 5,5 g/s of hydrogen mass flow rate and a very large oxidation power (around 800 kW). These conditions have not been obtained in the base case calculation (Figure 164).

Nevertheless, the huge hydrogen release measured during the cool down is not consistent with the absence of oxidation in the lower part of the test section (as observed according to the thermocouple). The experimentalists confirmed that the hydrogen release by the spectrometer during the cool down might be over-measured and needs to be re-evaluate by means of the carbon balance

During the quench phase, the Ar flow rate (Ar is used as the reference spectrometer gas) firstly decreased near to zero (during the first 30 seconds), then increased due to the injection of argon from the failed cooling jacket. Thus, even if the ratios CO/H<sub>2</sub> and CO<sub>2</sub>/H<sub>2</sub> remain well defined, uncertainties on the released gas flow rates are very high, and the overall released quantities are probably overestimated. More investigations are required to quantify the uncertainty on the H<sub>2</sub> release during the quench phase.

A second hypothesis to explain the discrepancy on the amount of hydrogen released could be the oxidation of other materials than claddings such as the molybdenum of the upper part of the electrodes for instance.

The comparison between the amount of B<sub>4</sub>C oxidised during the transient in the experiment and in the calculation is presented on the Figure 165. Based on the measurement of CO and CO<sub>2</sub>, the B<sub>4</sub>C oxidation during the cool down phase is also underestimated in this reference case calculation. Nevertheless, for the same reason than for the H<sub>2</sub> release measurement, the release of carbon oxides might be overestimated during the final cool down. This trend is confirmed by the analysis of measured carbon oxides releases that show 22 g of CO and 33 g of CO<sub>2</sub>. These quantities should have been produced by 93 g of B<sub>4</sub>C while the initial inventory is 78 g (Figure 165). The same trend is showed by the hydrogen released by the B<sub>4</sub>C oxidation, which is supposed to be equal to 33 g, whereas 23 g at a maximum can be obtained considering the maximum conversion rate into hydrogen of the initial inventory in B<sub>4</sub>C. It seems difficult to conclude regarding the total amount of B<sub>4</sub>C oxidised, even though the calculation seems anyway to underestimate it during the cool down. The post mortem analysis should give valuable information on this point. This underestimation in the calculation<sup>2</sup> come from the containment of

---

<sup>2</sup> The guide tube has to be broken to permit the boron carbide oxidation

the B<sub>4</sub>C mixtures in its guide tube in the lower part of the bundle, and probably also from the underestimation of the oxidation of B<sub>4</sub>C mixtures. Assuming that all the B<sub>4</sub>C relocated would have been oxidised, more than half of the initial B<sub>4</sub>C would have been oxidised in the calculation. A very strong oxidation of B<sub>4</sub>C/SS mixtures has been observed experimentally in SETs of the project (see § 3.10.3). A sensitivity calculation has been performed with a reduced relocation velocity of the B<sub>4</sub>C (1 cm/s instead of 60 cm/s) without obtaining much more oxidation of the B<sub>4</sub>C trapped in control rod mixtures.

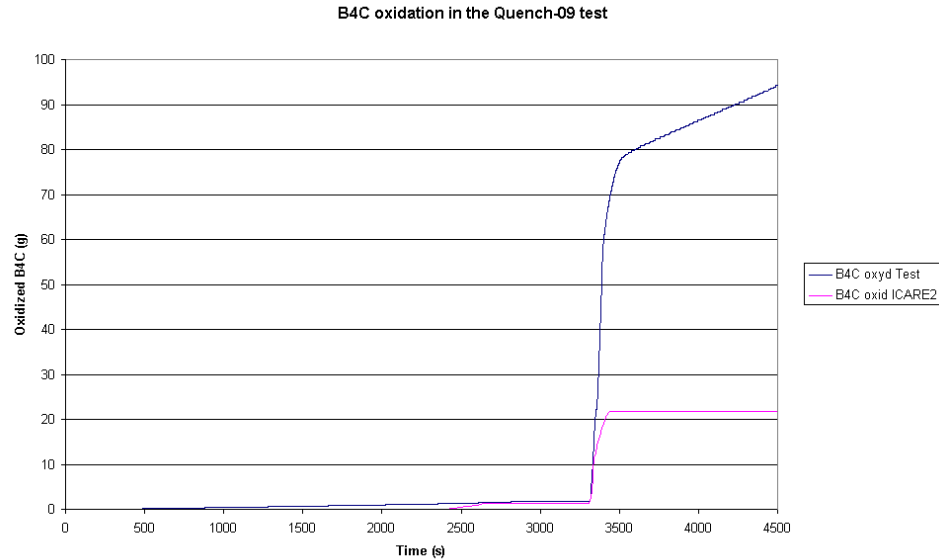


**Figure 165:** Comparison between the B<sub>4</sub>C oxidised in the calculation and in the test

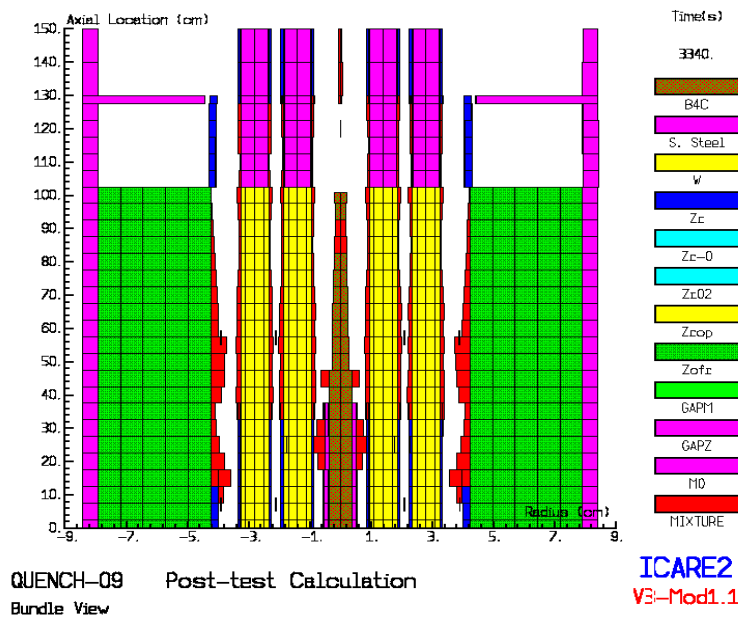


**Figure 166:** View of the bundle being degraded during the cool down phase

As an indication of the degradation of the test section simulated in the reference case calculation, the Figure 166 provides a view of the test section just after the onset of the cool down. In spite of the high temperature required to relocate the fuel rod Zr-rich mixtures, the test section is largely degraded.

### Calculation results taking into account oxidation of relocating materials

The purpose of this exploratory calculation was to enhance the oxidation process using an optional model of rapid oxidation of relocating materials. This calculation could not be performed until the end of the transient due to an unexplained code failure.

As expected, a large amount of hydrogen could then be calculated (Figure 167) as in the test before the code failure. On the other hand, this calculation shows a drastic temperature escalation with steam starvation and extended degradation almost everywhere in the bundle. The calculated oxidation escalation is overestimated at least in the lower part of the bundle. This disagreement underlined once again the overestimation of the measured hydrogen production or the existence of additional hydrogen sources. This exploratory calculation allowing strong oxidation of relocating mixtures shows also an enhanced B<sub>4</sub>C oxidation up to 77 % of the initial inventory at the moment of the calculation failure.

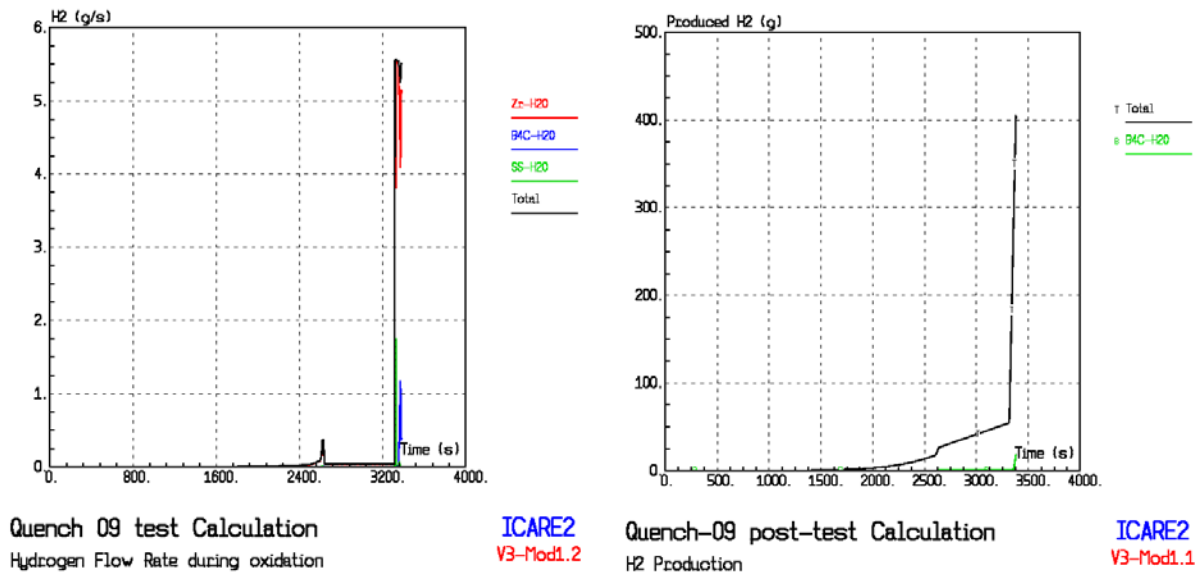


**Figure 167** : Hydrogen produced including the oxidation of relocating materials

### Conclusions

The QUENCH-09 post-test calculations show the ability of the ICARE2 code to simulate and analyse the test up to the onset of the final cool down phase.

A correct simulation required a detailed analysis of the temperature measurements permitting to get rid of the thermal shunting effect which jeopardized the thermal measurements at elevations 750 and 850 mm.

Sensitivity calculations showed that the transient is particularly sensitive to the steam inlet temperature because half of the power is extracted from the test section by convection. In other terms, there is no way to correctly calculate a threshold oxidation phenomenon.

The control rod degradation was fairly well simulated up to the onset of the final cool down, demonstrating by the way that the B<sub>4</sub>C oxidation model of ICARE2 takes into account correctly the effect of the low partial pressure during the starvation phase. During the final cool down phase, the thermal behaviour of the bundle is well reproduced in the lower part of the test section. It is difficult to conclude regarding this behaviour in the upper part because no measurements are available, the thermocouple having been destroyed by the violent final temperature escalation.

The total hydrogen production and B<sub>4</sub>C oxidation were underestimated. An exploratory calculation taking into account an enhanced oxidation of liquid mixtures during their flow down enable to reduce the disagreement. Nevertheless disagreements on the thermal behaviour of the bundle and on the amount of hydrogen released confirm the over-measurement of the H<sub>2</sub>, CO and CO<sub>2</sub> production or even the oxidation of the higher part of the electrodes.

Further efforts will be required to better analyse the final cooling phase taking into account the final post-test examinations and revised quantifications of gas measurements. Future calculations should be able to calculate CO and CO<sub>2</sub> taking into account the coupling of ICARE2 with a gas chemistry model.

## **4 Modelling tasks (WP7)**

Main topics investigated in the project through separate-effects tests such as degradation-oxidation of B<sub>4</sub>C control rods, dissolution of fresh and high burn-up UO<sub>2</sub> and MOX by Zircaloy, simultaneous dissolution of UO<sub>2</sub> and ZrO<sub>2</sub>, oxidation of U-O-Zr mixtures, enabled accompanying analytical investigations regarding modeling developments and validation in several SA computer codes. This section summarizes these activities

### **4.1 B<sub>4</sub>C-CR degradation and oxidation models (IRSN, EDF, FZK)**

#### **4.1.1 B<sub>4</sub>C oxidation model from IRSN**

IRSN was involved in the modelling of the oxidation of a B<sub>4</sub>C control rod which can occur during a high power PWR severe accident, the core being only cooled by steam.

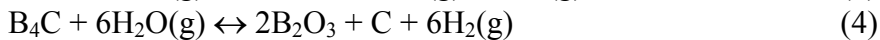
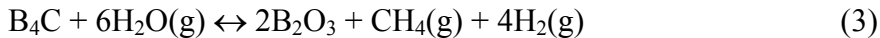
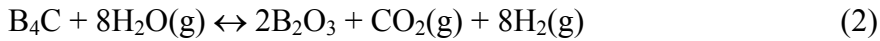
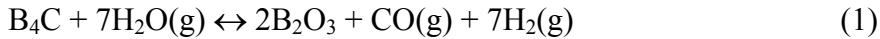
During an assumed severe accident transient, once the temperature of the control rod has reached approximately 1073 K, a solid/solid B<sub>4</sub>C/Stainless Steel (SS) interaction occurs, leading to a liquefaction of the reaction zone when the temperature exceeds 1500 K. Once the stainless steel is totally liquefied, that is, approximately near 1800 K, depending on the temperature transient and on the SS/B<sub>4</sub>C amount ratio, the liquid resulting from the aforementioned process interacts with the guide tube made of Zircaloy and thus, triggers its rupture. This event permits the flow down of the B<sub>4</sub>C/SS mixture to the lower part of the core, and the oxidation of the remaining B<sub>4</sub>C exposed to the steam flow.

A B<sub>4</sub>C oxidation model has been developed at IRSN and is implemented in the ICARE/CATHARE severe accident code. This section summarises main phenomenological aspects of the boron carbide oxidation, the modelling approach and the preliminary validation

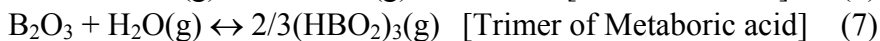
against separate-effects tests performed at IRSN and FZK during the project. More information can be found in Ref. [32] and Ref.[33].

### Main phenomenological aspects

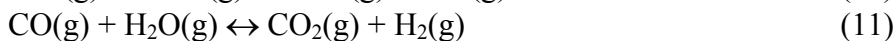
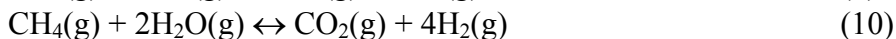
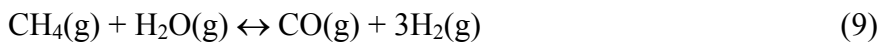
The boron carbide oxidation in steam can be described by the following reactions, forming hydrogen, carbonic compounds and boron oxide :



The resulting boric oxide (liquid or vapor depending on the conditions) can react with steam to form some combinations of acids (reaction 5 to 7) or can be vaporized according to reaction 8 :



In addition, three secondary gaseous reactions can take place and govern the carbonic compounds concentrations:



The boron carbide oxidation is an exothermal process. Without taking into account the  $\text{B}_2\text{O}_3$  consumption processes, the heat released by the oxidation is about 800 kJ per mole. The overall reaction heat can be drastically reduced taking into account the  $\text{B}_2\text{O}_3$  consumption. This is due to the endothermic reaction (5), which is the more favored scheme above 1600 K, and to the  $\text{B}_2\text{O}_3$  vaporization (8). Considering the equilibrium between the  $\text{B}_2\text{O}_3$  production and consumption, the reaction heat may be reduced to 100 kJ per mole of oxidised  $\text{B}_4\text{C}$ .

Beyond the reaction scheme presented above, a bibliographic (Ref [34]) of the experiments available up to now has shown that the kinetics feature depends on the  $\text{B}_2\text{O}_3$  behaviour :

- the kinetics is linear if no  $\text{B}_2\text{O}_3$  builds-up on the  $\text{B}_4\text{C}$  surface ( $\text{B}_2\text{O}_3$  consumption faster than  $\text{B}_4\text{C}$  oxidation) ;

- the kinetics is parabolic, then linear, if the  $\text{B}_2\text{O}_3$  accumulates ( $\text{B}_4\text{C}$  oxidation faster than  $\text{B}_2\text{O}_3$  consumption). In this case, the kinetics is driven by the diffusion in the  $\text{B}_2\text{O}_3$  layer (parabolic behaviour) that increases until the equilibrium between the boric oxide formation and consumption is reached. At this point, the  $\text{B}_2\text{O}_3$  thickness remains constant and the kinetics shows again a linear behaviour.

Finally, it was found that the experimental data base is very reduced regarding the high temperatures of interest in the case of an accident. As a consequence, results from tests performed at a temperature higher or even equal to 1400 °C are not available, except those carried out at IRSN and FZK (Ref. [35]) and (Ref. [36]) in the frame of the COLOSS project.

### Modelling approach

In severe accident conditions, the  $B_4C$  oxidation occurs at temperatures greater than 1500 K ( $B_4C$  exposure to steam after the control rod rupture) and the more favoured scheme for the  $B_2O_3$  consumption is the reaction with steam to form metaboric acid ( $HBO_2$ ).

This process is endothermic and can significantly reduce the exothermic character of the  $B_4C$  oxidation. Considering SA conditions, a linear kinetics assumption has been retained. This means that the thickness of the  $B_2O_3$  liquid film is equal to zero or more generally to a constant value (Figure 168). This assumption seems to be reasonable according to experimental data (Figure 170 and 171).

The governing chemical reactions system presented above has been simplified according to thermochemical calculations, whose examples at atmospheric pressure is presented on Figure 2. These calculations also permitted to assess the heat production (or consumption) resulting from the different reactions. These calculations have been performed using the COACH-V3.3 database couple with the GEMINI1-V3.3 software calculating the minimum Gibbs Energy of the system under constant pressure conditions.

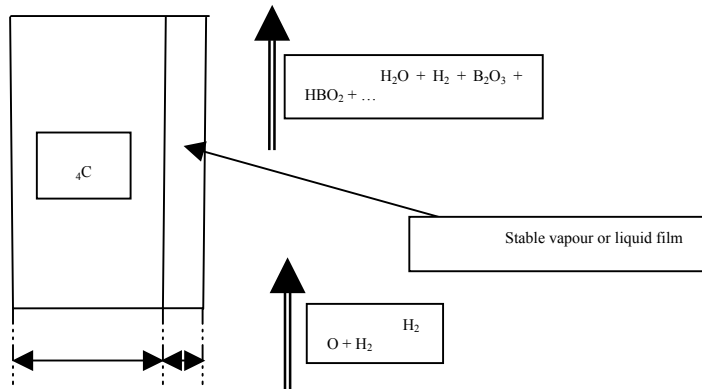


Figure 168: Modelling pattern

P = 1 atm; Initial number of moles : B4C=1 - H2O=100 - H2=0

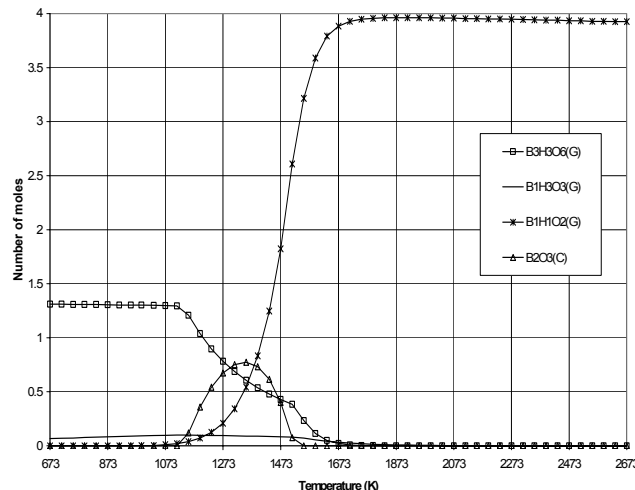
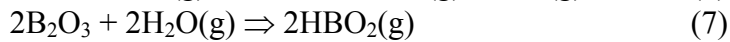
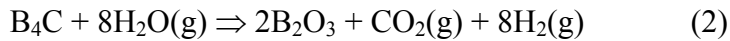
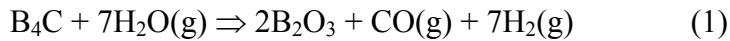


Figure 169 :  $B_4C$  oxidation products versus the temperature for an oxidising atmosphere

As a simplification, among the 4 reactions below, only 3 of them can be considered, retaining the reaction (1) or (1'), depending on the expected ratio between the CO and CO<sub>2</sub> concentration :



Moreover, taking into account the experimental results dealing with pellet oxidation tests (Ref.[37], Ref.[38 ] and Ref.[39 ] as well as the reaction pattern above, the parameters included in the kinetics law expressing the reaction rate are, the temperature, the pre-exponential factor, the steam partial pressure and the total pressure. The latter parameters have been chosen to best fit the test results available up to now including the COLOSS results. The resulting semi-empirical reaction rate can be expressed as:

$$k = k_0 e^{-\frac{E_a}{RT}} p_{\text{H}_2\text{O}}^\alpha p_{\text{Tot}}^\beta \quad (12)$$

With,  $k_0 = 34.17$ ,  $E_a/R = 19\,647$  (K),  $\alpha = 1.18$  and  $\beta = -0.78$ . Furthermore,  $k$  is expressed in mol/m<sup>2</sup>/s and the pressure in Pascal.

Implemented in ICARE/CATHARE, the B<sub>4</sub>C oxidation model takes into account the H<sub>2</sub> but not CO, CO<sub>2</sub> and CH<sub>4</sub> resulting of the B<sub>4</sub>C oxidation. This limitation is resulting from the thermal hydraulic model which do not enable more than two non-condensable gases.

### Validation of the B<sub>4</sub>C oxidation kinetics

In this section, an assessment of the modelling versus experimental tests is presented. Firstly, a validation of the semi-empirical kinetics law is provided. Afterwards, a validation of the modelling implemented in the ICARE2 code versus the VERDI experiments carried out at IRSN is also presented. A 1-D discretization of the VERDI test section has been used to compute the B<sub>4</sub>C pellet oxidation, taking into account the boundary conditions of the test. Moreover, in these ICARE2 calculations the steam partial pressure is evaluated in each representative mesh of the B<sub>4</sub>C pellet, providing by this way a better calculation of the amount of B<sub>4</sub>C oxidised.

### Validation of the kinetics law

This preliminary validation work has been realized based on test results realized at a pressure equal to 0.8 time the atmospheric pressure in the VERDI test section. The thermal-hydraulics conditions obtained in this facility were quite similar to those possible in a power plant accident case. In particular, the Reynolds number is of the same order of magnitude (Re ~100) and the flow configuration corresponds to an external flow along a pellet representing a portion of a control rod. The kinetics obtained in the VERDI tests are represented in the Figure 170 which, shows also results obtained in other facilities. The tests of Sato, Linjenzin and Elrick have been retained to adjust the coefficient of the semi-empirical expression of the reaction rate (12).

The Figure 170 shows clearly the dependency of the reaction rate on the temperature as in the Arrhenius law. Furthermore, the vertical shifting of the different sets of experiments indicates partial pressure and total pressure dependency. Thus, the VERDI results are consistent with the larger partial pressure than in other tests. VERDI and BOX experiments have been used for a validation of the preliminary kinetics law.

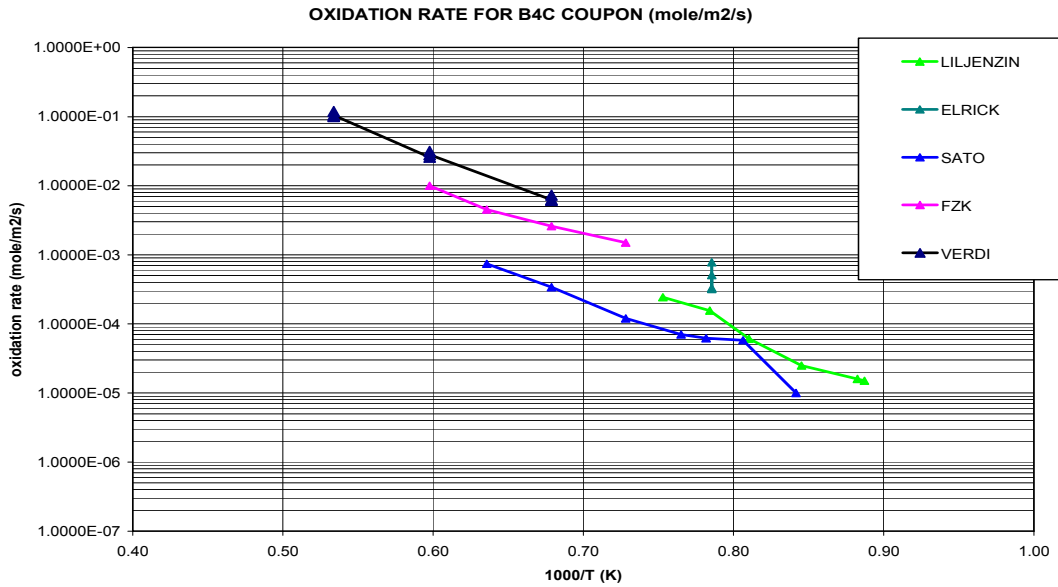


**Figure 170** : B<sub>4</sub>C pellets oxidation available experimental results

A comparison between the calculated and measured reaction rates are plotted on the Figure 171. The error symbols in the VERDI result are associated to the uncertainty affecting the surface temperature of the B<sub>4</sub>C pellet. This uncertainty has been assessed taken into account the boundary conditions of the test.. Despite a slight discrepancy between the reaction rate predicted and measured in the BOX tests at low temperature, the agreement between the calculated and measured reaction rate is quite acceptable. The departure of the modeled reaction rate from the measurement in these experiments at the lowest temperature could be explained, among other phenomena, by the presence of a growing liquid layer of B<sub>2</sub>O<sub>3</sub>.

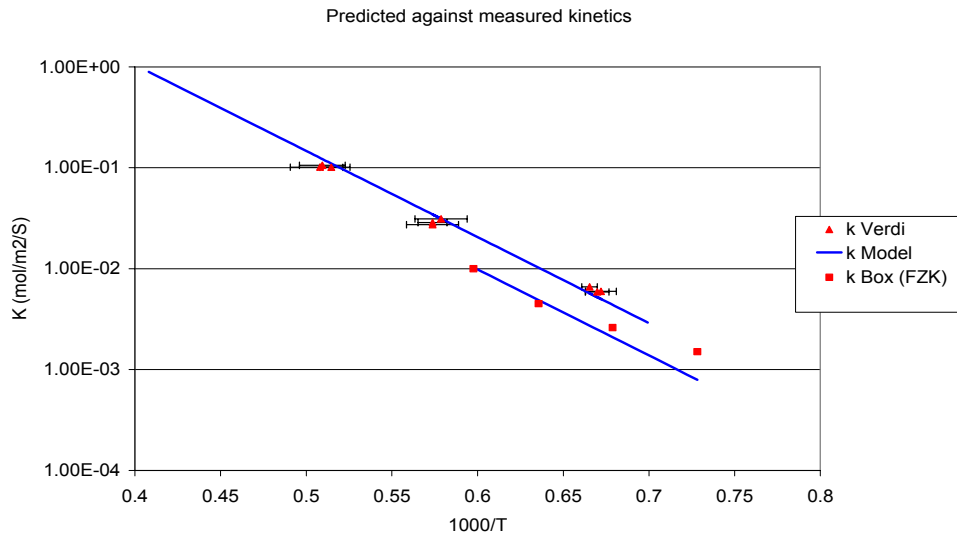


**Figure 171** : 0-D validation of the model reaction rate versus experiments

### 1-D validation of the ICARE2 code B<sub>4</sub>C oxidation modelling on VERDI tests

This validation versus the VERDI experiment has started during the final part of the project and will continue after it in the framework of the preparation of the PHEBUS FPT3. Validation on the first set of VERDI experiments carried out with a steam partial pressure of 0.8 bar and in the temperature range 1200-1600°C Verdi is described below.

The discretization of the VERDI test section in ICARE2 is presented on the Figure 172. Typical boundary conditions of a test performed at 1200 °C are also provided on the Figure 173. This latter figure exhibits a calculated difference between the fluid temperature, the heater temperature and the temperature of the wall of the B<sub>4</sub>C pellet.

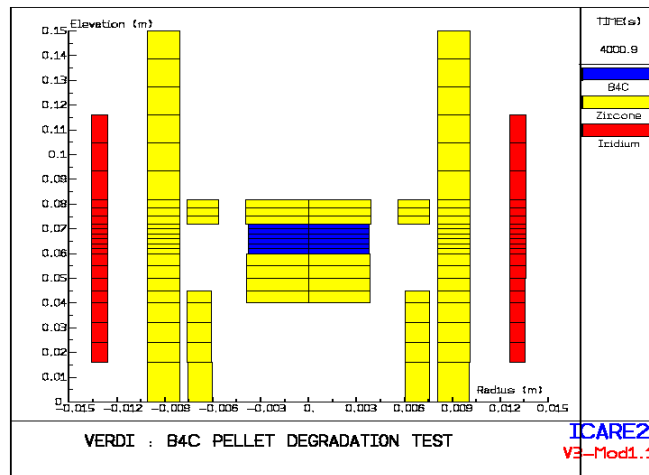


**Figure 172** : Discretization of the VERDI test section for a ICARE2 calculation

The only temperature measurement being located in the fluid and near the heater, the boundary conditions imposed in the ICARE2 calculation (Figure 173) have been established to reproduce the fluid temperature measurement. The axial evolution of the partial pressure of steam, Argon and Hydrogen is given on the Figure 174 at different temperatures condition (1200, 1400 and 1600°C as used in the tests).

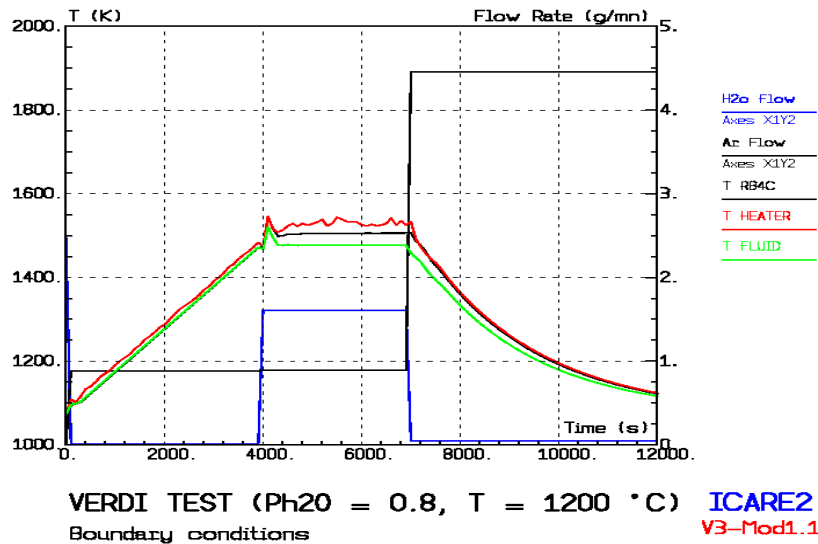


**Figure 174**: Typical boundary conditions of a VERDI test

The axial evolution of the partial pressure indicates that the decrease of the steam partial pressure due to the consumption of steam, during the oxidation, is correctly taken into account. This parameter illustrates the dependency of the oxidation reaction rate on the temperature. As a result, it can be observed that the higher the temperature, the larger the steam consumption is. Furthermore, Figure 174 shows also that the coupling between the thermal-hydraulic processes and the oxidation model permits to calculate the oxidation reaction rate, considering the correct steam partial pressure and temperature in each mesh representing a piece of the pellet.

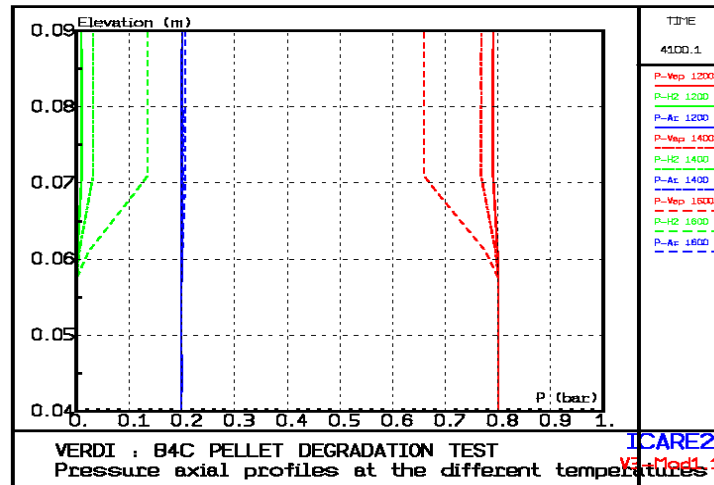


**Figure 174:** Axial profile of partial pressures (for H<sub>2</sub>, Ar and steam from the left to the right side and for in each case, 1200, 1400 and 1600°C)

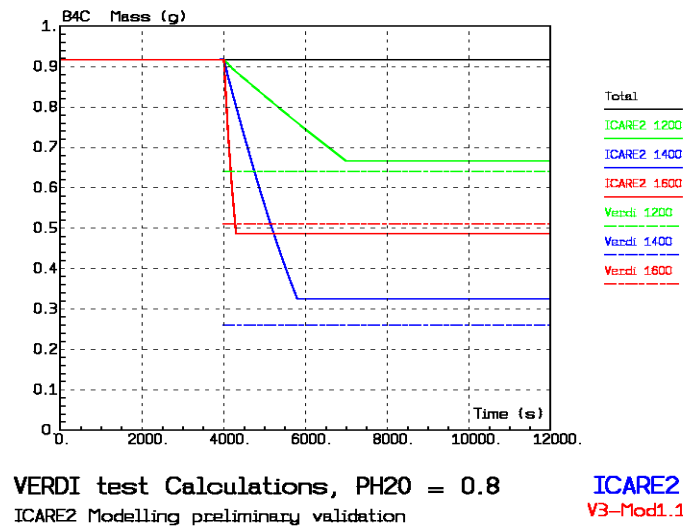


**Figure 175:** Comparison between the measurement (dot lines) and the calculation (solid lines) for tests at 1200, 1400 and 1600°C.

Finally, a comparison between the experiments (one at each targeted temperature in the VERDI tests) and the ICARE2 calculations is presented on the Figure 175. It can be seen that at the considered partial pressure, the results are fairly consistent.

## Summary

The reaction rate proposed by IRSN for the B<sub>4</sub>C oxidation in SA conditions is based on a classical Arrhenius law combined with additional terms to take into account the steam partial pressure and the total pressure. This law, which corresponds to a linear kinetics behavior, has been validated on analytical tests carried out in the project. The coupling between themalhydraulics and chemical processes is correctly taken into via the temperature, the steam pressure and the total pressure.

The present limitation regarding the lack of CO, CO<sub>2</sub> and CH<sub>4</sub> calculation will be overcome by the coupling between ICARE2 and thermochemical equilibrium tool (GEMINI2 code) to calculate the amount and the nature of the gases generated by the B<sub>4</sub>C oxidation.

### 4.1.2 B<sub>4</sub>C-CR degradation and oxidation models from EDF

EDF has developed a B<sub>4</sub>C model in the MAAP4 code with the following characteristics:

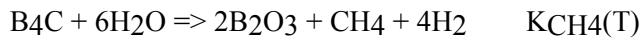
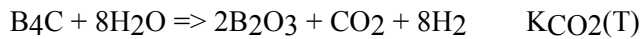
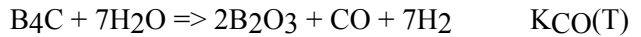
- In a first stage, the interaction of the B<sub>4</sub>C with the surrounding Stainless Steel cladding is considered. First, it is supposed an "instantaneous" formation of a B<sub>4</sub>C /Stainless Steel eutectic at 1500K. No kinetics of formation is taken into account in order to simplify the approach. One suppose that the eutectic content of B<sub>4</sub>C is about 9 % on the basis of previous experimental work made by FZK and UJP-Praha.
- In a 2<sup>nd</sup> stage between 1500 and 2700K, the remaining B<sub>4</sub>C supposed in a "pure" B<sub>4</sub>C state, is available for oxidation and/or melting.

**Table 24:** Three oxidation laws introduced in MAAP4.

The MELCOR B <sub>4</sub> C oxidation law: a Arrhenius temperature dependant law for the ratio "current mass to initial mass".	$MELCOR_{SANDIA} \quad - \frac{d\left(\frac{M_{B4C}}{M_{B4C}^0}\right)}{dt} = \left[\frac{9.973 \cdot 10^6}{60}\right]_{[s^{-1}]} e^{-\frac{22647.2}{T[K]}}$
The BOX test rig correlation from FZK (M. Steinbruck)	$STEINBRUCK_{FZK} \quad - \frac{1}{A_{oxyd}} \frac{dN_{B4C}}{dt} [mol/(m^2s)] = 0.0011 + 6800 e^{-\frac{188700}{R T[K]}}$
The ICARE2 correlation, validated against the VERDI tests	$ICARE_{IRSN} \quad - \frac{1}{A_{oxyd}} \frac{dN_{B4C}}{dt} [mol/(m^2s)] = 3417 e^{-\frac{163345}{R T[K]}} p_{H_2O[bar]}^{1.18} p_{total[bar]}^{-0.5}$

For the oxidation of the B<sub>4</sub>C /Stainless Steel eutectic, a dedicated oxidation correlation was not available but could be determine after project based on FZK SETs. The hypothesis of non-taking into account the oxidation of the eutectic melt is only supported in the case of a 'cold foot' situation (such as TMI-2, where assemblies lower part are cooled by liquid water all along the scenario) when the melt relocates downward to a water cooled region. The temperature is then so low that it is expected that oxidation of the melt is stopped.

Three different oxidation laws were introduced, the last two available from the project (Table 24). The oxidation of pure B<sub>4</sub>C produces mainly CO, CO<sub>2</sub>, CH<sub>4</sub> and H<sub>2</sub> with intermediate production of liquid B<sub>2</sub>O<sub>3</sub>



$$K_{\text{CO}}(T) = P_{\text{CO}} \left( \frac{P_{\text{H}_2}}{P_{\text{H}_2\text{O}}} \right)^7$$

$$K_{\text{CO}_2}(T) = P_{\text{CO}_2} \left( \frac{P_{\text{H}_2}}{P_{\text{H}_2\text{O}}} \right)^8$$

$$K_{\text{CH}_4}(T) = P_{\text{CH}_4} \frac{P_{\text{H}_2}^4}{P_{\text{H}_2\text{O}}^6}$$

The chemical constant, supposing an equilibrium state, can be written as seen above using the partial pressure in atmosphere. These parameters have been derived from an independent thermodynamic equilibrium analysis carried out with the GEMINI1/COACH package (Ref.[40]).

A first qualification of this model was made on the QUENCH-07 test and results are summarized in the § 4.14.1. In addition, this model was used to calculate with MAAP4 a « total loss of feedwater to the steam generators without safety injections » scenario (nicknamed « H2 without SI ») occurring on a PWR-1300. Results have been summarised in the Part 2 of the final COLOSS report (Ref.[1]).

#### 4.1.3 B<sub>4</sub>C oxidation model from FZK

The analysis of FZK results from the TG and BOX programmes showed that complex and competing phenomena are driving the B<sub>4</sub>C oxidation. The interpretation of these results required a modelling support and FZK decided to participate to the WP7.1 modelling task. In the preliminary version it was assumed that parabolic B<sub>2</sub>O<sub>3</sub> scale formation and linear B<sub>2</sub>O<sub>3</sub> evaporation are superposed and govern the B<sub>4</sub>C oxidation based on the following differential form:

$$\frac{dm_{\text{ox}}}{dt} = \frac{a}{m_o} \quad \text{with } m_{\text{ox}} = \text{specific mass of oxide film (g/cm}^2\text{)}$$

$$a = A_0 * e^{-A/T} \quad \text{and} \quad b = B_0 * e^{-B/T}$$

A preliminary model is given in § 3.8. A revised B<sub>4</sub>C oxidation kinetics was also proposed which has to be compared with other experimental results, in particular with those from the VERDI experimental programme. Additional improvement will consider the steam flow rate and steal partial pressure effects. By applying this model to tests on oxidation of pure dense B<sub>4</sub>C, mass losses, reaction rates, scale formation for TG as well as for BOX tests could be calculated with good conformity. Some comparisons with experimental data are illustrated in § 3.10.4. More information is available in Ref.[41].

## **4.2 Oxidation of U-O-Zr mixtures (IRSN, ALIAS CZ, JRC, IBRAE, RUB)**

Metal-rich U-O-Zr mixtures oxidise in steam during relocation and once frozen at lower core zones. This is a key source of H<sub>2</sub> during core degradation and particularly during reflooding. The corresponding oxidation modelling was either missing or inadequate in SA codes. One of the technical objectives of the project was to produce experimental data regarding oxidation of Zr-rich mixtures in order to enable preliminary modeling of this safety relevant phenomena considering both solid and liquid mixtures. Both ALIAS CZ and IBRAE were involved in this modeling activity. RUB did a complementary investigation on melt oxidation at high temperature, above the liquidus temperature of the formed oxide.

### **4.2.1 Modeling task on oxidation of solid U-Zr-O mixtures (ALIAS CZ)**

ALIAS CZ worked as a subcontractor of IRSN on the analysis and modelling of experimental data on U-Zr-O oxidation results produced by ÚJP PRAHA (former ŠKODA-ÚJP) in the WP3.1. The objective of this work was to improve the existing model ZROX used in ICARE/CATHARE on basis of the ÚJP PRAHA experimental programme (WP3.1). ALIAS CZ performed critical analysis of the oxidation model ZROX, implemented into ZROX the enhanced U-Zr-O oxidation kinetics and adjusted the ICARE2 source to preserve the thermal stability of the code in case of oxidation escalation (Ref.[42]).

The ÚJP tests showed that the presence of U and O in U-Zr-O mixtures enhances the oxidation kinetics at temperatures < 1400 °C compared to Zr or Zr1Nb (the effect of presence of oxygen is important, nevertheless limited effects were observed in the 2 - 5 wt% O range). ALIAS CZ collected and analysed the available experimental data on oxidation of U-Zr and U-Zr-O alloys. For U-Zr-O oxidation in steam it was only found one dataset (for 66U-30Zr-4O wt% alloy, 1415-2140 °C) measured at PNL by Prater & Courtright in 1987 (Ref.[15]). The PNL and ÚJP data are consistent at 1400 °C, but at low-temperature the ÚJP data show much higher oxidation than those of PNL extrapolated below 1400 °C. Both datasets obey parabolic law above 900 °C, but linear kinetics was observed by ÚJP between 450-900 °C. ALIAS CZ thus chose to model the U-Zr-O oxidation by using the parabolic reaction rates for oxygen weight gain  $\Delta G$ .

#### **Implementation of the ÚJP PRAHA data into the ZROX model**

The improvement of the ZROX model of ICARE2-V3mod1.2 was guided by the requirement to keep the modelling as simple as possible. The parabolic approach (used in the current model) was preserved. The ÚJP data were introduced into the EQUILIBR sub-model. The sub-model PROTECTI remains unchanged. The Arrhenius-type parabolic correlations were replaced by parabolic rate constants  $K_p$  tabulated over two parameters: Temperatures greater than 400°C and U-content in the U-Zr-O mixture (0-60 wt%). The database being not sufficient, the tabulated  $K_p$  rates could not be dependent on the oxygen content in the U-Zr-O mixture. Intermediate values are interpolated linearly as a function of temperature and U-content in the mixture (Figure 176) using a fast routine developed for this purpose.

The energy release from the exothermic U-Zr-O oxidation remains unmodified in the ZROX.

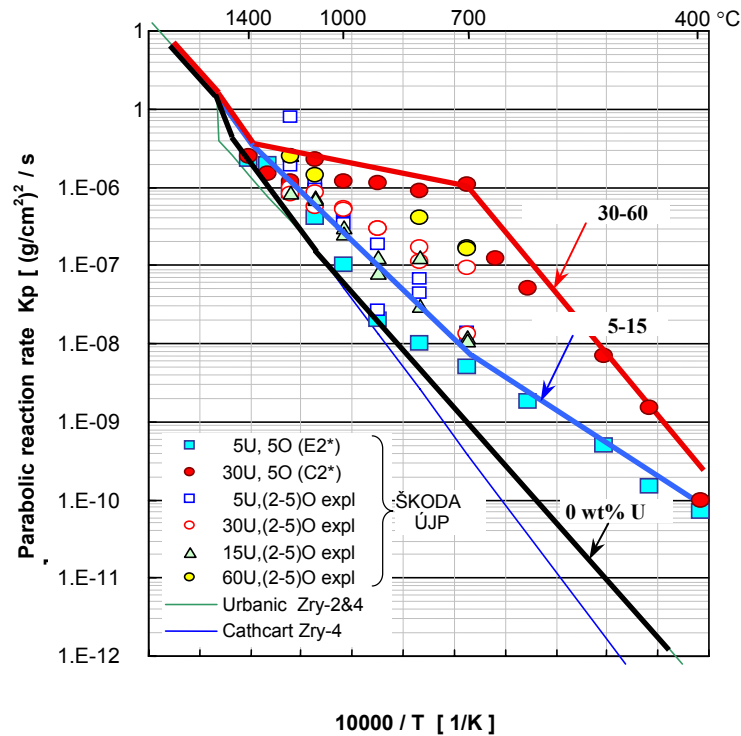


**Fig. 176:** ZROX model for solid mixtures: Reaction rates  $K_p$  as a function of temperature and U-content in the mixture.

### Validation of the improved oxidation model ZROX

The validation was performed against integral bundle experiments CORA-5, CORA-13, PBF 1-4 and FLHT-5 using the corresponding input decks (slightly modified) delivered with the ICARE2 code. The 1-D single-phase thermalhydraulics and user-defined parameter ZROX/MMI=0.8 and CAND/WETT ~0.1 were used in these calculations. The enhanced dissolution of irradiated  $UO_2$  in molten Zry (developed within WP1.2) was also activated when applicable. Table 25 shows that the largest improvement was achieved in tests, where steam starvation did not dominate as it is the case in CORA-5 and CORA-13.

**Table 25:** Total  $H_2$  production measured and calculated by the revised ZROX model of ICARE2.

	CORA-5	CORA-13	PBF 1-4	FLHT-5
Measured total $H_2$ [g]	~100	~210 (~165 <sup>A</sup> )	86 (126 <sup>B</sup> )	220-340
ZROX - original [g]	65.6	83.9	93.9	194.5
ZROX - improved [g]	105.5	144.5	107.6	212

<sup>A</sup> estimated before quench phase, <sup>B</sup> upper estimate

### Main outcomes

Main results of ÚJP have been introduced in ICARE/CATHARE. The improved oxidation model of mixtures has a potential to better predict the  $H_2$  release (total value & timing) from

relocated frozen mixtures especially in transients with rich steam supply, including quenching. The chosen parabolic reaction rates below 1400 °C are slightly conservative just to account for the 450-600 °C temperature range with U-rich alloys where linear kinetics would be more appropriate.

The enhanced oxidation of U-Zr-O alloys measured below 1400 °C by ÚJP-PRAHA and successfully implemented into ICARE2-V3mod1.2 improved both the timing and the total value of the hydrogen generation observed in bundle tests.

The model favours the hydrogen release but not sufficiently to simulate the hydrogen peak observed during quenching. For this, the model should be completed by an oxide ZrO<sub>2</sub> shattering or cracking effect that would expose some amount of fresh metallic surfaces to steam.

A complementary modeling activity has been carried out by IRSN (see § 4.2.3) to take into account the oxidation of U-O-Zr melts ( $T > 1850^{\circ}\text{C}$ ). This modeling has been implemented in the new MAGMA model of ICARE2 devoted to the calculation of the 2-D corium progression in a porous medium.

#### **4.2.2 Modeling task on oxidation of liquid Zr-O and U-Zr-O mixtures (JRC, IBRAE)**

The objective of this multi-partner task (JRC-Petten and IBRAE) was the development of models regarding the high temperature oxidation of U-O-Zr molten mixtures, in particular:

- Models that can adequately simulate the oxidation of U-O-Zr mixtures and related H<sub>2</sub> production during the core degradation phase of a severe accident.
- Models that can be integrated in SA codes.

In order to model the oxidation of Zr-O and U-Zr-O melts, available FZK data from post-test examinations of molten materials oxidation in the CORA and QUENCH bundle tests, as well as new FZK tests on ZrO<sub>2</sub> crucible dissolution by molten Zry were taken into account by IBRAE. These single-effect tests were specially designed for the investigation of long-term behaviour representative of the melt oxidation stage. Detailed analysis of post-test images of re-solidified Zr-O melts in the QUENCH-02 and 03 tests was performed. A close similarity was found with the melt appearance in the ZrO<sub>2</sub> crucible dissolution tests where oxide layer growth was accompanied by precipitation of ceramic particles in the corrosion (oxidation) stage.

On this basis, the new model for U-Zr-O melt oxidation under conditions of convection stirring was developed. The model explains the emergence of the ceramic precipitates induced by the temperature difference between the wall and the melt, and predicts continuous oxidation/precipitation process after attainment of the saturated state of the melt as well as a phase of ‘late dissolution’ as observed in the new FZK tests..

The developed model of oxidation of U-Zr-O and Zr-O melts in steam is based on the qualitative results of post-test observations of the melts in the bundle tests CORA and QUENCH. This work involved final formulation of the analytical model, development of the numerical model and validation of the model against FZK crucible test data.

The model was successfully validated against new FZK tests on ZrO<sub>2</sub> crucible dissolution by molten Zry, Figs. 177 and 178. The new model prediction concerning long-term behaviour in the oxidation stage of the tests (i.e. cessation of the oxide layer growth and commencement of its renewed dissolution) was confirmed by the FZK test results.

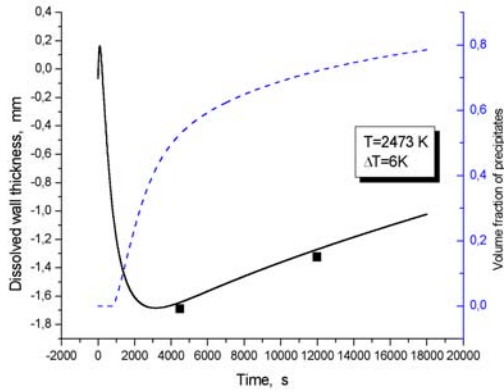


**Fig. 177:** Simulations of FZK tests on  $ZrO_2$  dissolution by molten Zry at melt temperature 2473 K and temperature difference 6 K. *Solid curves* – dissolved wall thickness; *dashed curve* – volume fraction of precipitates.

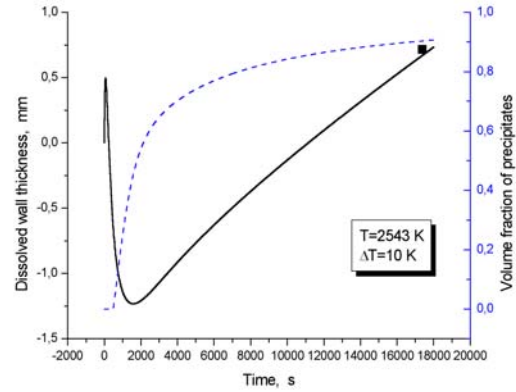
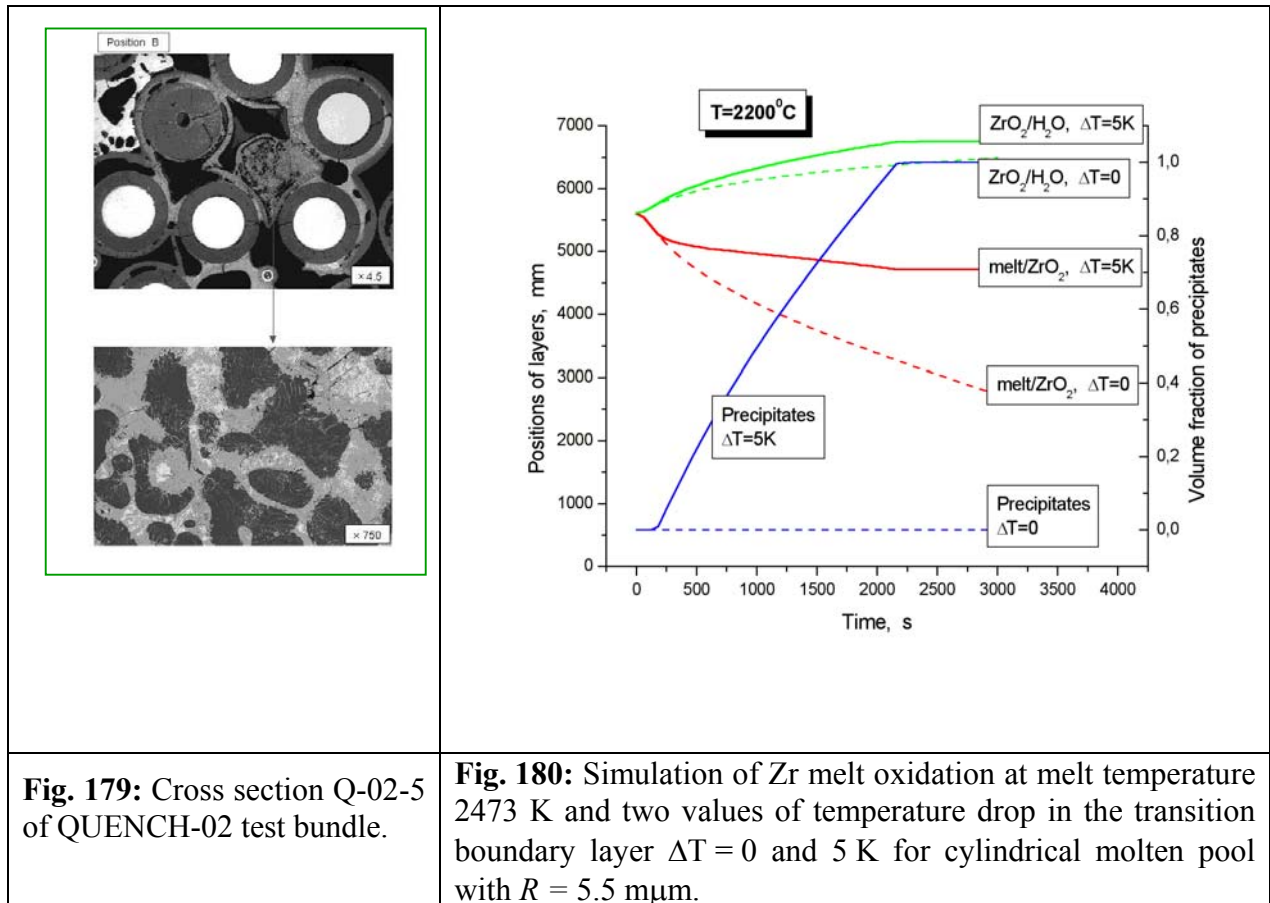


**Fig. 178:** Simulations of FZK tests on  $ZrO_2$  dissolution by molten Zry at melt temperature 2573 K and temperature difference 10 K. *Solid curves* – dissolved wall thickness; *dashed curve* – volume fraction of precipitates.



The model predicts a linear or close to linear time law for the rate of the  $ZrO_2$  ceramic phase (oxide layer + precipitates) growth during Zr melt oxidation that corresponds to a much

faster kinetics of Zr oxidation and hydrogen generation in comparison with the standard (parabolic) rate. The model predicts an enhancement of the oxidation kinetics in the presence of temperature gradient between melt and crucible wall due to precipitation of ceramic phase in the melt.

Calculations with the model allow quantitative interpretation of the vigorous melt oxidation and  $ZrO_2$  phase precipitation observed in the QUENCH tests, Figs. 179 and 180. These tests do not involve  $UO_2$  material and give illustration of relocated Zr-O mixtures within the bundle. In particular, it was demonstrated that complete solidification of the melts could occur rather quickly owing to formation of ceramic precipitates in the melt in the course of its oxidation. This explains the significant underestimation by standard oxidation models of hydrogen production measured in the integral tests characterised by large amount of melts.

The 2<sup>nd</sup> example of validation is based on the analysis of CORA mixtures involving  $UO_2$  material. Post-test images of re-solidified U-Zr-O melts in the CORA-W1 and W2 tests were additionally analysed. A behaviour of the ternary U-Zr-O melts similar to the previous case (i.e. continuous oxidation of oversaturated melts accompanied with precipitation of ceramic  $(U,Zr)O_{2-x}$  phase) were revealed also in these tests. Correspondingly, the new model was generalised for description of the ternary U-Zr-O melt oxidation. The main qualitative conclusion on the enhanced kinetics of melt oxidation and hydrogen generation due to  $(U,Zr)O_{2-x}$  phase precipitation is confirmed also for the ternary system. Calculations with the model allows quantitative interpretation of the vigorous melt oxidation and  $(U,Zr)O_2$  phase precipitation observed in the CORA tests (Fig. 181).

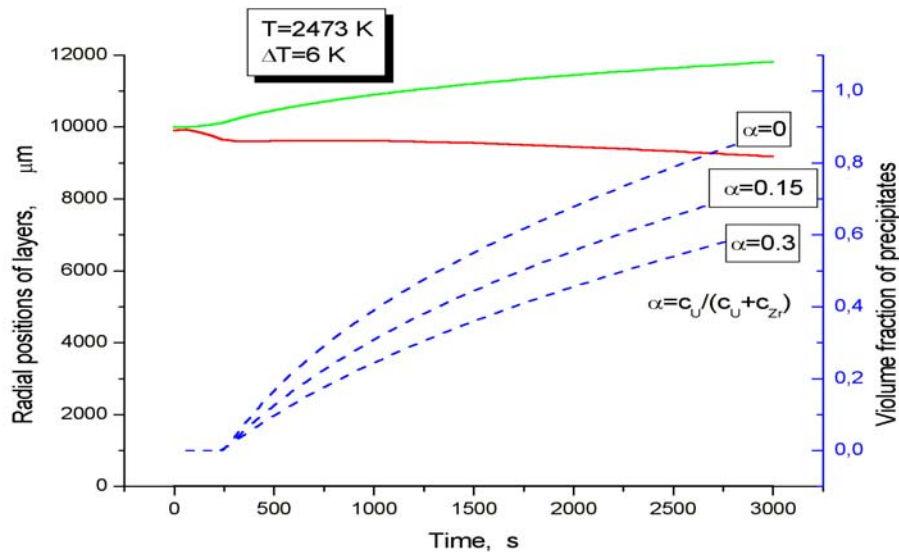


**Fig. 181:** Simulation of oxidation of U-Zr melt with three various compositions  $\alpha = c_U / (c_U + c_{Zr})$  at melt temperature 2473 K and temperature drop in the transition boundary layer  $\Delta T = 6$  K for cylindrical molten pool with  $R = 10$  mm

On the basis of the analysis performed for the binary Zr-O system behaviour (i.e. solid  $ZrO_2$  and Zr-O melt), it is anticipated that dissolution of  $UO_2$  fuel by the U-Zr-O melt is also strongly influenced by the temperature difference between heated fuel pellets and melt. This was the case in past experiments where dissolution was no longer restricted by the melt saturation

limit and proceed actively in the oversaturated melt. Such behaviour is possible in the bundle tests during the early fuel liquefaction.

The new mechanism provides a natural qualitative explanation of the early fuel destabilisation/liquefaction and enhanced melt oxidation accompanied with the ceramic phase precipitation (Ref.[43]). Implementation of this mechanism in the fuel dissolution model of SA codes for quantitative analysis of the bundle tests observations is recommended.

#### **4.2.3 Modeling on oxidation of liquid U-Zr-O mixtures (IRSN)**

First, among the numerous lessons drawn from the extended ICARE/CATHARE V1mod1 assessment, the lack of any dedicated melt (named MAGMA) oxidation model was identified to be one of the main shortcomings of the ICARE2 and ICARE/CATHARE code versions. Therefore, the development of a new oxidation model for MAGMA components (UZOX model) was launched at IRSN. This development not included in the initial IRSN work-plan of the project was carried out simultaneously with the improvement of the U-O-Zr oxidation model of ICARE/CATHARE for solid mixtures. IRSN developed the so-called "MAGMA oxidation model" (Ref. [44]) derived from the IBRAE modelling work (see previous section) based on the analysis of melt oxidation observed in CORA and QUENCH tests. The MAGMA oxidation model which is specific to the so-called "MAGMA" components could not be completed and validated in due time to be included to the V1mod1.3p version of ICARE/CATHARE issued to the PAG users in October 2002 (see Part 2 of the final report devoted to the WP8, Ref.[1]). Nevertheless, this version included the new alternative 2-D MAGMA model dealing with melt relocation in the core.

#### **4.2.4 Investigation on the melt oxidation above the liquidus temperature (RUB)**

In this temperature domain there is a very limited database available and no data were produced by the project. RUB/LEE did a state of the art on this topic (Ref. [16]). The lack of data was illustrated by the fact that even the rate controlling phenomena of molten Zr oxidation was not yet well understood. In addition, RUB did exploratory calculations using the RELOS code (*RE*lease of *LO*w volatile fission products from molten pool *S*urfaces) to illustrate uncertainties on the mechanism of oxidation. The exercise was based on the calculation of molten Zr configuration using the same boundary conditions and two extreme cases as controlling phenomena: a reaction at the melt's surface and a diffusion process. Due to the lack of appropriate experimental data, the task was limited to the comparison of the two calculations. The mechanism of melt oxidation proposed by IBRAE based on the precipitation of ceramic phase due to temperature difference between the melt and the crust has not been considered in this investigation.

In the case of reaction controlled oxidation it was assumed that in the melt, the transport is fast and the chemical equilibrium is reached quickly throughout the volume, thus, enabling the computer code RELOS to be applied for the simulation. This code has been developed at the Ruhr-University in projects of previous EC framework programs. It has been developed and used for investigations of combined diffusive and convective radionuclide release processes from molten corium pool surfaces into overlying cooler gas atmospheres. It is based on a mechanistic approach, introducing a coupling with a commercial thermochemical equilibrium code module, namely CHEMAPP, with a kinetic gas phase mass transfer coefficient formulation assuming heat

and mass transfer analogy. The driving force for diffusive and convective gas phase mass transfer is given by the partial density gradient established by the local, high-temperature conditions at the gas side of the molten pool surface and the bulk of the overlying cooler gas atmosphere. The chemical forms and gaseous partial densities of the relevant fission products at the molten pool surface and in the bulk of the gas phase are derived from multiphase thermochemical equilibrium conditions at the given pool and gas phase temperature, respectively. RELOS calculates time-dependent vaporisation rates of melt species or compounds of interest and is also able to treat transient pool compositions and atmospheric changes of the steam/hydrogen ratio caused by reduction processes near the molten pool surface. In contrast to the oxidation processes of solid U-Zr-O mixtures being modelled in leading severe accident analysis codes as a solid diffusion-controlled process by application of parabolic rate equations, RELOS calculates the time-dependent oxidation of the liquid melt assuming the oxidation to be limited by gas phase mass transfer.

While the equilibrium data necessary for the melt oxidation considerations with RELOS is available, the transport properties of the reactants in liquid Zirconia or in liquid corium are not known. But when the oxide phase can be assumed to be completely ionised, these properties can be estimated from other known properties. Especially the diffusion coefficient of oxygen can be calculated with the Nernst-Einstein correlation by using the electrical conductivity as a measure for the mobility of ions in the melt. Thus, the estimation of melt properties has been implemented into a numerical module describing one-dimensional diffusion processes. The relevant concentrations at the interfaces between the oxide on the one hand and the atmosphere and the metal, respectively, on the other hand are determined with the aid of phase diagrams.

In the second case of diffusion controlled oxidation, the oxygen was supposed to be dissolved into the very top of the oxide phase only and subsequent transport of the reactants leads to the growth of the oxide layer.

The boundary conditions chosen for the simulation were rather representative of typical experimental conditions. This enabled a basis for the choice of necessary experiments in future projects. The calculated oxidation behaviour is given in Figure 183.

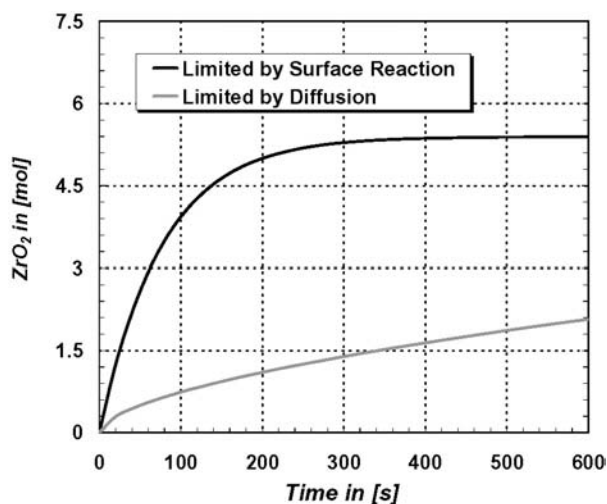


**Figure 182:** Progress of Zr-oxidation limited by surface reaction kinetics as well as by diffusion kinetics in the oxide layer.

It clearly can be seen, that the progress of oxidation is very different for the two cases of reaction controlled and diffusion controlled kinetics. Much faster reactions can be identified in the former case for the beginning of the simulation. The extent of the reaction kinetics leads to a complete oxidation of the available zirconium at a very early stage. Consequently, linear kinetics was not accomplished here except for the first 30 s. Afterwards the limited amount of remaining

Zirconium impacts the oxidation behaviour. In contrast, diffusion controlled oxidation approximately obeys the ideal parabolic law.

Since no experimental data is available yet, it cannot be concluded here, which controlling mechanism is the realistic one. Keeping in mind molten iron experiments, it can be expected that in the very beginning of oxidation of molten zirconium the rate is controlled by the reaction kinetics at the surface. Once a certain amount of Zirconia is formed, a distinct oxide layer will form on top of the melt and diffusion becomes rate controlling. The swap of kinetics will most probably take place after a few seconds only. To identify the transition and to validate the above models, experiments focussing on the oxidation of molten Zirconium are clearly desirable. Such experiments should be proposed in future projects.

### **4.3 Dissolution of fuel (IRSN, ALIAS CZ, IBRAE)**

There is a lot of data on fuel dissolution by molten Zr. In spite of the past efforts some significant uncertainties were remaining and related models in SA codes could not progress. The project intended to extend the existing database in order to improve dissolution models and reduce related uncertainties in the following two areas:

1/ Dissolution of irradiated fuel: Preliminary data on the burn-up effect on  $\text{UO}_2$  behaviour from PHEBUS FP, VERCORS and the 4<sup>th</sup> FP experimental programmes indicate significant differences between fresh and irradiated fuel with accelerated liquefaction due to burn-up. This affects the kinetics of FP release, the corium composition and finally its further progression. For MOX fuel, very few data exist for SA conditions whether for fresh or irradiated fuel. Uncertainties also exist for the  $\text{UO}_2$  high burn-up >33 GWd/t. Above this limit, there was in fact a lack of data for the modeling of the kinetics of dissolution by molten Zr and on the way the kinetics vary with burn-up.

2/ In the reactor case, the metallic Zr trapped between the  $\text{UO}_2$  pellet and the external  $\text{ZrO}_2$  layer on the cladding induce a simultaneous dissolution of the inner  $\text{UO}_2$  pellets and the external  $\text{ZrO}_2$  of the cladding. Preliminary results from the CIT project (4<sup>th</sup> FP) indicate an unexpected large dissolution of  $\text{UO}_2$  in the presence of  $\text{ZrO}_2$  which could not be calculated simply from the two separately-known interactions (Ref.[45]). Of course, the clad failure is affected by the above-mentioned interactions. In SA codes, the prediction of the amount of fuel dissolved in rod geometry is characterized by uncertainties even for low burn-up. In addition the related clad failure or rod collapse criteria used in codes are unable to predict the loss of geometry in different conditions. Code users have to tune these criteria often based on a temperature threshold in order to predict experimental results. The tuning is never the same for different experiments. In the PHEBUS FP tests, under oxidizing conditions, and in the VERCORS HT tests, unexpected loss of rod geometry occurred for temperatures as low as ~2200 °C which could not be predicted by SA codes (in blind conditions). At the beginning of the project, the coupling between fuel dissolution, related clad failure and final rod collapse was not sufficiently understood for modeling improvements in SA codes.

### 4.3.1 Dissolution of irradiated fuel (UO<sub>2</sub> & MOX) by molten Zr (IRSN, ALIAS CZ)

#### Background and objectives

The existing severe accident codes contain fuel dissolution models that are based on results for fresh UO<sub>2</sub>. JRC/ITU showed in experiments performed within both CIT and COLOSS projects that irradiated fuel has a tendency to be dissolved by molten Zircaloy more and faster than fresh fuel. This difference for UO<sub>2</sub> is in the order of ~30 % at 2000 °C but may be higher at lower temperatures. Irradiated MOX seems to be dissolved slightly less than irradiated UO<sub>2</sub>. The objective of this activity was to propose a preliminary model of dissolution of irradiated UO<sub>2</sub> & MOX and to introduce it in the simplified dissolution model UZRL of ICARE/CATHARE (V3mod1.2 version of the ICARE2 core module). This analytical task was carried out by ALIAS CZ in close co-operation by IRSN (Ref.[46 ]).

#### Interpretation of experimental data

Data from altogether three specimens with irradiated UO<sub>2</sub> (53 GWd/tU) were available from CIT (1740 and 2000 °C) and similarly three specimens with irradiated MOX (46 GWd/t) were available from COLOSS (2000 °C). The mean U-content in the melt is the most reliable parameter that quantifies the fuel dissolution. The volume fraction of dissolved pellet is an alternative parameter but it is very difficult to make a reliable estimate from one cross section. This parameter is often overestimated and must be corrected to be conforming to the melt composition. As the melt analysis for the COLOSS-MOX specimens was not available before the end of the project, the U-content was roughly estimated by ITU from the proportion of different phases (metallic/ceramic) and their approximate composition as observed in previous tests. The available experimental database is, thus, very limited and with uncertainties to be reduced with additional post-test examinations to be performed after the project. Consequently, the modelling of the enhanced dissolution due to burn-up was chosen as simple as possible. This preliminary model remains to be consolidated based on few complementary tests covering different burn-up and involving more precise post-test analysis.

**Table 26:** T-shift table for irradiated UO<sub>2</sub> fuel.

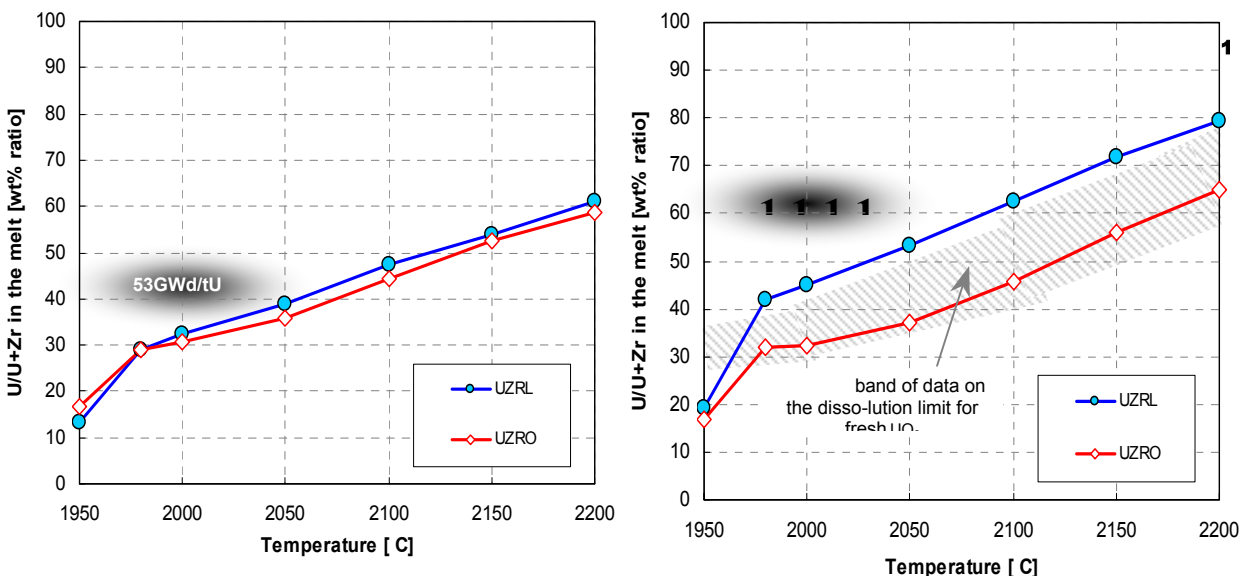
Temperature [°C]	Burn-up (GWd/tU)		
	0	10	90
1740	0	340	340
1800	0	280	280
1900	0	180	180
2000	0	90	90
2100	0	90	90
2200	0	90	90
2300	0	60	60
2400	0	30	30
2500	0	0	0

## Model description

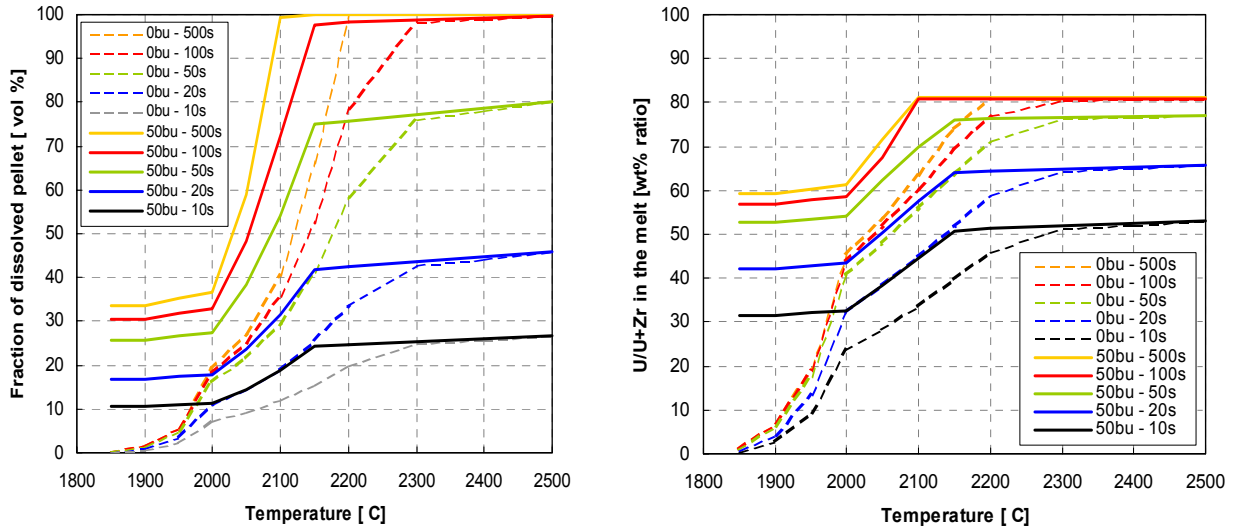
The UZRL model of ICARE2 (based on an empirical kinetics law) for fresh fuel was extended to take into account the enhance effect of the burn-up using a parametric approach. The faster kinetics for irradiated fuel were simulated by a higher “effective” temperature of interaction. The temperature shift (T-shift) between this effective temperature and the actual one depends on type of fuel, temperature, burn-up and is deduced from ITU dissolution tests with fresh and irradiated fuel. The T-shift is the largest near the melting point of Zircaloy but decreases with temperature up to zero at  $\sim 2500$  °C; see the T-shift table for irradiated  $\text{UO}_2$  in Table 26. The T-shift is assumed to increase with burn-up but not enough data is available to quantify this assumption. The dissolution between fresh MOX and fresh  $\text{UO}_2$  is assumed the same. Based on experimental results, the T-shift table for MOX was assumed  $\sim 50$  K smaller than for irradiated  $\text{UO}_2$ .

This simple approach enables higher dissolution kinetics as observed in the CIT and COLOSS tests with irradiated fuel. The more mechanistic dissolution model UZRO of ICARE2, which is based on the modelling of oxygen diffusion between the fuel and the cladding, was not modified.

This approach, which seems sufficient considering the limited experimental database available, does not increase the computational time of ICARE/CATHARE. Other parameters such as fuel porosity or fragmentation of irradiated fuel need not to be quantified before being considered in the model. The temperature shift is formulated in separate temperature-shift tables for each type of fuel and for selected temperatures and burn-up levels. Fast linear interpolation routine returns the temperature shift during core degradation calculations. These tables have to be fed by few additional experimental data.



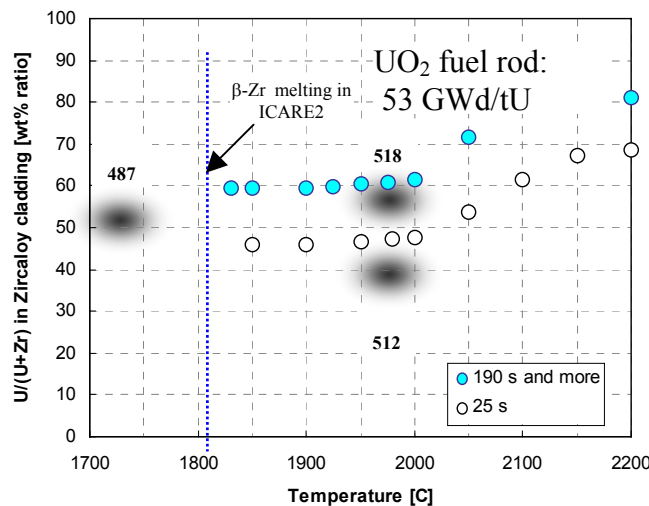
**Fig. 183:** Underestimation of the dissolution of irradiated fuel when using dissolution model derived from fresh fuel. Left: Fuel dissolution after 25s at 2000°C. Right: Fuel dissolution after 190s at 2000°C



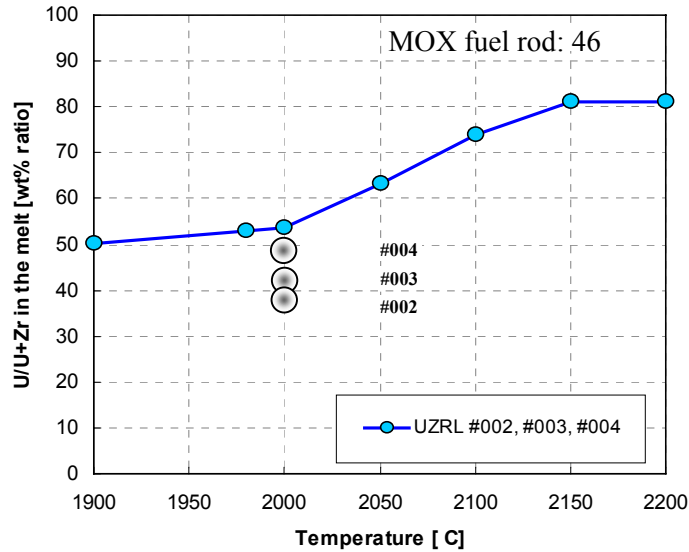
**Fig. 184:** Calculation by ICARE/CATHARE of the  $UO_2$  dissolution in a PWR fuel rod versus temperature and reaction time. Comparison between fresh fuel and irradiated fuel (50 GWd/tU). Left: Fraction of dissolved  $UO_2$  (vol %). Right: U/(U+Zr) in the melt (wt %)

Figure 183 shows calculations of the isothermal CIT dissolution tests with irradiated  $UO_2$  using the two initial dissolution models of ICARE2-V3mod1.2 (models without burn-up effect). The grey zones in plots a) and b) represent the CIT data for irradiated  $UO_2$  (53 GWd/tU). This comparison illustrates the underestimation of the irradiated fuel dissolution when using existing models validated on fresh fuel.

The difference between the predicted dissolution of fresh and irradiated fuel by the new UZRL of ICARE/CATHARE in a typical PWR fuel rod is shown in Figure 184. An important amount of irradiated fuel is now dissolved below 2000 °C even after short reaction times. The complete pellet dissolution in the molten Zircaloy cladding results in ~80 wt% U/U+Zr in the melt.



**Fig. 184:** Comparison of the upgraded UZRL model extended for irradiated  $UO_2$  with experiments of the CIT project.



**Fig. 186:** Comparison of the upgraded UZRL model for irradiated MOX fuel against the preliminary melt composition of COLOSS tests.

The prediction of the U-content in the melt in the three CIT specimens with irradiated  $UO_2$  and three COLOSS specimens with irradiated MOX is shown in Figures 185 and 178. The code-to-data agreement shows a correct enhancement factors due to the burn-up effect. For irradiated MOX the model is more conservative than for irradiated  $UO_2$ . Future post-test analysis of U-O-Zr mixtures planned by JRC/ITU are believed to shift the provisional estimation of the (U+Pu) contents in the melt to slightly higher values.

## Conclusions

- The UZRL model of ICARE2-V3mod1.2 was extended to irradiated  $UO_2$  and MOX. The upgraded UZRL reasonably predicts the fuel dissolution of the CIT and COLOSS specimens with irradiated fuel. The adopted empirical approach based on temperature-shift tables seems to be a suitable solution for SA codes considering the limited amount of data.
- Experimental results produced at the end of the COLOSS project need more precise post-test analysis in particular regarding the final melt composition.
- A limited amount of additional experiments with irradiated fuel is needed in order to complete the provisional T-shift tables. Data are especially needed for short reaction times (20 to 200 s) and temperatures  $<2000$  °C, 2100 and 2200 °C and for burn-ups in the range 32-62GWd/t.
- The preliminary model on the burn-up effect of fuel dissolution has to be confirmed and validated before being applied in plant calculations.

### 4.3.2 Simultaneous dissolution of $\text{UO}_2$ and $\text{ZrO}_2$ by molten $\text{Zr}$ (IBRAE)

On the base of the previously developed models within the CIT Project, based on separate dissolution of  $\text{UO}_2$  and  $\text{ZrO}_2$  by molten  $\text{Zr}$ , an upgraded model for simultaneous dissolution of these materials was developed at IBRAE for the mechanistic code SVECHA. The model considers interactions of solid materials with the convectively stirred melt during the two saturation and precipitation stages of interaction, and self-consistently describes either dissolution (erosion) or growth (corrosion) of  $\text{ZrO}_2$  layer during these interactions. The system of equations includes mass balances for three components (U, Zr, O) as well as flux matches (solid diffusion and melt convection) at two solid/melt interfaces.

This relatively simple approach was proposed, consistent with the level of modeling detail appropriate for the integral SA code, The model was thoroughly improved and validated against RIAR crucible dissolution tests (Ref.[48]) and demonstrated satisfactory agreement with the test measurements (Figs. 187 and 188).

The model predicts that the mass transfer mechanisms in the liquid phase is affected by the natural convection in the melt and, for this reason, the two problems of the  $\text{UO}_2$  and  $\text{ZrO}_2$  dissolution by the same melt cannot be described by the independent dissolution models. It is also anticipated that dissolution of  $\text{UO}_2$  fuel by the U-Zr-O melt is also strongly influenced by the temperature difference between heated fuel pellets and melt (Ref.[47]). This process was recently confirmed by the SETs on dissolution of  $\text{ZrO}_2$  by molten  $\text{Zr}$ . This was also the case in past experiments with  $\text{UO}_2$  crucibles where dissolution was no longer restricted by the melt saturation limit due to precipitation of ceramic phase in the oversaturated melt. Such behaviour is also possible in the bundle tests during the early fuel liquefaction for which a relatively quick transformation of the  $\text{UO}_2$  phase into the mixed (U,Zr) $\text{O}_2$  ceramic phase can be predicted.

The validation work based on RIAR tests showed that the temperature difference in the RIAR crucible wall, initially suspected to be large, was in fact small. The melt temperature measured by the pyrometer in the 1<sup>st</sup> set of tests was found to be unreliable while temperatures measured by thermocouple were found correct. Finally the first series of test was recalculated using TC readings and showed satisfactory agreement with measured dissolution kinetics (Figs. 189 and 190).

This model was implemented in the single-rod version of the SVECHA/QUENCH (S/Q) code and validated against AEKI short fuel rod dissolution tests (Ref.[48]).

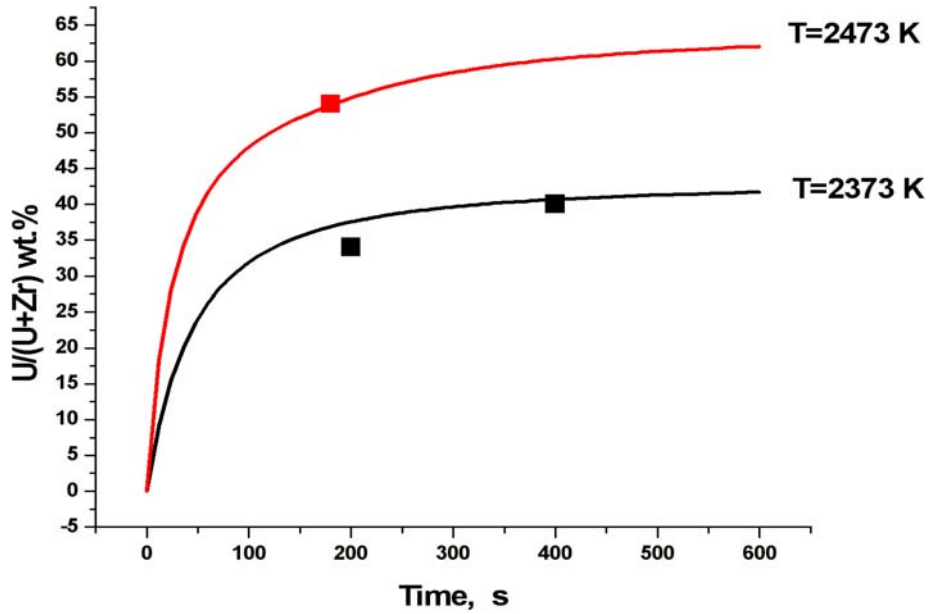


**Fig. 187:** Comparison of calculated and measured uranium weight content in the melt in the 2<sup>nd</sup> series of RIAR tests performed at 2100 and 2200°C.

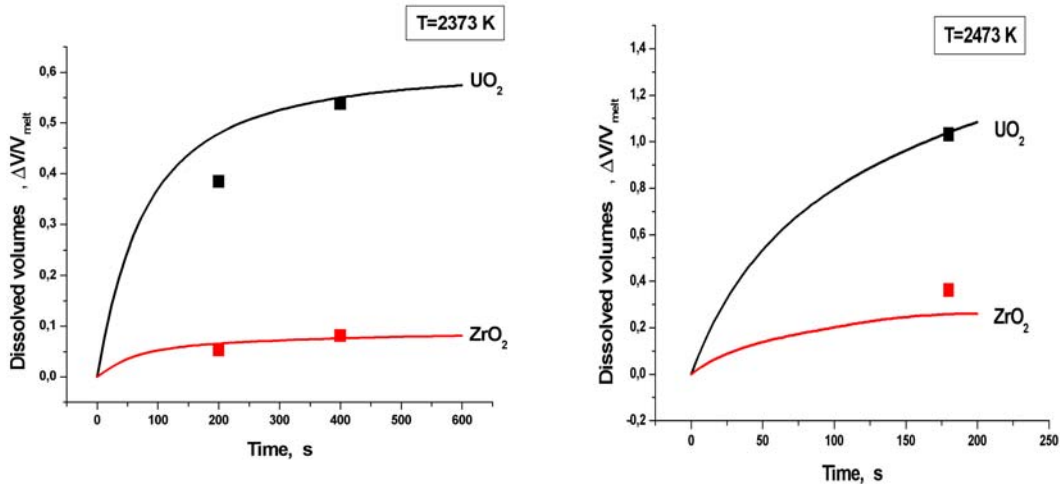


**Fig. 188:** Comparison of calculated and measured dissolved volumes of UO<sub>2</sub> and ZrO<sub>2</sub> in the melt

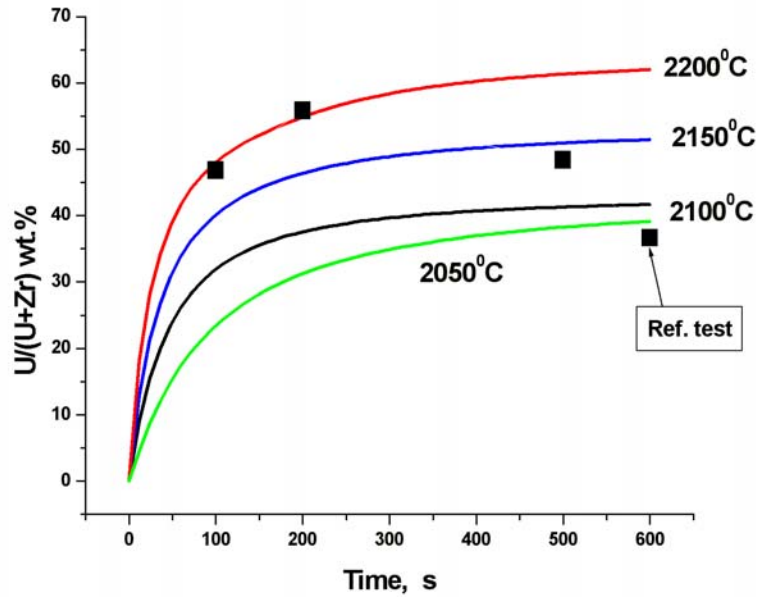


**Fig. 189:** Comparison of calculated and measured uranium weight content in the melt in the 1<sup>st</sup> series of RIAR tests performed at 2150 and 2200°C

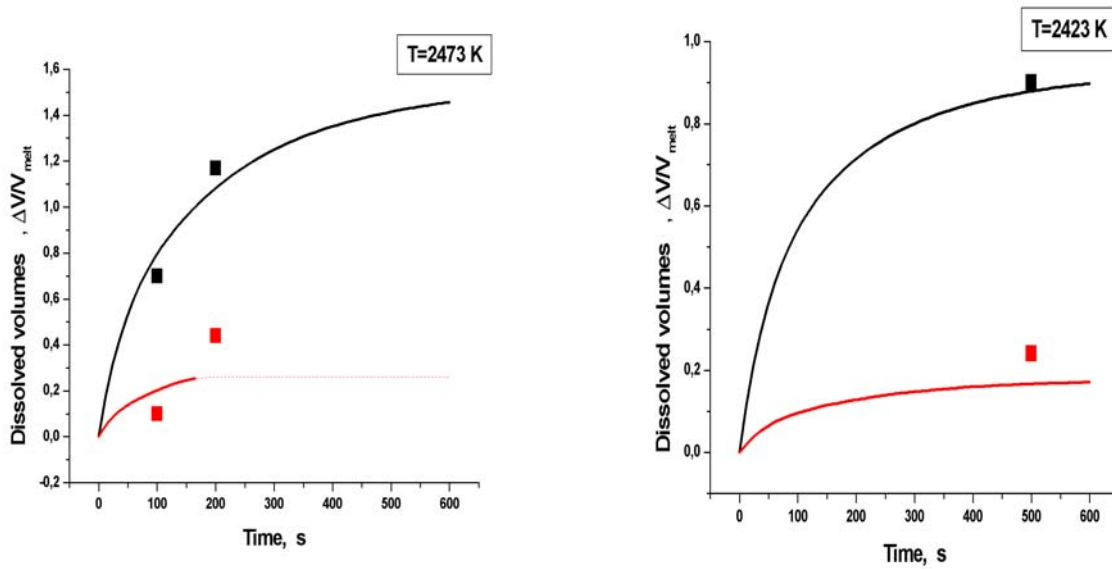


**Fig. 190:** Comparison of calculated and measured dissolved volumes of  $\text{UO}_2$  and  $\text{ZrO}_2$  in the melt

#### 4.4 Main improvements of SA codes in the project

The different modelling developments and improvements presented in this final extended Part 1 report could not be all implemented in SA codes due to the too short period available for modelling work between the completion of experimental tasks and the final plant calculations (WP8). Nevertheless, some new models and modelling improvements could be implemented in SA codes. This feedback could not be done easily in non-European codes such as SCDAP/R5 and MELCOR due to the lack of development possibilities.

In spite of these limitations, significant feedback could be done on SA codes having European developments teams. This section summarizes the modelling developments carried out directly in the WP7 - or outside based on data from the project - that could be implemented in SA code used in the project. Table 27 summarises this effort.

**Table 27:** Feedback of modelling activities on SA codes.

<b>Model developments or improvements developed in COLOSS (WP7)</b>	<b>Feedback from the modelling activity in SA codes</b>	<b>Comments</b>
Zr kinetics from Prater and Leistikov (recommended in the project)	SCDAP/R5, MELCOR	Still existing in other codes
B <sub>4</sub> C-CR degradation/oxidation	ASTEC, ICARE/CATHARE, MAAP4, ATHLET-CD, FZK-SM(*)	Already existing B <sub>4</sub> C models in MELCOR could not be improved
Oxidation of solid U-O-Zr mixtures	ICARE/CATHARE (**)	Missing or inadequate models in other codes
Oxidation of liquid mixture	SVECHA, ICARE/CATHARE (similar kinetics in the two codes)	Missing or inadequate models in other codes
Dissolution of UO <sub>2</sub> and ZrO <sub>2</sub> by molten Zr	SVECHA, ICARE/CATHARE, ASTEC	Dissolution of ZrO <sub>2</sub> only considered by ICARE/C.
Burn-up effect on dissolution	ICARE/CATHARE (**)	Missing models in other codes

(\*): Stand-Alone model, (\*\*): Preliminary model

- ICARE/CATHARE developers could achieve modelling improvements based on COLOSS results. This involved **B<sub>4</sub>C oxidation** considering the steam partial pressure effect, oxidation of relocated U-O-Zr mixtures (quasi-linear **U-O-Zr oxidation kinetics** under 1400 °C), **burn-up effect** on fuel rod dissolution and melt relocation. The improved version V1 mod1.3p ("p" as preliminary) was delivered by IRSN in October 2002 to the COLOSS partners in charge of reactor applications with ICARE/CATHARE (Ref.[49]). The 2<sup>nd</sup> set of plant calculations on TMI-2 transient and both LOCA and SBO sequences on a VVER-1000 were carried out successfully with this version. Simultaneously, IRSN has also developed the so-called "**MAGMA oxidation model**" based on the modelling work of IBRAE related with the oxidation of molten U-O-Zr mixtures. Finally, the **dissolution modelling improvement** carried out recently by IBRAE on the simultaneous dissolution of UO<sub>2</sub> and ZrO<sub>2</sub> by molten Zr is also planned to be included in ICARE/CATHARE as an alternative to the current model. The

V1mod1.3p version of ICARE/CATHARE issued to the project did not involve the MAGMA oxidation model.

- ASTEC V1 developers could issue mid-2002 a preliminary version of the new ASTEC V1 code to the partners in order to run the 2<sup>nd</sup> set of plant calculations (TMI-2 transient and PWR-1300 “H<sub>2</sub> sequence”). The code was already delivered with the improved B<sub>4</sub>C model of ICARE/CATHARE. A preliminary version of ASTEC V1 involving the IRSN B<sub>4</sub>C model modeling was issued to the PAG users in October 2002.
- MAAP4 was improved by EDF regarding the development and implementation of a new B<sub>4</sub>C control rod model which includes the production of H<sub>2</sub>, CO, CO<sub>2</sub> and CH<sub>4</sub> based on thermochemistry calculations carried out with the GEMINI/COACH gas thermodynamic system. The B<sub>4</sub>C oxidation kinetics proposed by FZK and IRSN have also been introduced. A similar model was also developed by Framatome-ANP SAS. Nevertheless this model was more limited regarding degradation and will be replaced by the EDF model.
- ATHLET-CD was also upgraded with a new B<sub>4</sub>C control rod model developed taking into account the new experimental database produced in the project. This model takes into account similar assumptions as the ICARE2 model.
- SCDAP/RELAP5 was also considered by FZK with respect to the development of a B<sub>4</sub>C oxidation model. Nevertheless, the lack of support from the USNRC hindered an effective work, and the necessary code extensions became laborious. Therefore a final boron carbide oxidation model, applicable for plant applications, was not working at the end of COLOSS in spite of the development of a FZK stand-alone model.
- MELCOR improvements were not possible by PSI and by Framatome-ANP GmbH having no code development teams. Nevertheless identified weaknesses and lacks, in particular regarding the B<sub>4</sub>C model, were transmitted to code developers at SNL.

In addition to this modelling effort, recommendations were specified regarding the choice of the following modelling options: a) the clad oxidation correlations based on a physically grounded examination of the existing database (Ref.[50]), b) the clad failure criteria (Ref.[1]) and c) the fuel rod collapse criteria based on the PHEBUS test analysis. Before clad failure, the H<sub>2</sub> production rate is mainly due to the oxidation of standing cladding. The main uncertainty comes from oxidation at high temperature (T > 1900 K). No conclusions could be drawn on the use of the Prater correlation above 1900K but additional investigations have been launched, out of the project, to finalize this issue Ref.[51, 52, 53] taking also into account at high temperature steam supply limitation and the impact of the total consumption of the β-Zr layer in the final stage of oxidation.

The modified versions of SA codes with model developments and improvements carried out in the project, have to be considered as preliminary due to the lack of time within COLOSS for sufficient checking and validation. Consolidation of these models is needed with the accompanying validation activity before application for safety studies.

In some cases, the effect of model improvements on SA codes has been illustrated by benchmarking between plant calculations using original and improved versions run respectively at the beginning and at the end of the project (see Part 2 of the final extended report, Ref. [1]). Of

course results are indicative of a first trend but this must be confirmed when models will be consolidated and validated.

## 5 Summary of the WP8 devoted to plant calculations of SA sequences

The large work-package WP8 was devoted to the applications of results to the calculation of selected SA sequences characterized by large core degradation. This activity has been reported in the “Part 2 of the final report” (B. Adroguer, 2003, <sup>54</sup>).

Eleven partners of the project were involved in this activity and formed the Plant Analysis Group (PAG) led by IRSN and Framatome-ANP SAS. The specific objectives were:

- to assess the ability of SA codes to calculate the core degradation and the related gas production, in particular those resulting from the degradation of B<sub>4</sub>C CR's,
- to identify improvement needs and give recommendations for future code developments,
- to evaluate implications of new results.

Main European plants involving B<sub>4</sub>C material were investigated, focussing on the impact of B<sub>4</sub>C on selected SA sequences. IRSN, EDF and ENEA were also involved in the calculation of the TMI-2 accident. Mainly the core and, to a lesser extent, the primary circuit were considered in these calculations.

Key SA codes such as the integral codes ASTEC, MAAP4 and MELCOR and the detailed codes ICARE/CATHARE and SCDAP/RELAP5 were used.

The work plan involved three stages:

1/ At the beginning of the project, a 1<sup>st</sup> set of calculations was performed for key SA sequences selected on various plant designs (Table 28). At this stage, the input decks were harmonised in order to facilitate code assessment and comparisons between calculations run with different codes.

2/ Afterwards, codes were upgraded and partially validated using experimental results of the bundle tests QUENCH-07, -09 and CODEX-B<sub>4</sub>C.project.

3/ At the end of the project, improved codes were run again to provide a 2<sup>nd</sup> set of calculations and assess the effect of new models and improvements compared with the 1<sup>st</sup> calculations.

**Table 28:** Plant calculation activity in COLOSS.

Plant designs	SA codes	Partners	SA sequences
PWR 1300	ASTEC-MAAP4	IRSN/EDF	“H2 sequence” (*)
PWR 900	ASTEC	IRSN	Same “H2 sequence”
BWR	MELCOR	PSI	Station Blackout (SBO)
VVER-1000	ICARE/CATHARE	KI/LTKK	Large break / SBO
EPR	MAAP4-MELCOR-SCDAP/R5	Fra-SAS/GmbH/FZK	SBO
TMI-2	ASTEC-SCDAP/R5- ICARE/CATHARE-MAAP4	IRSN/ENEA/ENEA/EDF	

(\*) Total loss of feedwater to the steam generator without safety injections.

Table 28 describes the SA calculations carried out during the project. For the 1<sup>st</sup> set of calculations run during the 1<sup>st</sup> year, code versions used were not able to take into account B<sub>4</sub>C

effects except MELCOR which had a parametric B<sub>4</sub>C model for BWRs. The 1<sup>st</sup> set of calculations produced useful results on code capabilities. Recommendations have been made on model improvements and associated experimental needs to help reduce code uncertainties in B<sub>4</sub>C and fuel rod dissolution modelling. Sensitivity studies on some user parameters known to affect the core degradation such as the Zr and B<sub>4</sub>C oxidation laws, ZrO<sub>2</sub> clad failure, fuel rod collapse criteria and some B<sub>4</sub>C modelling parameters were recommended for the final plant calculations (Ref.[55]). Benchmarks between calculations of SA sequences carried out in EVITA (Ref. [60]) and COLOSS projects were organised.

The 2<sup>nd</sup> set of plant calculations was performed with upgraded codes. The main improvements deal with boron carbide oxidation, Zircaloy oxidation kinetics, a first attempt to deal with the burn-up effect on fuel dissolution, an improved solubility limit of UO<sub>2</sub> in melts and oxidation of U-O-Zr mixtures as well as other improvements of core degradation and corium relocation modules. Accompanying sensitivity studies and code-to-code benchmarks enabled a general assessment of codes to calculate core degradation, more particularly core oxidation and H<sub>2</sub> production (both the rate and the total production), B<sub>4</sub>C effects, and corium formation resulting from fuel dissolution and burn-up effects. Based on these calculations, needs for short-term developments were also identified as well as implications of new results for safety.

### **5.1 Assessment of SA codes on H<sub>2</sub> production, B<sub>4</sub>C effects and corium formation**

Plant calculations, code-benchmarks and sensitivity studies on key parameters of the core degradation enabled the identification of abilities and deficiencies of codes and needs for improvements.

*H<sub>2</sub> production:* Sensitivity studies on early degradation models showed more significant effects on *H<sub>2</sub> rate* during early core heat-up or during quenching than on *total* production found to be in the 20-35% range depending on the SA sequence. The H<sub>2</sub> rate can be affected in particular by the user choice of the ZrO<sub>2</sub> clad rupture criteria and is certainly underestimated during melt relocation due to missing or incorrect melt oxidation models.

*Oxidation of mixtures:* This is a key weakness of SA codes resulting in the underestimation of the H<sub>2</sub> production during the early melt progression and, more important, during the quenching of a degraded core. In general, modelling is either missing or inadequate while experiments on oxidation of solid U-O-Zr and B<sub>4</sub>C-rich mixtures showed larger kinetics than for pure materials. A correct modelling of the oxidation of mixtures requires not only a specific mixture oxidation kinetic but also a 2D corium progression and thermal-hydraulic description in the core to take into account reasonably the corium-coolant surface interaction and the steam supply. These bi-dimensional aspects were missing in SA code versions available in the project.

*B<sub>4</sub>C oxidation:* Effects on core degradation were calculated as limited, nevertheless the B<sub>4</sub>C-induced degradation modelling is in general limited in present SA codes. Regarding gases produced, H<sub>2</sub> induced by B<sub>4</sub>C oxidation was often less than 10% of total H<sub>2</sub> and very little CH<sub>4</sub> was produced. More important for FP chemistry in the primary circuit are the CO, CO<sub>2</sub> and B-compounds productions. The rapid oxidation of B<sub>4</sub>C-melts is not yet modelled in spite of the large impact suspected on H<sub>2</sub> production during core quenching. In general, SA codes do not calculate the *gas chemistry* in the core (except MELCOR) and, more important, in the primary circuit (except ASTEC V1) where the FP chemistry, in particular iodine and cesium speciation, can be affected by B<sub>4</sub>C-gas production as indicated by exploratory ASTEC calculations.

*UO<sub>2</sub> dissolution by molten Zr and burn-up effect:* Large uncertainties on the corium formation were evidenced by large differences observed between SA codes on the modelling of fresh fuel dissolution. Main modelling differences concern the solubility limit of fuel in Zr-rich mixtures and the ZrO<sub>2</sub> clad failure criteria which limit the rod dissolution and drive the onset of U-O-Zr melt relocation. In addition, the burn-up effect known to enhance significantly UO<sub>2</sub> and MOX liquefaction and suspected to favour early rod collapse was not modelled in the majority of SA codes. When existing, such as in ICARE/CATHARE, the burn-up effect model is preliminary and needs consolidation for plant applications.

*Loss of rod geometry:* The user-effect linked with the **choice of the ZrO<sub>2</sub> clad failure** conditions was found to be core-condition dependent and also code-modelling dependent. Main effects were found on hydrogen release rate during core heat-up as well as on fuel dissolution and early corium composition. The **choice of a fuel rod collapse criterion** was also found to be an overwhelming parameter for the corium progression. Fuel rod collapse conditions, suspected to be dependent on core conditions and fuel burn-up, need to be more clearly identified to reduce large uncertainties induced on the further corium progression.

*Corium behaviour:* Large discrepancies were found between calculations on the prediction of the amount of corium produced, on its composition and on the distribution between core, core by-pass and lower head. The corium behaviour is affected by many degradation models. Nevertheless it was found to be more dependent on the late melt progression modelling than on that of the early degradation. One exception is the *fuel rod collapse criterion*, which controls the early formation of large quantities of corium and affects significantly the late corium behaviour, in particular the metal-oxide composition.

## **5.2 Needs for short-term code improvements**

Short-term code improvements were recommended in the continuation of the modelling effort carried out in the project in order to take full account of findings from experimental programmes of the project and from the ongoing QUENCH, PHEBUS and ISTC programmes. Main short-term needs on modelling improvements concern:

- B<sub>4</sub>C oxidation considering “all main gases” and B-compounds resulting from the B<sub>4</sub>C oxidation, the oxidation of “B<sub>4</sub>C-rich mixtures” and the implementation of a gas chemistry modelling in and beyond the core for the calculation of the gas and FP chemistry,
- fuel rod dissolution, including the burn-up effect taking into account results produced in the CIT and COLOSS projects and complementary ones expected in the ISTC project 1648 and in the SARNET network (6<sup>th</sup> FP),
- ZrO<sub>2</sub> clad failure criteria and fuel rod collapse conditions considering a wider set of loss of core geometry conditions,
- oxidation of solid and molten U-O-Zr mixtures taking into account results produced in the project and improved coupling between 2D thermal-hydraulic and melt progression behaviours,
- adaptation of the mixture oxidation models and validation on conditions representative of core reflooding.

### 5.3 Safety implications of results

The  $H_2$  rate during early core heat-up or during quenching is at least as important as the total  $H_2$  production regarding the explosion risk and the efficiency of  $H_2$  mitigation measures in the containment. This rate could be underestimated due to code weaknesses on the oxidation of mixtures. Indeed, experiments on oxidation of U-O-Zr and metallic  $B_4C$ -rich mixtures showed faster kinetics than for Zr and  $B_4C$  and indicate that mixtures can be a key source of  $H_2$ , in particular during core reflooding.

The main risk with  $B_4C$  oxidation comes from the production of CO and  $CO_2$  gases that can be converted into  $CH_4$  in the cooler zones of the primary circuit during  $H_2$ -rich phases. The formation of  $CH_3I$  has been predicted in demonstrative plant calculation, nevertheless the amount seems low compared to the production of  $CH_3I$  by heterogeneous reactions in the containment building itself. Significant effects of B-compounds were also found on Cs chemistry. The additional  $H_2$  production from  $B_4C$  oxidation is limited to about 10% of the total  $H_2$  production during core degradation (not taking into account oxidation of  $B_4C$ -rich metallic mixtures) but has to be taken into account correctly being produced during the largest  $H_2$  production phase during the largest  $H_2$  production phase resulting from the early core oxidation escalation.

*In-vessel corium behaviour* is affected by large uncertainties in the timing and amount of corium formation and in its oxidation which drive the metallic-oxidic composition and the final corium distribution between the core, the core by-pass and the lower head. Corium oxidation is a key factor affecting the late  $H_2$  release, the corium metal-oxide composition in the lower-head and the final vessel failure mode in case of unavailability of water safety injection.

## 6 European added value and dissemination of the results

The COLOSS project has attracted a great deal of interest because it concentrates on key safety related topics of particular interest for accident management and mitigations such as a) hydrogen generation not only during heat-up but also during cool-down and quenching, b) effects of  $B_4C$  on core degradation and on gas production focusing on the possible impact on the source term in the primary circuit and c) on the corium formation and progression in the core. The three topics have been investigated with the aim of applications in SA codes.

Progress meetings held twice a year together with the progress meetings of the ENTHALPY project (Ref.[56]) and linked with some QUENCH workshops (Ref.[57]) and PHEBUS meetings (Ref.[58]) provided a forum where the results could be widely discussed. In particular,  $B_4C$  results of particular interest for the preparation of the future PHEBUS FPT3 test and for the preparation and interpretation of QUENCH-07 and QUENCH-9 tests were commonly analysed (Ref.[23]).

Through various topical meetings and exchanges between EC projects, the project provided the opportunity to disseminate acquired knowledge and experience on core degradation under severe accident conditions among the European Nuclear Energy Community.

- Close exchanges between the PAG members of the COLOSS project and the EVITA partners involved in SA plant calculations contributed to reinforce the European dimension of the ASTEC code (Ref.[59]) commonly developed by GRS and IRSN. The code-benchmarking activity launched in the COLOSS project has been extended to the EVITA project (Ref.[60]) providing positive feedbacks on the ASTEC code. In this context, code users involved in the design, in the mitigation measures or in the emergency plans have gained important information about the uncertainties that exist when applying their tools for SA situations.

- Dissemination of knowledge acquired from experimental programmes was supported through various topical meetings and also through the distribution to the COLOSS and EVITA partners of improved ICARE/CATHARE and ASTEC codes.

- SA code weaknesses identified on safety relevant phenomena have been transmitted to the thematic network EURSAFE (Ref.[61], Ref.[62]) devoted to a PIRT focused on safety ranking priorities on SA phenomena. Links existed also with the thematic networks THENPHEBISP devoted on the ISP 46 based on the PHEBUS FPT1 test (Ref.[63], Ref.[64]). In particular, a final meeting was made between THENPHEBISP, COLOSS, EVITA and ENTHALPY projects where a synthesis was done on main outcomes and conclusions on core degradation, corium aspects and related SA code capabilities (Ref.[65]).

- The project was also the opportunity to build specific links with EC-ISTC projects devoted to corium behavior. Common meetings were held to discuss and define complementary R&D efforts, avoiding duplication and reinforcing complementarities between EURATOM and EC-ISTC projects. This cooperation enabled the definition of two well-shaped projects on core degradation which were accepted by ISTC.

The contribution of the COLOSS project to the networking of the European nuclear safety research will be continued in the 6<sup>th</sup> FP within the SARNET network of excellence (Ref.[66]).

## **7 Main achievements**

### **7.1 Fulfilling the terms of the contract**

The work performed in the project followed the specification laid out in the contract and in the amendment of the project accepted just after the Mid-Term Assessment meeting (Ref.[6]). The terms of the amended contract were fulfilled.

All experimental programmes, except melting point tests on U-O-Zr mixtures, all analytical and modelling tasks and all plant calculations were done. The missing experiments on the liquidus temperature of mixtures will be carried out by ITU in the framework of SARNET using an improved test rig. In this context, additional tests on irradiated UO<sub>2</sub> dissolution (medium burn-up) will also be carried out in order to compare better the dissolution of irradiated UO<sub>2</sub> and MOX fuel.

The new experimental database produced by the project, involving separate-effect tests and three large-scale tests, enabled significant extensions to current knowledge and led to improved models that are directly applicable to SA codes.

The success of the project was based on the availability of several test rigs, on the construction of new ones and on tight links between experimental teams and analysts:

- Five test rigs have been constructed and improved for performing various experimental tasks of COLOSS. They are available for future efforts at IRSN, FZK, UJP, AEKI and ITU on material interactions studies, the latter enabling experiments using irradiated material.

- Strong co-operative links between experimental and modelling works have been very fruitful in producing qualified data and consistent models. This co-operation must be recommended in future R&D activities of the EC.

A strong contribution to the diffusion of knowledge in EU including two NAS was achieved thanks to a large series of 80 technical documents: Contractual documents (Contract technical annex, Contract Amendment, semi annual reports, yearly reports, final reports), technical deliverables and journal papers. Intermediate results and discussions were reported in 16 Minutes of progress and topical meetings. All documents are given in Appendix 1.

## **7.2 Main achievements and perspectives**

### **Production of a very fruitful experimental database on B<sub>4</sub>C effects, fuel dissolution and oxidation of mixtures:**

- Main B<sub>4</sub>C oxidation issues have been covered thanks to several SETs carried out in different conditions with B<sub>4</sub>C material representative of different plant designs. The large database produced showed that in addition to the temperature dependence, the B<sub>4</sub>C oxidation kinetics is also dependent on material properties and even more on thermal-hydraulic conditions such as steam partial pressure and flow rate which control the mass transfer of the oxidizing phase. Production of gases such as H<sub>2</sub>, CO, CO<sub>2</sub>, very low CH<sub>4</sub> and very large amounts of aerosol were measured under severe accident conditions.

- Small scale B<sub>4</sub>C control rod tests enabled the identification of main degradation processes such as B<sub>4</sub>C/steel and Zr/steel eutectic interactions, crucible effect of the external ZrO<sub>2</sub> layer of the guide tube, failure conditions and final oxidation of the remaining B<sub>4</sub>C fragments (undissolved part of the B<sub>4</sub>C pellets) and metallic B<sub>4</sub>C-rich mixtures. Complementary tests with longer B<sub>4</sub>C-CR are needed for modeling improvement and validation purposes.

- Preliminary data obtained on the oxidation of B<sub>4</sub>C-rich metallic mixtures representative of the early degradation of B<sub>4</sub>C-control rods showed much more rapid kinetics than the oxidation of pure B<sub>4</sub>C materials. This kind of mixture is also suspected to enhance the H<sub>2</sub> peak production generated during quenching of degraded cores that are characterized by relocated B<sub>4</sub>C-rich mixtures. Again complementary tests are needed for modeling purposes.

- Three key large-scale bundle experiments characterized by a central B<sub>4</sub>C control rod have been carried out in the QUENCH and CODEX facilities with bundles representative of PWR (2 tests) and VVER designs respectively. The B<sub>4</sub>C was found to be a contributor to the core degradation nevertheless its contribution could not be quantified. No significant differences could be observed between PWR and VVER designs. For the first time, the gas production from B<sub>4</sub>C oxidation was measured. Significant quantities of CO, CO<sub>2</sub> and B-compounds (as large aerosol source) were produced during the degradation of the bundles while CH<sub>4</sub> release was very low. The behaviour of gases resulting from the B<sub>4</sub>C control rod degradation and oxidation was found to be closely dependent on the oxidizing conditions in the bundle. This B<sub>4</sub>C database represents very valuable results for code validation and for the future PHEBUS FPT3 test that also has a central B<sub>4</sub>C control rod in the bundle.

- Experimental data from the oxidation of U-O-Zr solid and molten mixtures showed faster kinetics than for pure Zr. These data confirm that Zr-rich metallic mixtures can be a significant source of rapid H<sub>2</sub> production during core degradation and, mainly, during core reflooding. This is a key insight for modeling. The oxidation of mixtures being in general absent or inadequate in

SA codes, this could explain why the H<sub>2</sub>-peak production observed during core reflooding is usually significantly underestimated by current SA codes.

- New results were produced on simultaneous dissolution of UO<sub>2</sub> and ZrO<sub>2</sub> by molten Zr. This interaction was investigated in a crucible geometry and in the fuel rod configuration where the molten Zr is trapped between fuel pellets and the external ZrO<sub>2</sub> layer of the cladding. These data enabled progress in the understanding of the mechanisms of this double interaction responsible for the early fuel liquefaction and failure of the external ZrO<sub>2</sub> layer of the cladding.

- Using a new test rig constructed in a hot cell, tests on dissolution of high burn-up UO<sub>2</sub> (65 and 90 GWd/tU) and MOX fuel (~45 GWd/tU) could be carried out for the first time. Compared with fresh fuel, enhanced kinetics and greater apparent dissolution and fuel decohesion were observed for UO<sub>2</sub> and MOX due to fuel cracking and fission gas and volatiles bubbling in the liquefied fuel. Whether UO<sub>2</sub> or MOX fuel of similar burn-up dissolves faster could not be concluded from these experiments, since the burn-ups of the two fuels were too different. These preliminary results require additional experiments covering a wider range of experimental conditions, in particular medium burn-up UO<sub>2</sub> fuel, and carried out with improved post-test examinations to confirm the findings.

### **Modelling and transfer of knowledge in SA codes:**

- Each experimental task was accompanied by a significant analytical activity enabling the production of models on B<sub>4</sub>C oxidation, fuel dissolution and oxidation of solid and molten mixtures.

- Models produced were implemented in SA codes by the project partners developing the ASTEC, ATHLET-CD, ICARE/CATHARE and SVECHA codes. This activity ensured the transfer of knowledge from experimental programmes to SA codes used for safety studies. The improved versions of SA codes could be used to carry out the final set of plant calculations.

- Models developed on B<sub>4</sub>C, fuel dissolution and oxidation of mixture were applied in the calculation of the global tests QUENCH-07, QUENCH-09 and CODEX-B<sub>4</sub>C for validation purposes. Modelling improvements and related validation were planned to continue after the project to take full account of experimental results produced near the end of the project.

- Preliminary versions of SA codes need to be consolidated and validated with complementary experimental results on B<sub>4</sub>C, fuel dissolution and oxidation of mixture expected in the short-term from ongoing PHEBUS FP, QUENCH and EC-ISTC projects on core degradation.

- Large user-effects were found in various calculations regarding the choice of oxidation kinetics law and that of fuel rod degradation criteria (ZrO<sub>2</sub> clad failure and fuel rod collapse). Based on an in-depth analysis of existing data, recommendations were given by FZK for the oxidation laws and by IRSN for the degradation criteria on the choice of these user-specified models in SA codes. The latter were based on PHEBUS PF results. For the Zr oxidation, the use of Leistikow (or Cathcart) correlation at low temperature (T <1800 K) and Prater-Courtright correlation at high temperature (T >1900 K) were recommended in the calculations of the project. More investigations were needed to conclude on the best Zry oxidation correlations, in particular there is a need at high temperature of modeling improvements regarding the steam supply

limitation before recommending Zr oxidation correlations for plant calculations. Additional studies were launched out of the project to clarify and improve the Zry oxidation modeling in SA codes.

### **Application of results to plant calculations of selected SA sequences:**

- Two large series of eleven severe accident sequences involving different plant designs such as PWR-900, PWR-1300, EPR, BWR and VVER and the TMI-2 accident were calculated using three integral codes ASTEC, MELCOR and MAAP4 and two mechanistic codes ICARE/CATHARE and SCDAP/RELAP5. The final calculations were run with improved codes and knowledge acquired during the project.

- Each series of plant calculations was enriched by sensitivity studies on key parameters of the core degradation (in particular Zr and B<sub>4</sub>C oxidation laws, B<sub>4</sub>C-CR and UO<sub>2</sub> rod degradation criteria) and by code-to-code benchmark exercises. This effort enabled a) the assessment of codes to calculate core degradation with the identification of main uncertainties and needs for short-term improvements and b) the identification of safety implications of new results.

- Three “Risk Relevant Parameters and Ranking Tables” have been compiled from plant calculations to identify relevant parameters affecting the modelling of H<sub>2</sub> production, B<sub>4</sub>C effects and corium behaviour. These tables include a ranking of each parameter relative to safety risks: H<sub>2</sub> explosion in the containment, impact of B<sub>4</sub>C on the source term and corium behaviour and in-vessel corium retention. These tables provide also valuable indications for future R&D efforts.

- The project enabled sufficient technical exchanges between different partners involved in plant calculations to organize a code-to-code comparison exercise for plant calculations carried out in the project. Code benchmarks were recognized as a useful exercise for code validation. Valuable results on respective code capabilities and uncertainties were obtained. Recommendations to optimise future benchmarks could be given regarding the harmonization of input decks, the choice of SA scenario and the need to limit user-effects.

- Key points arriving from plant calculations were:

*H<sub>2</sub> production:* Sensitivity studies on early degradation models showed more significant effects on *H<sub>2</sub> rate* during early core heat-up or during quenching than on *total H<sub>2</sub> production*. The scattering of code predictions on the total H<sub>2</sub> release was found to be in the range of 20-35%.

*ZrO<sub>2</sub> clad failure:* The assessment of codes on the ZrO<sub>2</sub> clad failure criteria evidenced large uncertainties, the effect being dependent on core conditions and also dependent on code modelling. The uncertainties would affect significantly the hydrogen release rate during core heat-up as well as the corium formation via the fuel dissolution by Zircaloy and its composition.

*Fuel rod collapse:* The fuel rod collapse criteria are clearly characterised by large uncertainties. Significant effects were found in plant applications on the mass of corium that is formed. It was recommended that sensitivity studies have to be performed on these criteria for plant applications.

*Oxidation of mixtures:* This is a key weakness of SA codes. Related models are either missing or inadequate. Consequently, the H<sub>2</sub> generated during melt relocation or during quenching is certainly underestimated due to the poor melt oxidation models. A better treatment of this oxidation could reduce the uncertainty on the H<sub>2</sub> production. Convincing results could be obtained in a demonstrative calculation using a melt oxidation model coupled with a 2D corium

relocation model and a 2D thermal-hydraulic behaviour to take account of correct steam supply. The provisional models need to be consolidated with supplementary data.

*B<sub>4</sub>C oxidation:* Effects on core degradation were calculated as limited although experimental observations suggest more important effects. H<sub>2</sub> from B<sub>4</sub>C was often found to be less than 10% of the total H<sub>2</sub> production. Very little CH<sub>4</sub> was directly produced. More important for FP chemistry in the primary circuit are the CO, CO<sub>2</sub> and B-compounds produced. It was found that CO and CO<sub>2</sub> can be converted into CH<sub>4</sub> in the cooler zones of the primary circuit during H<sub>2</sub>-rich phases. Then, non-negligible quantities of volatile CH<sub>3</sub>I, a key factor of radiological risk, could be formed. Large effects of B-compounds on the Cs chemistry were also found.

*UO<sub>2</sub> dissolution:* Substantial uncertainties were evidenced by large differences between models and results on UO<sub>2</sub> liquefaction. The *burn-up effect* known to enhance significantly UO<sub>2</sub> liquefaction and suspected to favour early rod collapse and FP release has to be modelled in SA codes. Again the provisional model needs to be consolidated using complementary data.

*Corium behaviour:* Large discrepancies were found between comparable calculations in the amount and timing of corium formation, in its composition and in the distribution between core, core by-pass and lower head. MAAP4, SCDAP/RELAP5 and ICARE/CATHARE were found to largely underestimate the mass of corium that was formed in TMI-2. Corium behaviour was found to be more dependent on the late melt progression modelling than on that of the early degradation. One exception is the *fuel rod collapse criterion*, which causes an early and large corium formation and significantly affects late corium behaviour, in particular the metal oxide corium composition which affects the corium stratification in the lower-head and finally the in-vessel corium retention.

### **Perspectives:**

Remaining uncertainties and SA code weaknesses in safety-relevant phenomena of core degradation have been transmitted to the PIRT review on SA carried out in the EURSAFE thematic network (5<sup>th</sup> FP) to be addressed in the SARNET network of excellence (6<sup>th</sup> FP). In particular results on dissolution of irradiated fuel and oxidation of metal-rich mixtures during core degradation and reflooding should be consolidated. The follow-up of the COLOSS activity on plant calculations with sensitivity studies and benchmarking exercises has also been recommended, the priority being put in SARNET on the European ASTEC code

## **Acknowledgements**

The partners of the COLOSS project warmly thank EC DGXII for their financial support under the 5<sup>th</sup> Framework programme on Nuclear Fission Safety, contract number FIKS-CT-1999-00002, and, in particular Dr Alejandro Zurita, for his deep interest and contribution as EC project manager.

## Appendix 1: COLOSS reports

## DOCUMENTS SAM-COLOSS-M00X

EURATOM RESEARCH FRAMEWORK PROGRAMME 1998-2002 Nuclear Fission Safety - Reactor Safety Catalogue of documents issued by COLOSS Project	Title of the project: <b>(COLOSS Project)</b> Contract FIKS-CT-1999-00002	Coordinator: Dr. B. Adroguer (CEA-IPSN Cadarache)
	Contractual period: 5 <sup>th</sup> FP 1998 - 2002	Responsible EC: A. Zurita

TITLE	AUTHORS	TYPE	REFERENCE	DATE
CORE LOSS DURING A SEVERE ACCIDENT COLOSS Technical Annex 1	B. Adroguer and partners of COLOSS project	Contract Annex 1	SAM-COLOSS-P000 (*)	25/01/2000
MINUTES OF THE COLOSS KICK-OFF MEETING	C. Duriez, B. Adroguer	Minutes of kickoff meeting	SAM-COLOSS-M001 (*)	01/04/2000
MINUTES OF THE 1 <sup>ST</sup> COLOSS-RIAR MEETING	B. Adroguer, D. Bottomley	Minutes of topical meeting	SAM-COLOSS-M002	01/06/2000
MINUTES OF COLOSS TOPICAL MEETING ON PLANT APPLICATIONS	G. Azarian	Minutes of topical meeting	SAM-COLOSS-M003	20/10/2000
MINUTES OF THE 1 <sup>ST</sup> PROGRESS-MEETING (Karlsruhe)	C. Duriez, B. Adroguer	Minutes of topical meeting	SAM-COLOSS-M004	01/10/2000
MINUTES OF THE 2 <sup>ND</sup> PROGRESS-MEETING (Paris-Clamart)	C. Duriez, B. Adroguer	Minutes of topical meeting	SAM-COLOSS-M005	01/03/2001
MINUTES OF THE COLOSS TOPICAL MEETING ON QUENCH-07 TEST	A. Miassoedov	Minutes of topical meeting	SAM-COLOSS-M006	/03/2001
MINUTES OF 2 <sup>ND</sup> COLOSS TOPICAL MEETING ON PLANT APPLICATIONS	G. Azarian	Minutes of topical meeting	SAM-COLOSS-M007	09/01/2001

(\*): P: Progress Report and technical documents, M: Minutes

## DOCUMENTS SAM-COLOSS-M00X

EURATOM RESEARCH FRAMEWORK PROGRAMME 1998-2002 Nuclear Fission Safety - Reactor Safety Catalogue of documents issued by COLOSS Project	Title of the project: <b>(COLOSS Project)</b> Contract FIKS-CT-1999-00002
	Coordinator: Dr. B. Adroguer (CEA-IPSN Cadarache)
	Contractual period: 5 <sup>th</sup> FP 1998 - 2002
	Responsible EC: A. Zurita

TITLE	AUTHORS	TYPE	REFERENCE	DATE
MINUTES OF THE 3 <sup>rd</sup> PROGRESS-MEETING (Budapest)	C. Duriez, B. Adroguer	Progress meeting	SAM-COLOSS-M008	25/09/2001
MINUTES OF THE 2 <sup>ND</sup> COLOSS TOPICAL MEETING ON QUENCH-07 TEST	A. Miassoedov	Topical meeting	SAM-COLOSS-M009	/10/2001
MINUTES OF 3 <sup>rd</sup> COLOSS PLANT ANALYSIS GROUP (Budapest)	G. Azarian	PAG Progress meeting	SAM-COLOSS-M010	/10/2001
MINUTES OF THE 4 <sup>th</sup> PROGRESS-MEETING (Bologna)	C. Duriez, B. Adroguer	Progress meeting	SAM-COLOSS-M011	25/02/2002
MINUTES OF 4 <sup>th</sup> COLOSS PLANT ANALYSIS GROUP (Bologna)	G. Azarian	PAG Progress meeting	SAM-COLOSS-M012	
MINUTES OF THE 5 <sup>th</sup> PROGRESS-MEETING (Madrid)	B. Adroguer, C. Duriez	Progress meeting	SAM-COLOSS-M013	06/2002
MINUTES OF 5 <sup>th</sup> COLOSS PLANT ANALYSIS GROUP (Madrid)	G. Azarian	PAG Progress meeting	SAM-COLOSS-M014	06/2002
MINUTES OF THE COLOSS TOPICAL MEETING ON FUEL DISSOLUTION	M. Barrachin et B. Adroguer	Minutes of topical meeting	SAM-COLOSS-M015	/10/2002
MINUTES OF 6 <sup>th</sup> COLOSS-PAG meeting (Paris)	G. Azarian and B. Adroguer	PAG Progress meeting	SAM-COLOSS-M016	/12/2002
MINUTES OF 7 <sup>th</sup> COLOSS-PAG meeting (Mol)	G. Azarian and B. Adroguer	PAG Progress meeting	SAM-COLOSS-M017	/04/2003
MINUTES OF THE 6 <sup>th</sup> PROGRESS-MEETING (Mol)	C. Duriez, B. Adroguer	Progress meeting	SAM-COLOSS-M018	05/2003

## Catalogue of COLOSS documents (SAM-COLOSS-P00X) (\*)

EURATOM RESEARCH FRAMEWORK PROGRAMME 1998-2002 Nuclear Fission Safety - Reactor Safety Catalogue of documents issued by COLOSS Project	Title of the project: Coordinator: Contractual period: Responsible EC:	<b>(COLOSS Project)</b> Contract FIKS-CT-1999-00002 5 <sup>th</sup> FP Dr. B. Adroguer (CEA-IPSN Cadarache) 1 <sup>st</sup> Feb. 00 - 1 <sup>st</sup> Feb. 03 A. Zurita
--	---	--

TITLE	AUTHORS	TYPE	REFERENCE	DATE
1 <sup>st</sup> Semi-Annual Progress Report	PARNERS OF COLOSS PROJECT	1 <sup>st</sup> semi-annual progress report	SAM-COLOSS-P001 (*)	01/10/2000
Thermodynamic Calculations In The B-C-H-O System	C. Duriez	Technical report	SAM-COLOSS-P002	01/10/2000
1 <sup>st</sup> Annual Progress Report (2000-2001)	PARNERS OF COLOSS PROJECT	1 <sup>st</sup> Annual Progress Report	SAM-COLOSS-P003	15/03/2001
Pre-Test Calculations of The CODEX -B <sub>4</sub> C Test	Volchek, Y. Zvonarev	Final report D16, Vol 1	SAM-COLOSS-P004	2001
Preliminary modelling of B <sub>4</sub> C oxidation in ICARE2	S. Ederli, O. Marchand.	Interim report D24	SAM-COLOSS-P005	2001
ICARE/COLOSS-IBRAE: Fuel dissolution modelling and validation	A.V. Berdyshev; A.V. Boldyrev and M.S. Veshchonov	Preliminary report D28	SAM-COLOSS-P008	March 2001
Pre-test calculation of CODEX -B <sub>4</sub> c test	G. Gyenes (KFKI)	Final report D16, Vol 2	SAM-COLOSS-P013	May 2001
Pre-test calculation of CODEX -B <sub>4</sub> c test	E. Virtanen (LTKK)	Final report D16, Vol 3	SAM-COLOSS-P014	June 2001

(\*): P: Progress Report and technical documents

## Catalogue of COLOSS documents (SAM-COLOSS-P00X)

EURATOM RESEARCH FRAMEWORK PROGRAMME 1998-2002 Nuclear Fission Safety - Reactor Safety Catalogue of documents issued by COLOSS Project	Title of the project:  Coordinator: Contractual period: Responsible EC:	<b>(COLOSS Project)</b> Contract FIKS-CT-1999-00002 5 <sup>th</sup> FP Dr. B. Adroguer (CEA-IPSN Cadarache) 1 <sup>st</sup> Feb. 00 - 1 <sup>st</sup> Feb. 03 A. Zurita
--	---	--

TITLE	AUTHORS	TYPE	REFERENCE	DATE
VVER-1000 LOCA CALCULATIONS	V. Kobzar, Y. Zvonarev (KI) E. Virtanen (LTKK):	Interim -PartA Interim -PartB D32	SAM-COLOSS-P006A SAM-COLOSS-P006B	2001 Undeway
PWR 1300 MWe	IPSN-SEAC: EDF	Interim -PartA Interim -PartB D30	SAM-COLOSS-P007A SAM-COLOSS-P007B	2001 2001
EPR	FZK: FRAMATOME-ANP/Paris FRAMATOME-ANP/Erlangen:	Interim -PartA Interim -PartB Interim -PartC D33	SAM-COLOSS-P009A SAM-COLOSS-P009B SAM-COLOSS-P009C	2001 2001 2001
BWR	PSI:	Interim report D31	SAM-COLOSS-P010A	2001
TMI-2	IPSN-SEMAR: ENEA:	Interim -PartA Interim -PartB D34	SAM-COLOSS-P011A SAM-COLOSS-P011B	2001
Post-test calculation of QUENCH-07 test with MAAP4.04c	J. S. Lamy (EDF) D19	D19	SAM-COLOSS-P012	2003
QUENCH-07 Preliminary Post-test Calculations using SCDAP/RELAP5/Mod3.2.	J. Birchley	D22	SAM-COLOSS-P015	2001

## Catalogue of COLOSS documents (SAM-COLOSS-P00X)

EURATOM RESEARCH FRAMEWORK PROGRAMME 1998-2002 Nuclear Fission Safety - Reactor Safety Catalogue of documents issued by COLOSS Project	Title of the project: Coordinator: Contractual period: Responsible EC:	<b>(COLOSS Project)</b> Contract FIKS-CT-1999-00002 5 <sup>th</sup> FP Dr. B. Adroguer (CEA-IPSN Cadarache) 1 <sup>st</sup> Feb. 00 - 1 <sup>st</sup> Feb. 03 A. Zurita
--	---	--

<b>TITLE</b>	<b>AUTHORS</b>	<b>TYPE</b>	<b>REFERENCE</b>	<b>DATE</b>
High temperature oxidation of an U-O-Zr alloys	T. v. Berlepsch, M. K. Koch, H. Unger	Interim report D8	SAM-COLOSS-P016 (*)	June 2001
MTA report	B. Adroguer et al.	MTA report	SAM-COLOSS-P017	June 2001
FISA-01 paper: Status of the COLOSS project	B. Adroguer et al.	FISA-01 symposium	SAM-COLOSS-P018	June 2001
Pre-Test Calculation Of Codex -B <sub>4</sub> C Test	IKE	Final report D16 Vol 4	SAM-COLOSS-P019	Undeaway
CODEX- B <sub>4</sub> C data report and file	AEKI	Data report (D17)	SAM-COLOSS-P020	October 2001
Pre-test calculations of AEKI VVER and PWR single rod tests	KI	Pre-test calculation D16	SAM-COLOSS-P021	Undeaway
AEKI short fuel rod tests series N°1.	Z. Hozer et al..	Interim data report (D5)	SAM-COLOSS-P022	January 2002
D18 Post-test calculation of the CODEX B <sub>4</sub> C commissioning test	A. VOLCHEK, Y. ZVONAREV (KI)	Interim data report (D18)	SAM-COLOSS-P023	January 2002
QUENCH-07 data report	FZK	Data report D21	SAM-COLOSS-P024	January 2002
QUENCH-07 data file	FZK	Data file D20	SAM-COLOSS-P025	January 2002

## Catalogue of COLOSS documents (SAM-COLOSS-P00X)

EURATOM RESEARCH FRAMEWORK PROGRAMME 1998-2002 Nuclear Fission Safety - Reactor Safety Catalogue of documents issued by COLOSS Project	Title of the project: Coordinator: Contractual period: Responsible EC:	<b>(COLOSS Project)</b> Contract FIKS-CT-1999-00002 5 <sup>th</sup> FP Dr. B. Adroguer (CEA-IPSN Cadarache) 1 <sup>st</sup> Feb. 00 - 1 <sup>st</sup> Feb. 03 A. Zurita
--	---	--

<b>TITLE</b>	<b>AUTHORS</b>	<b>TYPE</b>	<b>REFERENCE</b>	<b>DATE</b>
BOX Tests on B <sub>4</sub> C oxidation at high temperature. Test Data Report: FZK BOX rig tests	Steinbruck et al.	Deliverable D11 (Part 1)	SAM-COLOSS-P026	May 2002
B <sub>4</sub> C oxidation data report: FZK TG rig tests	Steinbruck et al.	Deliverable D11 (Part 2)	SAM-COLOSS-P027	Underway March 2002
Short B <sub>4</sub> C CR data report: FZK tests	Steinbruck et al.	Deliverable D13	SAM-COLOSS-P028	Underway March 2002
Modelling of simultaneous UO <sub>2</sub> and ZrO <sub>2</sub> dissolution of by molten Zr	A.V. Berdyshev, A.V. Boldyrev and M. Veshchunov	Interim modelling report D28	SAM-COLOSS-P029	March 2002
2 <sup>nd</sup> ANNUAL PROGRESS REPORT (2001-2002)	All COLOSS partners	2 <sup>nd</sup> Annual Progress Report	SAM-COLOSS-P030	15/03/2002
COLOSS Amendment	B. Adroguer and partners of COLOSS project	Contract amendment	SAM-COLOSS-P031	16/04/002
U-O-Zr oxidation model	M.S. Veshchunov	Interim Report D26	SAM-COLOSS-P032	May 2002
COLOSS paper. Special NED-FISA Issue	All COLOSS partners	Paper in a journal	SAM-COLOSS-P038	2003
2 <sup>nd</sup> SEMI-ANNUAL REPORT	All COLOSS partners	Semi-Annual	SAM-COLOSS-P034	2002
QUENCH-07 calculation with MAAP4	J.S Lamy, S. Marguet		SAM-COLOSS-P039	

## Catalogue of COLOSS documents (SAM-COLOSS-P00X)

EURATOM RESEARCH FRAMEWORK PROGRAMME 1998-2002 Nuclear Fission Safety - Reactor Safety Catalogue of documents issued by COLOSS Project	Title of the project: Coordinator: Contractual period: Responsible EC:	<b>COLOSS Project</b> Contract FIKS-CT-1999-00002 5 <sup>th</sup> FP Dr. B. Adroguer (CEA-IPSN Cadarache) 1 <sup>st</sup> Feb. 00 - 1 <sup>st</sup> Feb. 03 A. Zurita
--	---	--

TITLE	AUTHORS	TYPE	REFERENCE	DATE
VVER-1000 LOCA CALCULATIONS	KI: LTKK:	Final PartA Final PartB D32	SAM-COLOSS-P033A SAM-COLOSS-P033B	End 02- begin 03
PWR 1300 Mwe CALCULATIONS	IPSN-SEAC: EDF	Final-PartB D30	SAM-COLOSS-P038A SAM-COLOSS-P038B	End 02- begin 03
EPR CALCULATIONS	FZK: FRA-ANP/Paris FRA-ANP/Erlangen:	Final-PartA Final-PartB Final-PartC D33	SAM-COLOSS-P035A SAM-COLOSS-P035B SAM-COLOSS-P035C	End 02- begin 032003
BWR CALCULATIONS	PSI:	Final-PartA D31	SAM-COLOSS-P036A	End 02- begin 03
TMI-2 CALCULATIONS	IPSN-SEMAR: ENEA: EDF	Final-PartA Final-PartB D34	SAM-COLOSS-P037A SAM-COLOSS-P037B SAM-COLOSS-P037C	End 02- begin 03

## Catalogue of COLOSS documents (SAM-COLOSS-P00X)

EURATOM RESEARCH FRAMEWORK PROGRAMME 1998-2002 Nuclear Fission Safety - Reactor Safety Catalogue of documents issued by COLOSS Project	Title of the project: Coordinator: Contractual period: Responsible EC:	<b>COLOSS Project</b> Contract FIKS-CT-1999-00002 5 <sup>th</sup> FP Dr. B. Adroguer (CEA-IPSN Cadarache) 1 <sup>st</sup> Feb. 00 - 1 <sup>st</sup> Feb. 03 A. Zurita
--	---	--

<b>TITLE</b>	<b>AUTHORS</b>	<b>TYPE</b>	<b>REFERENCE</b>	<b>DATE</b>
Final Report on U-Zr-O Melt Oxidation Model	M.S. Veshchunov	Final modeling report Report D27	SAM-COLOSS-P039	August. 2002
Modelling of Zr-O and U-Zr-O melts oxidation and new crucible tests	M. S. Veshchunov, J. Stuckert, A.V. Berdishev	Technical report	SAM-COLOSS-P040	December 2002
QUENCH-09 Quick Look Report	FZK	Data report D12	SAM-COLOSS-P041	Sept. 2002
QUENCH-09 data file	FZK	Data file D14	SAM-COLOSS-P042	Sept. 2002
Recommendations and supporting Information on the choice of Zry Oxidation Models in Severe Accident Codes	G. Schanz, FZK	Technical report	SAM-COLOSS-P043	Oct. 2002
Simultaneous UO <sub>2</sub> and ZrO <sub>2</sub> dissolution of by molten Zr: Experimental database	A. Goryachev	Interim report D3	SAM-COLOSS-P044	Oct. 2002
A model for B <sub>4</sub> C degradation-oxidation in MAAP4	S. Marguet	Modeling D24	SAM-COLOSS-P045	Oct. 2002
U-O-Zr Oxidation (Experimental data)	UJP-PRAHA	Interim report	SAM-COLOSS-P046	January 2002
Simultaneous dissolution of UO <sub>2</sub> and ZrO <sub>2</sub> by molten Zr: Final experimental report	A. Goryachev	Final report D3	SAM-COLOSS-P047	2003

## Catalogue of COLOSS documents (SAM-COLOSS-P00X)

EURATOM RESEARCH FRAMEWORK PROGRAMME 1998-2002 Nuclear Fission Safety - Reactor Safety Catalogue of documents issued by COLOSS Project	Title of the project: Coordinator: Contractual period: Responsible EC:	<b>COLOSS Project</b> Contract FIKS-CT-1999-00002 5 <sup>th</sup> FP Dr. B. Adroguer (CEA-IPSN Cadarache) 1 <sup>st</sup> Feb. 00 - 1 <sup>st</sup> Feb. 03 A. Zurita
--	---	--

<b>TITLE</b>	<b>AUTHORS</b>	<b>TYPE</b>	<b>REFERENCE</b>	<b>DATE</b>
Modelling of simultaneous UO <sub>2</sub> and ZrO <sub>2</sub> dissolution of by molten Zr: Validation against AEKI single rod tests. Final report	A.V. Berdyshev, A.V. Boldyrev and M. Veshchunov	Final report D28	SAM-COLOSS-P048	March 2003
Calculations for QUENCH-07	C. Homann	D19 or D22	SAM-COLOSS-P049	
High temperature oxidation of an U-O-Zr alloys 2002	T. v. Berlepsch, I.D. Kleinhietpass, M. K. Koch, H. Unger, H.-J. Wagner	Final report D26	SAM-COLOSS-P050	March 2003
Final report on short fuel rod dissolution tests	AEKI	D4	SAM-COLOSS-P051	
CODEX-B <sub>4</sub> C post-test examination (D17-Part 2	AEKI	D17	SAM-COLOSS-P052	
CODEX-B <sub>4</sub> C post-test analysis (AEKI part)	AEKI	D17	SAM-COLOSS-P053	
Final B4C Report.	M. Steinbruck et al.	D15	SAM-COLOSS-P054	
Pre and post-test calculations for QUENCH-07	C. Homann et al. FZK-PSI-UPM	D19 and D22	SAM-COLOSS-P055	April 03
Synthesis report on QUENCH-07 and QUENCH-09 experiments	A. Miassoedov	D23	SAM-COLOSS-P056	

## Catalogue of COLOSS documents (SAM-COLOSS-P00X)

EURATOM RESEARCH FRAMEWORK PROGRAMME 1998-2002 Nuclear Fission Safety - Reactor Safety Catalogue of documents issued by COLOSS Project	Title of the project: Coordinator: Contractual period: Responsible EC:	<b>COLOSS Project</b> Contract FIKS-CT-1999-00002 5 <sup>th</sup> FP Dr. B. Adroguer (CEA-IPSN Cadarache) 1 <sup>st</sup> Feb. 00 - 1 <sup>st</sup> Feb. 03 A. Zurita
--	---	--

<b>TITLE</b>	<b>AUTHORS</b>	<b>TYPE</b>	<b>REFERENCE</b>	<b>DATE</b>
Pre and post-test calculations for QUENCH-09	C. Homann	D9	SAM-COLOSS-P057	April 03
WP3.1 : Final report on oxidation of U-O-Zr mixtures ; QUENCH calculations	V. Vrtilkova J. Birsley (PSI)	D8	SAM-COLOSS-P058 SAM-COLOSS-P059	March 03
A fast-running model for degradation and oxidation of B <sub>4</sub> C in MAAP4	S. Marguet (EDF)	Modeling report	SAM-COLOSS-P060	March 2003
Pre- and Post Test Calculations for the CODEX-B4C Experiment with ATHLET-CD	M. Buck (IKE)	D18 and D16	SAM-COLOSS-P061	March 2003
"Pre- and Post-test calculations for the QUENCH-07 Bundle Test with ATHLET-CD"	M. Buck (IKE)	D19 and D22	SAM-COLOSS-P062	March 2003
B <sub>4</sub> C modelling in ATLETH-CD	M. Buck (IKE)	D25	SAM-COLOSS-P063	March 2003

## Catalogue of COLOSS documents (SAM-COLOSS-P00X)

EURATOM RESEARCH FRAMEWORK PROGRAMME 1998-2002 Nuclear Fission Safety - Reactor Safety Catalogue of documents issued by COLOSS Project	Title of the project: Coordinator: Contractual period: Responsible EC:	<b>COLOSS Project</b> Contract FIKS-CT-1999-00002 5 <sup>th</sup> FP Dr. B. Adroguer (CEA-IPSN Cadarache) 1 <sup>st</sup> Feb. 00 - 1 <sup>st</sup> Feb. 03 A. Zurita
--	---	--

TITLE	AUTHORS	TYPE	REFERENCE	DATE
Dissolution of High Burn-up UO <sub>2</sub> and MOX by molten Zry. Analysis of JRC ITU tests and improvement of ICARE2 modelling	L. Belovsky (ALIAS CZ)	D29	SAM-COLOSS-P064	April 2003
Oxidation of U-O-Zr mixtures by steam Analysis of SKODA tests and improvement of ICARE2 modelling	L. Belovsky (ALIAS CZ)	D27	SAM-COLOSS-P065	April 2003
Analysis of the CODEX-B4C test and ICARE/CATHARE code validation against VVER tests CODEX-B4C and CORA-W2 Final report	A. Voltchek, Yu. Zvonarev (NSI/KI)	D-18	SAM-COLOSS-P066	January 2003
Analysis of AEKI VVER and PWR single rod tests. Final report D-7	A. Voltchek, Yu. Zvonarev (NSI/KI)	D7	SAM-COLOSS-P067	January 2003
ICARE/CATHARE V1mod1 application on VVER-1000 Large Break LOCA. Final report	V. Kobzar, Yu. Zvonarev (NSI/KI)	Report D32-1 (Part B)	SAM-COLOSS-P068	January 2003
Post-test calculations of QUENCH-09 with ICARE/CATHARE	F. Bertrand	D14	SAM-COLOSS-P069	June 2003
B <sub>4</sub> C modelling in ICARE/CATHARE	F. Bertrand	D25	SAM-COLOSS-P070	June 2003

## Catalogue of COLOSS documents (SAM-COLOSS-P00X)

EURATOM RESEARCH FRAMEWORK PROGRAMME 1998-2002 Nuclear Fission Safety - Reactor Safety Catalogue of documents issued by COLOSS Project	Title of the project: Coordinator: Contractual period: Responsible EC:	<b>COLOSS Project</b> Contract FIKS-CT-1999-00002 5 <sup>th</sup> FP Dr. B. Adroguer (CEA-IPSN Cadarache) 1 <sup>st</sup> Feb. 00 - 1 <sup>st</sup> Feb. 03 A. Zurita
--	---	--

Analysis of QUENCH-09 Test with ICARE/CATHARE Code	G. Bandini	D14	SAM-COLOSS-P071	May 2003
Analysis of AEKI PWR Fuel Rod Dissolution Tests with ICARE/CATHARE and SCDAP/RELAP5 Codes	G. Bandini	D7	SAM-COLOSS-P072	May 2003
Final experimental report on oxidation of U-O-Zr (WP 3.1)	L. Belovsky	D8	SAM-COLOSS-P073	June 2003
Simultaneous Dissolution of UO <sub>2</sub> and ZrO <sub>2</sub> by Molten Zircaloy. New Experiments and Modelling.	K. Müller, A.V. Goryachev, V.P. Smirnov, A.M. Svyatkin, J. Stuckert, M.S. Veshchunov, A.V. Berdyshev	D33	SAM-COLOSS-P074	Sept 03
Oxidation of B <sub>4</sub> C by steam in the VERDI induction furnace: Final report	N. Cocuaud, D. Drouan, G. Taraud	D14	SAM-COLOSS-P075	End 03
Final Progress Report (EDF)	S. Marguet	B <sub>4</sub> C Modelling D25	SAM-COLOSS-P076	May 2003

## Catalogue of COLOSS documents (SAM-COLOSS-P00X)

EURATOM RESEARCH FRAMEWORK PROGRAMME 1998-2002 Nuclear Fission Safety - Reactor Safety Catalogue of documents issued by COLOSS Project	Title of the project: Coordinator: Contractual period: Responsible EC:	<b>COLOSS Project</b> Contract FIKS-CT-1999-00002 5 <sup>th</sup> FP Dr. B. Adroguer (CEA-IPSN Cadarache) 1 <sup>st</sup> Feb. 00 - 1 <sup>st</sup> Feb. 03 A. Zurita
--	---	--

FISA-03 COLOSS project	B. Adroguer et al.	FISA-03 symposium	SAM-COLOSS-P077	June 2002
Final COLOSS summary report	B. Adroguer et al.	Contractual Doc.	SAM-COLOSS-P078	July 03
Final COLOSS extended report: Part 1	B. Adroguer et al.	Contractual Doc	SAM-COLOSS-P079	July 03
Synthesis on plant calculations (D35) Final COLOSS extended report: Part 2	B. Adroguer et al.	Contractual Doc D35	SAM-COLOSS-P080	July 03

- 
- 1 B. Adroguer et al., "Synthesis on plant calculations. Final COLOSS report Part 2", IRSN/DRS/SEMAR 03/92, SAM-COLOSS-P079, June 3003.
  - 2 B. Adroguer, et al., Corium Interactions and Thermochemistry. CIT project, FISA-99 Symposium, EUR 19532 EN, Lux., Nov. 1999.
  - 3 I. Shepherd et al., Investigation of Core Degradation, COBE project. FISA-99 Symposium, EUR 19532 EN, Lux, Nov.1999.
  - 4 M. Firnhaber et al., OECD/NEA CSNI International Standard Problem N° 31: CORA-13 Experiment on Severe Fuel Damage. Comparison Report, NEA/CSNI/R(93°17, July 1993.
  - 5 W. Hering et al., OECD/NEA CSNI International Standard Problem N° 45: QUENCH-06, Comparison and Interpretation Report, FZKA 6722, April 2002.
  - 6 B. Adroguer et al., « Mid-term Assessment Report », COLOSS project, Feb. 2000-June 2001, SAM-COLOSS-P017.
  - 7 G. Azarian. "Minutes of the 5<sup>th</sup> Plant Analysis Group Meeting, Madrid, June 19, 2002, SAM-COLOSS-M014.
  - 8 B. Adroguer et al., "Final report of the CIT project", INV-CIT(99)-P040, IRSN/DRS/SEMAR 99/123, Dec. 1999.
  - 9 B. Adroguer et al., "Status report on dissolution of fuel rods and related effects", CIT Project , 4<sup>th</sup> FP, INV-CIT(99)-D004, July 2000.
  - 10 P.J.Hayward, I.M.George, J. Nucl. Mater. 208 (1994) 35.
  - 11 V. Vrtílková, L. Novotný, L. Belovsky: Oxidation of U-Zr-O mixtures – Interim report. SAM-COLOSS P026 (2001).
  - 12 P.J. Hayward and I. M. George, "Dissolution of ZrO<sub>2</sub> in Molten Zry-4", J.Nucl.Mater., 265 (1999) 69.
  - 13 P. Hofmann, J. Stuckert, A. Miassoedov, M. S. Veshchunov, A. V. Berdyshev, A. V. Boldyrev. "ZrO<sub>2</sub> Dissolution by Molten Zr and Cladding Oxide Shell Failure. New Experimental Results and Modelling", FZKA 6383, Forschungszentrum Karlsruhe, 1999
  - 14 M.S.Veshchunov, J.Stuckert, A.V.Berdyshev, Modelling of Zr-O and U-Zr-O Melts Oxidation and New Crucible tests. Report FZKA 6792, SAM-COLOSS-P040, Karlsruhe, Germany, December 2002.
  - 15 J. T. Prater, E. L. Courtright: Properties of Reactor Fuel Rod Materials at High Temperatures. NUREG/CR-4891 (1987).
  - 16 T. v. Berlepsch, I. D. Kleinhietspass, M. K. Koch, H. Unger, H.-J. Wagner. „High Temperature Oxidation of U-Zr-O Alloys – Final Report”. Ruhr-University Bochum, SAM-COLOSS-P050, 2003.
  - 17 L. Belovsky et al., Chemical Interaction in B<sub>4</sub>C-filled Control Rod Segments above 1000°C under transient conditions, ICONE5, Nice, May 1997.
  - 18 B. Adroguer, "Status on B<sub>4</sub>C in Severe Accident Conditions. Uncertainties and Experiments Proposed", NT DRS/SEMAR 99/95, January 2000."
  - 19 B. Adroguer et al., Mid-Term Assessment report, COLOSS Project, SAM-COLOSS-P017, June 2001.
  - 20 M. Steinbrück, A. Meier, E. Nold, U. Stegmaier, Degradation and oxidation of B<sub>4</sub>C control rod segments at high temperatures, Report FZKA 6980, Forschungszentrum Karlsruhe, 2004.
  - 21 W. Krauss, G. Schanz, H. Steiner, TG-rig tests (thermal balance) on the oxidation of B<sub>4</sub>C. Basic experiments, modelling and evaluation approach, Report FZKA 6883, Forschungszentrum Karlsruhe, 2003.

- 
- 22 M. Steinbrück, W. Krauss, G. Schanz, H. Steiner, M. S. Veshchunov, A. V. Berdyshev. FZK Separate-effects Tests on B<sub>4</sub>C Oxidation; Final Analysis Report, SAM-COLOSS-P054, FZK/NUKLEAR 3385, Apr. 2003.
- 23 Miassoedov, A.: Minutes of the COLOSS Topical Meeting on QUENCH-07 Test, SAM-COLOSS-M006, Karlsruhe, Feb. 8, 2001.
- 24 Sanchez, V., Elias, E., Homann, Ch., Hering, W., Struwe, D.: Development and Validation of a Transition Boiling Model for the RELAP5/MOD3 Reflood Simulation, FZKA 5954, Sep. 1997
- 25 Hering, W., Homann, C.: Improvement of the Severe Accident Code SCDAP/RELAP5 mod 3.2 with respect to the FZK QUENCH facility, FZKA 6566, to be published.
- 26 Homann, Ch., Hering, W., Birchley, J., Fernandez Benitez, J. A., Ortega Bernardo, M.: Analytical Support for B<sub>4</sub>C Control Rod Test QUENCH-07, FZKA 6822, April 2003.
- 27 Homann, Ch., Hering, W., “Analytical Support for B<sub>4</sub>C Control Rod Test QUENCH-09”, FZKA 6853, to be published.
- 28 Miassoedov, A., “Minutes of the COLOSS Topical Meeting on QUENCH-09 and CODEX-B<sub>4</sub>C Experiments”, SAM COLOSS-M009, Karlsruhe, 22 and 23 Oct. 2002.
- 29 Duriez, Ch, Adroguer, B., “Minutes of the 4th Progress Meeting”, SAM-COLOSS-M011, Bologna, January 31, 2002.
- 30 J. Birchley. “Quench-07 Preliminary Post-test Calculation using SCDAP/RELAP Mod3.2”, (SAM-COLOSS-P015), PSI report, 2002.
- 31 J. Birchley. “Analysis of Quench-06, -07, and 09 Experiments using MELCOR 1.8.5. Preliminary Post-test Calculation using SCDAP/RELAP Mod3.2”, SAM-COLOSS-P015, PSI report, 2002.
- 32 S. Ederli and O. Marchand, “Oxidation of a B<sub>4</sub>C control rod by steam, implementation of a preliminary model in the ICARE2 code”, COLOSS Project, Interim Report D24, Jan. 2001.
- 33 F. Bertrand, O. Marchand and G. Repetto, “B<sub>4</sub>C control Rod Oxidation During a Severe Accident in a PWR Reactor, Separate Effect and Integral Tests Analysis for Modeling Purpose with the ICARE/CATHARE Code”, NURETH-10, Seoul, Korea, October 5-9, 2003.
- 34 M. Barrachin, Bibliographie sur l'oxydation du B<sub>4</sub>C, Technical Note, IRSN, NT DRS/SEMAR 99/121, 1999.
- 35 N. Cocuau, D. Drouan, G. Teraud, « Oxidation of B<sub>4</sub>C by steam in the VERDI induction furnace », NT LEA/DRS 04-080, SAM-COLOSS-P075, Dec. 2003.
- 36 M. Steinbrück, A. Meier, U. Stegmaier, L. Steinbock, “Experiments on the oxidation of boron carbide at high temperatures”, SAM-COLOSS-P054, Report FZKA 6979, Forschungszentrum Karlsruhe, 2004.
- 37 J.O. Liljenzin, R. Alenljung, L.G. Johansson, O. Lindquist, L. Hammar, A. Hautjarvi, J. Jokiniemi, J.P. Omtvedt, T. Raunemaa, K. Koistinen, P. Pasanen and U. Steiner Jensen, “The influence of chemistry on melt core accidents“, *Final report of the NKA Project ATKI-150*, 1990.
- 38 T. Sato, K. Haryu, T. Endo and M. Shimad, “*Oxidation of Nonoxide ceramics by Water Vapor at High Temperature*”, Fac. Eng. Tohoku Univ., Sendai, Japan, Zairyo, 37(412), 77-82, 1988.
- 39 R.M. Elrick, R.A. Sallach, A.L. Ouellette and S.C. Douglas, “Boron Carbide-Steam Reactions with Cesium Hydroxyde and Cesium Iodide at 1270 K in an Inconel 600 System” NUREG/CR-4963, 1987.
- 40 S. Marguet, “Final Progress Report”, SAM-COLOSS-P076, May 2003.
- 41 W. Krauss, “B<sub>4</sub>C oxidation tests in TG-unit and approach to evaluation”, 9<sup>th</sup> Inter. QUENCH Workshop, FZK Karlsruhe, Oct. 13-15, 2003.
- 42 L. Belovsky, “Oxidation of U-Zr-O alloys by steam: Analysis of ŠKODA-ÚJP experiments and improvement of ICARE2 (ZROX) modeling”, SAM-COLOSS-P065, NT-SEMAR 03/42, June 2003.

- 
- 43 M.S. Veshchunov, A.V. Berdyshev, "Final Report on U-O-Zr Melt Oxidation Model", JRC Technical Note N° P.02.84, SAM-COLOSS-P039, Petten, August 2002.
- 44 B. Lefèvre, "Magma oxidation: oxidation of the MAGMA components in ICARE2 code", CISI 2003/104 (V2.0), to be released.
- 45 B. Adroguer et al., Status report on dissolution of fuel rods and related clad failure, INV-CIT(99)-D004, Nov. 1999.
- 46 L. Belovsky, "Dissolution of High Burn-up UO<sub>2</sub> and MOX by molten Zry. Analysis of JRC ITU tests and improvement of ICARE2 modelling", SAM-COLOSS-P064, NT-SEMAR 2003/41, April 2003.
- 47 M.S. Veshchunov, A.V. Berdyshev, "Development of a model for the simultaneous dissolution of UO<sub>2</sub> and ZrO<sub>2</sub> by molten Zr", JRC/COLOSS-IBRAE, JRC Technical Note, N° P.03.78, SAM-COLOSS-P047, March 2003.
- 48 K. Müller, A.V. Goryachev, V.P. Smirnov, A.M. Svyatkin, J. Stuckert, M.S. Veshchunov, A.V. Berdyshev, "Simultaneous Dissolution of UO<sub>2</sub> and ZrO<sub>2</sub> by Molten Zircaloy. New Experiments and Modelling", Report FZKA 6947, SAM-COLOSS-P074, Karlsruhe, Germany, January 2004.
- 49 P. Chatelard et al., "ICARE/CATHARE V1mod1.3 : Release guide", NT. IRSN/DRS/SEMAR 03/51, 2003.
- 50 G. Schanz, "Recommendations and Supporting Information on the Choice of Zirconium Oxidation Models in Severe Accident Codes", FZKA 6827, SAM-COLOSS-P043, March 2003.
- 51 G. Schanz, B. Adroguer, A. Volchek, "Advanced Treatment of Zircaloy Cladding High-Temperature Oxidation in Severe Accident Code Calculations, PART I. Experimental database and basic modeling", To be published in Nucl. Eng. and Design.
- 52 A. Volchek, G. Schanz, Yu. Zvonarev, "Advanced Treatment of Zircaloy Cladding High-Temperature Oxidation in Severe Accident Code Calculations, PART II. Best-fitted parabolic correlations", To be published in Nucl. Eng. and Design.
- 53 F. Fichot, B. Adroguer, A. Volcheck and Yu. Zvonarev, "Advanced treatment of Zircaloy cladding, High-Temperature Oxidation in Severe Accidents Code Calculations, PART III. ", To be published in Nucl. Eng. and Design.
- 54 B. Adroguer et al., Synthesis on plant calculations. Final COLOSS report : Part 2, SAM-COLOSS-P080, IRSN/DRS/SEMAR 03/30, June 2003.
- 55 B. Adroguer et al., "Core Loss During a Severe Accident (COLOSS Project)", Nuclear Engineering and Design, 221, 55-76, 2003.
- 56 A. De Bremaecker et al., "European nuclear thermodynamic database for in- and ex-vessel applications (ENTHALPY)", FISA 01, Lux., Nov. 2001.
- 57 Steinbrück M. and Granosa M. (Editors), "8th International QUENCH Workshop", Karlsruhe, Oct.29-31, 2002.
- 58 A. Miassoedov et al., "Main Results of the Large-Scale Experiments QUENCH-07 and QUENCH-09 with B<sub>4</sub>C Control Rods", PHEBUS FP Information Meeting, JRC Petten, 26 March 2003.
- 59 J.P. Van Dorsselaere, F. Jacq, H.J. Allelein, B. Schwinges, "ASTEC status and applications", CSARP 2003, Bethesda (USA).
- 60 Allelein H.J. et al., European validation of the integral code ASTEC (EVITA), FISA 01, Lux., Nov. 2001.
- 61 D. Magallon et al., "European Expert Network for the Reduction of Uncertainties in Severe Accident Safety Issues", EURSAFE, FISA-03, Luxembourg, 10-13 Nov. 2003.
- 62 A. Mailliat et al., «EUROSAFE Project: The Status of the European Severe Accident PIRTs», EUROSAFE Seminar, Berlin, 4-5 Nov. 2002.

- 
- 63 T. Haste and B. Clément, Synthesis meeting between THENPHEBISP, COLOSS, ENTHALPY and EVITA, CR DRS/SEMAR 2003/037, June 2003.
- 64 B. Clément et al., “Thematic network for a PHEBUS FPT-1 International Standard Problem (THENPHEBISP)”, FISA 2003, Luxembourg 10-13 novembre 2003.
- 65 B. Clément and T. Haste, Minutes of the Application Workshop, Aix-en-Provence, 23<sup>rd</sup> June 2003.
- 66 J.C. Micaelli et al., “SARNET : Sustainable Integration of EU Research on Severe Accident Phenomenology and Management”, FISA-03, Luxembourg, 10-13 Nov. 2003.